NATURAL STREAM FLOW FIELDS: MEASUREMENTS AND IMPLICATIONS FOR PERIPHYTON

By

MARK CHARLES STONE

A dissertation submitted in partial fulfillment of
the requirements for the degree of

DOCTOR OF PHILOSOPHY IN CIVIL ENGINEERING

WASHINGTON STATE UNIVERSITY
Department of Civil and Environmental Engineering

MAY 2005

To the Faculty of Washington State University:

The members of the Committee appointed to examine the dissertation of MARK CHARLES STONE find it satisfactory and recommend that it be accepted.

_____
Chair

_____

_____

_____

ACKNOWLEDGMENT

I would like to express my sincere appreciation to my advisor, Dr. Rollin Hotchkiss, for providing professional and personal guidance through my undergraduate and graduate careers. I would also like to thank Dr. Michael Barber, Dr. Shulin Chen, and Dr. David Smith for serving on my graduate committee.

I would also like to thank Ryan Morrison for his contribution to this research. Additionally, I acknowledge the students of Albrook Hydraulics Laboratory for their support and guidance over the past several years.

Finally, I would like to thank my wife, Asako, and the rest of my family for their unconditional love and support.

NATURAL STREAM FLOW FIELDS: MEASUREMENTS AND

IMPLICATIONS FOR PERIPHYTON

Abstract

by Mark Charles Stone, Ph.D.
Washington State University
May 2005

Chair: Rollin H. Hotchkiss

To restore ecological processes and functions, we must advance our knowledge of natural stream flow fields and their influence on aquatic ecosystems. This research addressed this need by meeting the following objectives:

- Objective 1: a) Evaluate the adequacy of existing empirical relationships for describing natural stream flow fields and b) investigate spatial distributions of flow variables
- Objective 2: Test the adequacy of ADCP instruments for measuring velocity, shear stress, and turbulence distributions in cobble bed streams
- Objective 3: Investigate temporal variations in periphyton resistance to shear stress

Objective 1 was completed by conducting acoustic Doppler velocimeter (ADV) measurements in two stream reaches. Objective 2 was met by collecting ADCP and ADV data at nine coincident stations and statistically comparing the results. Objective 3 was met by colonizing periphyton assemblages on ceramic tiles in a stream and exposing the collected tiles to various levels of shear stress in a laboratory flume.

The results showed that existing empirical relationships were adequate for describing velocity and shear stress distributions, but empirical predictions of turbulence parameters were significantly different from observed values. The ADCP adequately measured velocity magnitude and shear stress values, but not three dimensional velocity components or turbulence parameters. Periphyton resistance to shear stress increased with successional development of the assemblage, but was not affected by time of the growth season.

The results have broad implications for evaluating and managing aquatic systems. The flow field measurements reveal that we must re-evaluate natural stream turbulence prediction techniques. Quantifiable descriptions of flow heterogeneity will improve restoration designs and communication between disciplines. Further, this data can be used for parameterization of numerical models. ADCP results verify the use of these instruments for velocity and shear stress measurements. This has implications for habitat evaluation, model calibration, sediment transport estimates, and evaluation of other stream processes. Results of the periphyton experiments can be used to improve reservoir release management, restoration designs, and assessment of instream flow requirements.

Table of Contents

List of Figures

List of Tables

Chapter 1: Introduction

Hydropower development, channelization of streams, water withdrawals, land use changes, and other anthropogenic activities have caused severe damage to aquatic ecosystems. To restore ecosystem processes and functions, we must advance our knowledge of these systems. This requires a better understanding of physical flow features and the influence of these features on aquatic organisms. Improved flow field descriptions will advance stream restoration efforts by allowing reproduction of important flow features. Advanced measurement techniques will allow for easier analysis of aquatic ecosystems. Increased knowledge of the influence of flow on aquatic organisms will improve our ability to manage and restore streams and rivers.

Objectives

The goal of this research was to improve descriptions of natural stream flow fields and the influence of flow on periphyton assemblages. This goal was met by completing the following three objectives and testing the associated hypotheses.

Objective 1: a) Evaluate the adequacy of existing empirical relationships for describing natural stream flow fields and b) investigate spatial distributions of flow variables

Hypothesis 1: Existing empirical equations are adequate for describing natural stream flow fields. It was predicted that there would be no significant difference between measured data and empirical relationships.

Hypothesis 2a: Mean and turbulent flow field parameters are good distinguishers of stream units (riffles, pools, and runs). It is predicted that there will be a significant difference in flow variables between riffle, pool, and run stream units.

Hypothesis 2b: It is also predicted that there will be a significant difference in flow variables at different relative depths.

Objective 2: Test the adequacy of ADCP instruments for measuring velocity, shear stress, and turbulence distributions in cobble bed streams

Hypothesis 3: ADCP measurements are adequate for describing velocity and shear stress distributions. It was predicted that there would be no significant difference between ADV and ADCP velocity and shear stress measurements.

Objective 3: Investigate temporal variations in periphyton resistance to shear stress scour

Hypothesis 4: Periphyton ash free dry mass (AFDM) is dependent on time of the growth season. It is predicted that periphyton assemblages will increase in AFDM with respect to time of the growth season.

Hypothesis 5: Periphyton AFDM is dependent on successional development. It is predicted that the periphyton AFDM will increase with colony age.

Hypothesis 6: The amount of periphyton scour is dependent on the level of shear stress. It is predicted that periphyton mass scour and percent scour will increase linearly as shear stress is increased.

Hypothesis 7: The effect of shear stress on periphyton scour is dependent on time of the growth season. It is predicted that periphyton mass scour will increase and percent scour will decrease with an increase in time.

Hypothesis 8: The effect of shear stress on periphyton scour is dependent on successional development. It is predicted that periphyton mass scour will increase and percent scour will decrease with colony age.

Overview of Experiments

These objectives were met through a combination of stream observations and laboratory experiments. Flow field measurements were conducted in the Potlatch River near Kendrick, Idaho and the St. Maries River near Clarkia, Idaho. Turbulent flow fields were mapped with an acoustic Doppler velocimeter (ADV). The stream flow fields were also measured with an acoustic Doppler current profiler (ADCP) and compared with ADV results. The data were used to investigate velocity, shear stress, and turbulence distributions. The measured data were compared with existing empirical relationships, developed primarily in laboratory experiments with statistical techniques.

Periphyton samples were colonized on unglazed ceramic tiles in the South Fork of the Palouse River in Pullman, Washington. Colonized tiles were transferred to Albrook Hydraulics Laboratory at Washington State University and subjected to four levels of shear stress. Periphyton scour was evaluated as a function of shear stress, time of the growth season, and successional development. The hypotheses were tested with statistical techniques.

Summary of Results

Results showed that existing empirical relationships were adequate for describing velocity and Reynolds shear stress values but not turbulence parameters. The log-law closely predicted the vertical velocity profile for all stream units and transverse locations. Although there was not a significant difference between measured and predicted Reynolds shear stress values, the results were marginal. Empirical turbulence equations were inadequate for describing turbulence intensities, turbulent kinetic energy, and integral time and length scales. ADCP velocity magnitude and shear stress estimates were

not significantly different from ADV results. The tested ADCP configuration was found inadequate of for measurement of three-dimensional velocity components and turbulence variables. Periphyton scour resistance was found to be a function of successional development but not time of the growth season. Periphyton scour was linearly proportional to shear stress.

Implications

Stream flow fields influence aquatic organisms through dispersal, habitat use, resource acquisition, and competitor/prey relationships. Despite the pervasive influence of flow on aquatic ecosystems and other stream processes, the details of natural flow fields are poorly described. To advance understanding of the affects of flow on aquatic ecosystems, improvements are desperately needed in the following areas (Hart and Finelli 1999): 1) flow field descriptions, 2) flow field measurement techniques, and 3) understanding of the linkages between the flow field and aquatic organisms. This research will address theses priorities as follows:

Flow field descriptions → Objective 1 → Chapter 2

Flow field measurement techniques → Objective 2 → Chapter 3

Flow field/aquatic organism linkages → Objective 3 → Chapter 4

The results of this research will improve efforts in reservoir release management, stream restoration, fish passage, and instream flow evaluations. General implications are discussed below with in-depth discussions within the specific chapters.

<u>Reservoir Release Management</u>

Study results will improve our ability to manage reservoir release schedules to enhance aquatic ecosystems. Damming of streams drastically modifies the aquatic

environment, including downstream flow regime. Reservoir release rates are generally dictated by power demand, reservoir volumes, flood control, irrigation demand, and other human needs. These complex demands result in unnatural flow fluctuations. Recently, increased environmental awareness and regulations, such as the endangered species act, have forced dam managers to consider environmental impacts of reservoir release schedules. Improved knowledge of flow impacts on periphyton communities will enhance our ability to manage reservoir releases in a manner which benefits the environment.

In river systems in which excess periphyton is a nuisance, reservoir discharge can be scheduled to manage the colonies. Although greater periphyton mass can be removed later in the growth season, advanced periphyton colony development will increase resistance to disturbance. The best results would be achieved through frequent flushing flows that prevent advanced successional development. Conversely, preservation of periphyton colonies is desired for energy limited streams. For such systems, it is desirable to promote successional development of the periphyton colonies and avoid late season flushing flows. A natural flow regime with a spring flush and low summer flows would be desirable.

Stream Restoration

This research will benefit stream restoration efforts. Current designs depend heavily on qualitative descriptions of stream flow fields, such as riffle, pool, and run stream units. The general approach is to increase flow heterogeneity by reproducing these habitat types. However, such features are difficult to define and flow field details are not known. This research will provide quantifiable details about the flow features found

within these qualitative habitat features. Flow heterogeneity is also increased by adding objects to the flow, such as large woody debris and fish rocks. The design and placement of such features will be improved through better flow field descriptions and measurement techniques.

Further, restoration efforts will be improved through greater knowledge of the impacts of shear stress on periphyton disturbance. Depending on productivity and energy input to the stream, channel geometry and structures can be adjusted to prevent or encourage periphyton scour.

Finally, to prevent streambank failure and bed degradation or aggradation, restoration designs must account for sediment transport. Sediment transport relationships depend on estimates of shear stress and turbulence distributions. Improved shear stress descriptions and measurement techniques will enhance these analyses.

Fish Passage

Improving fish passage at hydroelectric facilities, culverts, and other hydraulic structures is a priority for the recovery of salmonid species. This effort requires greater knowledge of natural and modified flow fields and the response of fish to these environments. Properly scaled turbulence provides habitat, increases swimming efficiency, and has been hypothesized to provide directional guidance to actively swimming fish (Cada and Odeh, 2001). The introduction of turbulent flows to attract upstream migrating adult salmon has been used for more than forty years. In order to capitalize on fish response to flow fields, a better understanding of the appropriate intensity and scale of turbulence required for fish attraction must be attained. The most logical turbulent attraction flow for migrating salmonids would be the turbulent flow

conditions in natural streams. This research contributes to this effort by improving descriptions and measurement techniques of natural stream flow fields.

Instream Flow Assessments

Proper water allocation and management decisions require suitable tools for assessing tradeoffs between competing interests. Assigning value to out-of-stream uses can be accomplished through traditional economic techniques. However, relating ecological benefits to in-stream flow is a more complicated task. Tools have been developed to relate the quantity of in-stream flow to the benefits produced by that flow. Models, such as the Physical Habitat Simulation Model (PHABSIM) and Ecosystem Diagnosis and Treatment (EDT), are used to analyze the relationship between stream flow and physical habitat by evaluating flow features such as water depth, velocity, and substrate features as they relate to target species. Current methods used for evaluating aquatic habitat rely on simplified representations of the flow field in the form of point measurements. These methods can be improved by incorporating important spatial and temporal flow field variations and through a better understanding of the complex relationships between the flow field and aquatic organisms (Crowder and Diplas, 2002). By improving flow field descriptions, measurement techniques, and knowledge of flow impacts on periphyton, this research will lead to improvement of these tools to better evaluate the ecological effects of changes in river flow regime. This will allow the water needs of society to be better assessed against the water needs of river ecosystems. This will improve our ability to make intelligent decisions regarding in-stream flow requirements, water rights, and stream improvements.

References

Cada, G.C., and Odeh M. (2001). “Turbulence at hydroelectric power plants and its potential effects on fish.” *Report, U.S. Department of Energy*, Bonneville Power Administration.

Crowder, D. W. and Diplas, P. (2002). Assessing changes in watershed flow regimes with spatially explicit hydraulic models. Journal of the American Water Resources Association, 38(2), 397-408.

Hart, D. D. and Finelli, C. M. (1999). Physical-biological coupling in streams: The pervasive effects of flow on benthic organisms. Annual review of ecology and systematics, 30, 363-395.

Chapter 2: Stream Flow Field Measurements

Abstract

Improving descriptions of natural stream flow fields is a critical step in restoring aquatic ecosystems. Current methods used for evaluating aquatic habitat rely on simplified representations of the flow field. These methods can be improved by incorporating important spatial and temporal flow field variations and more advanced habitat metrics, such as shear stress and turbulence properties. However, knowledge of velocity and turbulence distributions in natural streams is limited to laboratory derived empirical equations. Further, only limited experiments have been conducted in natural streams. The objective of this research was to evaluate the adequacy of existing empirical relationships for describing natural stream flow fields and to investigate spatial distributions of flow variables. In this research, acoustic Doppler velocimeter (ADV) measurements were conducted at the reach scale (approximately 5 stream widths) in two cobble-bed streams. The measurements encompassed riffle, pool, and run stream units. The results showed that velocity distributions were adequately predicted with the log-law for all stream units and transverse locations. The linear Reynolds shear stress distribution adequately predicted observed values. However, empirical turbulence intensity, turbulent kinetic energy, and integral length scale equations inadequately described measured values. Flow variables displayed greater variation with stream units (riffles, pools, and runs) than with depth. This was likely due to turbulence generation from stream banks, bedforms, obstructions, and other stream features. A turbulent kinetic energy budget approach was recommended as a possible improvement over existing empirical predictions of turbulence distributions in natural channels.

Introduction

Flow is one of the most dominant variables influencing stream processes. For example, aquatic habitat is affected by dispersal, habitat use, resource acquisition, and competitor/prey relationships. Mixing of nutrients, contaminants, and dissolved gases depend on velocity and turbulence distributions. Sediment transport is influenced by velocity, shear stress, and turbulence fluctuations. Despite the pervasive effects of flow on aquatic processes, little is known about the details of natural stream flow fields. Most of our knowledge is derived from laboratory studies or limited field observations. This lack of quantifiable data has limited us to qualitative stream descriptions such as riffles, pools, and runs. The recent development of field equipment, capable of measuring more advanced flow variables, has improved stream measurement techniques. However, only a small number of studies with rather limited scopes have been conducted. A detailed investigation of flow features at the reach scale has not been completed.

Objective

The objective of this research was to a) evaluate the adequacy of existing empirical relationships for describing natural stream flow fields and b) investigate spatial distributions of flow variables. This objective was met by testing the following hypotheses.

Hypothesis 1: Existing empirical equations are adequate for describing natural stream flow fields. It was predicted that there would be no significant difference between measured data and empirical relationships.

Hypothesis 2a: Mean and turbulent flow field parameters are good distinguishers of stream units (riffles, pools, and runs). It is predicted that there will be a significant difference in flow variables between riffle, pool, and run stream units.

Hypothesis 2b: It is also predicted that there will be a significant difference in flow variables at different relative depths.

Background

Influence of Flow

Flow plays an important role in nearly every stream process. Mean velocity and turbulence distributions influence aquatic ecosystems, energy transfer, geomorphology, and contaminant and nutrient transport.

Flow is regarded as a key driver of stream ecology (Bunn and Arthington 2002). Velocity and turbulence distributions can strongly affect habitat characteristics, dispersal, resource acquisition, competition, and predator-prey interactions (Hart and Finelli 1999). These processes and associated flow field influences are summarized in Table 2.1.

Table 2.1. Summary of the affects of the flow field on aquatic processes

Process	**Influence**
Dispersal	Entrainment, in-stream transport, settlement
Habitat Use	Habitat structure, disturbance regime, energy expenditure
Resource Acquisition	Resource distribution, capture efficiency, drag costs
Competition	Exploitation, interference, spacing
Predator-Prey Interactions	Encounter probability, escape tactics, and cover

Human activities modify natural flow fields. Given the pervasive effects of flow on aquatic organisms, it is not unexpected that these activities often have adverse affects on aquatic ecosystems. For example, sediment depleted water released from dams erodes fine sediments from the streambed, resulting in a coarsened particle size distribution. This can reduce habitat availability for organisms using the interstitial spaces and spawning gravels for salmon and trout (Poff 1997). By improving our understanding of spatial and temporal flow field variations, it will be possible to improve water resources management to better balance human and environmental needs (Naiman 2002).

Flow Field Descriptions

The description of flow fields can be separated into mean velocity and turbulent fluctuations. Mean velocity is typically time-averaged at a point in the flow field. This definition can be expanded to a depth-integrated mean and often as a cross-sectional mean. Turbulence can be investigated statistically as velocity fluctuations at a point or through the study of coherent structures. Both mean and turbulent features must be considered in the analysis of shear stress distributions, ecological investigations, and hydrodynamic model development. The physical implication of mean velocity and turbulent fluctuations is the transfer of mass, momentum, and energy through the flow field.

The separation of flow descriptions into mean and turbulent features is formalized through the Reynolds decomposition (Reynolds 1974):

$$u_i' = u_i - \overline{u}_i \qquad \text{(Equation 2.1)}$$

where u_i', u_i, and $\overline{u}_i$ denote the fluctuating, instantaneous, and time averaged velocities in each coordinate direction, respectively. The fluctuating velocity components are evaluated through statistical techniques. The standard deviation of the velocity fluctuation is referred to as the turbulence intensity (TI) and is calculated as follows:

$$TI_i = \sqrt{\overline{u_i'^2}} \qquad \text{(Equation 2.2)}$$

where TI_i is the turbulence intensity in each coordinate direction. Higher order statistical moments can also be evaluated, including the skew and kurtosis.

Another common evaluation parameter for turbulent velocity fluctuations is the turbulent kinetic energy (TKE). TKE is analogous to mean kinetic energy and is calculated as:

$$TKE = \frac{\overline{u_i u_i}}{2} \qquad \text{(Equation 2.3)}$$

where $u_i u_i$ is the sum of the squared velocity fluctuations in each coordinate direction. TKE can be used to study the flow field energy budget and is an important parameter in turbulence modeling.

Statistical turbulence descriptions can be expanded with correlation functions. The covariance is the correlation between velocity fluctuations in two coordinate directions and is calculated as:

$$\overline{u_i' u_j'} = \frac{1}{t_a} \int_{t_o}^{t_o + t_a} u_i' u_j' dt \qquad \text{(Equation 2.4)}$$

where $\overline{u_i' u_j'}$ is the covariance and t_o and t_a are the initial and averaging times, respectively. The covariance can be multiplied by the fluid density to determine the Reynolds shear stress:

$$\tau_R = -\rho \overline{u_i' u_j'} \qquad \text{(Equation 2.5)}$$

where τ_R is the Reynolds shear stress and ρ is the fluid density. This term represents turbulent momentum transfer through the flow field. For shear flows, such as streams, the streamwise-vertical term ($\overline{u_S' u_V'}$) is dominant (Nezu and Nakagawa 1993 pg. 13).

More information about the turbulent features of the flow field can be gained through investigation of coherent structures. This is accomplished by calculating time and length scales. Time scales can be determined through investigation of auto-correlation

functions. Auto-correlation functions are derived by calculating the correlation of the time series with itself at an increasing level of lag interval as follows:

$$R(t) = \frac{1}{t_a \, TI_i^2} \int_{t_o}^{t_o + t_a} u_i'(x_p, t) u_i'(x_p, t + \Delta t) dt \qquad \text{(Equation 2.6)}$$

where R(t) is the auto-correlation function. The average persistence of turbulent activity at a point is the integral time scale and it is calculated by integrating the auto-correlation function as:

$$T = \int_0^{t_R} R(t)\, dt \qquad \text{(Equation 2.7)}$$

where T is the integral time scale and t_R is the correlation time. t_R is defined as the time at which the correlation function goes to zero.

Length scales can be used to measure the average spatial extent of the velocity fluctuations. Integral length scales can be calculated from integral time scales using Taylor's Frozen Turbulence Hypothesis as follows:

$$L = \overline{u}_S T \qquad \text{(Equation 2.8)}$$

where L is the integral length scale, and $\overline{u}_S$ is the mean streamwise velocity. Taylor's hypothesis has been confirmed valid in open channel flows for relative depths greater than 20% (Shteinman et al. 1996).

Predictive Equations

The distribution of mean and turbulent flow parameters in open-channels has been the topic of numerous investigations. Nearly all have been conducted in laboratory flumes and have resulted in a series of predictive empirical equations.

The ‘law of the wall’ or ‘log-law’, developed by Prandtl (1932) and von Karman (1930) for smooth-boundaries, was modified by Nikuradse (1933) and others (Rotta 1962) to the following log-law for rough boundaries:

$$\frac{\bar{u}}{u*} = \frac{1}{\kappa}\ln\left(\frac{z+\Delta z}{k_s}\right) + B \qquad \text{Equation 2.9}$$

where $\bar{u}$ is the local time-averaged velocity, u* is the friction velocity, κ is the von Karman constant, z is the distance from the bed, Δz is the displacement length, k_s is the roughness height and B is an integration constant. In this paper Z=z+Δz, where Z is the distance above the point were the velocity profile equals zero. Details of log-law application to measured data are found in Chapter 3 and Appendix A.

The friction velocity is directly related to the bed shear stress as:

$$u_* = \sqrt{\tau_0 / \rho} \qquad \text{Equation 2.10}$$

where τ_o is the bed shear stress and ρ is the fluid density. u_* is often the desired result of Equation 2.9 and is determined from measured velocity data using a regression technique. It also can be estimated at the reach scale, referred to as global in this document, from the bed shear stress as determined from the water surface slope as:

$$\tau_g = \gamma R_H S \qquad \text{Equation 2.11}$$

where γ is the fluid specific weight, R_H is the stream hydraulic radius, and S is the water surface slope. The shear stress can also be estimated from the Reynolds shear stress distribution, τ_R. The total shear stress is the result of viscous and Reynolds stresses, which can be represented for two-dimensional flow as:

$$\tau = \mu \bar{u}_{i,j} - \rho\overline{u_i' u_j'} \qquad \text{Equation 2.12}$$

For natural streams, τ_R dominates, and the viscous term can be neglected (Nezu and Nakagawa 1993). By integrating the Navier-Stokes equations for the water depth, h, a theoretical τ_R distribution can be derived for two-dimensional flow as:

$$\frac{-\overline{u_S' u_V'}}{u_*^2} = 1 - \frac{Z}{h} \qquad \text{Equation 2.13}$$

Researchers have also suggested universal functions for TI_i and TKE. Using the *k*-ε turbulence model, the turbulence intensity and turbulent kinetic energy distributions can be developed as follows:

$$TI_S = a\,u_* \exp\left(-C_k \, Z/h\right) \qquad \text{Equation 2.14a}$$

$$TI_T = b\,u_* \exp\left(-C_k \, Z/h\right) \qquad \text{Equation 2.14b}$$

$$TI_V = c\,u_* \exp\left(-C_k \, Z/h\right) \qquad \text{Equation 2.14c}$$

$$TKE = d\,u_*^2 \exp\left(-2C_k \, Z/h\right) \qquad \text{Equation 2.14d}$$

where TI_S, TI_T, and TI_V are the streamwise, transverse, and vertical turbulence intensities at an elevation above the origin of the velocity profile Z, at a station with a total depth of h. TKE is the turbulent kinetic energy and a, b, c, d, and C_k are empirical constants. C_k is approximately equal to unity in the log-law region. Nezu and Nakagawa (1993) suggested the following values for the empirical constants: a=2.30, b=1.27, c=1.63, and d=4.78.

Nezu and Nakagawa (1993) suggested the following two-part empirical equation for integral length scale profiles:

$$L/h = \beta (Z/h)^{1/2} \text{ for } Z/h < 0.6 \qquad \text{Equation 2.15a}$$

$$L/h = 0.77\beta \text{ for Z/h>0.6} \qquad \text{Equation 2.15b}$$

where L is the integral length scale and β is an empirical constant equal to approximately 1 for high Reynolds numbers.

Recent Research in Non-Laboratory Environments

The studies summarized above have been completed under carefully controlled experimental conditions, which meet the assumptions of the underlying models. However, assumptions such as two-dimensional, uniform flow are rarely met in investigations of natural stream flow. Recently, instrument advances have allowed researchers to observe turbulence features in natural rivers. Nikora and Smart (1997) completed turbulence characterizations of three New Zealand gravel-bed rivers with fast response electronic pitot tubes. Although only streamwise velocity components could be measured, the authors completed a thorough evaluation of velocity distributions and structure functions. Sukhodolov et al. (1998) completed a detailed investigation of turbulence structure around sand dunes in a straight low-land river with an ADV and a micropropeller system. The researchers found that empirical expressions for flow field properties were only valid for the central region of the channel. Further, they reported a clear difference in the empirical parameters for the observed data from those reported by Nezu and Nakagawa (1993). Rennie et al. (1999) conducted ADV measurements in a reach of the Salmon River in British Columbia, Canada. The measurements provided information about the spatial variability of turbulence parameters. However, measurements were only conducted at 20% of the flow depth, preventing a thorough investigation of the flow field distributions or comparison with empirical equations. Buffin-Belanger et al. (2000) used an array of electromagnetic current meters to confirm the existence of large-scale flow

structures in the Eaton North River, Quebec, Canada. They reported a complex organization of large-scale coherent structures with no preferred sequence of events. Smith (2003) conducted ADV measurements across a range of fish habitat types. He reported probable focal positions of salmonids in small streams could be distinguished using turbulence parameters but not average velocities. Tritico and Hotchkiss (in press) completed turbulence observations behind boulders in two cobble-bed rivers in northern Idaho, USA. The researchers found elevated TI and TKE and reduced integral time scales in the wake of the obstructions. The turbulence parameters did not appear to be a function of obstruction shape.

A thorough investigation of turbulence distributions at the reach scale has not been completed. Turbulence distributions in cobble-bed rivers have not been reported. Also, empirical relationships for turbulence distributions have only been tested in a straight low-land river. Further, a quantifiable evaluation of turbulence across stream units (riffle, pools, and reaches) has not been completed. This research addresses these shortcomings in previous turbulence observations.

Methods

Site Characterization

Measurements were conducted in a 75m reach of the St. Maries River near Clarkia, Idaho and a 65m reach of the Potlatch River near Kendrick, Idaho (Figure 2.1). Stream geometry data were collected with a total station using standard surveying

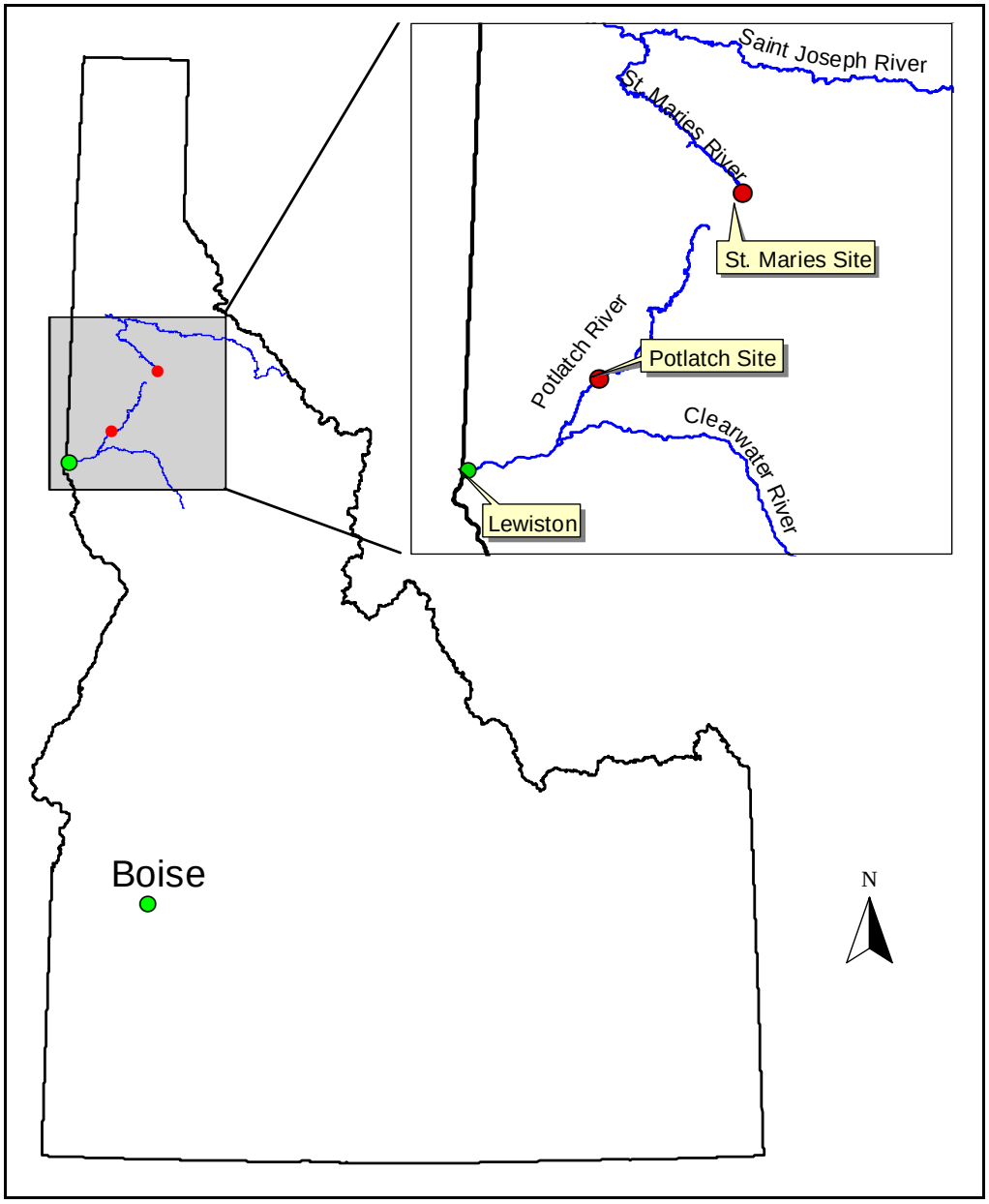

Figure 2.1. Location map for Potlatch and St. Maries sampling reaches

techniques (including stream banks, water surface and bed slopes, and cross-section geometries). Survey data were used to calculate mean depth (H), hydraulic radius (R_H), top width (T_w), Reynolds number (Re), Froude number (Fr), and global shear stress (τ_g).

The sediment particle size distributions (psd) were described using a Wolman pebble count (Wolman 1954). Approximately 100 samples were collected within each cross section. Median particle diameters were 10.5 and 10.8 cm for the St. Maries and Potlatch rivers, respectively. Both reaches were classified as cobble bed (Bunte and Abt 2001). The critical shear stress values, τ_c, were estimated for the d_{50} using the Shields parameter. Global shear stress estimates were far below critical values.

Data were collected at four cross sections in the St. Maries River (Figure 2.2) and three cross sections in the Potlatch River (Figure 2.3). St. Maries cross sections 1, 2, 3 and 4 were classified as run, run, riffle, and pool, respectively. The Potlatch cross sections 1, 2, and 3 were classified as riffle, run, and pool, respectively. These subjective classifications were based on observed flow velocities and depths. Table 2.2 contains geometric and hydraulic data for sampled cross-sections.

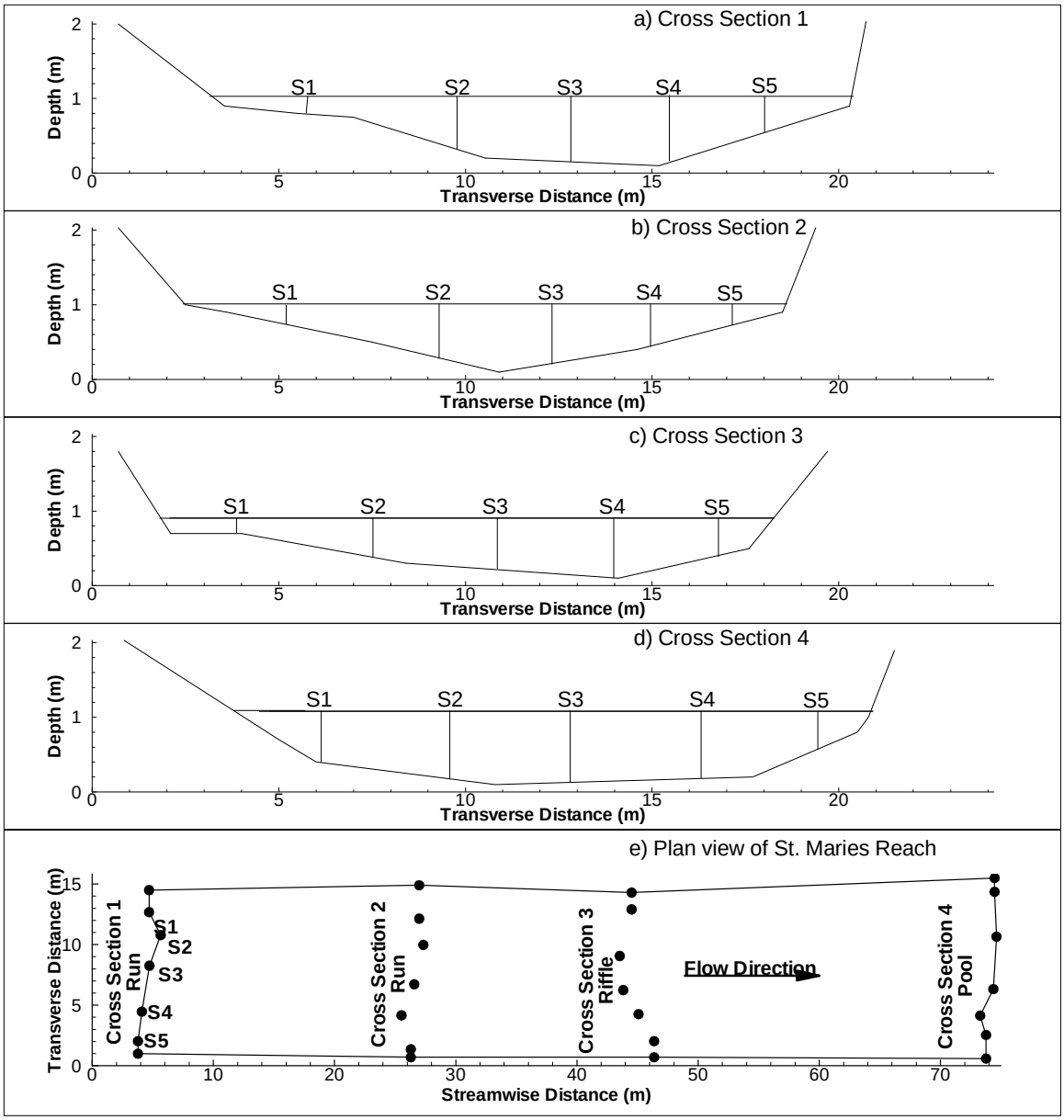

Figure 2.2. Cross section and plan geometry of the St. Maries sampling reach

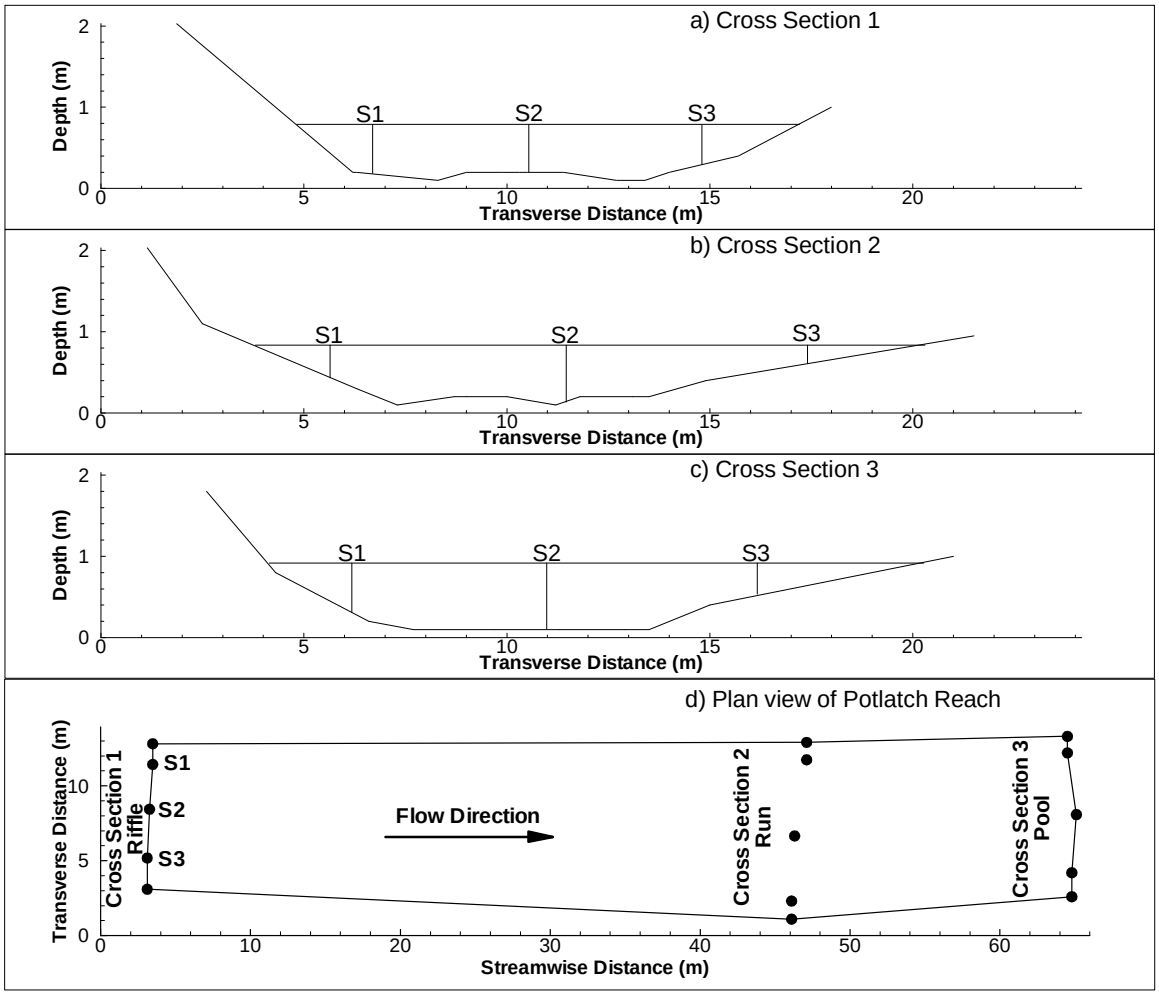

Figure 2.3. Cross section and plan geometry of the Potlatch sampling reach

Table 2.2. Hydraulic and geometry characteristics of the sampled cross-sections

	St. Maries Reach				Potlatch Reach		
Cross-Section	1	2	3	4	1	2	3
Discharge, Q (m^3/s)	3.1	3.1	3.1	3.1	1.5	1.5	1.5
Mean Velocity, U (cm/s)	32.1	42.8	71.9	20.8	41.7	32.6	17.8
Mean Depth, H (m)	0.49	0.41	0.39	0.70	0.35	0.40	0.73
Hydr. Rad. R_H (m)	0.44	0.38	0.36	0.67	0.32	0.36	0.68
Top Width, T_W (m)	15.6	16.4	15.6	16.9	10.9	11.3	11.1
Aspect Ratio, T_W/H	31.6	39.6	40.0	24.0	31.5	28.0	15.2
Froude Number, Fr	0.15	0.22	0.38	0.08	0.24	0.17	0.07
Reynolds Num., Re	1.41E+05	1.63E+05	2.59E+05	1.39E+05	1.33E+05	1.17E+05	1.21E+05
Bed Slope, S_b	0.0018	0.0018	0.0018	0.0018	0.00038	0.00038	0.00038
Water Slope, S	0.0012	0.0012	0.0012	0.0012	0.00024	0.00024	0.00024
Global Friction Velocity, u_{*g} (m/s)	0.074	0.074	0.074	0.074	0.033	0.033	0.033
Global Shear Stress, τ_g (N/m^2)	5.4	5.4	5.4	5.4	1.1	1.1	1.1
d_{50} (cm)	10.9	10.6	11.8	8.5	11.4	11.0	9.9
Relative Roughness, d_{50}/H	0.22	0.26	0.30	0.12	0.33	0.27	0.14
Critical Shear, τ_c (N/m^2)	88	86	95	69	92	89	80

Flow Measurements

The flow field was measured with a Sontek Field ADV. Details of ADV operating principles and performance can be found in Voulgaris and Trowbridge (1998). The ADV was mounted on a custom built sampling stand that was 1 meter wide and 0.5 meters long and fitted with four adjustable legs and an adjustable sampling arm (Figure 2.4). The sampling arm extended a maximum of 0.5 meters from the stand's front to avoid flow field interference, while cross-bracing prevented flow induced stand vibrations. The ADV processing canister and laptop computer were set on top of the stand. The ADV position was measured with a combination of vernier scales.

Figure 2.4. ADV, sampling stand, and laptop computer in the Potlatch River

Samples were collected at three to five stations within each cross section. A vertical profile was measured at each station at heights above the streambed of 1cm, 2cm, and 5cm along with 20%, 40%, 60% and 80% of the flow depth. The distance between the sampling volume and the bed were determined using the ADV as a sounder for the first three measurements. The vernier scales were used to position the instrument for the top four measurements. Data were collected for 2-minutes at each location at a sampling frequency of 25-Hz. The suitability of the 2-minute sample duration was validated by collecting 8-minute samples at several stations and observing the convergence of

statistical properties. At all tested locations, convergence occurred at 40 seconds or less. This was consistent with physical expectations of coherent structure size.

The streamwise coordinate system was used in the data analysis. The data was rotated in post-processing to ensure that the mean transverse and vertical velocity components were zero for each profile (Wilczak et al. 2001). This resulted in unique streamwise, transverse, and vertical coordinate systems at each station. The data were rotated back to a standard Cartesian coordinate system for plotting.

The data were filtered at a minimum signal to noise ratio of 15 and a minimum correlation value of 70 using WinADV (Wahl 2000). This eliminated about 7% of the data. The data was exported and processed using a custom developed FORTRAN code (Appendix F). The FORTRAN program rotated the data and computed the flow field parameters including mean velocities, TI, TKE, correlations, time scales, and length scales.

Results

The flow field observations were investigated as vertical profiles and as spatial distributions. The vertical profiles were used to test existing empirical equations. The spatial distributions improved understanding of heterogeneous natural stream flows.

Velocity Profiles

Streamwise (u_s), transverse (u_t), and vertical (u_v) velocity profiles for all stations are shown in Figure 2.5. u_s was generally the highest in riffles and lowest in pools with an expected increase in magnitude with distance from the bed, Z. By definition, mean u_t and u_v values were set equal to zero for each vertical profile. The magnitude of u_t tended to be slightly larger than u_v. The magnitudes of u_t and u_v were highest in riffle units.

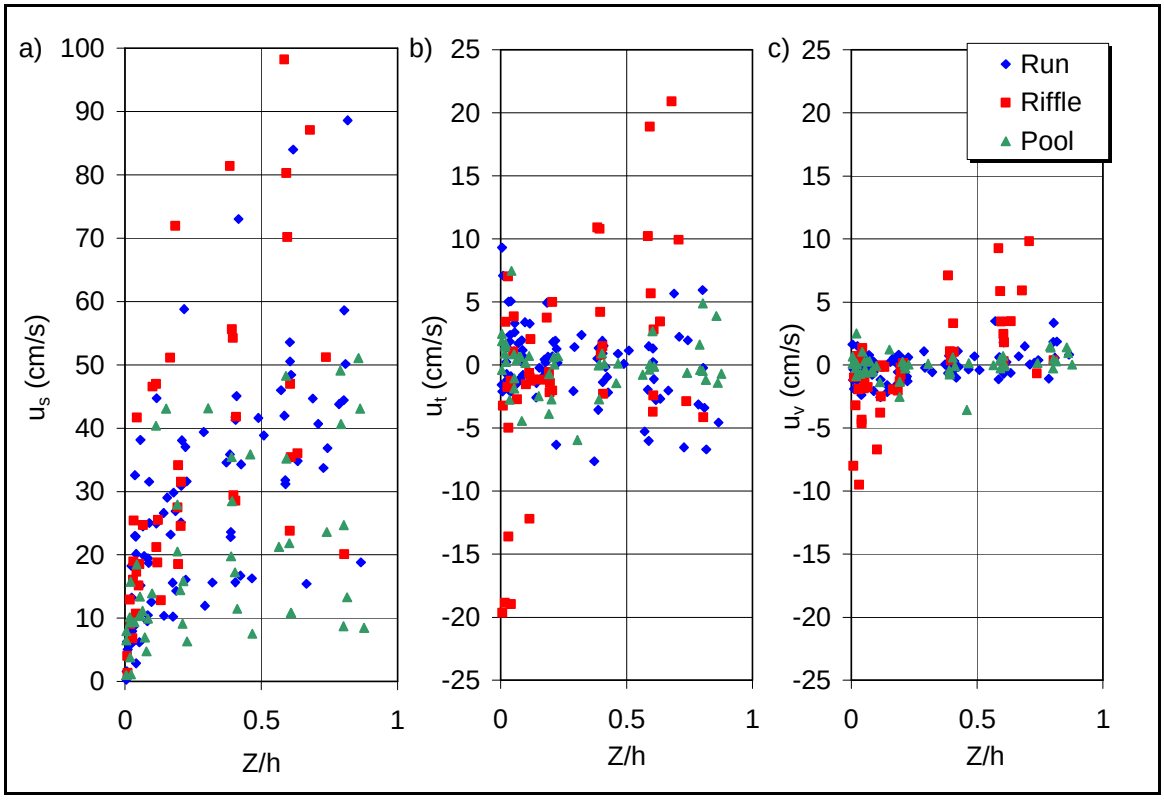

Figure 2.5. a) Streamwise, b) transverse, and c) vertical velocity profiles

The streamwise velocity components were non-dimensionalized with the friction velocity, u*, for comparison with the log-law. To evaluate log-law performance, the velocity profiles were categorized by stream unit (run, riffle, and pool) and by transverse location (edge, transition, and center). The stream unit velocity profiles are displayed in Figure 2.6. Best-fit regression lines were found using the least-squares technique for each stream unit. The pool and run regression equations showed nearly perfect agreement with the log-law. The log-law did not perform as well in riffle units.

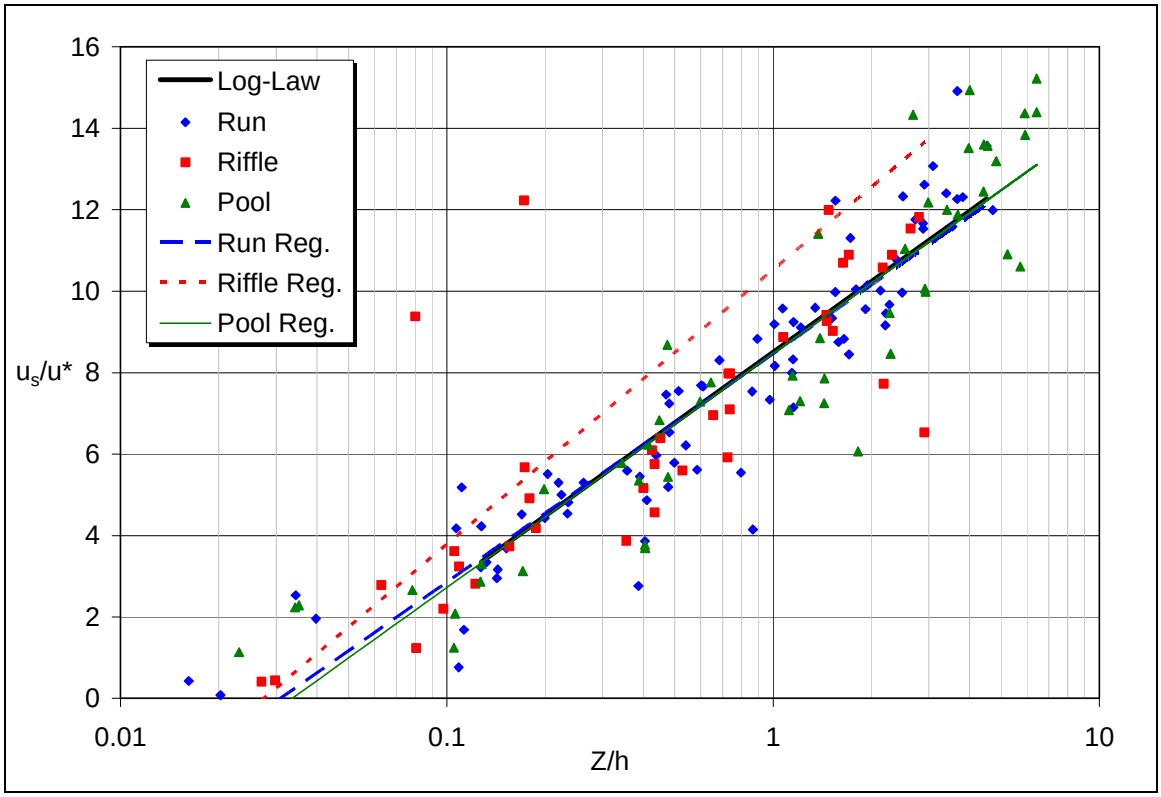

Figure 2.6. Velocity profiles and regression lines by stream transverse location

The adequacy of the log-law was tested using a Chow Test. Results of the Chow test showed no significant difference between the log-law and measured data for the run ($F(2,348)=0.0024$, non. sig.), riffle ($F(2,348)=1.20$, non. sig.), pool ($F(2,348)=0.029$, non. sig.), or combined ($F(2,348)=0.69$, non. sig.) datasets.

The velocity profiles categorized by transverse location are shown in Figure 2.7. The velocity profiles collected at the centerline and near the banks showed a strong agreement with the log-law. The log-law tended to underestimate the velocity in the transitional profiles. This was likely due to elevated velocities in this region, caused by secondary currents, as discussed later (Transverse Velocity Distributions). Chow test results showed no significant differences between log-law and measured data for the center ($F(2,94)=0.020$, non. sig.), transition ($F(2,104)=0.76$, non. sig.) and edge ($F(2,142)=0.083$, non. sig.) regions.

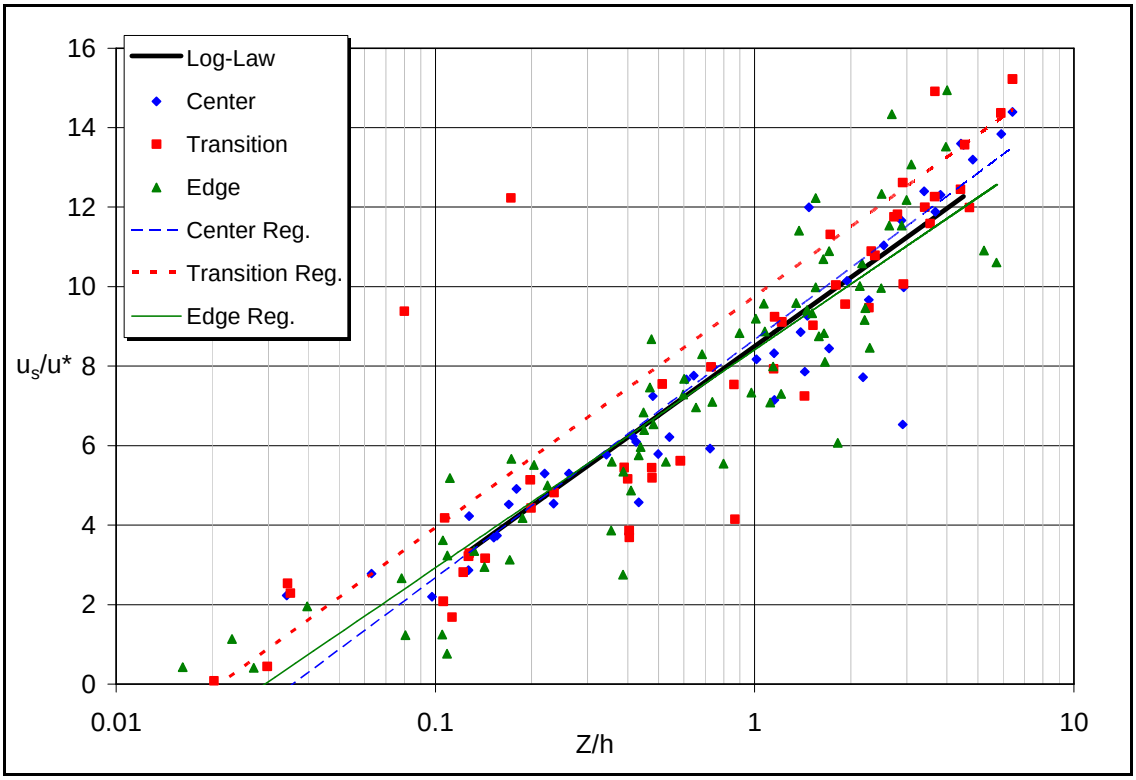

Figure 2.7. Velocity profiles and regression lines by stream transverse location

Turbulence Intensity Profiles

Streamwise (TI_s), transverse (TI_t) and vertical (TI_v) turbulence intensity profiles are shown in Figure 2.8. As expected, TI components were generally highest in riffles and lowest in pools. Additionally, TI_s was generally higher than TI_t and TI_v. However, TI_t

vales were slightly higher than TI_v values, which contradicts previous experiments. The elevated TI_t levels were likely caused by secondary currents.

The TI data were non-dimensionalized with the friction velocity and plotted in Figure 2.9, along with corresponding empirical equations (Equations 2.14a-d). Although the empirical equations were of the same magnitude as the measured data, no predictive ability was observed. The inadequacy of the empirical equations was verified with a series of Chow tests. The tests showed a significant differences between measured and predicted values for TI_s ($F(2,348)=49.41$, $p<0.05$), TI_t ($F(2,348)=134.40$, $p<0.05$), and TI_v ($F(2,348)=13.10$, $p<0.05$). Attempts to develop best-fit regression equations were unsuccessful due to extremely high sample variances. Additionally, an exploratory analysis (correlation and regression) failed to identify a trend between TI observations and hydraulic or geometric data.

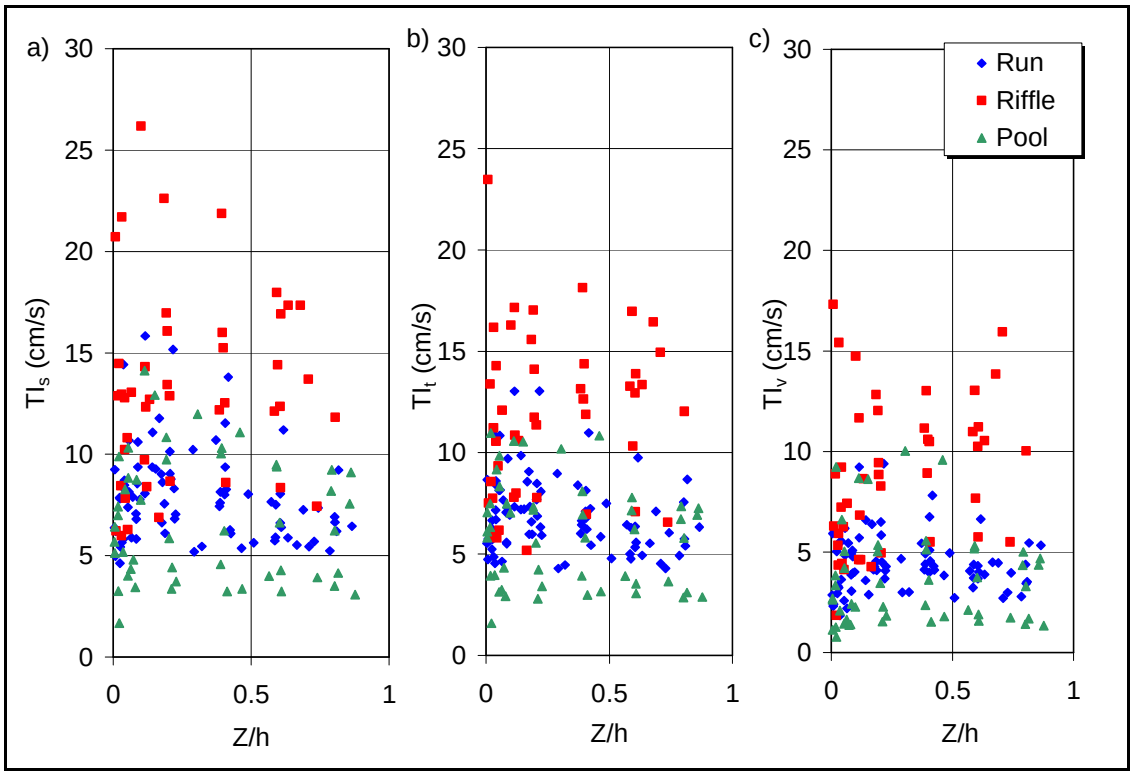

Figure 2.8. Streamwise, transverse, and vertical turbulence intensity profiles

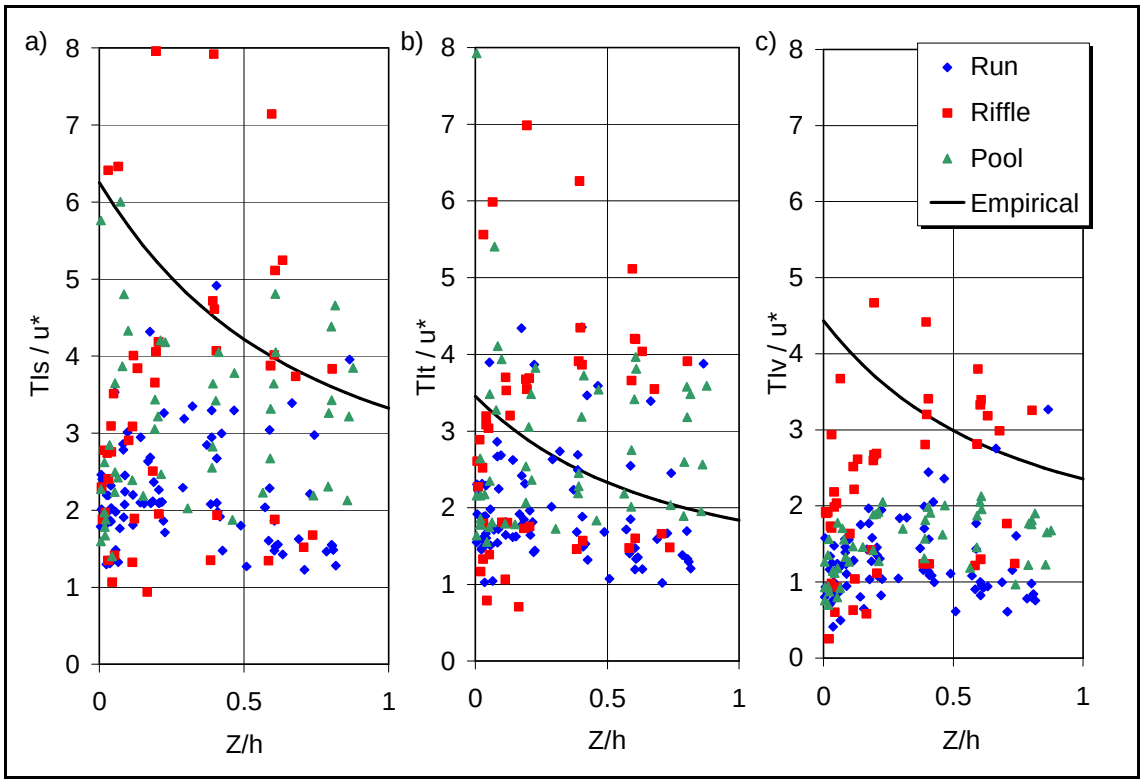

Figure 2.9. Dimensionless a) streamwise, b) transverse, and c) vertical turbulence intensities and empirical equations

Turbulent Kinetic Energy Profiles

Dimensional and dimensionless TKE profiles are displayed in Figure 2.10. As expected, TKE levels were generally lowest in pools and highest in riffles with values ranging from 0 to 650 cm^2/sec^2. Figure 2.10b contains the predicted values from the empirical TKE equation (Equation 2.14d). The predicted values were far below measured values except near the bed. The expected exponential decline in TKE with depth was not observed. The Chow test verified the inadequacy of the TKE equation by finding a significant difference between measured and predicted values ($F(2,348)=101.9, p<0.05$). As with TI, high sample variance prevented the reasonable application of a regression equation.

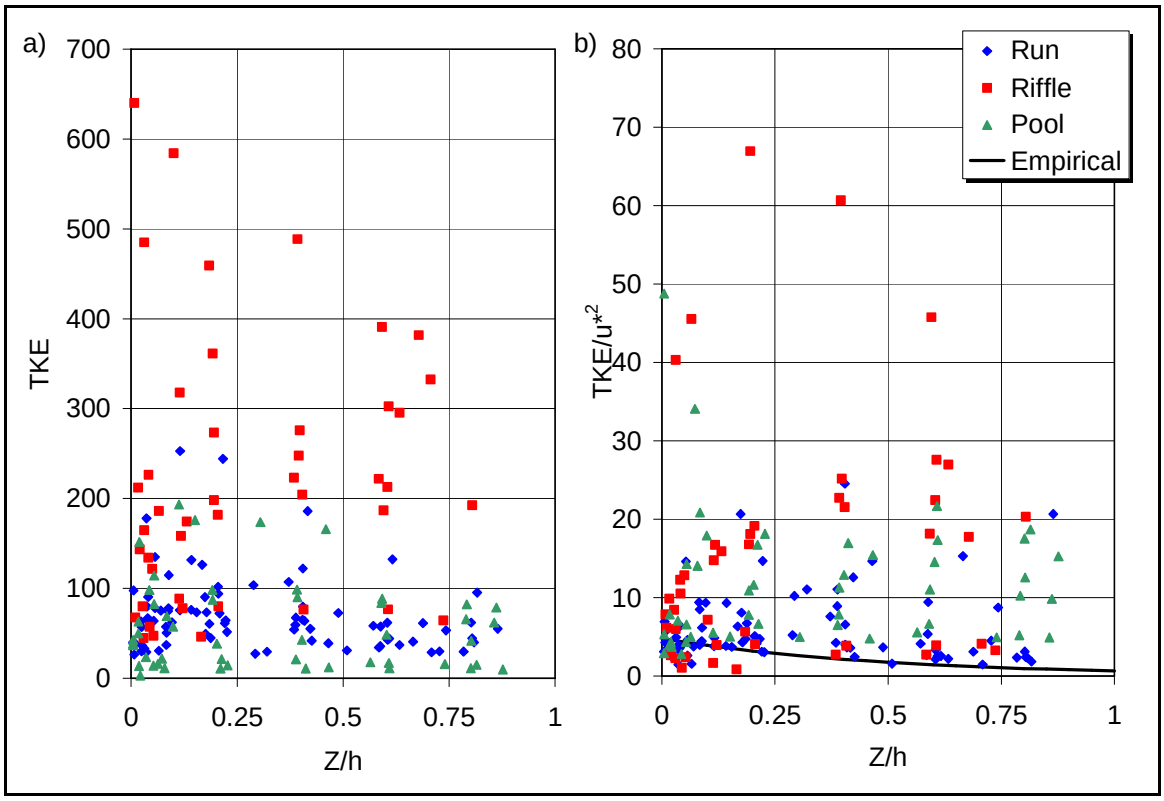

Figure 2.10. a) TKE and b) dimensionless TKE profiles

Reynolds Shear Stress

Dimensional and dimensionless Reynolds shear stress (τ_R) profiles are shown in Figure 2.11. The τ_R values were similar between stream units, with slightly higher values observed in riffles. Most τ_R values were greater than zero, demonstrating the expected momentum flux toward the streambed. The predicted dimensionless τ_R distribution and best-fit regression line are shown in Figure 2.11b. Although the empirical equation reasonably predicted the magnitude of τ_R values, the observed data showed a weaker reduction in τ_R with distance from the streambed. Further, the measured data had a high level of variance, with an R^2 value of 0.05 for the best-fit line. However, the Chow test did not find a significant difference between measured and predicted values

(F(2,348)=2.49, non. sig.). This result was marginal, indicating the equation should be used with caution. The best-fit regression equation for the observed data was as follows:

$$\frac{-\overline{u_S' u_V'}}{u_*^2} = 1.1 - 0.41\frac{Z}{h} \qquad \text{Equation 2.16}$$

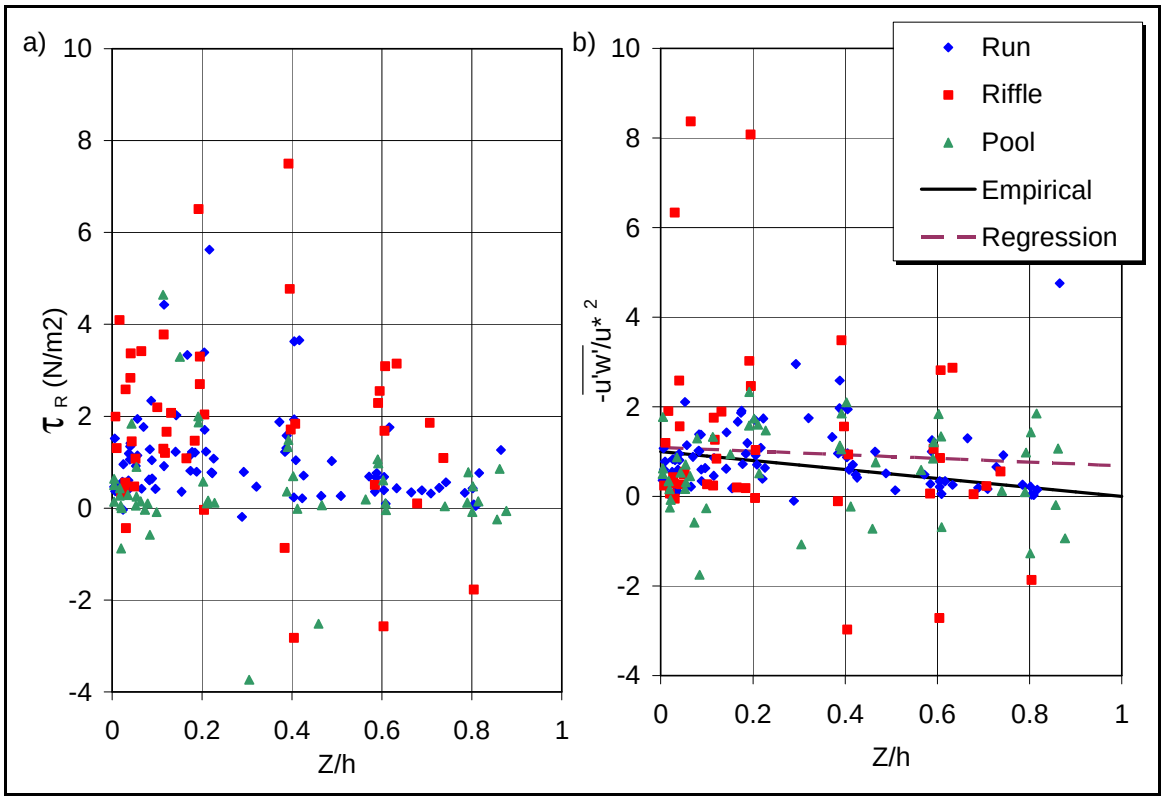

Figure 2.11. a) Reynolds shear stress and b) dimensionless shear stress profiles

Integral Scales

Integral time and length scales are shown in Figures 2.12 and 2.13, respectively. As expected, integral scales were largest in the pool and lowest in the riffles. The distinction between stream units is less obvious for length scales due to the influence of velocity in the calculations with Taylor's frozen turbulence hypothesis. Length scale values less than 0.2h were shaded because the application of Taylor's hypothesis in this region is questionable (Shteinman et al. 1996).

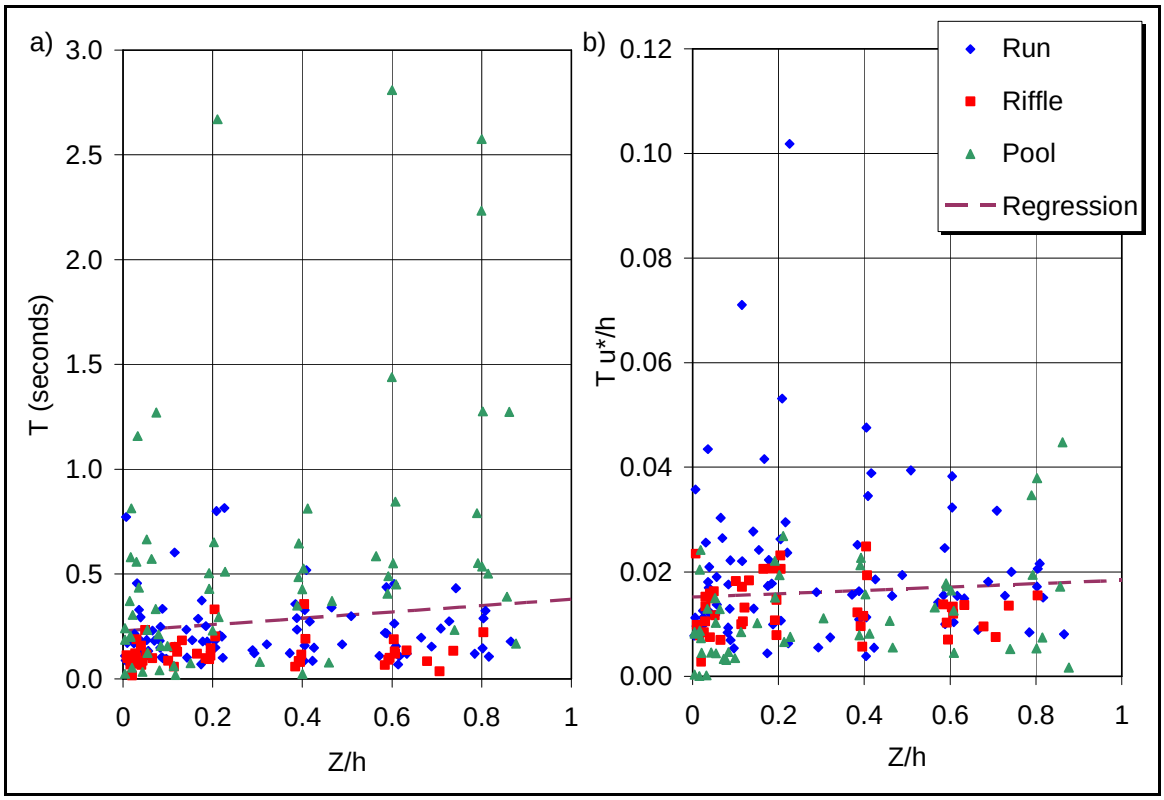

Figure 2.12. a) Integral time scales and b) dimensionless integral time scales

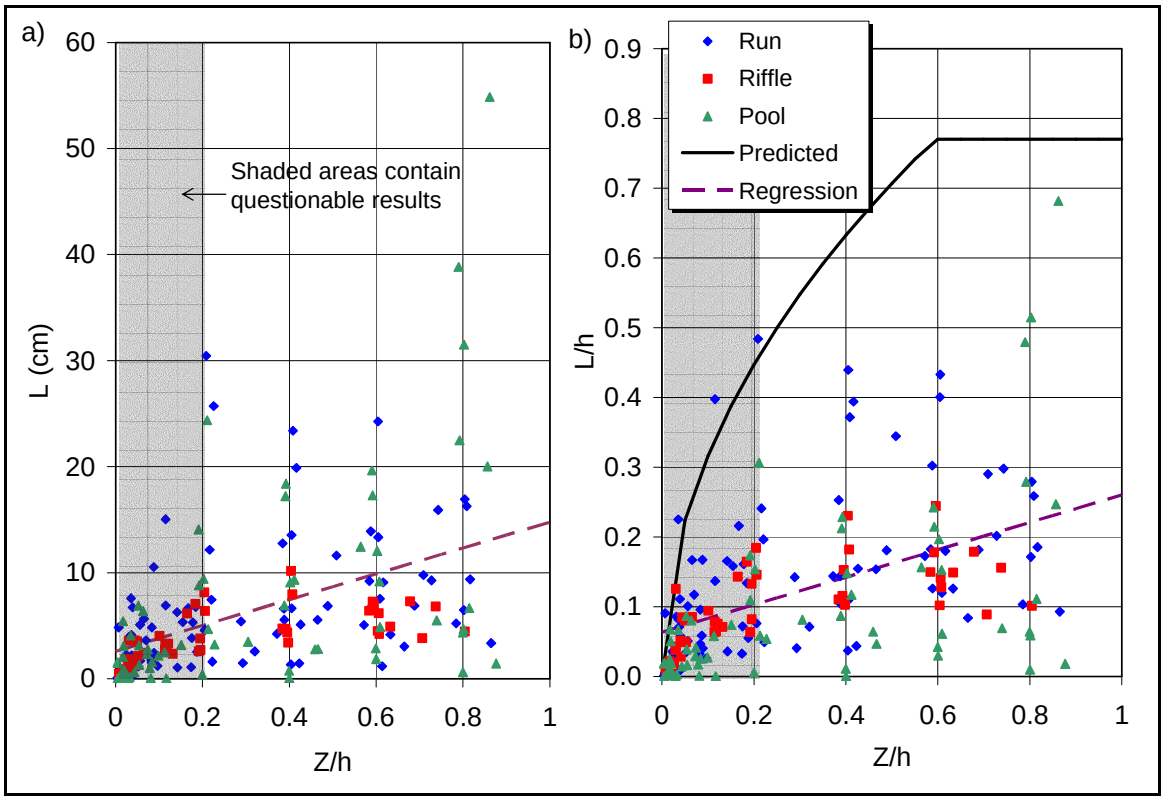

Figure 2.13. a) Integral length scales and b) dimensionless integral length scales

No accepted empirical equations exist for integral time scale distributions. A regression line was fitted to the dimensional and dimensionless data, shown in Figure 2.12. The regression equation for the dimensional data revealed a slight increase in time scale with depth with an R^2 value of only 0.020. The regression equation for the dimensionless data also showed an increase in time scale with depth, but the R^2 value was even lower at 0.005. The resulting regression equations were as follows:

$$T = 0.15\frac{Z}{h} + 0.228 \qquad \text{Equation 2.17a}$$

$$\frac{T\,u_*}{h} = 0.0032\frac{Z}{h} + 0.0151 \qquad \text{Equation 2.17b}$$

The integral length scale empirical equation (Equation 2.15) is shown with the measured data in Figure 2.13b. Equation 2.15 greatly over-predicted observed values. Linear regression equations were fitted to the observed L and L/h data using a least-squares method. The resulting equations were as follows with an R^2 value of 0.20 for both equations:

$$L = 12.18\frac{Z}{h} + 2.57 \qquad \text{Equation 2.18a}$$

$$\frac{L}{h} = 0.20\frac{Z}{h} + 0.063 \qquad \text{Equation 2.18b}$$

When categorized by stream unit, the R^2 value of the dimensionless regression equations were improved to 0.40 and 0.29 for the riffle and pool and reduced to 0.13 for the run. Regression equations for the riffle, run and pool are given below.

$$\frac{L_{Riffle}}{h} = 0.15\frac{Z}{h} + 0.061 \qquad \text{Equation 2.18c}$$

$$\frac{L_{Run}}{h} = 0.19\frac{Z}{h} + 0.097 \qquad \text{Equation 2.18c}$$

$$\frac{L_{pool}}{h} = 0.24\frac{Z}{h} + 0.022 \qquad \text{Equation 2.18e}$$

Streamwise Velocity Distributions

Streamwise velocity distributions and velocity vectors for the St. Maries reach are shown in Figure 2.14. The Figure contains hypothetical, horizontal slices cut through the reaches at 1cm, 2cm, and 5cm above the streambed and at 20, 40, 60, and 80% of the flow depth. As expected, the velocity increased towards the surface in both reaches. Velocity was generally highest in riffles and lowest in pools. Steep velocity gradients were observed near the banks and near the riffle. The peak velocities in the St. Maries reach were observed near the center of the riffle. ANOVA statistics were conducted in order to investigate the effects of stream unit (riffle, pools, and runs) and relative depth on the flow parameters. The results showed that there was a significant difference between stream units for both the St. Maries ($F(2,119)=30.68$, $p<0.001$) and Potlatch reach ($F(2,42)=19.64$, $p<0.001$). Further, a significant difference was observed between velocity distributions by depth for both the St. Maries ($F(2,119)=14.63$, $p<0.001$) and Potlatch ($F(2,42)=5.50$, $p<0.001$) reaches. Streamwise velocity distributions for the Potlatch reach are shown in Appendix C (Figure C.15).

Transverse and Vertical Velocity Distributions

The transverse velocity distributions for the St. Maries reach are shown in Figure 2.15. u_t distributions reveal the occurrence of secondary currents. The secondary currents are observed by a shift between positive and negative u_t values with depth. A strong secondary cell was observed along the left bank of the St. Maries reach where transverse velocities varied from less than -10 cm/s at the bottom to above 10 cm/s at the surface. The Potlatch reach displayed similar trends with velocities ranging from -5 cm/s at the bottom to above 5 cm/s at the surface (Figure C.16). Transverse velocities

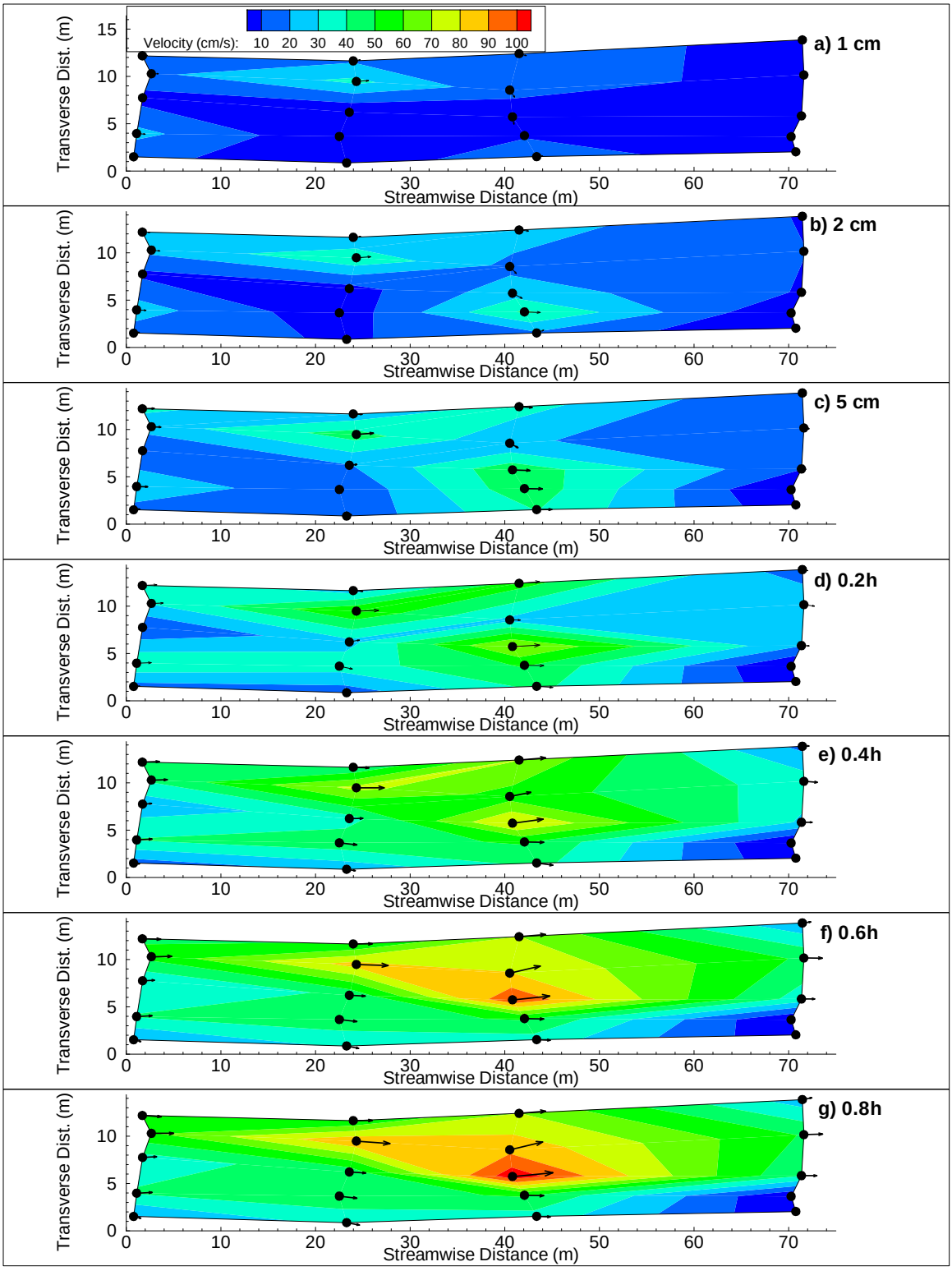

Figure 2.14. St. Maries reach streamwise velocity distributions and velocity vectors

were not significantly different between stream units for the St. Maries ($F(2,119)=0.21$, 0.812) or Potlatch ($F(2,42)=0.14$, $p=0.99$) reaches.

Vertical velocity distributions are shown in Appendix C (Figures C.17 and C.18). Magnitudes were relatively small, generally less than 2 cm/s. Spatial trends further demonstrated the existence of secondary currents. Vertical velocities were not significantly different between stream units for the St. Maries ($F(2,119)=0.321$, $p=0.73$) or Potlatch ($F2,42)=0.023$, $p=0.977$) reaches.

Turbulence Intensity Distributions

Dimensionless streamwise turbulence intensities (TI_s/u^*) for the St. Maries reach are shown in Figure 2.16. TI_s was highest in riffles and lowest in pools. ANOVA results revealed a significant difference in TI_s between stream units for both the St. Maries ($F(2,119)=56.67$, $p<0.001$) and Potlatch ($F2,42)=54.99$, $p<0.001$) reaches. TI_s was not significantly different between depths for the St. Maries ($F(2,119)=1.84$, $p=0.10$) or Potlatch ($F2,42)=0.75$, $p=0.62$) reaches. Streamwise turbulence intensity distributions for the Potlatch reach (Figure C.19) and transverse turbulence intensity distributions (Figures C.20 and C.21) for both reaches are shown in Appendix C. A significant difference in TI_t was observed between stream units for the St. Maries ($F(2,119)=52.81$, $p<0.001$) and Potlatch reaches ($F(2,42)=56.54$, $p<0.001$). A significant difference was also observed in TI_v between stream units for the St. Maries ($F(2,119)=39.17$, $p>0.001$) and Potlatch reaches ($F(2,42)=86.75$, $p>0.001$). There was not a significant difference in TI_t or TI_v between depths in either reach.

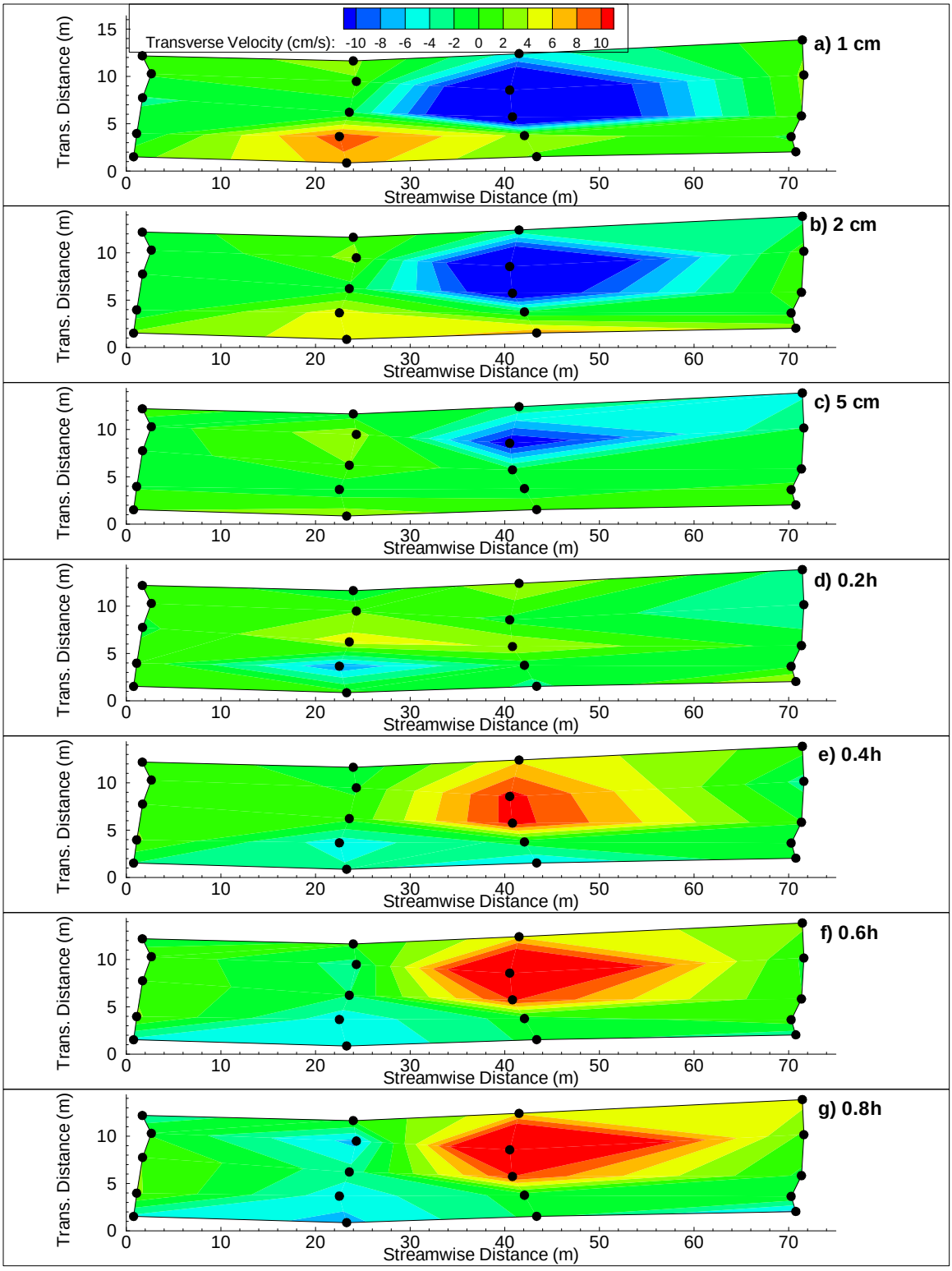

Figure 2.15. St. Maries reach transverse velocity distributions

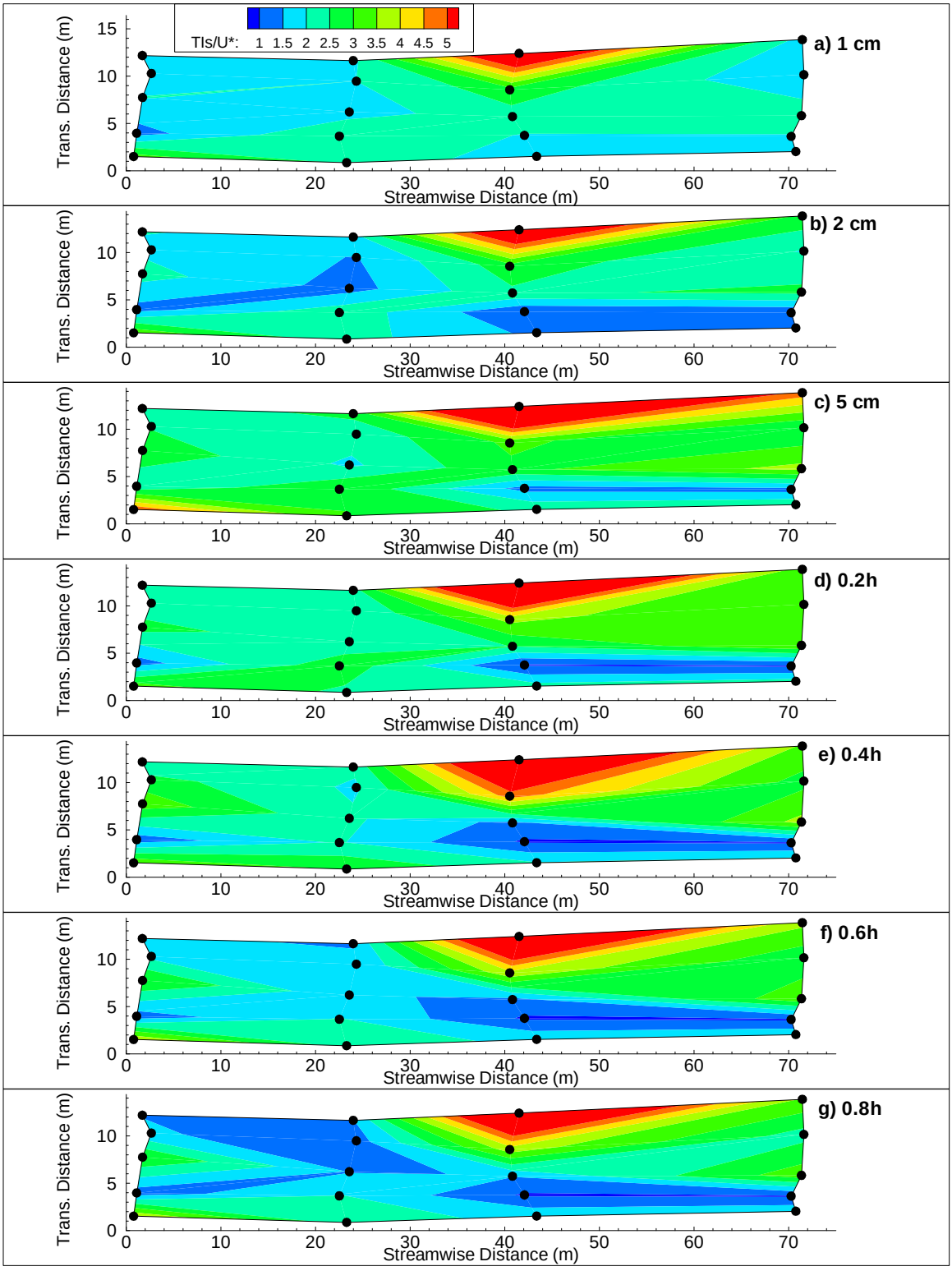

Figure 2.16. St. Maries reach streamwise turbulence intensity distributions

Turbulent Kinetic Energy Distributions

Dimensionless TKE distributions (TKE/u^{*2}) for the St. Maries reach are shown in Figure 2.17 and for the Potlatch reach in Figure C.22. Similar TKE magnitudes were observed between the sample reaches. TKE was highest in riffles and lowest in pools. Elevated TKE values were associated with high velocity gradients. Horizontal TKE heterogeneity appeared to be much stronger than vertical variability. A significant difference in TKE was observed between stream units for both the St. Maries ($F(2,119)=57.44$, $p<0.001$) and Potlatch ($F2,42)=38.38$, $p<0.001$) reaches. However, no significant difference in TKE was observed between depths for the St. Maries ($F(2,119)=0.84$, $p=0.544$) or Potlatch ($F2,42)=0.75$, $p=0.613$) reaches.

Shear Stress Distributions

Shear stress distributions for the St. Maries reach are shown in Figures 2.18. Figure 2.18a contains bed shear stress values calculated from the friction velocity determined with the log-law. Figure 2.18b through g contains Reynolds shear stress values calculated from the turbulence correlations using Equation 2.12. The shear stress was highest in riffles and lowest in the pools. A significant difference in τ_R was observed between stream units for both the St. Maries ($F(2,119)=16.52$, $p<0.001$) and Potlatch ($F2,42)=3.94$, $p<0.05$) reaches. The spatial variability of τ_R demonstrates the inadequacy of reach scale estimates. This is especially true for processes that are sensitive to shear stress, such as sediment transport and benthic habitat disturbance. A significant difference in τ_R was observed between depths for the St. Maries reach ($F(2,119)=2.42$, $p<0.05$) but not for the Potlatch reach ($F(2,42)=0.47$, $p=0.83$). Shear stress distributions for the Potlatch river can be found in Figure C.23.

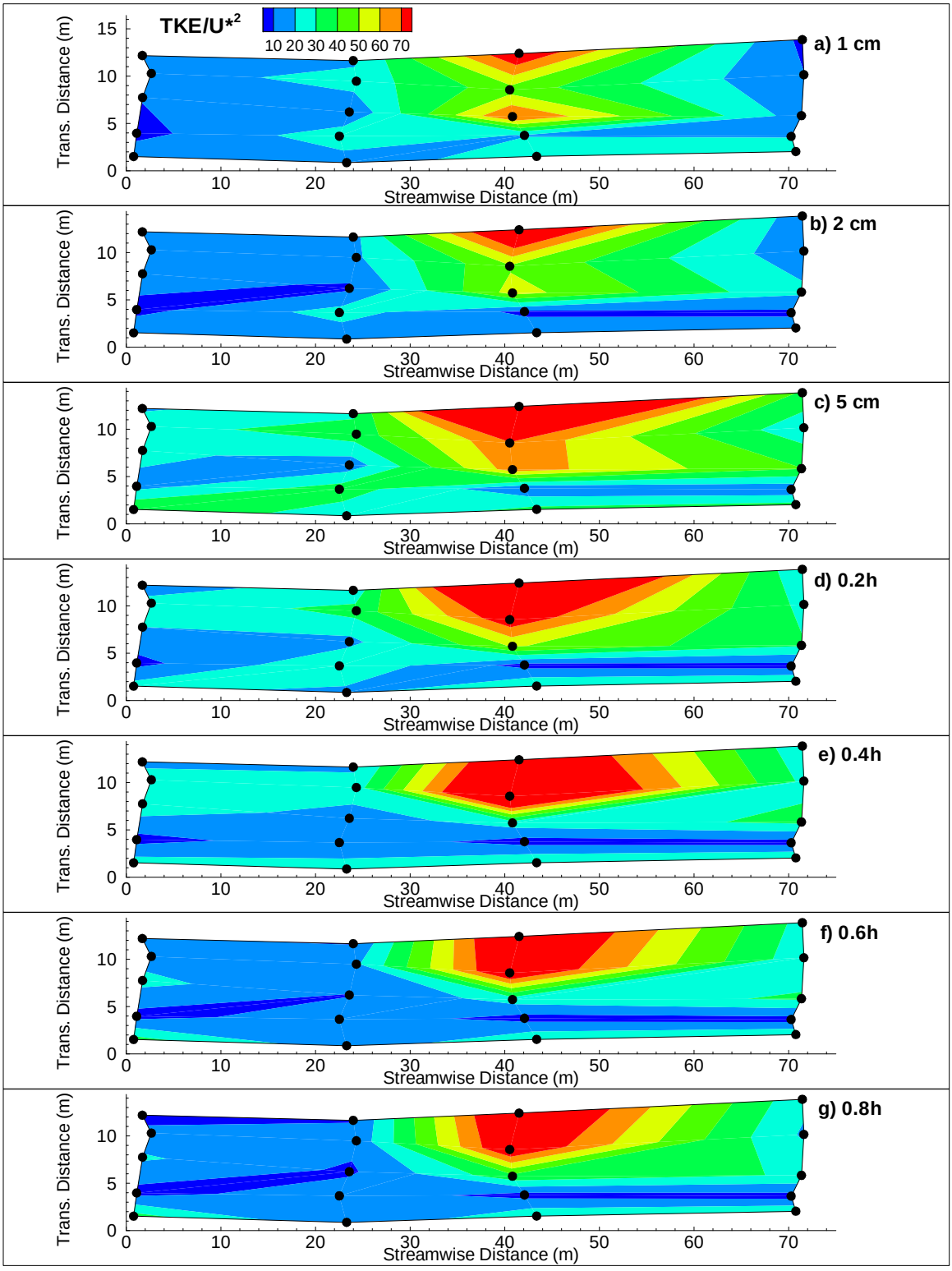

Figure 2.17. St. Maries reach TKE distributions

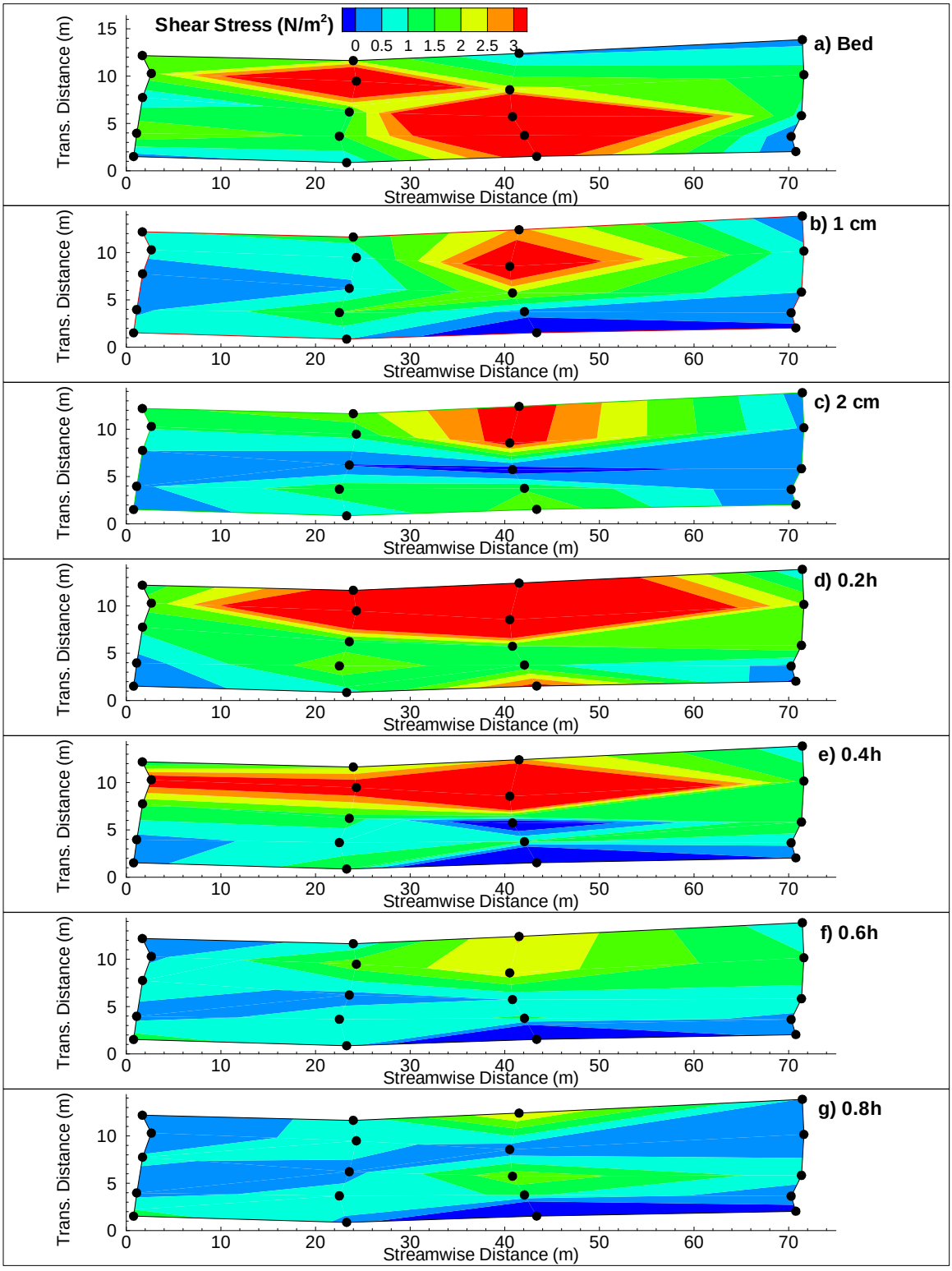

Figure 2.18. St. Maries reach shear stress distributions

Integral Time Scale Distributions

Distributions of integral time scales for the St. Maries reach are shown in Figure 2.19. Although most values were between 0 and 1 second, values as high as 2.7 seconds were observed (Figure 2.11). A clear distinction between run, riffles, and pool units was observed. A significant difference in T was found between stream units for both the St. Maries ($F(2,119)=20.06$, $p<0.001$) and Potlatch ($F(2,42)=0.82$, $p<0.005$) reaches. Although the value of T changed with depth, no obvious trends were observed. The differences in T with depth was significant for the St. Maries reach ($F(2,119)=2.29$, $p<0.005$) but not for the Potlatch reach ($F(2,42)=0.82$, $p=0.558$). Integral time scale distributions for the Potlatch reach are shown in Figure C.24.

Length Scale Distributions

Distributions of integral length scales for the St. Maries reach are shown in Figure 2.20. Most of the values ranged from 0 to 22cm, but length scales as large as 55cm were observed (Figure 2.12). Due to the influence of velocity on the calculations, a stronger trend with depth was observed, but the distinction between stream units was reduced. A significant difference in L was observed between stream units for the St. Maries reach ($F(2,119)=3.24$, $p<0.05$) but not for the Potlatch reach ($F(2,42)=0.46$, $p=0.64$). The distributions revealed the existence of large scale eddies in both pools and runs. The difference in L between depths was significant for the St. Maries reach ($F(2,119)=5.68$, $p<0.001$) but not for the Potlatch reach ($F(2,42)=0.51$, $p=0.80$). Although results are shown for all measured depths, the values for depths less than 0.2h are questionable because Taylor's hypothesis has not been verified in this region (Shteinman et al. 1996). Potlatch reach integral length scale distributions are shown in Figure C.25.

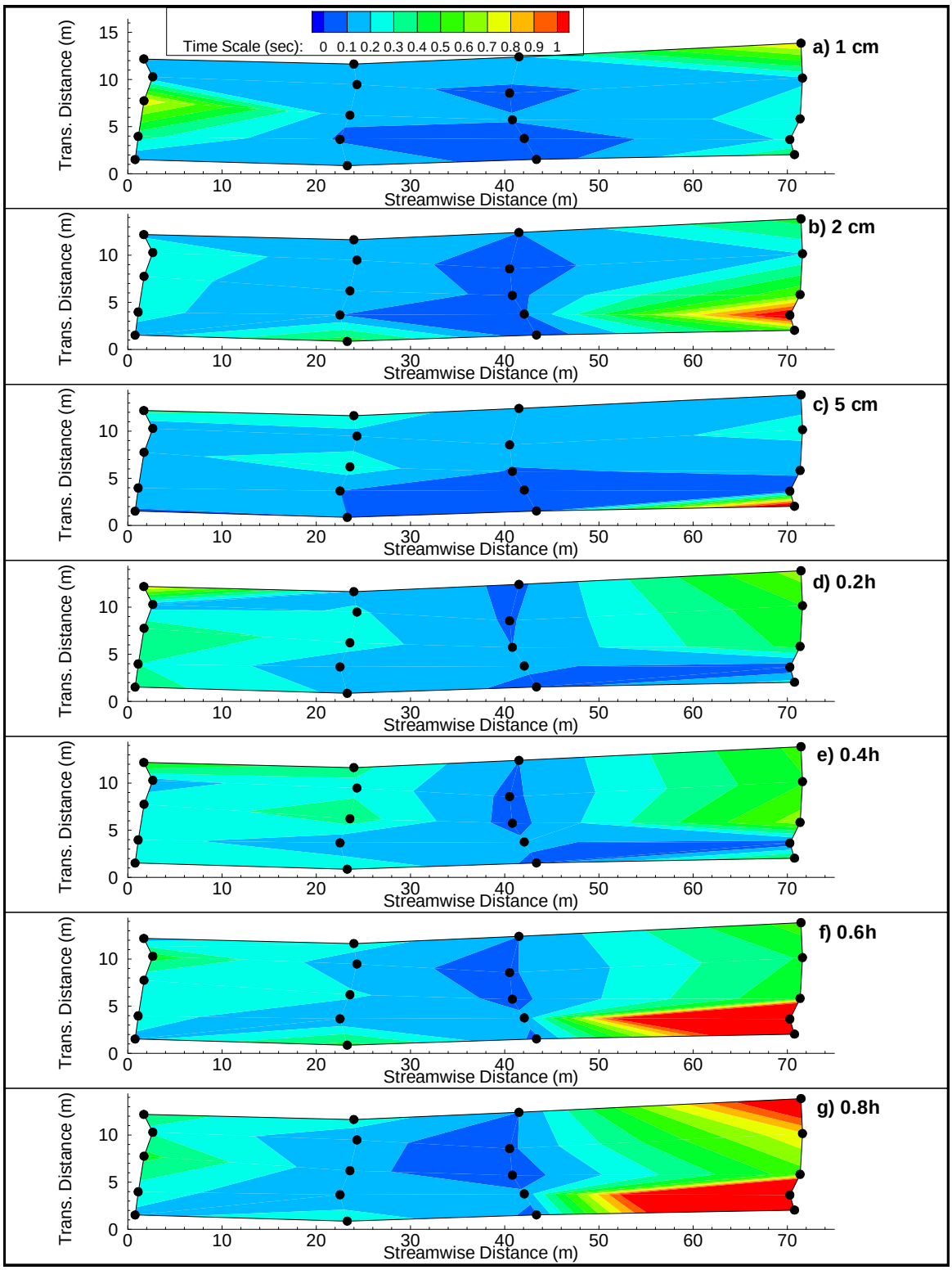

Figure 2.19. St. Maries reach integral time scale distributions

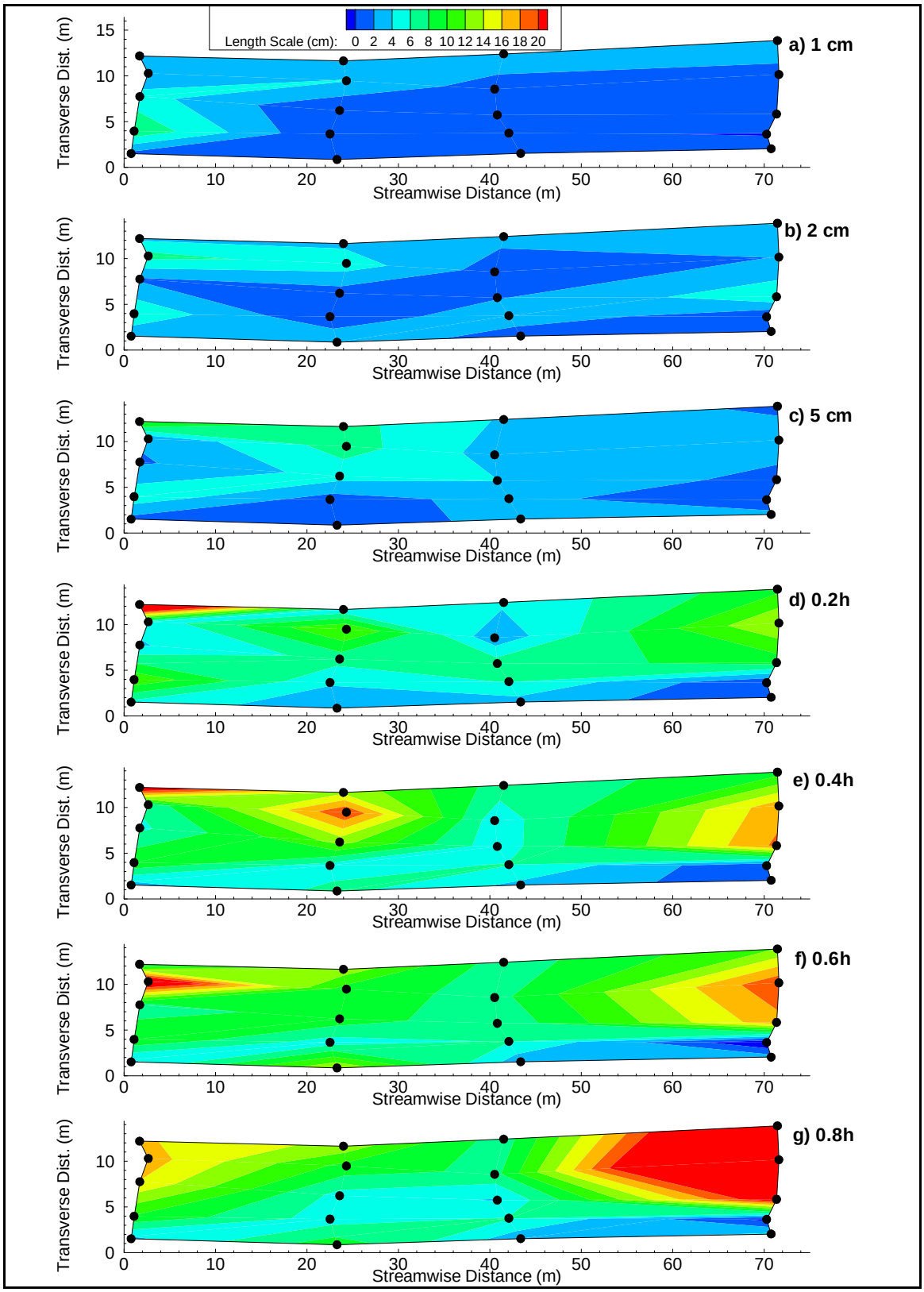

Figure 2.20. St. Maries reach integral length scale distributions

Hypothesis Testing

The results confirmed hypothesis 1 for velocity and shear stress profiles. However, hypothesis 1 was rejected for TI_s, TI_t, TI_v, TKE, T, and L profiles. New regression equations were presented for τ_R, T, and L. The results confirmed hypothesis 2a for the variables u_s, u_t, TI_s, TI_t, TI_v, TKE, τ_R, and T for both streams and L for the St. Maries reach only. Hypothesis 2a was rejected for L in the Potlatch reach. The results also confirmed hypothesis 2b for u_s and T for both reaches. the St. Maries reach and U_s and T for the Potlatch reach. Hypothesis 2b was also confirmed for TI_s and L for the St. Maries reach. Hypothesis 2b was rejected for all other variables. Results of the hypothesis tests are summarized in Table 2.3.

Table 2.3. Results of hypothesis tests for the St. Maries (SM) and Potlatch (PL) reaches (C=confirmed, R=rejected, NA=not applicable)

	Hypothesis and Reach				
Variable	1	2a SM	2a PL	2b SM	2b PL
U_s	C	C	C	C	C
U_t	NA	C	C	R	R
U_v	NA	R	R	R	R
TI_s	R	C	C	C	R
TI_t	R	C	C	R	R
TI_v	R	C	C	R	R
TKE	R	C	C	R	R
τ_R	C	C	C	R	R
T	NA	C	C	C	C
L	R	C	R	C	R

Discussion

The objective of this research was to a) test the adequacy of existing empirical formulas for velocity and turbulence distributions in natural streams and b) to investigate flow field distributions at the reach scales. These objectives were met by conducting ADV measurements in two natural stream reaches.

It was found that the log-law adequately predicted velocity profiles at all transverse locations and stream units in the sample reaches. The empirical shear stress equation also performed adequately, but the results were marginal. Empirical relationships for turbulence intensity, turbulent kinetic energy, and integral length scale were inadequate for predicting measured data. Best-fit regression equations for Reynolds shear stress and integral time and length scales were presented. A high level of spatial heterogeneity was observed between stream units (riffles, pools, and runs) but not between different depths.

These results have important implications for the understanding of natural flow fields because they contradict existing concepts of open channel turbulence. The most accepted model is that turbulence is primarily generated by boundary shear and bursting events and then diffused towards the surface while dissipating. Further, it is generally believed that contributions from other features, such as the stream banks and bedforms, are small and localized. This study found that turbulence heterogeneity was stronger between stream units (horizontally) than between depths (vertically). Most turbulence variables showed no significant trends with depth. TKE values were near predicted values near the bed, but much higher than predicted values higher in the water column. This suggests that turbulence generation at the bed with diffusion to the surface was not

the dominant mechanism. This can be explained through substantial turbulence generation associated with stream banks, bedforms, vegetation, obstructions, channel curvature, and other channel features. This finding suggests that a different approach must be used in the prediction of natural stream turbulence. A turbulent kinetic energy budget approach, which accounts for turbulence generation from the channel features mentioned above, may provide an improved estimate of turbulence distributions.

Although this work has advanced our understanding of natural stream flow fields, several limitations exist in the current study. First, the observations were only conducted in two stream reaches. Also, the reaches were similar in terms of discharge, channel geometry, and bed roughness. Additionally, instrumentation limited the measurement resolution and investigation of coherent structures. Future work should investigate additional reaches with a wider range of hydraulic and geometric characteristics. An array of ADVs would provide greater data resolution. Instrument advancements, such as the use of acoustic Doppler current profilers (ADCP), may also improve the quality of measurements.

References

Blanckaert, K., and Graf, W. H. (2001). "Mean flow and turbulence in open-channel bend." *Journal of Hydraulic Engineering*, 127(10): 835-847.

Buffin-Belanger, T., Roy, A. G., and Kirkbride, A. D. (2000). "On large-scale flow structures in a gravel-bed river." *Geomorphology*, 32(3-4): 417-435.

Bunn, S. E., and Arthington, A. H. (2002). "Basic principles and ecological consequences of altered flow regimes for aquatic biodiversity." *Environmental Management*, 30(4), 492-507.

Bunte, K., and Abt, S. R. (2001). "Sampling surface and subsurface particle-size distributions in wadable gravel- and cobble-bed streams for analyses in sediment transport, hydraulics, and streambed monitoring / Kristin Bunte, Steven R. Abt." U.S. Dept. of Agriculture, Forest Service, Rocky Mountain Research Station, Fort Collins, CO .

Chen, X., and Chiew, Y. M. (2003). "Response of velocity and turbulence to sudden change of bed roughness in open-channel flow." *Journal of Hydraulic Engineering*, 129(1): 35-43.

Hart, D. D., and Finelli, C. M. (1999). "Physical-biological coupling in streams: The pervasive effects of flow on benthic organisms." *Annual Review of Ecology and Systematics*, 30: 363-395.

Naiman, R. J., Bunn, S. E., Nilsson, C., Petts, G. E., Pinay, G., and Thompson, L. C. (2002). "Legitimizing fluvial ecosystems as users of water: An overview." *Environmental Management*, 30(4), 455-467.

Nezu, I., and Nakagawa, H. (1993). "Turbulence in open-channel flows." A.A.Balkema, Rotterdam,Netherlands/Brookfield,VT.

Nezu, I., and Onitsuka, K. (2001). "Turbulent structures in partly vegetated open-channel flows with LDA and PIV measurements." *Journal of Hydraulic Research*, 39(6), 629-642.

Nikora, V. I., and Smart, G. M. (1997). "Turbulence characteristics of New Zealand gravel-bed rivers." *Journal of Hydraulic Engineering*, 123(9): 764-773.

Nikora, V. I., and Goring, D. (2000). "Flow turbulence over fixed and weakly mobile gravel beds." *Journal of Hydraulic Engineering*, 126(9): 679-690.

Nikuradse, J. (1933). "Stromungsgesetze in rauhen Rohren." Heft 361, Berlin.

Poff, N. L., Allan, J. D., Bain, M. B., Karr, J. R., Prestegaard, K. L., Richter, B. D., Sparks, R. E., and Stromberg, J. C. (1997). "The natural flow regime." *Bioscience*, 47(11), 769-784.

Prandtl, L. (1932). "Zur turbulenten Stromung in Rohren und langs Platten." *Ergebnisse der Aerodynamischen Versuchsantalt zu Gottingen*, 4, 18-29.

Raupach, M. R., Antonia, R. A., and Rajagopalan, S. (1991). "Rough-wall turbulent boundary layers." *Applied Mechanics Review* , 44(1): 1-25.

Rennie, C. D., Fisher, T. S. R., and Millar, R. G. (1999). "Spatial variability of turbulent velocity structure in a natural river." Seattle.

Reynolds, A. J. (1974). "Turbulent flows in engineering." John Wiley, New York.

Rotta, J. (1962). "Turbulent boundary layers in incompressible flow." *Progress in Aeronautical Science*, 2, 1-219.

Shteinman, B., Nikora, V., Ekhnich, M., and Sukhodolov, A. (1996). "Experimental validation of the `frozen' turbulence hypothesis for river flows." Lausanne, Switz, 531.

Smith, D. L. (2003). "*The* shear flow environment of juvenile salmonids." Ph.D. Dissertation, University of Idaho.

Song, T and Chiew, Y M. (2001). Turbulence Measurement in Nonuniform Open-Channel Flow Using Acoustic Doppler Velocimeter (ADV). *Journal of Engineering Mechanics*, 127(3):219-233.

Song, T., Lemmin, U., and Graf, W. H. (1994). "Uniform-Flow in open channels with movable gravel-bed." *Journal of Hydraulic Research*, 32(6): 861-876.

Sukhodolov, A. N., Thiele, M., and Bungartz, H. (1998). "Turbulence structure in a river reach with sand bed." *Water Resources Research*, 34(5): 1317-1334.

Tritico, H. M., and Hotchkiss, R. H. (2005). "Unobstructed and obstructed turbulent flow in gravel bed rivers." *Journal of Hydraulic Engineering*, Accepted for publication.

von Karman, T. (1930). "Mechanische ahnlichkeit und turbulenz." *Gottinger Nachrichten, Math. Phys. Klasse*, 58-60.

Voulgaris, G., and Trowbridge, J. H. (1998). "Evaluation of the acoustic Doppler velocimeter (ADV) for turbulence measurements." *Journal of Atmospheric and Oceanic Technology*, 15: 272-289.

Wahl, T. L. (2000). "Analyzing ADV Data Using WinADV." American Society of Civil Engineers. Minneapolis.

Wilczak, J. M., Oncley, S. P., and Stage, S. A. (2001). "Sonic anemometer tilt correction algorithms." *Boundary-Layer Meteorology*, 99: 127-150.

Wolman, M. G. (1954). "A method of sampling coarse bed material." *Transactions of the American Geophysical Union*, 35: 951-956.

Chapter 3: Adequacy of ADCP velocity, shear stress, and turbulence measurements

Abstract

Accurate flow field measurements in rivers are necessary for many applications including biological investigations and numerical model development. Unfortunately, data availability is very limited due to inadequate measurement techniques. Acoustic Doppler Current Profilers (ADCP) provide a promising alternative to traditional point-velocity measurements. However, these instruments have not been thoroughly tested against accepted measurement techniques in natural streams. The objective of this research was to evaluate the adequacy of ADCP to measure velocity, turbulence, and shear stress distributions in cobble bed rivers. Comparison with Acoustic Doppler Velocimeter (ADV) data showed that ADCP instruments accurately measured velocity magnitude and bed shear stress distributions in two cobble bed rivers. However, ADCP measurements of three-dimensional velocity components and turbulence parameters were significantly different than ADV results. This has broad implications considering the use of thousands of ADCPs by the USGS and other agencies. This will greatly improve our ability to measure natural stream flow fields for numerical model calibration, habitat assessments, and other stream investigations.

Introduction

Accurate flow field descriptions in rivers are important for the investigation of stream processes. For example, velocity distributions impact aquatic habitat and mixing phenomena, bed shear stress influences sediment transport and benthic organism development, and numerical models require flow field descriptions for boundary conditions and calibration.

Despite the need for flow field information, measurement challenges have limited data availability. Traditional techniques utilize point-measurements conducted at several locations. This is usually completed with a Price or Pygmy current meter. More advanced instruments, such as the Acoustic Doppler Velocimeter (ADV), are increasingly being used. These point-measurement techniques share several drawbacks including safety considerations (fast or deep flow) and prohibitive time requirements to collect an adequate number of measurements.

A possible alternative to these point-measurement instruments is the Acoustic Doppler Current Profiler (ADCP). Originally developed for marine flow environments, the technology was first applied to rivers in the early 1990s. The popularity of ADCP stream discharge measurements has grown consistently (Simpson 2001). Recently, researchers have investigated the use of ADCPs to measure spatial flow features including velocity and turbulence distributions (Muste et al. 2004a; Muste et al. 2004b; Shields et al. 2003; Schemper and Admiraal 2002). However, the validity of ADCP velocity measurements have not been adequately tested against accepted techniques in natural streams.

Objective

The objective of this research was to evaluate the adequacy of ADCP instruments for measuring velocity, shear stress, and turbulence distributions in cobble bed streams. This was accomplished by conducting ADCP and ADV measurements at nine coincident stations in two rivers. The observation data were used to test the following hypothesis:

Hypothesis 3*:* ADCP measurements are adequate for describing velocity and shear stress distributions. It was predicted that there would be no significant difference between ADV and ADCP velocity and shear stress measurements.

Background

Significance

Velocity is a dominant variable influencing many stream processes including aquatic habitat, contaminant transport, and geomorphology. Velocity and shear stress distributions influence aquatic organism energy expenditure, food delivery, waste removal, predator avoidance, and physical disturbance (Hart and Finelli 1999). Aquatic habitat evaluation is usually accomplished through point measurements, while neglecting important spatial variations (Crowder and Diplas 2000). Improving measurement techniques is necessary to advance habitat assessment procedures (Bunn and Arthington 2002; Hardy 1998).

Proper placement of wastewater and stormwater outfalls requires knowledge of mixing processes. Velocity gradients and turbulent fluctuations influence mixing of contaminants, nutrients, sediments, and dissolved gases (Martin McCutcheon 1999). Predicting contaminant and nutrient mixing requires accurate flow field measurements. Sediment transport calculations also require knowledge of velocity and shear stress distributions.

River analysis is often accomplished using one-, two-, and three-dimensional stream models (Biron et al. 2004; Crowder and Diplas 2002; Lane et al. 2004). Flood prediction, hydraulic design, sediment and contaminant transport, and ecosystem restoration are a few of the simulated processes. Model development requires accurate flow field and geometry data for boundary conditions and calibration. The desired data are rarely available due to collection difficulties.

Flow Characteristics

Stream flow fields are often described through a combination of theoretical and empirical equations. The 'law of the wall' developed by Prandtl (1932) and von Karman (1930) for smooth-boundaries was modified by Nikuradse (1933) and others (Rotta 1962) to the following log-law for rough boundaries:

$$\frac{\bar{u}}{u_*} = \frac{1}{\kappa}\ln\left(\frac{z+\Delta z}{k_s}\right) + B \qquad \text{Equation 3.1}$$

where $\bar{u}$ is the local time-averaged velocity, u_* is the friction velocity, κ is the von Karman constant, z is the distance from the bed, Δz is the displacement length, k_s is the roughness height and B is an integration constant.

Log-law application to measured data is dependent on assumptions made in choosing Equation 3.1 parameters. The appropriate assumptions depend on project objectives, flow conditions, and data availability. Extensive laboratory and field experiments have demonstrated that κ can be assumed between 0.4 and 0.41 for fixed beds (Nikora and Goring 2000; Kirkgoz 1989) and B is approximately 8.5 for equilibrium flow conditions (Song and Chiew 2001).

The roughness height is a function of the boundary roughness. For a uniform grain distribution, it is appropriate to use the particle diameter (Nikuradse 1933). However, k_s is not clearly defined for heterogeneous streambeds and can be further complicated by the presence of bedforms. k_s is often assumed as a particle size distribution statistic such as the median particle size, d_{50} (Blanckaert and Graf 2001; Papanicolaou and Hilldale 2002).

The displacement length is a correction from the local streambed elevation to the velocity profile origin (u=0 and z+Δz=0). The profile origin is difficult to define for natural streams as it depends on local bed geometry. Δz is often determined by curve-fit to collected data or neglected altogether (Nikora et al. 2002).

Details for determining friction velocity (u_*), shear stress (τ), the correlation function (R), integral time scale (T), and integral length scales (L) is found in Chapter 2 and Appendix A.

Instruments

The details of ADCP operation are described by numerous authors (Mueller 2003; Stacey 2003) and are briefly summarized here. A 1200 kHz Workhorse ADCP, manufactured by RD Instruments, was used in this research. The ADCP transmits and receives an acoustic signal with four beams, each separated by 90 degrees (Figure 3.1a). Each beam is oriented outward 20 degrees from the vertical. This configuration results in four control volumes (bins), which increase in size and diverge with distance from the ADCP. Velocity profile data are collected at uniformly spaced bins.

Several limitations result from the ADCP sampling technique. First, flow field heterogeneity across the four diverging beams results in measurement error. The error can be substantial when applied to natural streams. Second, velocity in the top 10 to 50 cm and bottom 6% of the water column cannot be measured due to acoustic ringing and echoes. This is a serious limitation if boundary data are required or when operating in shallow flow. Additionally, the large sampling volume, which increases with depth, makes it impossible to measure small scale turbulent fluctuations.

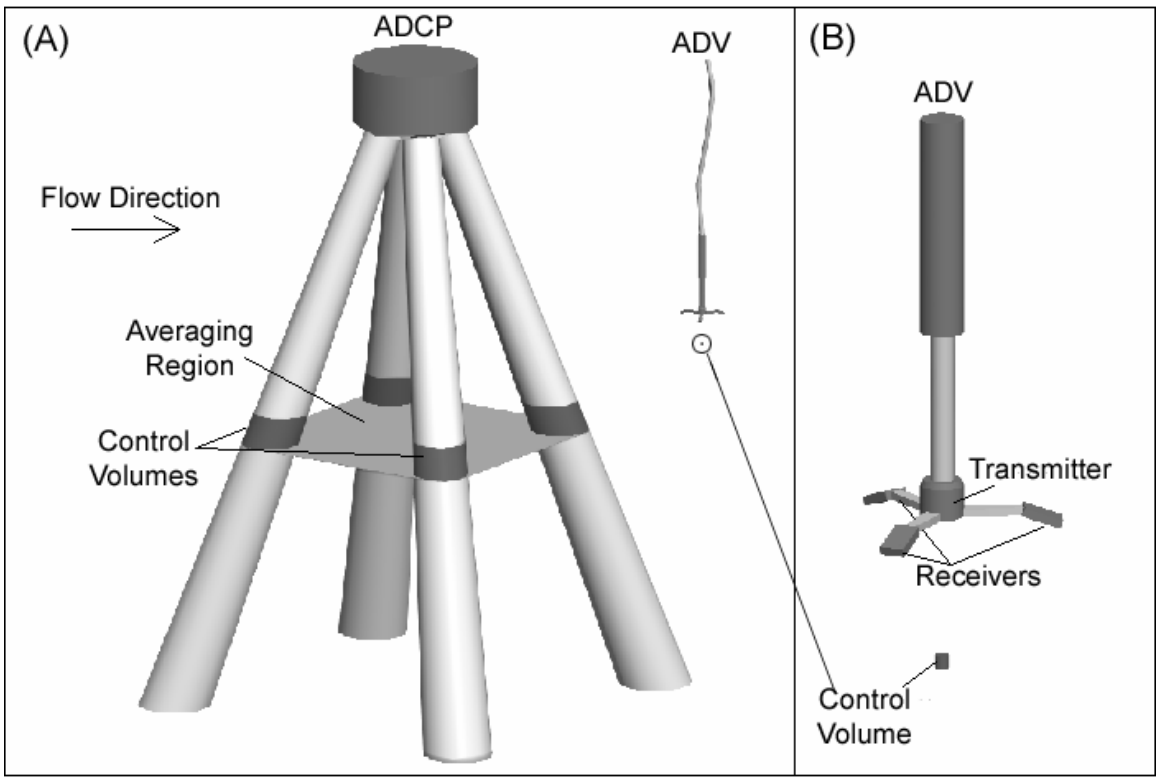

Figure 3.1 a) ADCP and ADV instruments and control volumes, b) Expanded view of the ADV probe and control volume

Alternatively, flow fields may be characterized using an ADV instrument. A 16 MHz MicroADV, manufactured by Sontek/YSI, was used for this research. A detailed description of ADV operation principles can be found in Song and Chiew (2001). The ADV operates on a pulse-to-pulse coherent Doppler shift. An acoustic signal is emitted by a transducer towards a sampling volume located approximately 5 cm away. The signal is reflected by ambient particles in the flow field and measured by three receivers separated 120 degrees and approximately 7 cm (Figure 3.1b). The Doppler shift frequency along each receiver is used to calculate the 3D water velocity. The resulting control volume is 0.09 cc with a 50 Hz maximum sampling rate. Figure 3.1 demonstrates the contrast in ADCP and ADV sampling volumes.

The ADV configuration allows analysis of detailed flow features including small-scale turbulent fluctuations. ADV instruments have been used to describe velocity and turbulence distributions in laboratory flumes (Ferro 2003), irrigation canals (Nikora and Goring 2000), and natural channels (Rennie et al. 1999; Tritico and Hotchkiss in press). However, this technique has several drawbacks compared to the ADCP approach. Foremost, the small sampling volume makes characterization of large areas very time consuming. Further, instrument placement can be difficult and dangerous in deep or rapid flows.

Methods

Site Characterization

Measurements were conducted at two cross-sections in the St. Maries River near Clarkia, Idaho and two cross-sections in the Potlatch River near Kendrick, Idaho. Stream geometry data were collected with a total station using standard surveying techniques (including stream banks, water surface and bed slopes, and cross-section geometries). Survey data were used to calculate mean depth (H), hydraulic radius (R_H), top width (T_w), Reynolds number (Re), Froude number (Fr), and global shear stress (τ_g). Table 3.1 contains physical and hydraulic descriptions of the sampled reaches and stream geometries are shown in Figure 3.2.

Table 3.1. Physical and hydraulic descriptions of the sampled reaches

	Potlatch Reach	St. Maries Reach	How determined
Discharge, Q (m^3/s)	11.4	7.9	ADCP measurement
Mean Velocity, U (cm/s)	87.6	61.5	ADCP measurement
Mean Depth, H (m)	0.81	1.02	Survey
Hydr. Rad. R_H (m)	0.77	0.87	Survey
Top Width, T_W (m)	15.4	12.8	Survey
Aspect Ratio, T_W/H	19.0	12.5	Survey
Froude Number, Fr	0.31	0.21	$U/(gR_H)^{0.5}$
Reynolds Num., Re	$6.0x10^5$	$4.8x10^5$	$\rho UR_H/\mu$
Bed Slope, S_b	0.00081	-0.00012	Survey
Water Slope, S	0.001	0.0005	Survey
Global Friction Velocity, u_{*g} (m/s)	0.088	0.066	Eq. 2 and 3
Global Shear Stress, τ_g (N/m^2)	7.8	4.4	Eq. 3
d_{16}, d_{50}, d_{84} (cm)	7.2,11.4,18.7	5.8,10.9,16.8	Wolman
Relative Roughness, d_{50}/H	0.14	0.11	Wolman, Survey
Critical Shear, τ_c (N/m^2) for d_{50}	92	88	Shields Parameter

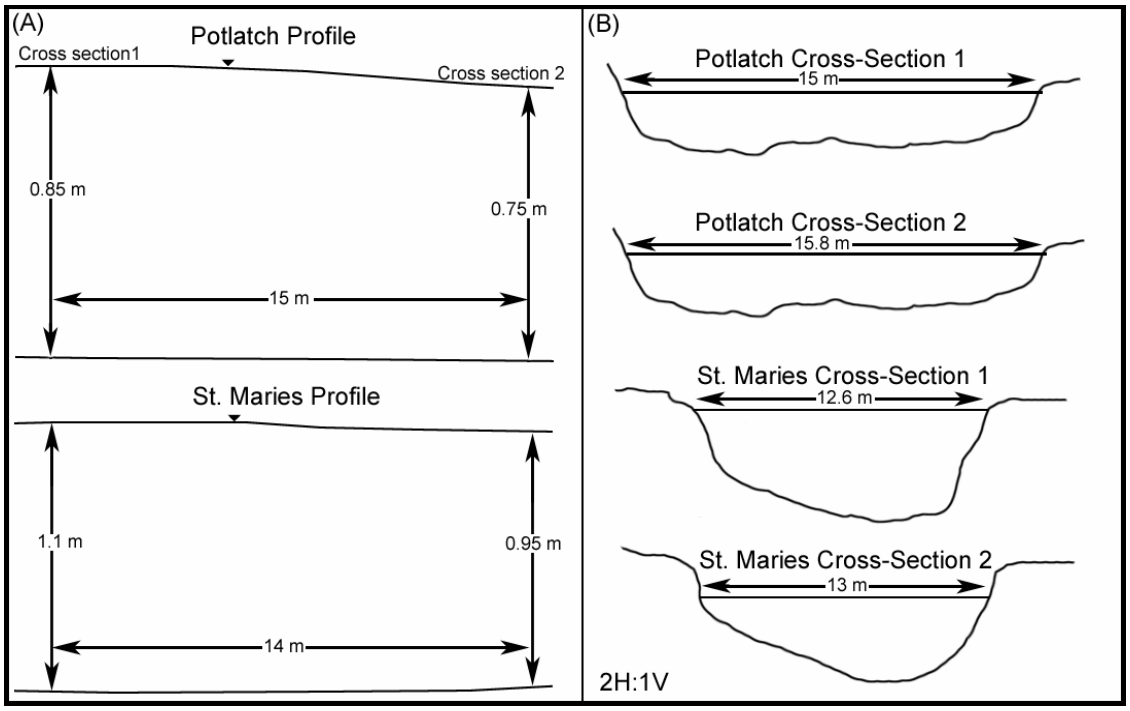

Figure 3.2. a) Elevation and b) cross-section views of the sample reaches

The sediment particle size distributions (psd) were described using a Wolman pebble count (Wolman 1954). Approximately 150 samples were collected at a series of transects within each reach. Median particle diameters were 10.9 and 11.4 cm for the St. Maries and Potlatch rivers, respectively; both reaches were classified as cobble bed (Bunte and Abt 2001). The critical shear stress values, τ_c, were estimated for the d_{50} using the Shields parameter. Global shear stress estimates were far below critical values.

The Potlatch River reach is a high gradient stream producing coarse sediment, high mean velocity, and shallow depth. The left bank is nearly vertical bedrock and the right bank is vegetated cobble. The St. Maries reach has a more moderate slope and therefore, a lower mean velocity and finer sediment. The reach has a minor lateral expansion but an increase in bed elevation results in a moderate flow acceleration. Both banks are covered with grass, which was submerged at the time of sampling.

ADCP Sampling

The ADCP was mounted within a RiverBoat, manufactured by OceanScience. Two taglines were attached to the Riverboat and threaded through eyebolts, which were driven into the river banks. The RiverBoat was fitted with flow-vanes to align the ADCP and was moved to the desired location and anchored by tying the taglines to the eyebolts. Data were collected for 20 minutes at each station, providing approximately 1200 samples. ADCP data were transferred to a laptop computer with wireless modems. The instrument configuration was adjusted to optimize data quality. Due to high velocity and turbulence levels, the ADCP was operated in mode 12 with a 5cm bin size. Although more robust, mode 12 provides less precision than the available pulse-to-pulse coherent modes (5, 8, and 11). For the St. Maries reach, two stations were sampled in each cross-section at one-third the stream width from each bank. In the Potlatch reach, three stations were sampled in each cross-section at the centerline and one-quarter the top width from each bank.

ADCP data were analyzed with vendor and custom software programs. WinRiver (RD Instruments) was used for instrument configuration, data archiving, and data extraction. A custom FORTRAN code was written to compute velocity, correlation, and spectral density values.

ADV Measurements

An aluminum sampling stand was built to hold the ADV. The stand was 1 meter wide and 0.5 meters long and fitted with four adjustable legs and an adjustable sampling arm (Figure 2.4). The sampling arm extended a maximum of 0.5 meters from the stand's front to avoid flow field interference, while cross-bracing prevented flow induced stand

vibrations. The ADV processing canister and laptop computer were set on top of the stand. The ADV position was measured with a combination of vernier scales.

Following ADCP data collection, instrument location was surveyed and marked with a florescent monument. The ADV was positioned over the monument and the location was verified by surveying the probe. The streambed, water surface, and all four stand legs were also surveyed. The ADV was initially positioned with the control volume approximately 1 cm from the streambed. Data were collected for 2 minutes at a frequency of 50 Hz. The adequacy of the 2 minute sample duration was confirmed by collecting data at one point for 20 minutes and evaluating divergence of velocity statistics. Data were collected at 10 elevations within each vertical profile. The data were processed using WinADV (Sontek/YSI) and custom FORTRAN codes.

Results

Velocity

ADCP velocity measurements were evaluated against ADV data. Time-averaged velocity magnitudes and three-dimensional components were examined. ADCP error was assessed by assuming ADV measurements represented reality (Voulgaris and Trowbridge 1998). The significance of measurement techniques was statistically tested.

ADCP measurements of velocity magnitude closely resembled ADV results. ADCP and ADV depth-integrated velocity magnitudes for all nine stations are summarized in Table 3.2 (U_{ADV} and $U_{ADCP\ Mag}$). The mean depth-integrated ADCP error was -2.8 cm/s or -4.8%.

A typical velocity profile (St. Maries, Station 2) is shown in Figure 3.3a. ADCP measurements closely approximated ADV data throughout the vertical profile. A comparison between ADCP and ADV point-velocity measurements at all coinciding locations is shown in Figure 3b. Most ADCP measurements were close to the one-to-one line. Mean point-velocity errors for each station are summarized in Table 3.2 (E_{Mag}). The mean ADCP error for all data points was -1.2%. ADCP and ADV velocity magnitudes were compared using a two-sample t-test. The results showed that the mean difference between ADCP and ADV velocity magnitude measurements was not statistically significant ($t(40)=0.47$, $p=0.32$).

ADCP and ADV measurements were also compared by decomposing the velocity magnitudes into streamwise, transverse, and vertical components using a streamline coordinate system (Wilczak et al. 2001). Figure 3.3 also contains streamwise velocity data for both instruments. ADV streamwise velocity data were very similar to

Table 3.2. Physical and hydraulic station data where: where: H=depth, U_{ADV}=ADV depth integrated mean velocity magnitude, $U_{ADCP-Mag}$=ADCP depth integrated mean velocity magnitude, $U_{ADCP-SW}$=ADCP depth integrated mean streamwise velocity, E_{Mag}=mean ADCP error in point velocity magnitude, E_{sw}=mean ADCP error in point streamwise velocity, τ_{ADV}=ADV log-law derived bed shear stress, $\tau_{ADCP-Mag}$=ADCP log-law velocity magnitude derived bed shear stress, $\tau_{ADCP-SW}$=ADCP log-law streamwise velocity derived bed shear stress, τ_{RSS} =ADV Reynolds shear stress derived bed shear stress, d_{50}=median particle size, Δz_{ADV}=ADV log-law displacement length, Δz_{ADV}=ADCP log-law displacement length, R^2_{ADV}=ADV log-law correlation coefficient, R^2_{ADCP}=ADCP log-law correlation coefficient, $TI_{ADV\ 0.5H}$=ADV velocity turbulence intensity at mid-water column, $TI_{ADCP\ 0.5H}$=ADCP velocity turbulence intensity at mid-water column, $T_{ADV\ 0.5H}$ =ADV integral time scale at mid-water column, $T_{ADCP\ 0.5H}$ =ADCP integral time scale at mid-water column, L_{ADV} 0.5H =ADV integral length scale at mid-water column, $L_{ADCP\ 0.5H}$ =ADCP integral length scale at mid-water column.

River	Potlatch					St. Maries			
Station	1	2	3	4	5	1	2	3	4
H (cm)	65	84	94	83	81	106	113	87	102
U_{ADV} (cm/s)	80.3	84.7	81.9	82.8	71.4	74.3	79.1	72.7	81.4
$U_{ADCP-Mag}$ (cm/s)	78.7	84.1	81.0	82.8	69.2	70.9	72.9	67.3	67.1
$U_{ADCP-SW}$ (cm/s)	75.0	80.1	78.1	79.0	66.4	67.8	69.4	64.9	64.2
E_{Mag} (%)	-0.1	1.4	3.2	-0.2	3.7	-1.8	-2.4	-1.2	-14.6
E_{SW} (%)	-8.5	-6.4	-2.7	-5.5	-7.5	-8.5	-8.4	-9.8	-23.0
τ_{ADV} (N/m^2)	5.8	5.7	6.0	5.6	4.2	4.1	4.4	4.2	4.9
$\tau_{ADCP-Mag}$ (N/m^2)	5.5	5.6	5.9	5.6	4.0	3.7	3.8	3.6	3.3
$\tau_{ADCP-SW}$ (N/m^2)	5.0	5.1	5.5	5.1	3.7	3.4	3.4	3.4	3.1
τ_{RSS} (N/m^2)	4.2	4.9	5.1	3.3	3.0	3.1	4.0	2.9	1.8
d_{50} (cm)	10.4	10.4	15.3	10.9	11.2	11.0	10.8	11.1	10.8
Δd_{ADV} (cm)	2.9	1.0	-4.3	-1.6	0.0	2.9	-0.5	5.3	-2.7
Δd_{ADCP} (cm)	3.3	2.7	0.1	-1.0	-4.4	3.2	-1.8	1.2	-3.6
R^2_{ADV} Log	0.99	0.99	0.99	0.99	0.99	0.99	0.98	0.97	0.97
R^2_{ADCP} Log	0.99	0.99	0.99	0.98	0.96	0.99	0.98	0.99	0.98
$TI_{ADV\ 0.5H}$	11.6	10.1	12.8	11.4	10.8	8.6	8.7	10.9	6.4
$TI_{ADCP\ 0.5H}$	27.2	28.2	27.5	27.1	27.0	26.2	26.8	26.9	26.3
$T_{ADV\ 0.5H}$ (sec)	2.50	2.82	3.25	1.17	1.59	1.70	3.50	1.10	1.93
$T_{ADCP\ 0.5H}$ (sec)	0.55	0.52	0.52	0.51	0.55	0.52	0.57	0.52	0.57
$L_{ADV\ 0.5H}$ (sec)	230	254	243	102	67	134	310	87	168
$L_{ADCP\ 0.5H}$ (sec)	43	44	42	42	38	40	44	38	42

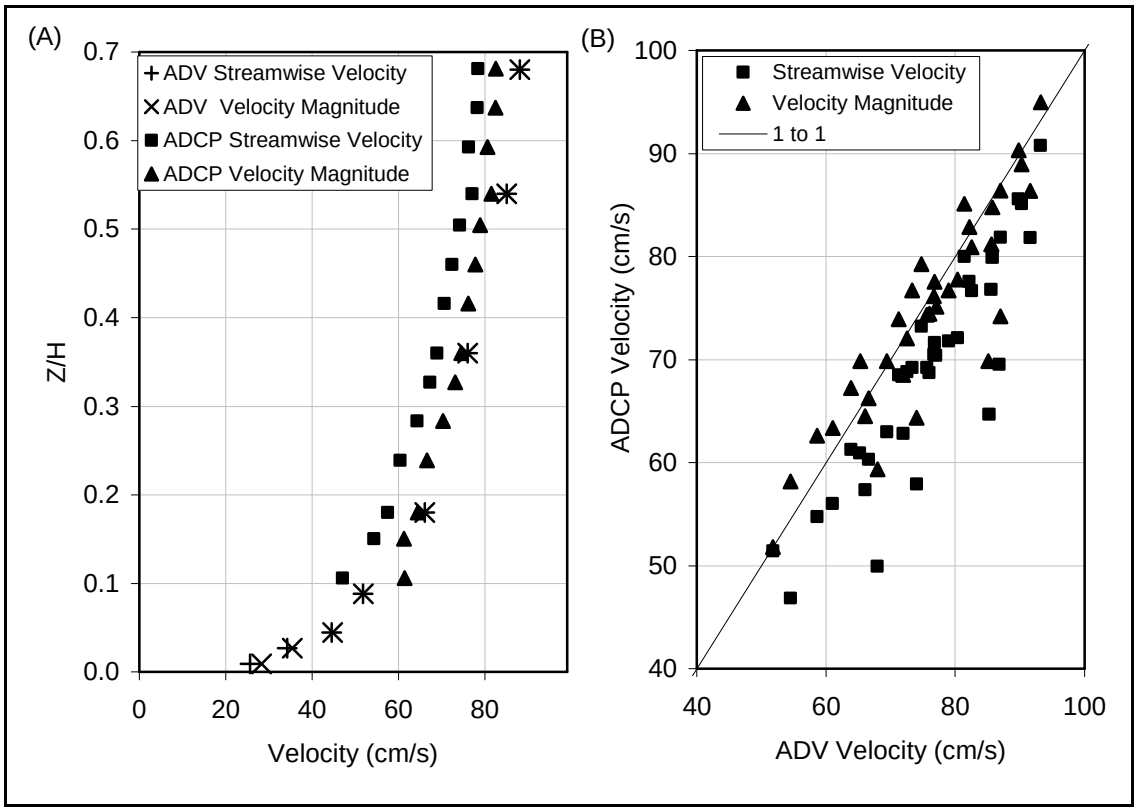

Figure 3.3. (A) ADV and ADCP streamwise velocity and velocity magnitude profiles for Station 2 of the St. Maries River, (B) ADCP velocities vs. ADV velocities for all points

corresponding velocity magnitudes. However, due to large fluctuations in transverse and vertical velocity measurements, ADCP streamwise velocity data were noticeably reduced. The result was a much larger mean error in ADCP depth-averaged streamwise velocities ($U_{ADCP\,SW}$) at -8.9%. The point-velocity errors for each station are summarized in Table 3.2 (E_{SW}) and displayed in Figure 3.3b. The result of a two-sample t-test revealed a statistically significant difference in mean ADCP and ADV streamwise velocity measurements ($t(40)=2.68$, $p<0.05$).

The measured vertical velocity profiles were compared with the predicted log-law distributions (Figure 3.4) showing dimensionless profiles and log-law functions for all stations. The log-law was applied by solving for the friction velocity and displacement length using a least-squares method. Measured data from both instruments closely

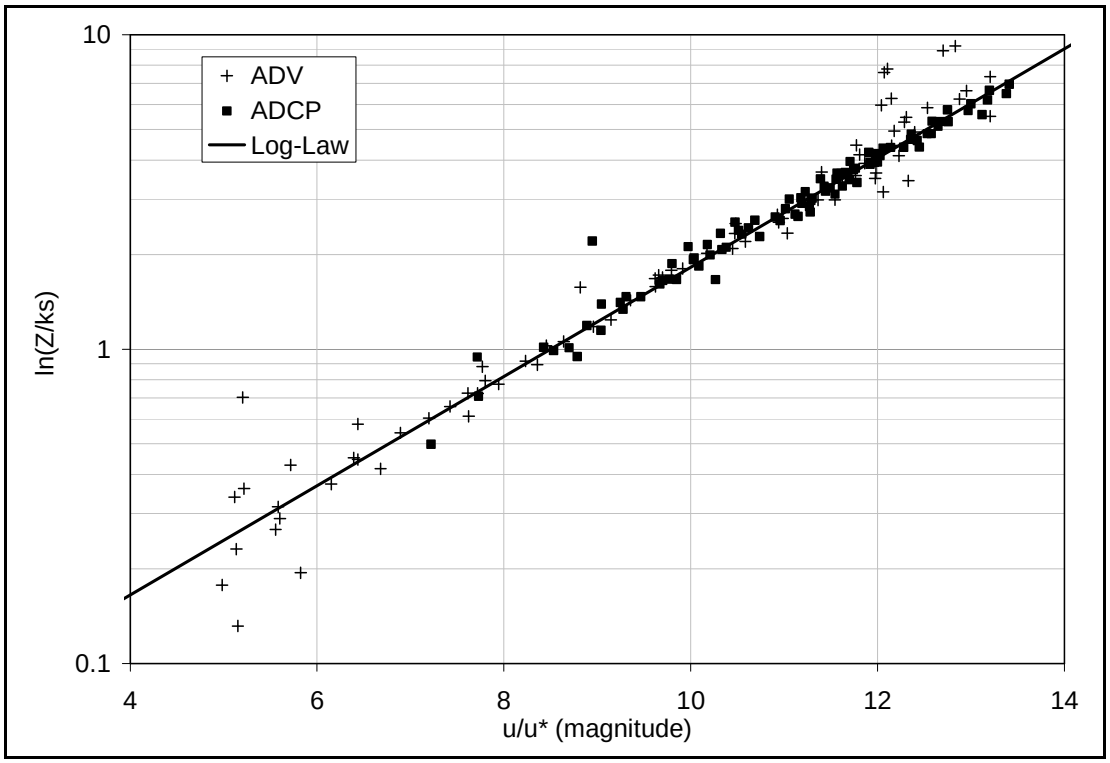

Figure 3.4. ADV and ADCP logarithmic velocity profiles and the theoretical log-law

resembled the log-law profile. Resulting log-law parameters and correlation (R^2) values are shown in Table 3.2. R^2 values were greater than 0.96 for all stations. Displacement lengths, Δz, varied from -4.4 to 5.3 cm, which were less than the median particle size diameter for all profiles. Friction velocity values will be addressed below with shear stress results.

Turbulence

The adequacy of ADCP turbulence measurements was evaluated by comparison with ADV data. ADV performance has been thoroughly tested and was assumed to represent reality for this study (Voulgaris and Trowbridge 1998). Turbulence intensity (TI), integral time (T) and length scales (L), and spectral densities were compared.

Figure 3.5 contains typical TI vertical profiles as measured by ADCP and ADV instruments (St. Maries, Station 2). Due to high instrument uncertainty when operated in mode 12, ADCP standard deviation was about three times larger than ADV results. The effects of artificially elevated standard deviations can be observed using velocity histograms. Figure 3.6 contains ADCP and ADV streamwise velocity histograms for one point in the St. Maries River (Station 2, z=0.5h). As expected, the elevated ADCP standard deviation resulted in a broader velocity distribution. Gaussian distributions for sample means and standard deviations are also shown. Measurements from both instruments resembled Gaussian distributions.

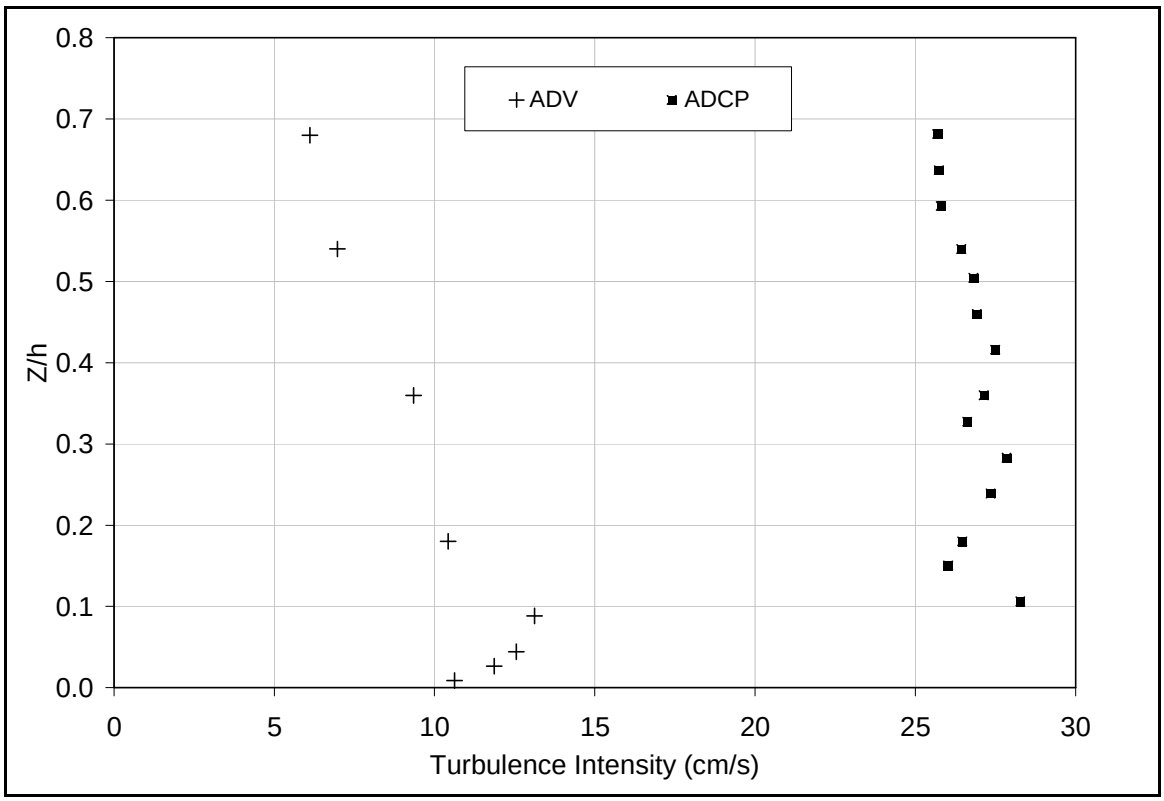

Figure 3.5. ADV and ADCP velocity magnitude TI profiles for Station 2 of the St. Maries River

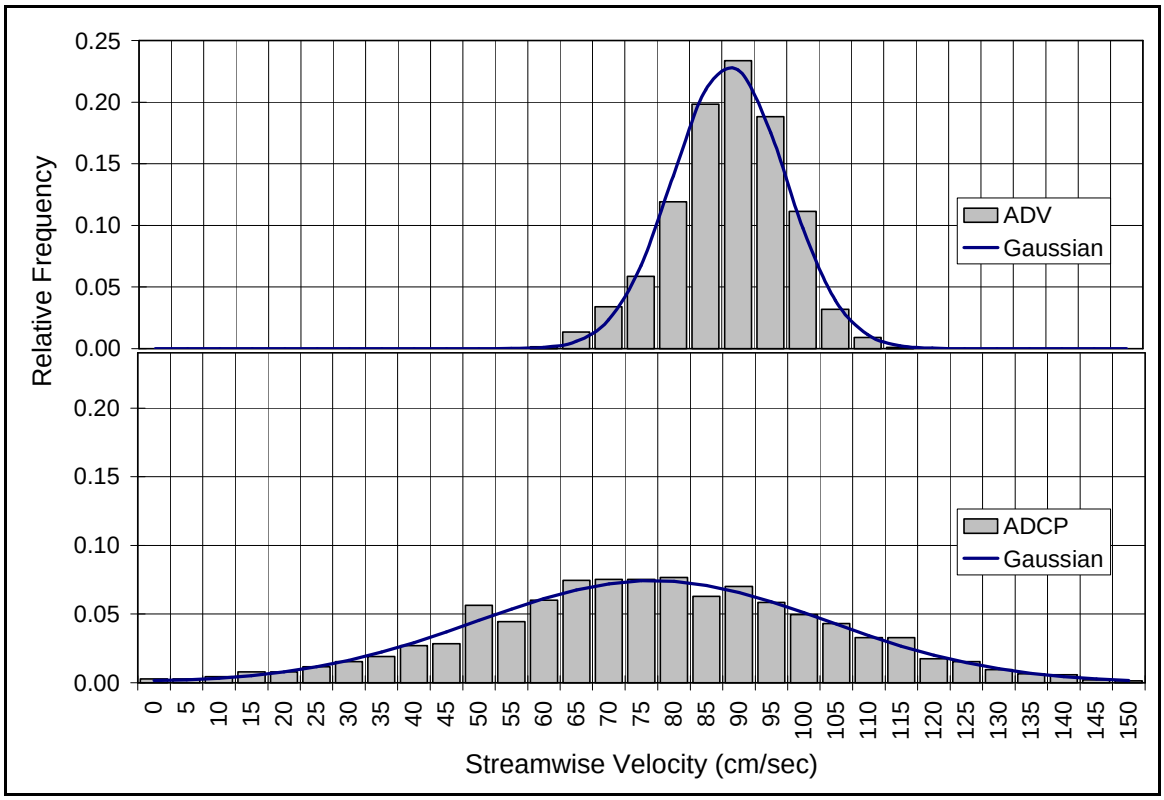

Figure 3.6. ADV and ADCP streamwise velocity histograms for mid-water column of Station 2 in the St. Maries River

Turbulent integral time and length scales provide greater insight into flow structure and instrument performance. ADCP measurements were evaluated through comparison to ADV results. Additionally, ADV scale measurements were used to test instrument criteria as discussed above. Figure 3.7a contains typical ADCP and ADV correlation functions for one location in the St. Maries River (Station 2, z=0.5h). The correlation data illustrate the drastic difference in ADCP (approximately 1 Hz) and ADV (50 Hz) sampling frequencies. The correlation functions were integrated to determine turbulent time scales (Table 3.2 and Figure 3.7b). For the data displayed in Figure 3.7a, the ADCP and ADV integral time scales were 0.57 and 3.5 seconds, respectively. The ADCP time scale is less than the instrument sampling frequency and only slightly greater than the theoretical minimum of one-half the sampling time step (0.5 seconds).

Investigation of time scales at other stations (Table 2) and depths (Figure 7b) reveals that ADV time scales vary with location, while ADCP scales remain near one-half the sampling frequency.

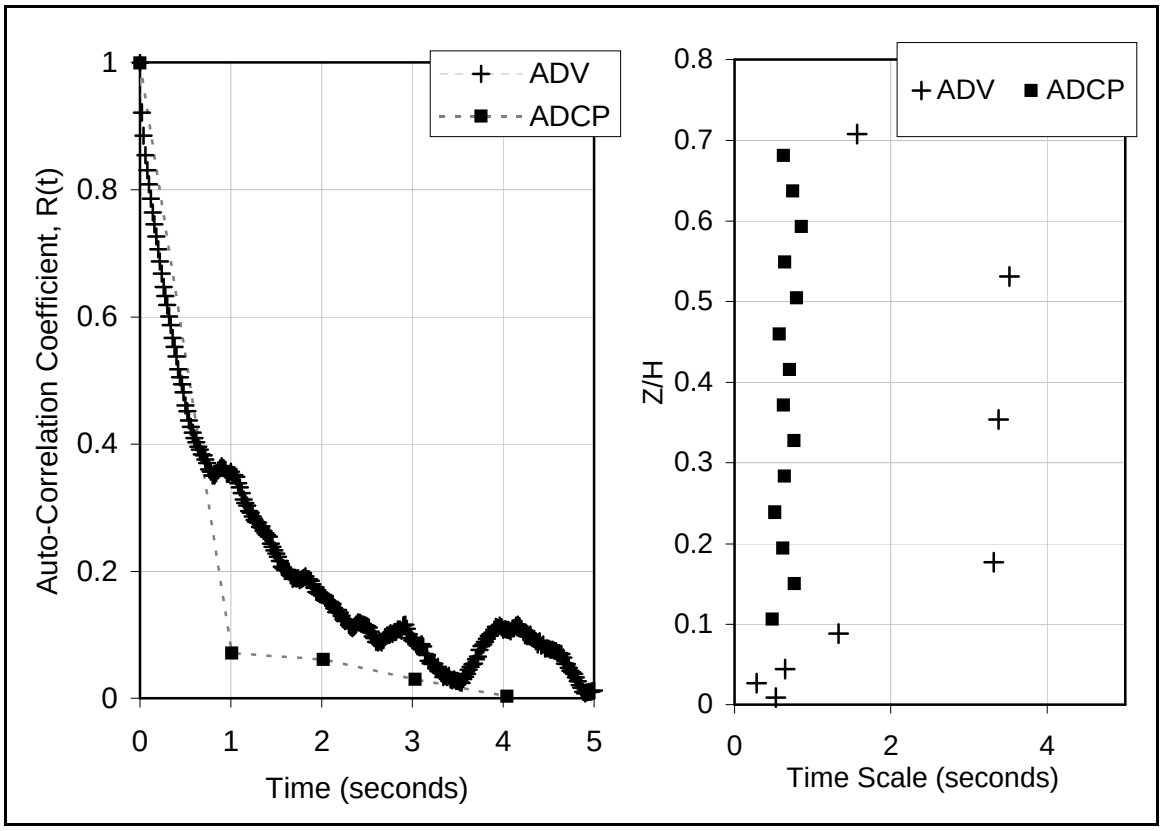

Figure 3.7. (A) ADV and ADCP correlation functions for mid-water column of Station 2 in the St. Maries River, (B) ADV and ADCP integral time scale profiles for Station 2 of the St. Maries River

Turbulent integral length scales were also compared to evaluate the adequacy of ADCP sampling volumes for measuring coherent structures. Table 3.2 contains mid-water column integral length scales for both instruments. As with time scales, ADCP length scales varied little between stations ranging from 38 to 44 cm. These scales were far less than corresponding ADV measured scales (67 to 310 cm) and similar to the length of the ADCP sampling regions (30 to 50 cm).

ADCP performance was further evaluated by investigating turbulence spectral densities. Figure 3.8 contains spectral densities as derived from both instruments in the St. Maries River (Station 2, z=0.5h). ADV measurements demonstrated the well known Kolmogoroff -5/3 power law (Monin and Yaglom 1971). Turbulence generation occurred in the region between 0.1 and 1 Hz, consistent with integral time scales. The turbulence spectrum indicates dissipative time scales of 0.02 seconds or less. ADCP results do not accurately describe the turbulence spectrum. High frequency scales were truncated by the low sampling frequency. The lack of high frequency data also introduced erroneous low frequency data points (<0.1 Hz) due to aliasing. These results indicate that the ADCP sampling frequency was too low and the sampling volume too large to properly measure turbulence features.

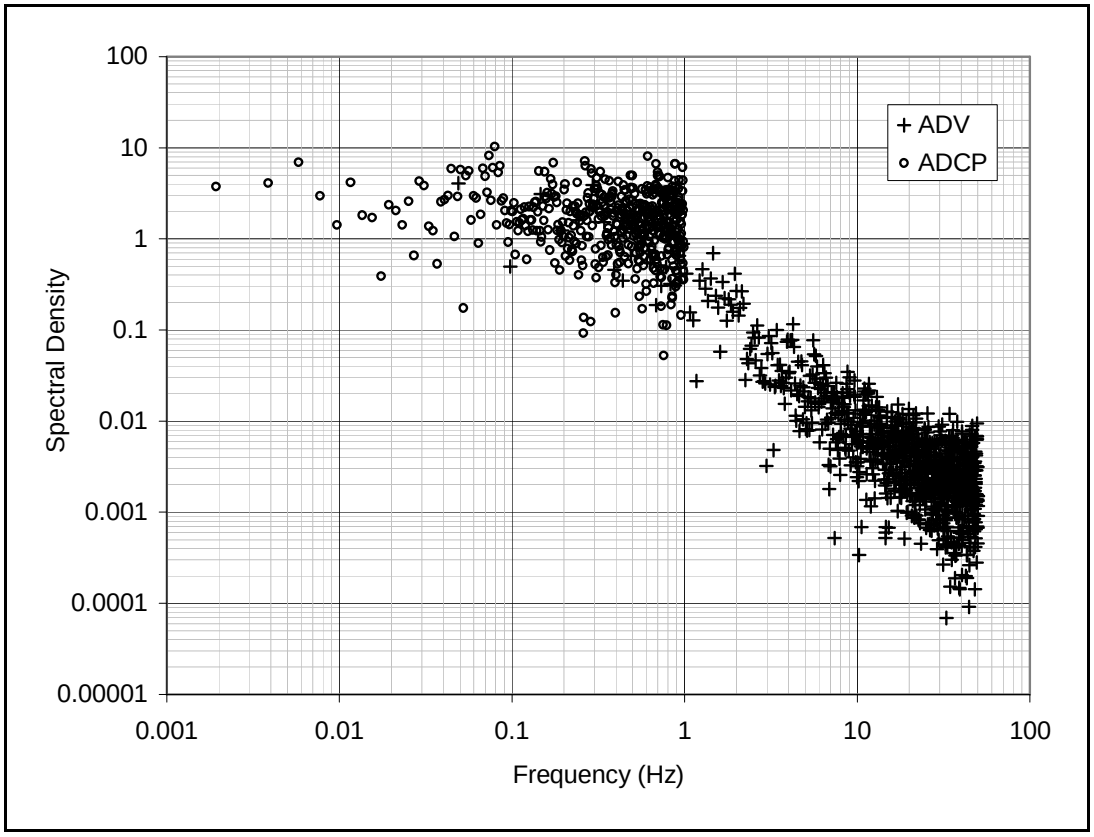

Figure 3.8. ADV and ADCP spectral density distributions for mid-water column of Station 2 in the St. Maries River

Shear Stress

The adequacy of ADCP derived shear stress estimates was assessed through comparison with ADV and water surface slope methods. The log-law (Equation 3.1) was used to estimate bed shear stress using ADV and ADCP streamwise velocity data and ADCP velocity magnitudes. ADV velocity magnitudes were not included because they were nearly identical to streamwise values. ADV Reynolds shear stress measurements (τ_R) were also used to estimate local bed shear stress while water surface slopes were used to estimate global shear stress, τ_g. ADCP Reynolds shear stress measurements were not used because the preceding results demonstrated the inadequacy of ADCP turbulence measurements.

Bed shear stress estimates are contained in Table 3.2. For nearly every value, global shear stress was greater than the local estimates. Results of a one-sample t-test showed a significant difference between global and local bed shear stress estimates. Among local shear stress estimates, ADV log-law values were the highest and τ_R estimates were the lowest. ADV τ_R estimates were considered less reliable due to low correlation values in calculations from Equation 2.13 ($R^2<0.4$). ADCP log-law estimates compared well with ADV values. As with velocity data, shear stress estimates from ADCP velocity magnitudes more closely matched ADV results. The results of a two-sample t-test showed that the mean difference between ADCP and ADV shear stress estimates from streamwise velocities was statistically significant ($t(9)=1.98$, $p<0.05$). However, the mean difference between ADCP and ADV shear stress estimates from velocity magnitudes was not statistically different ($t(9)=0.99$, $p=0.17$). In other words, ADCP shear stress values derived from velocity magnitudes using the log-law adequately matched ADV results.

Summary

Improved flow-field descriptions are needed for a wide range of applications. ADCP instruments provide a potential alternative to traditional point-measurement techniques. The objective of this paper was to investigate the accuracy and adequacy of ADCP velocity, bed shear stress, and turbulence measurements in cobble bed rivers. This was accomplished by comparing ADCP and ADV measurements at nine coincident stations in two rivers. Results showed that the ADCP accurately measured velocity magnitude but under-evaluated the streamwise velocity component. ADCP measured velocity profiles closely resembled theoretical logarithmic distributions. Investigation of turbulence parameters revealed the inadequacy of ADCP turbulence measurements in this environment. The ADCP TI values were elevated due to high instrument noise. Investigation of turbulent scales and spectral densities showed that ADCP sampling frequency was too low and the sampling region too large to adequately capture turbulence structure. Comparison of shear stress results showed that ADCP values derived from velocity magnitudes, using the log-law, adequately estimated ADV results. Further, ADCP estimates of local shear stress were significantly better than global estimates using water surface slopes, which tended to overestimate local values.

In conclusion, ADCP measurements of velocity magnitude and bed shear stress were adequate when compared with ADV results in two cobble bed rivers. Therefore, ADCP instruments may provide a preferred alternative to traditional point-measurement techniques. However, higher instrument sampling frequencies and reduced sampling volumes are necessary to describe three-dimensional velocity components and turbulence parameters.

References

Biron, P. M., Ramamurthy, A. S., and Han, S. (2004). "Three-dimensional numerical modeling of mixing at river confluences." *Journal of Hydraulic Engineering*, 130(3), 243-253.

Blanckaert, K., and Graf, W. H. (2001). "Mean flow and turbulence in open-channel bend." *Journal of Hydraulic Engineering*, 127(10), 835-847.

Bunn, S. E., and Arthington, A. H. (2002). "Basic principles and ecological consequences of altered flow regimes for aquatic biodiversity." *Environmental Management*, 30(4), 492-507.

Bunte, K., and Abt, S. R. (2001). "Sampling surface and subsurface particle-size distributions in wadable gravel- and cobble-bed streams for analyses in sediment transport, hydraulics, and streambed monitoring / Kristin Bunte, Steven R. Abt." U.S. Dept. of Agriculture, Forest Service, Rocky Mountain Research Station, Fort Collins, CO .

Crowder, D. W., and Diplas, P. (2000). "Evaluating spatially explicit metrics of stream energy gradients using hydrodynamic model simulations." *Canadian Journal of Fisheries and Aquatic Sciences*, 57(7), 1497-1507.

Crowder, D. W., and Diplas, P. (2002). "Assessing changes in watershed flow regimes with spatially explicit hydraulic models." *Journal of the American Water Resources Association*, 38(2), 397-408.

Ferro, V. (2003). "ADV measurements of velocity distributions in a gravel-bed flume." *Earth Surface Processes and Landforms*, 28(7), 707-722.

Hardy, T. B. (1998). "The future of habitat modeling and instream flow assessment techniques." *Regulated Rivers: Research and Management*, 14(5), 405-420.

Hart, D. D., and Finelli, C. M. (1999). "Physical-biological coupling in streams: The pervasive effects of flow on benthic organisms." *Annual review of ecology and systematics*, 30, 363-395.

Kirkgoz, M. S. (1989). "Turbulent velocity profiles for smooth and rough open channel flow." *Journal of Hydraulic Engineering*, 115(11), 1543-1561.

Lane, S. N., Hardy, R. J., Elliott, L., and Ingham, D. B. (2004). "Numerical modeling of flow processes over gravelly surfaces using structured grids and a numerical porosity treatment." *Water Resources Research*, 40(1).

Martin, J. L., and McCutcheon, S. C. (1999). "Hydrodynamics and Transport for Water Quality Modeling." Lewis Publishers, New York.

Monin, A. S., and Yaglom, A. M. (1971). "Statistical fluid mechanics; mechanics of turbulence, Volume1." MIT Press, Cambridge, MA.

Mueller, D. S. (2003). "Field Evaluation Of Boat-Mounted Acoustic Doppler Instruments Used To Measure Streamflow.".

Muste, M., Yu, K., and Spasojevic, M. (2004). "Practical aspects of ADCP data use for quantification of mean river flow characteristics; Part I: moving-vessel measurements." *Flow Measurement and Instrumentation*, 15(1), 1-16.

Muste, M., Yu, K., Pratt, T., and Abraham, D. (2004). "Practical aspects of ADCP data use for quantification of mean river flow characteristics; Part II: fixed-vessel measurements." *Flow Measurement and Instrumentation*, 15(1), 17-28.

Nezu, I., and Nakagawa, H. (1993). "Turbulence in open-channel flows." A.A.Balkema, Rotterdam,Netherlands/Brookfield,VT.

Nikora, V. I., and Goring, D. (2000). "Flow turbulence over fixed and weakly mobile gravel beds." *Journal of Hydraulic Engineering*, 126(9), 679-690.

Nikora, V. I., Koll, K., McLean, S., Dittrich, A., and Aberle, J. (2002). "Zero-plane displacement for rough-bed open-channel flows.".

Nikuradse, J. (1933). "Stromungsgesetze in rauhen Rohren." Heft 361, Berlin.

Papanicolaou, A. N., and Hilldale, R. (2002). "Turbulence characteristics in gradual channel transition." *Journal of Engineering Mechanics-ASCE*, 128(9), 948-960.

Prandtl, L. (1932). "Zur turbulenten Stromung in Rohren und langs Platten." *Ergebnisse der Aerodynamischen Versuchsantalt zu Gottingen*, 4, 18-29.

Rennie, C. D., Fisher, T. S. R., and Millar, R. G. (1999). "Spatial variability of turbulent velocity structure in a natural river.".

Reynolds, A. J. (1974). "Turbulent flows in engineering." John Wiley, New York.

Rotta, J. (1962). "Turbulent boundary layers in incompressible flow." *Progress in Aeronautical Science*, 2, 1-219.

Shields, F. D., Knight, S. S., Testa, S., and Cooper, C. M. (2003). "Use of acoustic Doppler current profilers to describe velocity distributions at the reach scale." *Journal of the American Water Resources Association*, 39(6), 1397-1408.

Simpson, M. (2001). "Discharge Measurements Using a Broad-Band Acoustic Doppler Current Profiler." *Rep. No. Open Report 01-01*, U.S. Geological Survey.

Song, T., and Chiew, Y. M. (2001). "Turbulence measurement in nonuniform open-channel flow using acoustic Doppler velocimeter (ADV)." *Journal of Engineering Mechanics-Asce*, 127(3), 219-232.

Stacey, M. T. (2003). "Estimation of diffusive transport of turbulent kinetic energy from acoustic Doppler current profiler data." *Journal of Atmospheric and Oceanic Technology*, 20(6), 927-935.

Stone, M. C., Tritico, H. M., Hotchkiss, R. H., and Flanagan, P. (2003). "Turbulence characteristics in obstructed gravel bed flow.".

von Karman, T. (1930). "Mechanische ahnlichkeit und turbulenz." *Gottinger Nachrichten, Math. Phys. Klasse*, 58-60.

Wilczak, J. M., Oncley, S. P., and Stage, S. A. (2001). "Sonic anemometer tilt correction algorithms." *Boundary-Layer Meteorology*, 99, 127-150.

Wolman, M. G. (1954). "A method of sampling coarse bed material." *Transactions of the American Geophysical Union*, 35, 951-956.

Chapter 4: Influence of successional development on periphyton disturbance

Abstract

Disturbance is known to be a dominant variable in stream ecology. Disturbance can be the result of hydraulic or physical modifications to the environment. Periphyton assemblages are composed of attached algae, bacteria, and fungi growing on the streambed. The assemblages can be viewed as a necessity or a nuisance depending on stream productivity. Periphyton community structure is highly dependent on disturbance regime. The objective of this research was to investigate temporal variations in periphyton resistance to shear stress. The research was accomplished by colonizing ceramic tiles in a natural stream for various time periods. The tiles were periodically collected and subjected to increasing levels of shear stress in a laboratory flume. The tiles were then analyzed to determine the level of periphyton scour. It was found that periphyton ash free dry mass increased significantly with colony age and time of the growth season. Periphyton resistance to scour increased with colony development but was not significantly influenced by time. The results can be used to improve restoration and management of stream systems.

Introduction

Periphyton assemblages are composed of attached algae, bacteria, and fungi growing on the streambed (Barbour et al. 1999). Periphyton are primary producers and form the base of autochthonous stream food webs. As a result, stream productivity is often dependent on periphyton development. For streams with abundant allochthonous inputs or high nutrient concentrations, periphyton can overwhelm the stream and become a nuisance (Allen 1995). Therefore, understanding periphyton assemblages is an important step for managing and restoring stream functions (Hart and Finelli 1999)

The successional development of periphyton colonies has been studied under a range of conditions. Additionally, the effects of the flow field on periphyton colonies have been investigated by several researchers. However, the influence of successional development on periphyton scour resistance has not been directly investigated. Such knowledge is needed to better understand the influence of natural disturbances and water management on stream processes.

Objectives

The objective of this research was to investigate temporal variation in periphyton resistance to shear stress scour. This objective was met by testing the following hypotheses.

Hypothesis 4: Periphyton ash free dry mass (AFDM) is dependent on the time of the growth season. It is predicted that periphyton assemblages will increase in AFDM with respect to time.

Hypothesis 5: Periphyton AFDM is dependent on successional development. It is predicted that the periphyton AFDM will increase with colony age.

Hypothesis 6: The amount of periphyton scour is dependent on the level of shear stress. It is predicted that periphyton mass scour and percent scour will increase as shear stress is increased.

Hypothesis 7: The effect of shear stress on periphyton scour is dependent on time of the growth season. It is predicted that periphyton mass scour will increase and percent scour will decrease with an increase in time.

Hypothesis 8: The effect of shear stress on periphyton scour is dependent on successional development. It is predicted that periphyton mass scour will increase and percent scour will decrease with colony age.

Background

Successional Development

The temporal sequence of periphyton assemblage development in streams has been the topic of several investigations. Successional development is defined as a directional change or sequence in the relative abundance of species and structure in a community (Poff et al. 1990). The development of periphyton assemblages has been described analogous to higher plant succession, including vertical community development from low to high structures and the progressive slow-down in the rate of succession. This analogy was first made for lentic periphyton assemblages by Hoagland et al. (1982). The authors reported that the periphyton developed from structurally simple, horizontal assemblages, characterized by diatoms and bacteria to more complex vertical communities consisting of an understory of diatoms and an overstory of stalked diatoms and filamentous algae. However, development is less clear for lotic assemblages. Steinman and McIntire (1986) did not observe the analogy between vertical stratification in lotic periphyton and higher plant communities. They found that the taxonomic structure of the periphyton assemblage is apparently determined by several environmental variables, including the species pool and the physical environment.

Periphyton Disturbance

Disturbance is widely recognized as a fundamental determinant of community development in most ecosystems (Poff and Ward 1990). Resistance and recovery of periphyton communities to disturbance are important considerations for stream ecology (Stevenson 1990). Hydraulic disturbance by floods may be the major mechanism controlling differences in periphyton biomass and structure (Biggs and Close 1989).

Further, successional trajectories of periphyton communities are rarely able to evolve to climax stage without interruption (Steinman and McIntire 1986).

Numerous studies have investigated the impact of hydraulic disturbance on periphyton assemblages. Steinman et al. (1990) reported that the type and duration of disturbance may be more important to stream ecosystems than nutrient levels and species interactions. Field studies completed by Biggs and Close (1989) showed that the proportion of periphyton lost in floods of similar magnitude varied among streams and was not a linear function of shear stress. Peterson and Stevenson (1992) reported that resistance was generally lower in slow current communities. The authors concluded that disturbance timing, successional state, and habitat affect the susceptibility to disturbance.

An example of the response of periphyton communities to disturbances was reported by the USGS (1997). The researchers investigated periphyton cell densities before and after two flood events on Big Darby Creek in Ohio. The researchers found that algal-cell densities varied seasonally with scour ranging from 0 to 76%. The diverse range of disturbance responses between streams and events underscores the need for additional research on this topic.

Flow Field Influence on Periphyton

The influence of flow on periphyton communities can be described through two counteracting processes. A rise in velocity produces a steeper diffusion gradient and increased turbulent fluctuations, resulting in greater material exchange of nutrients to the periphyton community (Whitford 1960). Concurrently, increased velocity results in elevated form drag and skin friction causing scour (Horner and Welch 1981). These competing processes would suggest the existence of an optimal flow velocity for

periphyton growth. However, this concept is greatly complicated by tremendous variation in periphyton communities, including taxonomic composition and developmental stage, and environmental variables including water velocity, nutrient concentrations, light, and substrate.

A large number of studies have investigated the relationship between flow and periphyton communities. Stevenson (1983) reported that immigration rates were increased by six-fold when flow velocity was elevated. McIntire (1966) reported that an accumulation of biomass was more rapid for fast currents but similar biomass was observed by the end of the experiments. Horner and Welch (1981) found that the erosive effects of current would retard periphyton accumulation unless nutrient availability was high enough to be influenced by turbulent diffusion. Nikora et al. (1998) developed a conceptual model of the interaction between periphyton and flow. The authors described three regions of periphyton-flow interaction: buoyancy dominant, drag dominant, or both forces important. The model was tested with laboratory experiments. These results support the concept of offsetting mechanisms between increased diffusion and scour from increased velocity.

The complex relationships between the flow field and aquatic organisms can be better understood by investigating more advanced flow metrics (Godillot et al. 2001; Crowder and Diplas 2002). Shear stress is a result of near bed velocity gradients and turbulent velocity fluctuations. Thus, it is an appropriate parameter for investigating the counteracting processes of near bed diffusion and flow induced scour. Biggs and Thomsen (1995) investigated the resistance of stream periphyton to structural disturbance by subjecting samples to increasing levels of shear stress. Results showed that shear

stress can potentially have widely differing effects on periphyton depending on the initial taxonomic composition of resident communities.

A description of flow field parameters, measurement techniques, and calculation procedures can be found in Chapter 2 and Appendix C.

Methods

The experiment involved periphyton colonization of ceramic tiles in a stream and shear stress tests in a laboratory flume. Two sets of tiles were placed in the study stream representing "developed" and "time-specific" conditions. The entire developed tile set was placed in the stream at the onset of the project and collected incrementally, every two weeks, throughout the study. The time-specific tiles were collected and replaced every two weeks. The procedure was conducted over a three month period for a total of six sampling events. Following tile collection, the samples were exposed to four shear stress levels in a laboratory flume to evaluate scour tolerance. Periphyton ash free dry mass (AFDM) was evaluated for pre- and post-shear stress test conditions. Periphyton scour was analyzed as the change in AFDM and percentage of AFDM removed.

Field sample collection

The samples were colonized in a straight reach of the South Fork of Palouse River in Pullman, Washington. Twelve 6.45cm^2 (1 square-inch) unglazed ceramic tiles were placed in a series of custom built periphytometers. The periphytometers were built from small acrylic rectangles (10cm x 35cm) with a groove beveled down the center. The tiles were flush with the top of the periphytometers. The periphytometers were fixed to the streambed with wire pins. Seventy-two tiles were initially placed in the stream (60 developed and 12 time-specific). After two weeks, twelve developed and twelve time-specific tiles were collected from the periphytometers (Figure 4.1).

Figure 4.1. Periphytometer holding ceramic tiles following river collection

The tiles were stored in plastic containers with water from the sample site and transferred to Albrook Hydraulics Laboratory. Twelve new tiles were placed in the time-specific periphytometer to start colonization for collection two weeks later.

Laboratory experiments

The shear stress tests were conduced in a tilting flume, located in Albrook Hydraulics Laboratory at Washington State University. The flume is 21m long, 0.89m wide and 0.21m deep. To resemble the hydraulic characteristics of a natural stream, a 2m by 0.89m gravel covered fiberboard was attached to the flume bottom. A periphytometer was attached to the downstream side of the fiberboard (Figure 4.2). The periphytometer was planed flush with the fiberboard. The flume slope and discharge were adjusted to produce the desired bed shear stress, estimated using Equation 2.11. The local bed shear stress above the sample tiles was determined by measuring the velocity and τ_R profiles with an acoustic Doppler velocimeter (ADV). To verify fully developed flow conditions, the velocity profile and bed shear stress was also measured 0.5m upstream from the sample tiles. Details of the flow measurements can be found in Appendix E and are summarized in Table 4.1. The tiles were exposed to the flow for 20 minutes each, as suggested by Biggs and Thomsen (1995).

Table 4.1. Estimated and measured shear stress levels

Method	Shear Stress (N/M^2)			
Slope Estimate, Eq. 2.11	10.1	20.0	30.0	40.1
ADV, above Tiles, Eq. 2.13	12.1	22.1	29.4	43.8
ADV, 0.5m upstream, Eq. 2.13	12.4	21.4	28.1	42.1

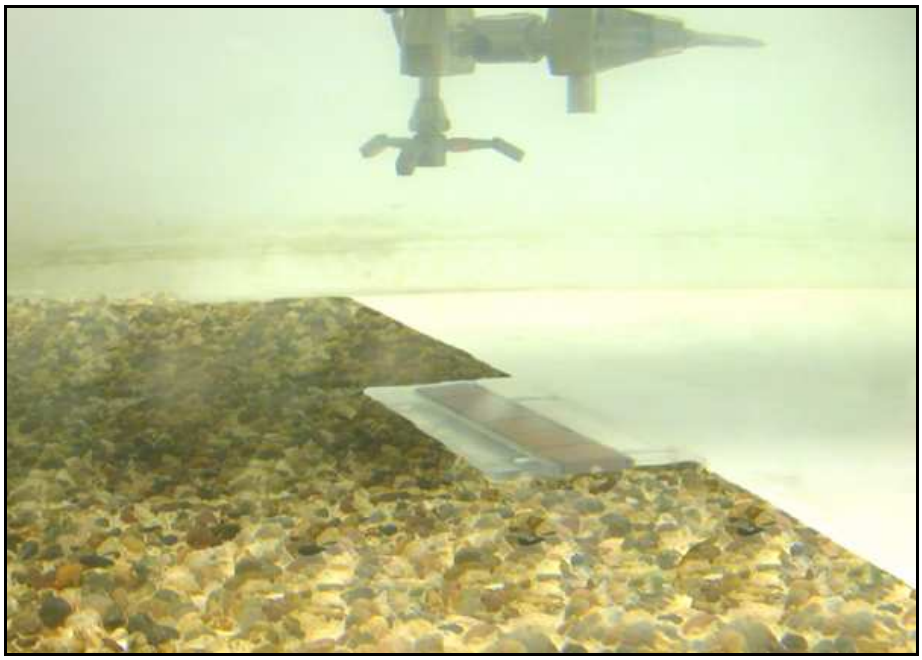

Figure 4.2. Periphytometer, gravel fiberboard, and ADV in the tilting flume

Figure 4.3 contains water surface elevations required in the colonization cross section to produce the first three shear stress values (10, 20, and 30 N/m^2), bank full discharge, maximum shear stress, and the 100 year flood. The bank full discharge was estimated at 47 cms, producing a shear stress of 36 N/m^2. The maximum shear stress achievable in this reach is 39 N/m^2, resulting from a discharge of 68 cms. Figure E.5 contains shear stress, water surface elevation, top width, and flow area as a function of discharge. These estimates were produced with a HEC-RAS simulation of the colonization reach.

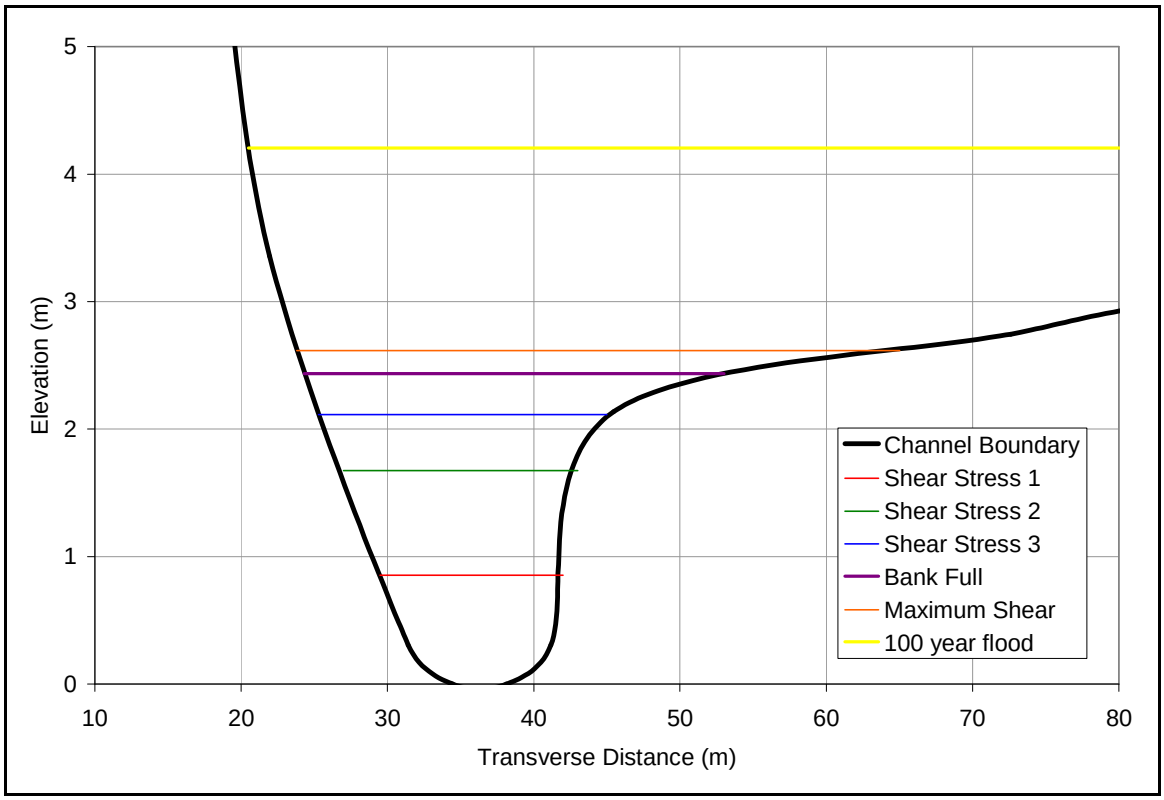

Figure 4.3. Water surface elevations in the colonization reach to produce the shear stress test levels.

Following each shear stress test, the tiles were removed from the periphytometers and the remaining periphyton was scraped from the tile surface using a razor blade. The AFDM for each sample was determined using standard methods (Hauer and Lamberti, 1998). Mass scour was calculated as the difference in AFDM between the sample and control. Percent scour of AFDM was also calculated by dividing the mass scour by the control mass.

Results

The project hypotheses were tested through a series of analysis of variance (ANOVA) statistical tests. The significant relationships were further investigated through linear regression analyses. The results from these tests are discussed below.

Hypothesis 4 (AFDM as a function of time of the growth season)

A one-way between ANOVA with 6 levels was conducted in order to test Hypothesis 4. Independent variables were time (6 levels) and control. The dependent variable was AFDM. The result was significant ($F(5, 41)= 6.60$, $p<0.001$), such that AFDM increased as time increased. In other words, AFDM increased significantly throughout the growth season. The analysis was limited to the time-dependent samples to eliminate the influence of successional development. Therefore, all samples were colonized for two weeks. Periphyton AFDM as a function of time is shown in Figure 4.3. A linear-regression was used to further evaluate the relationship. An R^2 value of 0.81 was found.

Hypothesis 5 (AFDM as a function of successional development)

A one-way within ANOVA with 6 levels was conducted in order to test Hypothesis 5. Independent variables were age (6 levels) and control (shear stress=0). The dependent variable was AFDM. The result was significant ($F(5, 86)= 71.24$, $p<0.001$), such that AFDM increased as age increased. In other words, AFDM increased with periphyton successional development. AFDM is plotted as a function of colony age in Figure 4.4. A linear-regression of this relationship produced an R^2 value of 0.83.

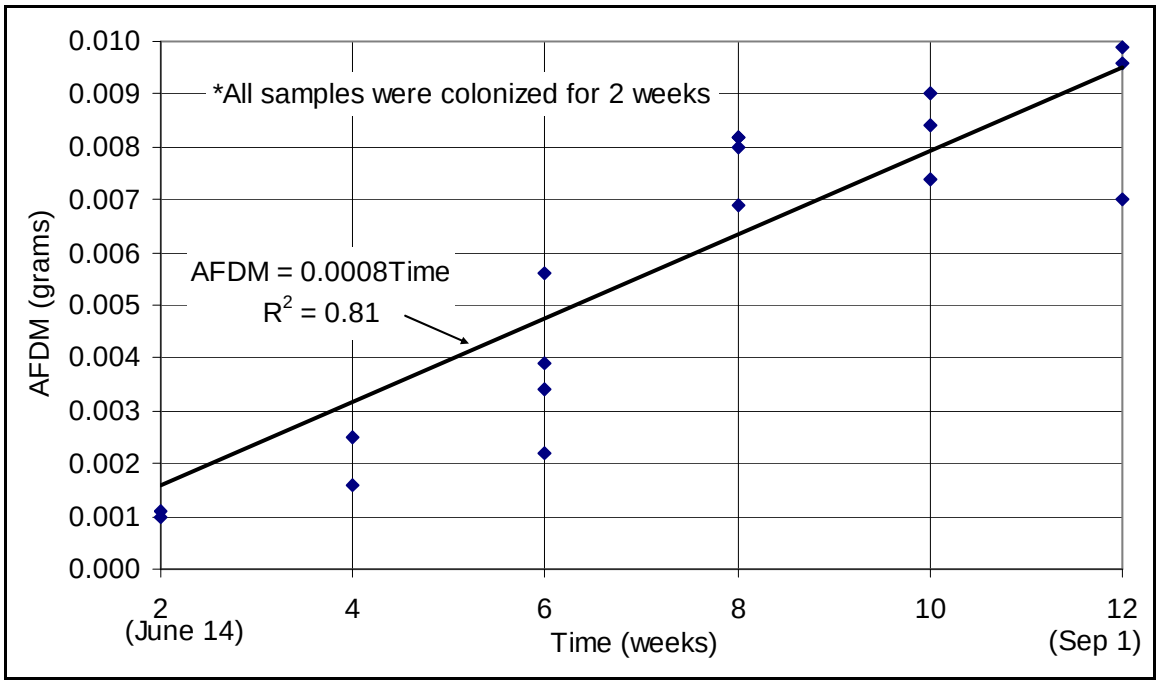

Figure 4.4. Periphyton AFDM versus time of the experimental growth season

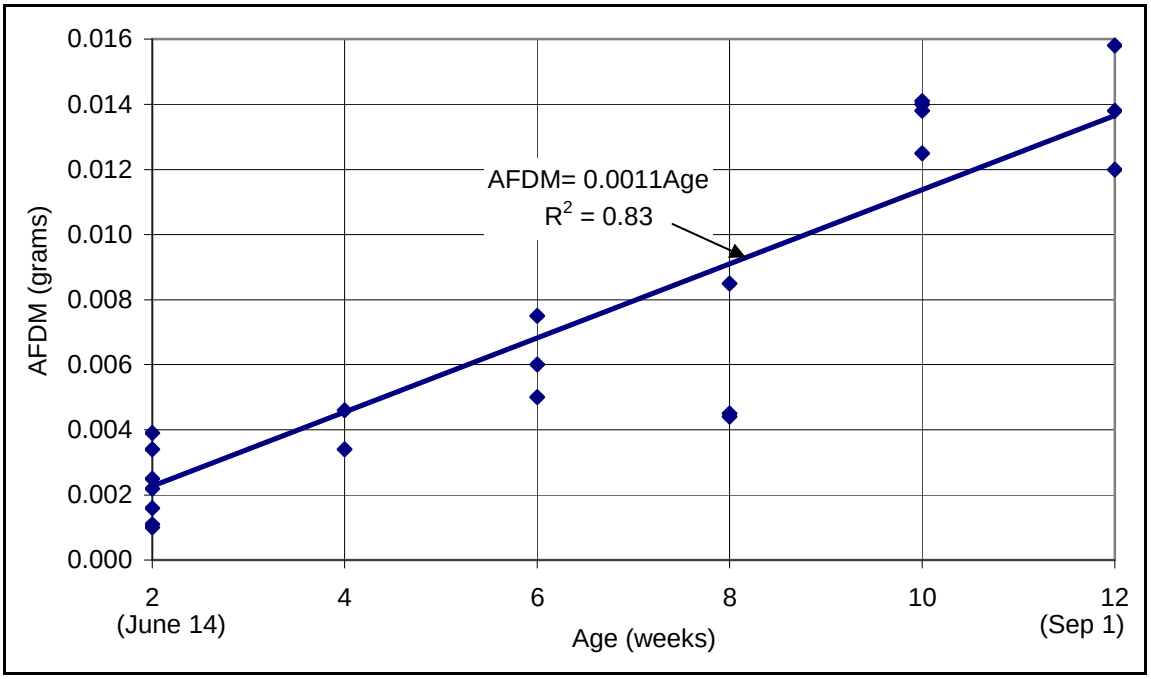

Figure 4.5. Periphyton AFDM versus colony age (successional development)

Hypothesis 6 (periphyton scour as a function of shear stress)

Two one-way between ANOVA tests with 4 levels were conducted in order to test Hypothesis 6. The independent variable was shear stress (4 levels) and dependent variables were mass scour and percent scour. The results for both dependent variables were significant (mass scour $F(3, 87)= 12.81$, $p<0.005$; percent scour $F(3, 87)= 20.43$, $p<0.001$), such that both mass scour and percent scour increased as shear stress increased. In other words, an increase in shear stress level caused an increase in periphyton scour. Mass scour and percent scour are plotted versus shear stress level in Figure 4.5. The mass scour and percent scour R^2 values were 0.96 and 0.99 respectively.

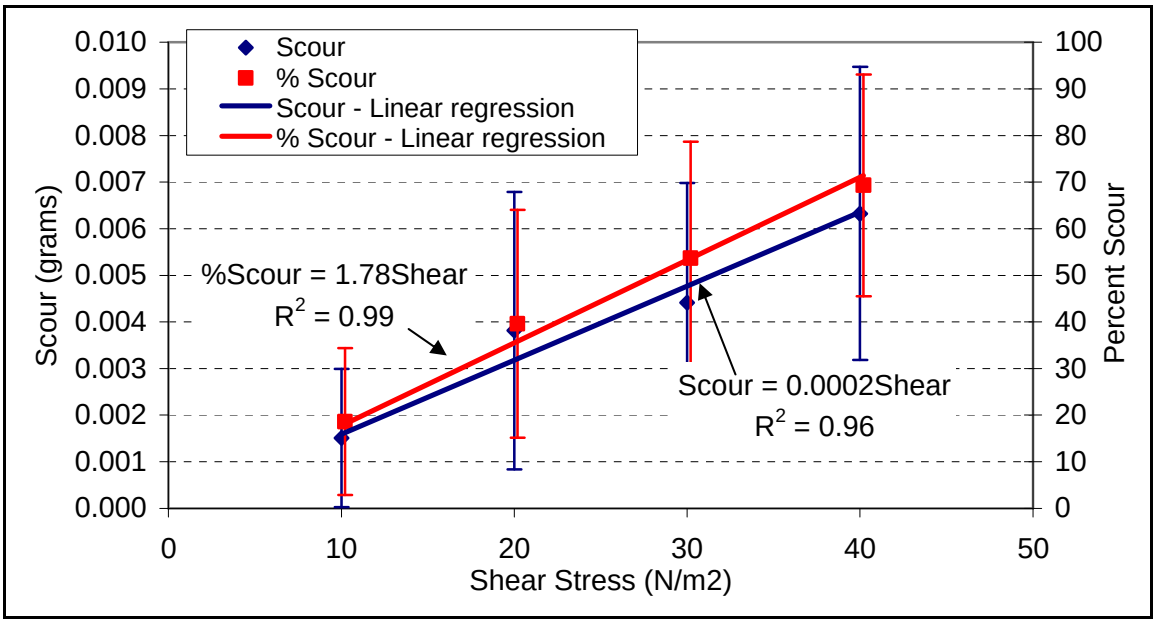

Figure 4.6. Periphyton mass and percent scour versus shear stress (error bars show max and min)

Hypothesis 7 (periphyton scour as a function of time of the growth season)

Two one-way between ANOVA tests with 6 levels were conducted in order to test Hypothesis 7. The independent variable was time (6 levels) and the dependent variables

were mass scour and percent scour. The result for mass scour was significant ($F(5, 87)= 15.76$, $p<0.001$), such that mass scour increased as time increased. However, there was no statistical significance in the effect of time on percent scour ($F(5, 87)= 0.89$, $p=0.448$). The results may be explained by increased AFDM throughout the growth season. Mass scour increased due to increased mass of periphyton. Mass scour and percent scour are plotted versus time in Figure 4.6. A linear-regression was fitted to the mass scour data to further investigate the relationship between mass scour and time. The resulting R^2 value was 0.87.

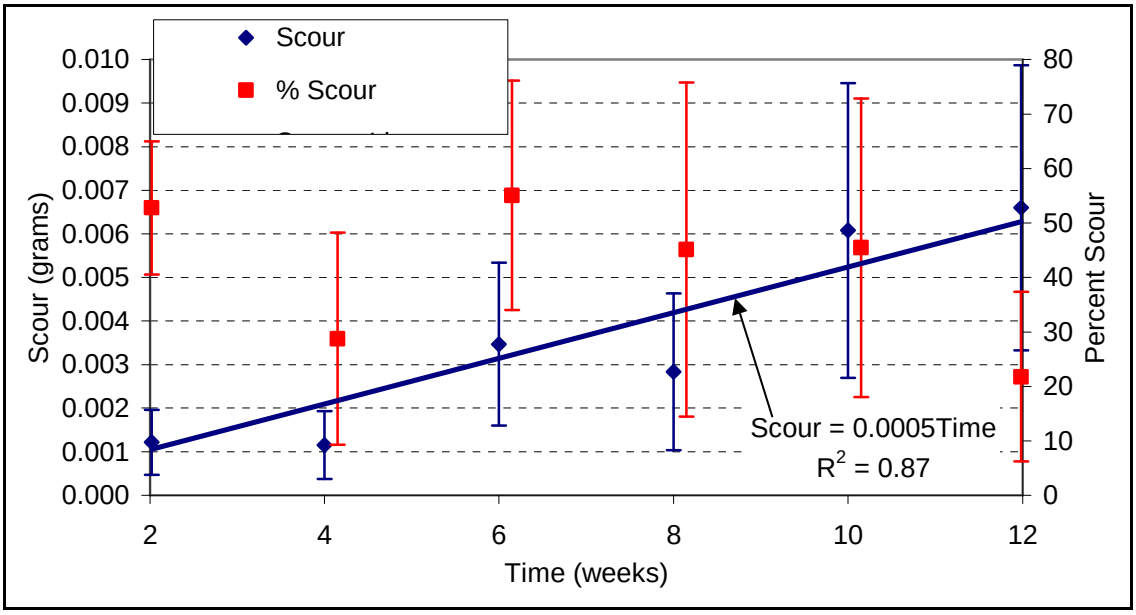

Figure 4.7. Periphyton mass and percent scour versus time of the growth season

Hypothesis 8 (periphyton scour as a function of successional development)

Two one-way between ANOVA tests with 6 levels were conducted in order to test Hypothesis 8. The independent variable was successional development or age (6 levels) and the dependent variables were mass scour and percent scour. The results for both mass scour and percent scour were significant, such that mass scour increased as periphyton

assemblage age increased ($F(5, 86)= 5.218$, $p<0.001$) whereas percent scour decreased as age increased ($F(5, 86)= 5.687$, $p<0.001$). The results are consistent with the findings in Hypothesis 3 and highly relevant to the findings in Hypothesis 6. Mass scour increased because of the increase in AFDM and percent scour decreased due to increased resistance to scour. Periphyton mass scour and percent scour are plotted as functions of colony age in Figure 4.7. Linear-regression functions were fitted to both datasets. The regressions resulted in R^2 values of 0.89 and 0.86 for mass scour and percent scour, respectively.

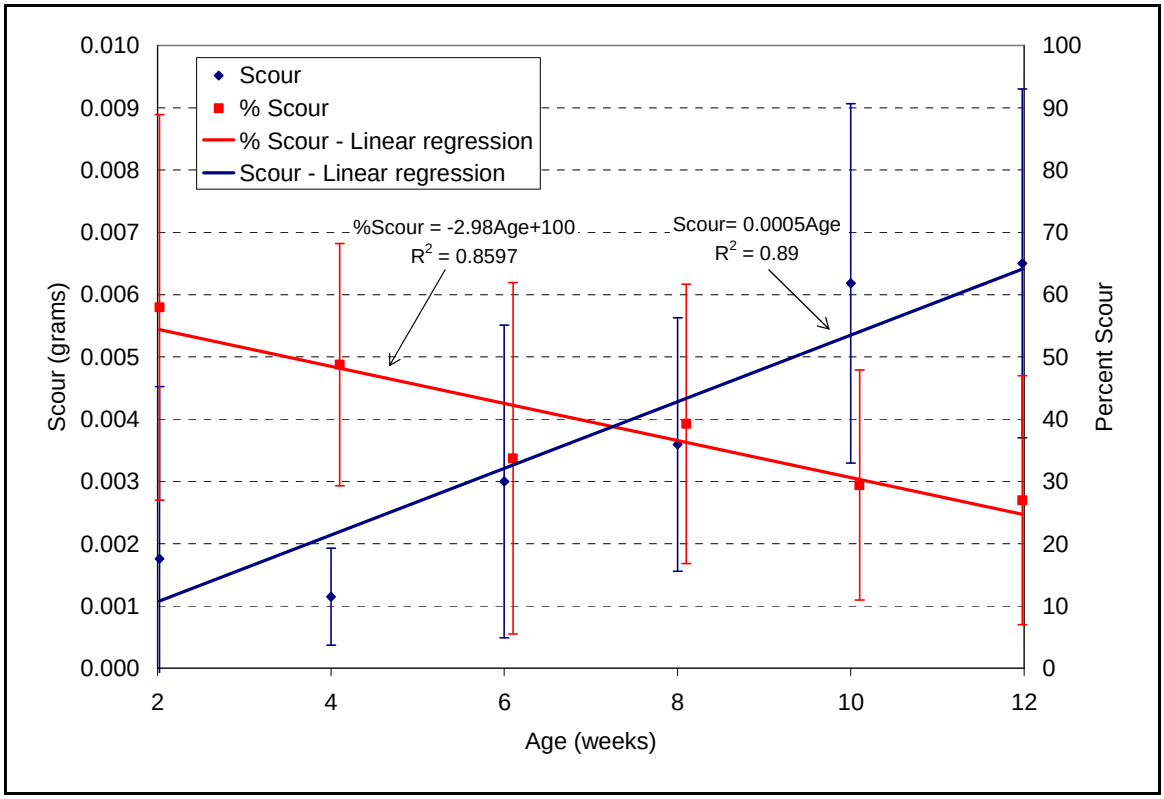

Figure 4.8. Periphyton mass scour and percent scour versus age (successional development)

Conclusion

The experimental results confirmed that AFDM increased with time through the growth season and with successional development of the periphyton colony. Additionally, periphyton mass scour and percent scour increased significantly with shear stress through the experimental range. The AFDM results provide insight for interpretation of scour results and the shear stress tests verify the appropriateness of the selected shear stress levels. Further the high R^2 values indicate that these processes are described well as linear relationships.

The periphyton mass scour increased with time of the growth season, but the percent scour did not change significantly. This suggests that periphyton resistance to shear stress is not a function of time of the growth season. The increase in mass scour can be explained through the increase in AFDM through the growth season.

The mass periphyton scour increased with successional development. However, percent scour decreased with successional development. These results suggest that periphyton resistance to shear stress scour increases with successional development. The increase in mass scour is explained by the increase in AFDM with colony development.

These results have increased our knowledge of the impacts of disturbance on stream ecosystems and improved our ability to restore stream processes and functions. The significance can be demonstrated through the example of reservoir release schedules. In river systems in which excess periphyton is a nuisance, reservoir discharge can be scheduled to manage the colonies. Although greater periphyton mass can be removed later in the growth season, advanced periphyton colony development will increase

resistance to disturbance. The best results would be achieved through frequent flushing flows that prevent advanced successional development.

On the other hand, preservation of periphyton colonies is desired for energy limited streams. For such systems, it is desirable to promote successional development of the periphyton colonies and avoid late season flushing flows. A natural flow regime with a spring flush and low summer flows would be desirable.

Although this research provides insight to the influence of temporal variables on periphyton response to shear stress scour, several limitations exist. First, the colonized slides were all collected from a single stream station. Future research should be conducted in multiple streams with tiles colonized in a range of hydraulic conditions. Second, this research was conducted over a three month time period. Observations over a complete year or multiple years would provide improved information. Finally, biological analyses were limited to AFDM. Future experiments should investigate more advanced biological variables such as chlorophyll concentrations and taxonomic structure.

References

Allen, J. D. (1995). "Stream Ecology: structure and function of running waters." Chapman and Hall, London, UK.

Barbour, M. T., Gerritsen, J., Snyder, B. D., and Stribling, J. B. (1999). "Rapid Bioassessment Protocols for Use in Streams and Wadeable Rivers: Periphyton, Benthic Macroinvertebrates and Fish, Second Edition." *Rep. No. EPA 841-B-99-002*, U.S. Environmental Protection Agency; Office of Water, Washington, D.C.

Biggs, B. J. F., and Close, M. E. (1989). "Periphyton biomass dynamics in gravel bed rivers: the relative effects of flow and nutrients." *Freshwater Biology*, 22, 209-231.

Biggs, B. J. F., and Thomsen, H. A. (1995). "Disturbance of Stream Periphyton by Perturbations in Shear-Stress - Time to Structural Failure and Differences in Community Resistance." *Journal of Phycology*, 31(2), 233-241.

Crowder, D. W., and Diplas, P. (2002). "Vorticity and circulation: spatial metrics for evaluating flow complexity in stream habitats." *Canadian Journal of Fisheries and Aquatic Sciences*, 59(4), 633-645.

Godillot, R., Caussade, B., Ameziane, T., and Capblancq, J. (2001). "Interplay between turbulence and periphyton in rough open-channel flow." *Journal of Hydraulic Research*, 39(3), 227-239.

Hart, D. D., and Finelli, C. M. (1999). "Physical-biological coupling in streams: The pervasive effects of flow on benthic organisms." *Annual Review of Ecology and Systematics*, 30, 363-395.

Hauer, F. R., and Lamberti, G. A. (1998). "Methods in Stream Ecology." Academic Press, San Diego, CA.

Hoagland, K. D., Roemer, S. C., and Rosowski, J. R. (1982). "Colonization and community structure of two periphyton assemblages, with emphasis on the diatoms (Bacillariophyceae)." *American Journal of Botany*, 69(2), 188-213.

Horner, R. R., and Welch, E. B. (1981). "Stream periphyton development in relation to current velocity and nutrients." *Canadian Journal of Fisheries and Aquatic Sciences*, 38, 449-457.

McIntire, C. D. (1966). "Some Effects of Current Velocity on Periphyton Communities in Laboratory Streams." *Hydrobiologia*, 27, 559-570.

Nezu, I., and Nakagawa, H. (1993). "Turbulence in open-channel flows." A.A.Balkema, Rotterdam,Netherlands/Brookfield,VT.

Nikora, V. I., Goring, D. G., and Biggs, B. J. F. (1998). "A simple model of stream periphyton-flow interactions." *Oikos*, 81(3), 607-611.

Peterson, C. G., and Stevenson, R. J. (1992). "Resistance and Resilience of Lotic Algal Communities - Importance of Disturbance Timing and Current." *Ecology*, 73(4), 1445-1461.

Poff, N. L., Voelz, N. J., Ward, J. V., and Lee, R. E. (1990). "Algal Colonization Under Four Experimentally-Controlled Current Regimes in A High Mountain Stream." *Journal of the North American Benthological Society*, 9(4), 303-318.

Poff, N. L., and Ward, J. V. (1990). "Physical Habitat Template of Lotic Systems - Recovery in the Context of Historical Pattern of Spatiotemporal Heterogeneity." *Environmental Management*, 14(5), 629-645.

Steinman, A. D., and McIntire, C. D. (1986). "Effects of current velocity and light energy on the structure of periphyton assemblages in laboratory streams." *Journal of Phycology*, 22, 352-361.

Steinman, A. D., Mulholland, P. J., Palumbo, A. V., Flum, T. F., Elwood, J. W., and DeAngelis, D. L. (1990). "Resistance of lotic ecosystems to a light elimination disturbance: a laboratory stream study." *Oikos*, 58, 80-90.

Stevenson, R. J. (1983). "Effects of current and conditions simulating autogenically changing microhabitats on benthic diatom immigration." *Ecology*, 64(6), 1514-1524.

Stevenson, R. J. (1990). "Benthic algal community dynamics in a stream during and after a spate." *Journal of the North American Benthological Society*, 9(3), 277-288.

United States Geological Survey (1997). "Hydrologic disturbance and response of aquatic biota in Big Darby Creek basin, Ohio." *Rep. No. Water resources investigations report, 96-4315*.

Whitford, L. A. (1960). "The Current Effect and Growth of Fresh-Water Algae." *Transactions of the microbiological society*, 79, 302-309.

Chapter 5: Summary

Hydropower development, channelization, water withdrawals, land use changes, and other anthropogenic activities have caused severe damage to aquatic ecosystems. To restore ecosystem processes and functions, we must advance our knowledge of these systems. This requires a better understanding of physical flow features and the influence of these features on aquatic organisms. The goal of this research was to improve descriptions of natural stream flow fields and the influence of flow on periphyton assemblages. This goal was met through a combination of field observations and laboratory experiments. Project objectives and results are summarized below.

Natural Stream Flow Field Measurements

Improving descriptions of natural stream flow fields is a critical step in restoring aquatic ecosystems. However, knowledge of velocity and turbulence distributions in natural streams is limited to laboratory derived empirical equations. Further, these equations have not been validated in natural streams. The objective of this research was a) to evaluate the adequacy of existing empirical relationships for describing natural stream flow fields and b) to investigate spatial distributions of flow variables. This objective was accomplished by conduction ADV measurements in two cobble-bed streams. The measured data was compared with empirical predictions using statistical techniques. The results showed that velocity distributions were adequately predicted with the log-law for all stream units and transverse locations. The linear Reynolds shear stress distribution adequately predicted observed values. However, empirical turbulence intensity, turbulent kinetic energy, and integral length scale equations inadequately described measured

values. A high level of spatial heterogeneity was observed between stream units (riffles, pools, and runs) but not between different depths.

These results have important implications for the understanding of flow fields because they contradict existing concepts of open channel turbulence. This study found that turbulence generation at the bed with diffusion to the surface was not the dominant mechanism. This can be explained through substantial turbulence generation associated with stream banks, bed-forms, vegetation, obstructions, channel curvature, and other channel features. This finding suggests that a different approach must be used in the prediction of natural stream turbulence. A turbulent kinetic energy budget approach, which accounts for turbulence generation from the channel features, is recommended to improve estimates of turbulence distributions.

This study also provides the first comprehensive quantifiable description of flow characteristics for stream units (riffles, runs, and pools). This information will improve communication between biologists, engineers, geologists, and other professionals working in the riverine environment. Further, the data gathered through this study will improve parameterization of stream numerical models.

This research was limited to two sample reaches. Further, measurements were taken at a fairly course spatial resolution. Future work should investigate additional reaches with a wider range of hydraulic and geometric characteristics. An array of ADVs would provide greater data resolution. Instrument advancements, such as the use of ADCPs may also improve the quality and resolution of measurements.

ADCP Measurements

The flow field observations described above demonstrate the limitations to point measurement techniques. ADCPs provide a promising alternative to traditional point-velocity measurements. However, these instruments have not been thoroughly tested against accepted measurement techniques in natural streams. The objective of this research was to evaluate the adequacy of ADCP to measure velocity, turbulence, and shear stress distributions in cobble bed rivers. This was accomplished by comparing ADCP and ADV measurements at nine coincident stations in two rivers. Results showed that the ADCP accurately measured velocity magnitude but under-evaluated the streamwise velocity component. ADCP measured velocity profiles closely resembled theoretical logarithmic distributions. Investigation of turbulence parameters revealed the inadequacy of ADCP turbulence measurements in this environment. Analysis of turbulent scales and spectral densities showed that ADCP sampling frequency was too low and the sampling region too large to adequately capture turbulence structure. Comparison of shear stress results showed that ADCP values derived from velocity magnitudes, using the log-law, adequately estimated ADV results.

These results support the use of ADCP instruments to measure velocity magnitude and shear stress. This will greatly improve our ability to measure natural stream flow fields for numerical model calibration, habitat assessments, and other investigations. This has broad implications considering the use of thousands of ADCPs by the USGS and other agencies. However, the results indicate that ADCP turbulence measurements should not be used in this environment.

This research was limited to measurements at nine stations in two rivers. This study should be expanded to a wider range of flow conditions. Further, for consistency all measurements were conducted with the standard instrument configuration. Future work should investigate the influence of configuration variables on instrument performance. For example, bin size, water mode, blanking distance, and pings per ensemble should be tested and optimized.

Periphyton Disturbance

Disturbance is known to be a dominant variable in stream ecology. Periphyton community structure is highly dependent on disturbance regime. The objective of this research was to investigate temporal variations in periphyton resistance to shear stress scour. This was accomplished by colonizing ceramic tiles in a natural stream for various time periods. The tiles were periodically collected and subjected to increasing levels of shear stress in a laboratory flume. The tiles were then analyzed to determine the level of periphyton scour. Results confirmed that AFDM increased with time through the growth season and with successional development of the periphyton colony. Additionally, periphyton mass scour and percent scour increased significantly with shear stress through the experimental range. The periphyton mass scour increased with time of the growth season, but the percent scour did not change significantly. The mass periphyton scour increased with successional development. However, percent scour decreased with successional development. These results suggest that periphyton resistance to shear stress scour increases with successional development.

These results increased our knowledge of the impacts of disturbance on stream ecosystems and improved our ability to restore stream processes and functions. This

knowledge can be used to improve reservoir release management, stream restoration efforts, and evaluation of instream flow. For example, results indicate that frequent flushing flows should be applied to control nuisance periphyton while a spring flush which emulates natural conditions should be used to protect essential assemblages.

Proposed Future Research

Flow Field Descriptions

To further the investigation of turbulence in natural streams, development of a conceptual TKE budget is proposed. Such a model would account for TKE sources, diffusion and dissipation. The TKE transport equation would be used as the basis for this approach.

$$\frac{D(TKE)}{Dt} = -\underbrace{\left(\overline{u_j' p'} + \rho \overline{u_j' \frac{u_i' u_i'}{2}} \right)_{,j}}_{Term\ I} - \underbrace{\rho \overline{u_i' u_j'} \overline{u_{i,j}}}_{Term\ II} + \underbrace{\mu \left(\overline{u_i' u_{i,j}'} \right)_{,j}}_{Term\ III} - \underbrace{\mu \overline{u_{i,j}' u_{i,j}'}}_{Term\ IV} \quad \text{(Equation 5.1)}$$

Term I represents diffusion of TKE, Term II is TKE production, Term III is the work done against TKE by viscous effects (usually neglected), and Term IV is TKE dissipation.

Generation of TKE is associated with areas of high strain rate, typically near the bed, banks, and obstructions. The conceptual model would quantify the contribution of TKE from these sources, such as TKE production per square unit of bed. The bed TKE production would be a function of flow Reynolds and Froude numbers, particle Reynolds number, and turbulence Reynolds number. The diffusion and dissipation would also be functions of the Reynolds and Froude numbers. By establishing general predictions of these terms as functions of environmental variables, the budget can be applied to estimate TKE distributions throughout the reach.

To develop such a model, an intensive flow measurement and modeling exercise is proposed. This would involve combined ADV and ADCP sampling in several river reaches with diverse characteristics. A series of ADVs should be used to investigate TKE distributions near boundaries, including the bed, banks, and obstructions. The ADV array should also be used to quantify TKE diffusion and dissipation. An ADCP should be used to thoroughly map the flow field. Moving-vessel measurements should be conducted to map velocity distributions. Stationary-vessel measurements of velocity profiles and bed shear stress should also be completed. ADCP measurements could also be used to supplement survey data of stream geometry.

Although a great deal of information could be gained from the measuring routine described above, a numerical model will allow for a deeper investigation into flow features and extrapolation to a wider range of flow conditions. The most appropriate modeling technique should be selected based on available resources and latest technology. Direct numerical simulation (DNS) is not yet feasible for complex flow fields, and large eddy simulation (LES) models have not been applied at high Reynolds numbers and are likely not yet feasible for natural streams. A Reynolds stress model or k-ε model are probably more likely alternatives. These approaches do not directly model TKE transport and would provide much less insight than DNS or LES. A possible compromise could be the sub-depth scale approach proposed by Nadaoka and Yagi (1998), which separates the energy cascade into multiple ranges.

This intensive measuring and modeling approach should be applied to several reaches, with increasing levels of hydraulic complexity. A test case could be developed in a laboratory flume and then expanded to natural streams. Further, the intensive sampling

reaches could be completed in cooperation with biological experiments to investigate linkages between the flow field and ecological processes.

ADCP Experiments

The current research validates the use of ADCP velocity and shear stress measurements. To utilize the thousands of ADCPs currently in use by the USGS and other agencies, it is proposed to expand on the work by Crowder and Diplas (2002) and Shields (2003) by developing habitat suitability indices based on ADCP data. Such functions could improve traditional point metrics used in models such as PHABSIM, by incorporating spatial flow features known to be important for habitat.

This research should be completed through combined ADCP flow measurements and biological observations. Fish utilization could be monitored with traditional techniques, such as snorkeling, or with advanced technology, such as acoustic cameras. Previously proposed metrics (Crowder and Diplas 2002) should be tested in addition to the development of new parameters.

The knowledge gained through this approach could be used to improve existing habitat evaluation techniques, such as PHABSIM, or to develop more advanced methods based on 2D or 3D models. This work could be conducted in concert with the intensive flow field investigation described above.

Periphyton Investigations

The goal of future work in this area is to develop a predictive model to evaluate the effects of water management and restoration efforts on periphyton assemblages. This work should expand on this study and also investigate in-stream periphyton colonies. The

current work should be extended by colonizing tiles in a wider range of streams and by conducting experiments for a much longer period of time.

In-stream experiments should include long-term, continuous monitoring of periphyton assemblages, flow characteristics, and environmental variables including light, temperature, and nutrient concentrations. These observations should be completed in a wide range of background conditions. Due to high spatial and temporal variability in periphyton assemblages and the large number of environmental variables, it will likely require a very large number of samples to develop a predictive model.

The end result of this work will be a numerical model that allows engineers to predict the influence of management and design decisions on periphyton assemblages. For example, reservoir release schedules could be simulated to optimize ecological impacts. This model would also allow for optimization of stream restoration designs.

Conclusion

This research has improved understanding of natural stream flow fields, advanced flow field measurement techniques, and improved knowledge of the impacts of disturbance on periphyton assemblages. Results have fundamental and applied implications for advancing understanding, management, and restoration of streams and rivers.

References

Crowder, D. W., and Diplas, P. (2002). "Vorticity and circulation: spatial metrics for evaluating flow complexity in stream habitats." *Canadian Journal of Fisheries and Aquatic Sciences*, 59(4), 633-645.

Nadaoka, K., and Yagi, H. (1998). "Shallow-water turbulence modeling and horizontal large-eddy computation of river flow." *Journal of Hydraulic Engineering*, 124(5), 493-500.

Shields, F. D., Knight, S. S., Testa, S., and Cooper, C. M. (2003). "Use of acoustic Doppler current profilers to describe velocity distributions at the reach scale." *Journal of the American Water Resources Association*, 39(6), 1397-1408.

Appendix A: Open Channel Turbulence

Turbulent transport of momentum, heat, and mass dominates the flow field of natural streams. Turbulence influences nearly all open channel properties and processes including velocity and shear stress distributions, energy loss, sediment transport, contaminant mixing, and aquatic habitat. Turbulence measurements in water flows began in the 1970s with the advent of hot-film anemometers and flow visualization techniques. Subsequently, numerous open channel turbulence observations have been completed. However, most investigations have been completed in laboratory flumes or in uniform artificial channels. This appendix will introduce turbulence concepts and review previous research on this topic.

The following definition of turbulence will be used for this report:

"The small-scale flow variations correlated with each other in space and time superimposed on the main large-scale flow."

Small-scale is defined as less than physical constraints (i.e. flow depth and channel width). Turbulent flow contains fluid particles with ordered motion which experience a life cycle including birth, development, interactions, and breakdown. These fluid particles, often referred to as eddies, are created in regions of shear and decompose into smaller parcels in a process known as the energy cascade. Eventually the coherent structures decompose to the Kolmogoroff scale at which point they dissipate due to viscosity. Hence, eddy scales are constrained by stream geometry (large scale) and viscosity (small scale).

Basic Equations

In order to understand the concepts of open channel turbulence, it is necessary to examine the basic equations of motion. The Navier-Stokes equations for open channel flow can be represented as (White 1991):

$$\rho \frac{\partial u_i}{\partial t} + \rho u_{i,j} u_j = \rho g_i - p_{,i} + \mu u_{i,jj} \qquad \text{(Equation A.1a)}$$

$$\frac{\partial \rho}{\partial t} + \left(u_i \rho\right)_{,i} = 0 \qquad \text{(Equation A.1b)}$$

where i=x, y, and z, u_i is the instantaneous velocity in the streamwise, transverse, and vertical directions, ρ and μ are the fluid density and viscosity respectively, p is the mechanical pressure, and g is the gravitational acceleration.

In order to apply the Navier-Stokes equations to engineering flows, A.J. Reynolds introduced the concept of time-averaged flows. Reynolds decomposed the velocity into three elements (Reynolds 1974):

$$u_i' = u_i - \overline{u}_i \qquad \text{(Equation A.2)}$$

where u_i', u_i, and $\overline{u}_i$ denote the fluctuating, instantaneous, and time averaged velocities, respectively. Reynolds used this concept to time-average the Navier-Stokes equations as follows:

$$\rho \frac{\partial \overline{u}_i}{\partial t} + \rho \overline{u}_{i,j}\, \overline{u}_j = \rho g_i - \overline{p}_{,i} + \mu \overline{u}_{i,jj} - \rho\left(\overline{u_i' u_j'}\right)_{,j} \qquad \text{(Equation A.3a)}$$

$$\overline{u_{i,i}} = 0 \qquad \text{(Equation A.3b)}$$

where the terms $\rho\left(\overline{u_i' u_j'}\right)_{,j}$ are referred to as the Reynolds shear stresses. The Reynolds shear stresses arise from momentum exchange through turbulent kinetic energy. The

result is a new apparent stress analogous to viscosity but attributed to the flow rather than the fluid. Equations A.3a and A.3b are referred to as the Reynolds Averaged Navier-Stokes (RANS) equations.

Turbulent flow can be further described using the concept of the kinetic energy associated with the turbulence. It is possible to define the turbulent kinetic energy (TKE) as:

$$TKE = \frac{\overline{u_i u_i}}{2} \qquad \text{(Equation A.4)}$$

A fundamental equation for k can be derived using the Navier-Stokes equations. The resulting turbulent kinetic energy equation is:

$$\frac{D(TKE)}{Dt} = -\underbrace{\left(\overline{u'_j p'} + \rho \overline{u'_j \frac{u'_i u'_i}{2}} \right)_{,j}}_{Term\ I} - \underbrace{\rho \overline{u'_i u'_j} \overline{u_{i,j}}}_{Term\ II} + \underbrace{\mu \left(\overline{u'_i u'_{i,j}} \right)_{,j}}_{Term\ III} - \underbrace{\mu \overline{u'_{i,j} u'_{i,j}}}_{Term\ IV} \qquad \text{(Equation A.5)}$$

Term I represents diffusion of TKE, Term II is TKE production from velocity gradients, Term III is the work done against TKE by viscous effects (usually neglected), and Term IV is TKE dissipation. The TKE equation can be used to improve experimental design and data analysis.

Nikora et al. (2001) separated the flow field into five conceptual layers as described below and illustrated in Figure A.1. These layers improve our ability to describe and communicate flow field characteristics.

Outer layer: The viscous effects and form induced fluxes are negligible and the spatially averaged equations are identical to the time-averaged equations. The velocity distribution in this layer is described by the velocity defect law. The outer only exists under relatively low relative roughness and in the top 10 to 20% of the water column.

Logarithmic layer: The viscous effects and form-induced fluxes are negligible the distribution of in this layer follows the logarithmic formula. A condition for the existence of this layer is H >>d_{50}.The logarithmic layer occupies the flow region $2d_{50}$ < z/H < 0.7H.

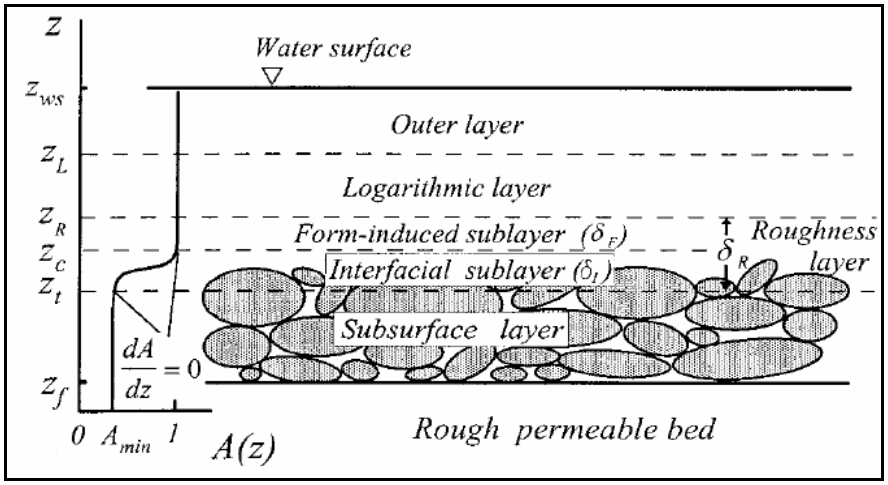

Figure A.1. Flow subdivisions for a gravel bed stream (Nikora et al., 2001)

Form-induced layer: The flow is influenced by individual roughness. The form-induced layer occupies the region just above the roughness crests.

Interfacial layer: This layer is also influenced by individual roughness elements and occupies the flow region between roughness crests and troughs.

Subsurface layer: The flow in this layer occupies pores between granular particles and is driven by the gravity force and momentum fluxes from the above layers.

Velocity Profiles

The description of open-channel velocity profiles are separated into inner and outer regions. The inner, or wall, region (y/h<0.2) can be further subdivided into viscous and fully-turbulent sublayers. The viscous sublayer is dominated by viscous forces and the velocity profile is linear (Klebanoff 1954).

$$\frac{\bar{u}}{u_*} = \frac{u_* z}{\nu} \qquad \text{(Equation A.6)}$$

where $\bar{u}$ is the time-averaged velocity as a function of distance from the boundary, z, ν is the kinematic viscosity, and u* is the shear velocity. The viscous sublayer does not exist for hydraulically rough boundaries, such as gravel-bed rivers, because roughness elements protrude through the layer. Interstitial flow is often assumed to demonstrate viscous behavior (Nikora et al. 2004).

The fully-turbulent sublayer is described with a logarithmic profile and is commonly referred to as the "law of the wall"(Prandtl 1932; von Karman 1930):

$$\frac{\bar{u}}{u_*} = \frac{1}{\kappa}\ln\left(\frac{u_* z}{\nu}\right) + B_0 \qquad \text{(Equation A.7)}$$

where κ is the von Karmen's constant (assumed as 0.40 or 0.41) and B_0 is an integration constant (approximately 5.6).

For hydraulically rough flows, the influence of roughness elements exceeds that of viscosity and the logarithmic profile is modified to account for grain roughness (Nikuradse 1933):

$$\frac{\bar{u}}{u_*} = \frac{1}{\kappa}\ln\left(\frac{z}{k_s}\right) + B_1 \qquad \text{(Equation A.8)}$$

where k_s is the roughness length and B_1 is an integration constant (usually assumed 8.5). As the bed becomes increasingly rough, the location of the bed origin is not clearly defined. The rough boundary logarithmic profile can be modified to account for the reference shift (Rotta 1962):

$$\frac{\bar{u}}{u_*} = \frac{1}{\kappa}\ln\left(\frac{z + \Delta z}{k_s}\right) + B_1 \qquad \text{(Equation A.9)}$$

where Δz is the zero-plane displacement height. Equations A.7 through A.9 apply to the logarithmic layer shown in Figure A.1.

In the outer region of turbulent boundary layers, the velocity profile is described by the velocity-defect law (Clauser 1956):

$$\frac{\overline{u}_m - \overline{u}}{u_*} = \frac{1}{\kappa}\ln\left(\frac{z}{\delta}\right) + B_2 \qquad \text{(Equation A.10)}$$

where δ is the distance to the maximum velocity and B_2 is an integration constant (equal to 8.5 for hydraulically rough boundaries). Coles (Coles 1956) extended the "law of the wall" to describe the outer region by introducing an empirical function known as the "law of the wake":

$$\frac{\overline{u}}{u_*} = \frac{1}{\kappa}\ln\left(\frac{u_* z}{\nu}\right) + B_0 + \frac{\Pi}{\kappa} 2\sin^2\left(\frac{\pi z}{2\delta}\right) \qquad \text{(Equation A.11)}$$

where Π is the wake factor, a function of channel uniformity. Zippe and Graf (Zippe and Graf 1983) demonstrated that the "law of the wake" could be applied to rough boundaries as follows:

$$\frac{\overline{u}}{u_*} = \frac{1}{\kappa}\ln\left(\frac{z}{k_s}\right) + B_1 + \frac{\Pi}{\kappa} 2\sin^2\left(\frac{\pi z}{2\delta}\right) \qquad \text{(Equation A.12)}$$

If the "law of the wake" is written for the boundary and then subtracted from itself, a velocity-defect distribution can be written as (Kirkgoz 1989):

$$\frac{\overline{u}_m - \overline{u}}{u_*} = \frac{1}{\kappa}\ln\left(\frac{z}{\delta}\right) + B_1 + \frac{\Pi}{\kappa} 2\cos^2\left(\frac{\pi z}{2\delta}\right) \qquad \text{(Equation A.13)}$$

As can be seen from the descriptions above, the vertical velocity profile takes on many forms depending on the water column location, bed roughness, and flow conditions. Each equation has multiple parameters which are difficult to determine. This makes the application of these formulas to experimental data complex. Techniques for applying these equations are discussed below.

The viscous sublayer velocity profile can be described completely by determining the shear velocity with Equation A.6. However, this region is difficult to measure and does not exist for hydraulically rough flow. Interstitial flow is often assumed to exhibit linear behavior like that of the viscous sublayer.

The "law of the wall" can be applied to smooth walls by determining the shear velocity with Equation A.6 and then using regression techniques to solve for parameters within Equation A.7. Often, the von Karmen constant is assumed equal to 0.40 or 0.41 and measured data is used to find the integration constant. If the von Karmen constant is not assumed in advance, a least-squared method is applied to simultaneously find κ and B.

The application of the "law of the wall" to hydraulically rough surfaces is less direct because as many as five parameters are unknown (u^*, ks, Δz, κ, and B_1). This problem is simplified by assuming values for κ and B1 from previous controlled experiments. For an immobile bed, κ can be assumed to take a value of 0.40 to 0.41 and B_1 can be set equal to 8.5 (Kirkgoz 1989). This still leaves three unknown variables. The assumptions used to determine the remaining parameters depend on experimental conditions and objectives. Below are four examples of the methods used to apply the "law of the wall" to hydraulically rough open channels.

Method 1 (Papanicolaou and Hilldale 2002)

- Assume the displacement length is equal to zero
- Approximate ks from grain roughness (for example, d50 or 0.1d84)
- Find the shear velocity using a regression technique

Method 2 (Kirkgoz 1989)

- Assume the interstitial flow shows laminar characteristics

- Extend the velocity profile below the lowest reading, □u
- Use □u and □z to find the shear velocity in the interstitial (laminar) region
- Use the logarithmic portion to find the roughness parameter, ks

Method 3 (Nikora and Goring 2000)

- In the fully-turbulent region, assume Δz is zero and κ is 0.40
- Solve for the shear velocity and roughness length using the least-squares method

Method 4 (Nikora and Goring 1999)

- Obtain the shear velocity using the Reynolds shear stress distribution
- Solve for ks and Δz simultaneously using the least-squares method

Several other methods have also been employed using combinations of those described above. A combination of Methods 1 and 3 were used for this report. k_s, κ, and B were assumed equal to the d_{50}, 0.41, and 8.5 respectively. u* and Δz were determined simultaneously using a least-squares method.

Turbulence Properties

Time averaging the Navier-Stokes equations to produce the RANS equations resulted in the fluctuating velocity products $\overline{u_i' u_j'}$ which represent the Reynolds shear stresses when multiplied by the fluid density. These statistical properties are called correlation functions. A correlation function can be defined between any two fluctuating variables and the case of $\overline{u_i' u_j'}$ is often called the covariance. The covariance is calculated as follows:

$$\overline{u_i' u_j'} = \frac{1}{t_a} \int_{t_o}^{t_o + t_a} u_i'(x_p, t) u_j'(x_p, t) dt \qquad \text{(Equation A.14)}$$

where x_p is the coordinate of the sampling point, t is the time at which the two measurements are made, and t_a is the averaging period.

The magnitude of $\overline{u_i' u_j'}$ depends on the intensities of u', v', and w' and the degree of interdependence of the two fluctuations. This relationship is called the correlation coefficient calculated as:

$$R = \frac{\overline{u_i' u_j'}}{TI_i TI_j} \qquad \text{(Equation A.15)}$$

where R is a dimensionless correlation coefficient and TI_i is the turbulence intensity. TI is the root mean square of the velocity fluctuations, calculated as:

$$TI_i = \sqrt{\overline{(u_i - \overline{u}_i)^2}} \qquad \text{(Equation A.16)}$$

This is often displayed as the relative turbulence intensity:

$$\frac{TI_i}{u_*} \qquad \text{(Equation A.17)}$$

In addition to the covariance, several other correlation functions can be described including autocorrelations and spatial correlations. Autocorrelations are the correlations that a signal has with itself at times separated by the lag interval Δt:

$$\overline{u_i'(t) u_i'(t+\Delta t)} = \frac{1}{t_a} \int_{t_o}^{t_o + t_a} u_i'(x_p, t) u_i'(x_p, t+\Delta t) dt \qquad \text{(Equation A.18)}$$

The autocorrelation function is then calculated as follows:

$$R(t) = \frac{\overline{u_i'(t) u_i'(t+\Delta t)}}{TI_i^2} \qquad \text{(Equation A.19)}$$

Spatial correlations involve two signals separated by a distance r at the same time. Spatial correlations can be calculated with a similar formula:

$$\overline{u_i'(x_p)u_j'(x_p+r)} = \frac{1}{t_a}\int_{t_o}^{t_o+t_a} u_i'(x_p,t)u_j'(x_p+r,t)dt \qquad \text{(Equation A.20)}$$

The spatial correlation coefficient is denoted as:

$$R(r) = \frac{\overline{u_i'(x_p)u_j'(x_p+r)}}{\sigma_i\sigma_j} \qquad \text{(Equation A.21)}$$

However, measurement of spatial correlations, particularly at important small scales, is very difficult due to instrument limitations.

Time Scales

Time scales can be defined using autocorrelation curves. The average persistence of turbulent activity at a point is the integral time scale calculated as:

$$T = \int_0^{R=0} R(t)\,dt \qquad \text{(Equation A.22)}$$

where T is the integral time scale.

The micro time scale is defined to characterize the small turbulence scales. The micro time scale is determined by describing the shape of the autocorrelation function with Δt near zero. The micro time scale is calculated as:

$$t_E = -\left[\frac{2}{\left(\partial^2 R / \partial t^2\right)}\right]^{1/2} \approx \frac{TI_i}{\left(\partial u_i' / \partial t\right)_{rms}} \qquad \text{(Equation A.23)}$$

where t_E is the micro time scale. Calculation of t_E requires a sampling frequency of at least twice the highest turbulence frequency of at least twice the highest turbulence frequency in order to adequately describe the shape of the autocorrelation function with Δt near zero.

Length Scales

Length scales can be used to measure the average spatial extent or coherence of the fluctuations. The integral length scale is defined as:

$$L = \int_0^\infty R(r)\,dr \qquad \text{(Equation A.24)}$$

The micro length scale in the streamwise direction is calculated as:

$$l = -\left[\frac{\overline{u'^2}}{\left(\overline{\partial^2 u'/\partial x^2}\right)}\right]^{1/2} \qquad \text{(Equation A.25)}$$

It is difficult to directly measure length scales because it requires the deployment of multiple interfaced instruments in very close proximity. An alternative method for calculating length scales involves the use of Taylor's hypothesis of frozen turbulence. Taylor argued that the sequence of events at a fixed point is nearly equivalent to the movement of an unchanging pattern of turbulence past a point. Using Taylor's hypothesis, we can calculate integral length scale as:

$$L \approx \bar{u}\int_0^\infty R(t)\,dt \qquad \text{(Equation A.26)}$$

The micro length scale can be calculated as:

$$l \approx \bar{u}\,\frac{TI_i}{\left(\partial u_i'/\partial t\right)_{rms}} \qquad \text{(Equation A.27)}$$

Application of Taylor's hypothesis requires that the turbulence intensity is small compared to the convective velocity. Experimental investigations have shown the hypothesis validity as long as $TI_i/\bar{u} < 0.1$ and the measurement is in the outer 90 to 95%

of the boundary layer. Additionally, in open channels the Taylor Hypothesis has only been validated for relative depths greater than 20% (Shteinman 1997).

Additional turbulence parameters are determined from higher order statistics, including skewness and kurtosis calculated as follows:

Skewness (third-order moment)

$$S = \frac{\overline{\left(u_i - \overline{u}_i\right)^3}}{TI_i^3} \qquad \text{(Equation A.28)}$$

Kurtosis (forth-order moment)

$$T = \frac{\overline{\left(u_i - \overline{u}\right)^4}}{TI_i^4} \qquad \text{(Equation A.29)}$$

Previous Research

Open-channel flow measurements have advanced from mean velocity profiles in the 1930s and 1940s to the instantaneous three-dimensional laser sheet measurements of today. The first investigations of velocity fluctuations in open-channels were conducted with hydrogen bubbles and hot-film anemometers in the 1960s and 1970s (Nezu and Nakagawa 1993). The first measurement of the three-dimensional turbulence intensities in an open channel was by Nakagawa et al. (1975). Further flume experiments by Nezu (1977a; 1977b) and others (Li et al. 1980; Griffith and Grinwood 1981) led to the development of the aforementioned empirical distributions (Eq. 2.9 through 2.15)

The bulk of our knowledge about open-channel flow fields has been developed through flume experiments with laser Doppler velocimeters (LDV) and more recently acoustic Doppler velocimeters (ADV). These experiments have been used to test and refine physical turbulence descriptions over a range of conditions.

The empirical turbulence equations were tested for conditions of static and mobile beds by Song et al. (1994). Using an ADV, the researchers described mean and turbulence parameters and found a good fit between the empirical equations and measured data for the velocity and turbulence intensity profiles. Kumar et al. (1998) investigated turbulence in a laboratory flume using particle image velocimetry (PIV). The researchers studied surface features such as upwellings, downdrafts, and spiral eddies. They found that eddies often merge if rotating in the same direction or form pairs if rotating in the opposite direction. Kadota and Nezu (1999) furthered the investigation of coherent structures by investigating the three-dimensional structure of vortices behind a dune crest using and two LDVs and dye visualization. The researchers proposed a refined physical model of coherent vortices in open-channels. Recently, Nikora et al. (2004) suggested the use of the double-averaged Navier-Stokes equations for the description of turbulent flow fields over rough-bed open-channels. The researchers used flume measurements with an ADV to test various models of space-averaged velocity distributions within the roughness layer. Results showed that a linear distribution, analogous to the viscous sublayer, was most appropriate.

The influence of hydraulic features, including channel roughness, transitions, bends, bed motion, vegetation, and suspended particles, have all been investigated through carefully controlled flume experiments. Channel roughness has been shown to increase TI and TKE (Raupach 1981). Lopez and Garcia (1999) suggested a universal value for the normalized vertical flux of TKE. They used ADV measurements over hydraulically smooth, transitional, and rough beds to investigate a theoretical TKE budget. They found good agreement with the suggested universal expression. Chen and

Chiew (2003) observed the response of velocity and turbulence profiles to sudden changes in bed roughness using two ADVs and a LDV. The researchers verified the increase in TI with an increase in bed roughness. However, they reported a slow response in turbulence parameters to a sudden change in bed roughness. They also found that a change in bed roughness disrupts the linear distribution of Reynolds shear stresses.

Song and Chiew (2001) conducted turbulence measurements in a non-uniform flume using an ADV. They investigated the use of a pressure gradient parameter, related to channel expansions and contractions, to describe velocity distributions in non-uniform channels. They found that the log-law was valid for accelerating and decelerating flows if the pressure gradient term was incorporated. The authors also reported a decrease in TI and Reynolds stresses for accelerating flows and an increase for decelerating flows.

The influences of channel bends were investigated by Blanckaert and Graf (2001). Using a custom-built acoustic Doppler velocity profiler (ADVP), the researchers investigated velocity and turbulence distributions in the outer-half of a 120 degree bend with a radius of 2 meters. They observed the presence of two circulation cells in the channel. The outer half of the bend experienced elevated velocities and retarded turbulence distributions. A stronger transverse trend in turbulence parameters was also observed. The results demonstrated the inadequacy of the empirical velocity and turbulence distributions, as a function of relative depth, for this flow condition.

The influence of bed motion was investigated by Song et al (1994) in a laboratory flume and Nikora and Goring (2000) in a trapezoidal irrigation canal. Song et al. (1994) reported only a week influence of bed motion on velocity and turbulence distributions. However, Nikora and Goring (2000) found that bed motion influenced the von Karman

constant of the log-law along with TI and TKE distributions. They suggested modified equations for TI and TKE vertical distributions.

Nezu and Onitsuka (2001) investigated the influence of vegetation on turbulence parameters using LDV and PIV measurements of a flow field with artificial vegetation in a laboratory flume. They found that vegetation caused secondary currents and an increase in TKE. The researchers reported that the secondary currents were created by the anisotropy of turbulence as investigated with the vorticity equation.

Turbulence characteristics in particle-laden flows were investigated using a laser light sheet in a laboratory flume by Nezu and Azuma (2004). The researchers found that fluid-sweep events contributed more to the motion of particles than fluid-ejections. Further, they found that sweeps also transport more momentum to the fluid, leading to an increase in TI.

Recently, instrument advances have allowed researchers to observe turbulence features in natural rivers. Nikora and Smart (1997) completed turbulence characterizations of three New Zealand gravel-bed rivers with fast response electronic pitot tubes. Although only streamwise velocity components could be measured, the authors completed a thorough evaluation of velocity, TI, TKE, and structure functions. Validation of the empirical relationships was not possible as the measurements were conducted from bridge crossings. Sukhodolov et al. (1998) completed a detailed investigation of turbulence structure around sand dunes in a straight low-land river with an ADV and a micropropeller system. The researchers found that analytical expressions for flow field properties were only valid for the central region of the channel. Further, they reported a clear difference in the empirical parameters for the observed data. The

log-law and turbulence equations were only valid 0.3 channel widths from the banks. Rennie et al. (1999) conducted ADV measurements in a reach of the Salmon River in British Columbia, Canada. The measurements provided information about the spatial variability of turbulence parameters. However, measurements were only conducted at 20% of the flow depth, preventing a thorough investigation of the distributions or comparison with empirical equations. Buffin-Belanger et al. (2000) used an array of electromagnetic current meters to confirm the existence of large-scale flow structures in the Eaton North River, Quebec, Canada. They reported a complex organization of large-scale coherent structures with no preferred sequence of events. Smith (2002) conducted ADV measurements across a range of fish habitat types. He reported no significant relationship between fish focal points and turbulence characteristics. Tritico and Hotchkiss (2005) completed turbulence observations behind boulders in two cobble-bed rivers in northern Idaho, USA. The researchers found elevated TI and TKE and reduced integral time scales in the wake of the obstructions. The turbulence parameters did not appear to be a function of obstruction geometry.

Efforts to model stream flow fields has advanced recently with increasing computational ability and data availability. Nadaoka and Yagi (1998) proposed an improved computational fluid dynamics (CFD) method for open channel flows that separates subdepth-scale turbulent processes from horizontal large-scale processes. They applied the proposed technique to a laboratory flume with a rough bottom and artificial vegetation. They reported that the horizontal large-scales dominated the horizontal mixing. Crowder and Diplas (2000a; 200b; 2002) proposed the use of a two-dimensional, depth-averaged hydrodynamic model to describe natural river flow fields and evaluate

habitat quality. The researchers successfully applied the model to a river reach with and without boulders and demonstrated its ability to evaluate trout habitat.

Although a wide range of velocity and turbulence measurements have been completed, most of the studies described above were conducted in laboratory flumes or in limited field observations. A thorough investigation of turbulence distributions at the reach scale has not been completed. Detailed measurements of turbulence distributions in cobble-bed rivers have not been conducted. Also, empirical relationships for turbulence distributions have only been tested in a straight low-land river. Further, a quantifiable evaluation of turbulence across stream units (riffle, pools, and reaches) has not been completed. This report addresses these shortcomings in previous turbulence research.

References

Blanckaert, K., and Graf, W. H. (2001). "Mean flow and turbulence in open-channel bend." *Journal of Hydraulic Engineering*, 127(10), 835-847.

Buffin-Belanger, T., Roy, A. G., and Kirkbride, A. D. (2000). "On large-scale flow structures in a gravel-bed river." *Geomorphology*, 32(3-4), 417-435.

Chen, X., and Chiew, Y. M. (2003). "Response of velocity and turbulence to sudden change of bed roughness in open-channel flow." *Journal of Hydraulic Engineering*, 129(1), 35-43.

Clauser, F. H. (1956). "The turbulent boundary layer." *Advances in applied mechanics*, 4, 1-51.

Coles, D. (1956). "The law of the wake in the turbulent boundary layer." *Journal of Fluid Mechanics*, 1, 191-226.

Crowder, D. W., and Diplas, P. (2000). "Using two-dimensional hydrodynamic models at scales of ecological importance." *Journal of Hydrology*, 230(3-4), 172-191.

Crowder, D. W., and Diplas, P. (2002). "Assessing changes in watershed flow regimes with spatially explicit hydraulic models." *Journal of the American Water Resources Association*, 38(2), 397-408.

Griffith, O. F., and Grimwood, C. (1981). "Turbulence measurement study." *Journal of the Hydraulics Division, ASCE*, 107(3), 311-326.

Kadota, A., and Nezu, I. (1999). "Three-dimensional structure of space-time correlation on coherent vortices generated behind dune crest." *Journal of Hydraulic Research*, 37(1), 59-80.

Kirkgoz, M. S. (1989). "Turbulent velocity profiles for smooth and rough open channel flow." *Journal of Hydraulic Engineering*, 115(11), 1543-1561.

Klebanoff, P. S. (1954). "Characteristics of turbulence in a boundary layer with zero pressure gradient." *Rep. No. 3178*, Washington D.C.

Kumar, S., Gupta, R., and Banerjee, S. (1998). "Experimental investigation of the characteristics of free-surface turbulence in channel flow." *Physics of Fluids*, 10(2), 437-456.

Li, R., Schall, J. D., and Simons, D. B. (1980). "Turbulence prediction in open channel flow." *Journal of the Hydraulics Division, ASCE*, 106(4), 575-587.

Lopez, F., and Garcia, M. H. (1999). "Wall similarity in turbulent open-channel flow." *Journal of Engineering Mechanics-Asce* , 125(7), 789-796.

Nadaoka, K., and Yagi, H. (1998). "Shallow-water turbulence modeling and horizontal large-eddy computation of river flow." *Journal of Hydraulic Engineering*, 124(5), 493-500.

Nakagawa, H., Nezu, I., and Ueda, H. (1975). "Turbulence of open channel flow over smooth and rough beds." *Proceedings of the Japan Society of Civil Engineers*, 241, 155-168.

Nezu, I., and Azuma, R. (2004). "Turbulence Characteristics and Interaction between Particles and Fluid in Particle-Laden Open Channel Flows." *Journal of Hydraulic Engineering*, 130(10), 988-1001.

Nezu, I. (1977). "Turbulent structure in open-channel flows.", Kyoto University.

Nezu, I. (1977). "Turbulence intensities in open-channel flows." *Proceedings of the Japan Society of Civil Engineers*, 261, 67-76.

Nezu, I., and Nakagawa, H. (1993). "Turbulence in open-channel flows." A.A.Balkema, Rotterdam,Netherlands/Brookfield,VT.

Nezu, I., and Onitsuka, K. (2001). "Turbulent structures in partly vegetated open-channel flows with LDA and PIV measurements." *Journal of Hydraulic Research*, 39(6), 629-642.

Nezu, I. (2005). "Open-Channel Flow Turbulence and Its Research Prospect in the 21st Century." *Journal of Hydraulic Engineering*, 131(3), 229-246.

Nikora, V. I., and Smart, G. M. (1997). "Turbulence characteristics of New Zealand gravel-bed rivers." *Journal of Hydraulic Engineering*, 123(9), 764-773.

Nikora, V. I., and Goring, D. G. (1999). "Effects of bed mobility on turbulence structure." *Rep. No. 48*, National Institute of Water and Atmospheric Research.

Nikora, V. I., and Goring, D. (2000). "Flow turbulence over fixed and weakly mobile gravel beds." *Journal of Hydraulic Engineering*, 126(9), 679-690.

Nikora, V. I., Goring, D., McEwan, I., and Griffiths, G. (2001). "Spatially averaged open-channel flow over rough bed." *Journal of Hydraulic Engineering*, 127(2), 123-133.

Nikora, V., Koll, K., McEwan, I., McLean, S., and Dittrich, A. (2004). "Velocity distribution in the roughness layer of rough-bed flows." *Journal of Hydraulic Engineering*, 130(10), 1036-1042.

Nikuradse, J. (1933). "Stromungsgesetze in rauhen Rohren." Heft 361, Berlin.

Papanicolaou, A. N., and Hilldale, R. (2002). "Turbulence characteristics in gradual channel transition." *Journal of Engineering Mechanics-Asce*, 128(9), 948-960.

Prandtl, L. (1932). "Zur turbulenten Stromung in Rohren und langs Platten." *Ergebnisse der Aerodynamischen Versuchsantalt zu Gottingen*, 4, 18-29.

Raupach, M. R., and Thom, A. S. (1981). "Turbulence in and above plant canopies." *Annual Review of Fluid Mechanics*, 13, 97-129.

Raupach, M. R., Antonia, R. A., and Rajagopalan, S. (1991). "Rough-wall turbulent boundary layers." *Applied Mechanics Review* , 44(1), 1-25.

Rennie, C. D., Fisher, T. S. R., and Millar, R. G. (1999). "Spatial variability of turbulent velocity structure in a natural river.".

Reynolds, A. J. (1974). "Turbulent flows in engineering." John Wiley, New York.

Rotta, J. (1962). "Turbulent boundary layers in incompressible flow." *Progress in Aeronautical Science*, 2, 1-219.

Shteinman, B., Nikora, V., Ekhnich, M., and Sukhodolov, A. (1996). "Experimental validation of the `frozen' turbulence hypothesis for river flows." Lausanne, Switz, 531.

Smith, D. L. (2003). "The shear flow environment of juvenile salmonids." Ph.D. Dissertation, University of Idaho.

Song, T., Lemmin, U., and Graf, W. H. (1994). "Uniform-Flow in open channels with movable gravel-bed." *Journal of Hydraulic Research*, 32(6), 861-876.

Song, T., and Chiew, Y. M. (2001). "Turbulence measurement in nonuniform open-channel flow using acoustic Doppler velocimeter (ADV)." *Journal of Engineering Mechanics-Asce*, 127(3), 219-232.

Sukhodolov, A. N., Thiele, M., and Bungartz, H. (1998). "Turbulence structure in a river reach with sand bed." *Water Resources Research*, 34(5), 1317-1334.

Tritico, H. M., and Hotchkiss, R. H. (2005). "Unobstructed and obstructed turbulent flow in gravel bed rivers." *Journal of Hydraulic Engineering*, Accepted for publication.

von Karman, T. (1930). "Mechanische ahnlichkeit und turbulenz." *Gottinger Nachrichten, Math. Phys. Klasse*, 58-60.

White, F. M. (1991). "Viscous Fluid Flow." McGraw-Hill.

Zippe, H. J., and Graf, W. H. (1983). "Turbulent boundary-layer flow over permeable and non-permeable rough surfaces." *Journal of Hydraulic Research*, 21(1), 51-65.

Appendix B: Periphyton Background Information

Introduction

Periphyton assemblages are composed of attached algae, bacteria, and fungi growing on the streambed (Barbour et al., 1999). Periphyton are primary producers and form the base of the food web of autochthonous streams. As a result, stream productivity is often dependent on periphyton development. For streams with abundant allochthonous inputs or high nutrient concentrations, periphyton can overwhelm the stream and become a nuisance (Allen, 1995).

The development of periphyton is dependent on many factors including nutrient concentrations, light, current velocity, substrate, and grazing. Current provides counteracting processes by improving nutrient transfer with increased velocity which also leads to elevated form drag and skin friction. Successional development of periphyton is highly dependent on disturbance regime. Resistance to disturbance is not well understood but it is dependent on taxonomic community structure. Few studies have investigated relationships between advanced flow metrics (i.e. shear stress and velocity gradients) and periphyton assemblages. This section will describe previous research regarding interactions between the flow field, periphyton development, successional development, and resistance to disturbance.

Successional development

The temporal sequence of species replacements among periphyton communities in streams has been the topic of several investigations. Observations of transitions from structurally simple, horizontal assemblages, characterized by diatoms and bacteria to more complex vertical communities consisting of an understory of

diatoms and an overstory of stalked diatoms and filamentous green and blue-green algae have been made in both lentic and lotic systems. The process might be accelerated under faster currents. However, the generality of this sequence for periphyton assemblages is not yet clear.

One of the first detailed studies on periphyton successional development was completed by Hoagland et al. (1982). The authors defined succession as a directional change or sequence in the relative abundance of species in a community. The research investigated periphyton collected on glass slides in two Nebraska reservoirs over a one-year duration. The three dimensional structure of the periphyton communities were studied using a scanning electron microscope. The observed colonization sequence involved an organic coating, followed by a variety of bacteria, low profile diatoms, and finally an upper-story of stalked and large rosette diatoms. The authors drew an analogy to higher plant succession including the vertical community development from low to high structures and in the progressive slow-down in the rate of succession. The periphyton community was heterogeneous and spatially and temporally dynamic throughout colonization and development.

Steinman and McIntire (1986) investigated the effects of current velocity and light energy on the taxonomic and physiognomic characteristics of periphyton assemblages in laboratory streams. The authors found that the initial rate of colonization was affected by flow velocity while difference in light energy accounted for community structure by the end of the experiment. They found a different successional sequence than that reported by Hoagland et al. (1983). The researchers observed large rosette and chain forming species followed by development of an understory with no strong bacterial

presence. They did not observe the analogy between vertical stratification in lotic periphyton and higher plant communities. The researchers found that the taxonomic structure of the periphyton assemblage is apparently determined by:

1. Composition of the species pool
2. Dispersal and colonization rates
3. Competitive interactions among the community constituents
4. Herbivory
5. Chemical and physical environment
6. Spatial and temporal patterns of disturbance

They concluded that successional trajectories of lotic periphyton communities are rarely able to evolve to climax stage without interruption. The significance of disturbance will be explored in the following section.

McCormick and Stevenson (1991) investigated how species-specific life history strategies and interspecific interactions contribute to such short-term successional patterns in stream algal assemblages. The researchers observed algal succession and production in a third-order stream in Kentucky. Results showed the importance of contrasting life history strategies in determining succession patterns. The authors found that autogenic factors are more important than allogenic factors for short-term community development. They also reported that strategies depend on the flow field environment.

A study completed by Poff et al. (1990) in four current controlled channels investigated the effect of flow on successional development. The results showed that current regime was an important determinant of periphyton species composition,

successional trajectories, and physiognomy. Scanning electron microscope observations did not generally support the successional pattern described by Hoagland et al. (1983).

Results from these studies suggest that the successional development of periphyton communities are complex and still not well understood. Taxonomic structure is dependent on many variables. Increased velocity accelerates colonization but short-term community development is more closely related to autogenic factors. The current research will address the effects of the physical environment and the spatial and temporal patterns of disturbance as outlined by Steinman and McIntire (1986).

Disturbance

Disturbance is widely recognized as a fundamental determinant of community development in most ecosystems (Poff and Ward, 1990). Resistance and recovery of periphyton communities to disturbance are an important consideration for stream ecology (Stevenson, 1990). Hydraulic disturbance by spates may be the major mechanism controlling differences in periphyton biomass and structure (Biggs and Close, 1989). Successional trajectories of lotic periphyton communities are rarely able to evolve to climax stage without interruption (Steinman and McIntire, 1986). Several studies have investigated the significance and recovery of periphyton as discussed below.

Steinman et al. (1990) investigated the resistance of stream ecosystems to minor disturbances using laboratory experiments. The researchers reported that the type and duration of disturbance may be more important to stream ecosystems than nutrient levels and species interactions. Field studies completed by Biggs and Close (1989) showed that the proportion of periphyton lost in spates of similar magnitude varies among streams and is not a linear function of intensity even within the same community. This creates

difficulty in predicting ecosystem depopulation from measurements of other variables such as stream discharge (Biggs and Thomsen, 1995).

Peterson and Stevenson (1992) examined the effects of disturbance timing on resistance and resilience of algal communities in fast and slow currents. They reported that resistance was generally lower in slow current communities. The researchers also found a temporal dependence to resistance in slow currents but not fast currents; meaning autogenic factors influence slow currents more than fast currents. The authors concluded disturbance timing, successional state, and habitat affect the susceptibility to disturbance and result in temporal and heterogeneity of periphyton communities.

Uehlinger et al. (1996) evaluated stream process influence on periphyton using a numerical model. The model incorporated major stream processes, including spates and hydrologic variables, in order to evaluate their relative significance. The researchers compared model predictions to periphyton data from four streams that were sampled bi-weekly. The best fitting model incorporated biomass-dependent growth rates, detachment rates that were directly proportionally to discharge and biomass, and catastrophic loss during bed moving spates. The temporal patterns of periphyton development were described by a series of growth curves periodically truncated by disturbances.

Biggs et al. (1999) tested the hypothesis that resource stressed communities would have lower resistance and resilience to scour than resource replete communities. The researchers tested the hypothesis using four artificial streams exposed to a combination of light and nutrients. Results showed that scour disturbance caused a reduction in growth rates of the regenerating communities relative to the undisturbed control communities. Also, disturbance had a longer-term influence on resource stressed communities.

An example of the response of periphyton communities to disturbances was reported by the USGS (1997). The USGS investigated periphyton cell densities before and after two flood events on Big Darby Creek in Ohio. The researchers found that algal-cell densities varied seasonally and were greater in the spring than in the summertime. Cell densities were lower following flood events at nearly every sampling location. Results showed that reduction in cell densities ranged from 0 to 76%. This variation demonstrates the significance of improving our understanding of periphyton disturbance.

Resistance of periphyton to disturbance is major mechanism controlling differences in biomass and structure. Disturbance response is related to a number of variables including type and duration of the event, timing, and resource stress. The diverse range of disturbance responses between streams and events underscores the need for additional research on this topic.

Influence of Flow

The influence of flow on periphyton communities can be described through two counteracting processes. A rise in velocity produces a steeper velocity gradient and increased turbulent fluctuations resulting in greater material exchange of nutrients to the periphyton community. Concurrently, increased velocity results in elevated form drag and skin friction causing sloughing. This simple concept is greatly complicated by tremendous variation in periphyton communities including taxonomic composition and developmental stage. A large number of studies have investigated relationships between velocity and periphyton communities as summarized below.

Whitford (1960) was one of the first researchers to recognize that in quiet water, a film deficient in vital materials forms near the streambed. Whitford suggested that current

affects algae growth due to the action of sweeping away material, producing a steep diffusion gradient, and increasing material exchange. Using field observations and laboratory experiments, he demonstrated that many species grow best in high currents but only after current exceeds 15 cm/sec. McIntire (1966) described characteristics and responses of two periphyton communities in a laboratory stream with current velocities of 9 and 38 cm/sec. He reported that an accumulation of biomass was more rapid for fast currents but similar biomass was observed by the end of the experiments.

Horner and Welch (1981) performed a multiple regression analysis on stream samples to evaluate periphyton development in relation to current velocity and nutrient concentrations. The researchers tested the hypothesis that the erosive effects of current would retard periphyton accumulation unless nutrient availability was high enough to influence the turbulent diffusion of dissolved substances so that cell growth would overcome frictional shear. The researchers found that development was inversely proportional to velocity unless phosphorus concentrations were high. The results support the concept of offsetting mechanisms between improved diffusion and scour from shear stress.

Stevenson (1983) investigated the influence of microhabitats (flow condition and substrate) on diatom immigration rates. Studies were completed in two Michigan streams. Results showed that immigration rates were increased by six-fold when currents near the substrate surface were interrupted and by two-fold when substrates were coated with agar (representing autogenic changes). The author attributed the increased impingement rates to elevated turbulence and a decrease in the laminar sublayer thickness. Results

demonstrated the interrelatedness of autogenic (within the community) and allogenic (external) variables.

Steinman and McIntire (1986) investigated the effects of current velocity and light energy on the successional development of lotic algal assemblages in relation to the taxonomic and physiognomic components of community structure. The study was completed using laboratory streams fed with natural stream water. The researchers monitored ash free dry weight and successional development with a scanning electron microscope. They found that fast currents inhibit initial colonization, but once established, the growth of a periphyton assemblage was enhanced by rapid exchanges of nutrients and dissolved gasses between algal cells and moving currents. Once cells were attached to the tile surface, the authors observed eddy formation downstream of attached particles which apparently enhanced community production.

Gosh and Gaur (1998) investigated colonization of periphytic algae on glass slides exposed to four current regimes. They found an inverse relationship between periphytic accumulation and current velocity. Results showed a preference for pool habitat for a majority of the species observed. These results contradicted earlier studies which reported an increase in periphyton accumulation with velocity until a threshold was passed.

Biggs et al. (1998) studied periphyton spatial heterogeneity by comparing several communities from a gradient of velocities. The authors hypothesized that the counteracting processes of flow on periphyton depend on growth form. The researchers compared data collected from four rivers and an artificial stream. They found mucilaginous community biomass increased with velocity, stalked/short filamentous

communities displayed a unimodal distribution, and long filamentous algal communities decreased with velocity. The important results supported their hypothesis that community growth form determines periphytal responses to spatial variations in velocity within a stream.

The effects of velocity on periphyton communities are complex and depend on a number of variables including resource availability and community composition. Increased velocity enhances impingement and diffusion but also results in greater sloughing. Although a number of studies have been completed on this topic, differences in results emphasize the complexity of periphyton-flow field interactions and the need for improved descriptions and understanding of these processes.

Advanced Flow Studies

The complex relationships between the flow field and aquatic organisms can be better understood by investigating more advanced flow metrics (Crowder and Diplas, 2002). Greater attention to the suitability of advanced flow descriptions will markedly enhance our understanding of physical-biological coupling in streams (Hart and Finelli, 1999). Recently, studies have begun investigating relationships between periphyton communities and flow field descriptions such as velocity gradients, shear stress, and turbulence characteristics. Most of the research involving advanced flow descriptions has been completed by Biggs, Nikora and their colleagues at the National Institute of Water and Atmospheric research (NIWA) in New Zealand. The NIWA researchers have completed a range of experiments, both in natural streams and laboratory flumes, to investigate flow field-periphyton interactions.

Biggs and Thomsen (1995) investigated the resistance of stream periphyton to structural disturbance by increases in shear stress. The researchers used artificial substrates (glass slides) to collect samples from natural streams. The samples were then transferred to the laboratory and subjected to increasing shear stress levels. Results showed that spates can potentially have widely differing disturbance effects on periphyton depending on the initial taxonomic composition of resident communities.

Nikora et al. (1997) observed the affects of periphyton on turbulence characteristics in a laboratory flume (diatoms on a concrete bed). The presence of periphyton influenced longitudinal velocity, Reynolds stresses, eddy diffusivity, velocity, and cross-spectra. Periphyton also affected the roughness sublayer and logarithmic sublayer. The roughness length was five times greater for the measurements with periphyton and the roughness coefficient was 20 to 25% higher.

Nikora et al. (1998a) studied the effects of aquatic moss on near-bed flow structure. The moss reduced longitudinal velocity, Reynolds shear stresses, and turbulent kinetic energy. Turbulence intensity was much higher in the presence of the moss. The internal boundary layer thickness increased with flow.

Nikora et al. (1998b) developed a conceptual model of the interaction between periphyton and flow. The authors described three regions of periphyton-flow interaction – buoyancy dominant, drag dominant, or both forces important. The model can be used for experimental design and interpretation. The researchers tested the model with laboratory experiments in which it performed well.

Godillot et al. (2001) investigated mutual ‘periphyton-flow’ interactions. The researchers measured the near-bed region in experimental flow with increasing

periphyton growth. It was found that periphytic characteristics differ with hydrodynamic conditions. Additionally, flow properties were modified by the periphytic matrix.

Nikora et al. (2002) studied periphyton-flow interactions conducted in a specially designed outdoor hydraulic flume. The goal was to identify the potential effects of periphyton-flow interactions and potential mechanisms of mass transfer. It was found that turbulence shifts the bed origin upwards (z_o increased by 16 to 21%). Below the roughness tops, periphyton suppresses mean velocity, Reynolds shear stresses, turbulence intensity, and the vertical turbulent flux of turbulent energy and Reynolds stress.

These experiments demonstrate the value of using advanced flow descriptions to investigate interactions with periphyton. The presence of periphyton on a stream bed impacts the flow field by shifting the bed origin upwards and modifying turbulence characteristics. The flow features can also be used to evaluate the effects of flow on the periphyton assemblages including response to shear stress. Many questions remain to be addressed on this topic.

References

Allen, J. D. (1995). "Stream Ecology: structure and function of running waters." Chapman and Hall, London, UK.

Barbour, M. T., Gerritsen, J., Snyder, B. D., and Stribling, J. B. (1999). "Rapid Bioassessment Protocols for Use in Streams and Wadeable Rivers: Periphyton, Benthic Macroinvertebrates and Fish, Second Edition." *Rep. No. EPA 841-B-99-002*, U.S. Environmental Protection Agency; Office of Water, Washington, D.C.

Biggs, B. J. F., and Close, M. E. (1989). "Periphyton biomass dynamics in gravel bed rivers: the relative effects of flow and nutrients." *Freshwater Biology*, 22, 209-231.

Biggs, B. J. F., and Thomsen, H. A. (1995). "Disturbance of Stream Periphyton by Perturbations in Shear-Stress - Time to Structural Failure and Differences in Community Resistance." *Journal of Phycology*, 31(2), 233-241.

Biggs, B. J. F., Goring, D. G., and Nikora, V. I. (1998). "Subsidy and stress responses of stream periphyton to gradients in water velocity as a function of community growth form." *Journal of Phycology*, 34(4), 598-607.

Biggs, B. J. F., Tuchman, N. C., Lowe, R. L., and Stevenson, R. J. (1999). "Resource stress alters hydrological disturbance effects in a stream periphyton community." *Oikos*, 85(1), 95-108.

Crowder, D. W., and Diplas, P. (2002). "Assessing changes in watershed flow regimes with spatially explicit hydraulic models." *Journal of the American Water Resources Association*, 38(2), 397-408.

Ghosh, M., and Gaur, J. P. (1998). "Current velocity and the establishment of stream algal periphyton communities." *Aquatic Botany*, 60(1), 1-10.

Godillot, R., Caussade, B., Ameziane, T., and Capblancq, J. (2001). "Interplay between turbulence and periphyton in rough open-channel flow." *Journal of Hydraulic Research*, 39(3), 227-239.

Hart, D. D., and Finelli, C. M. (1999). "Physical-biological coupling in streams: The pervasive effects of flow on benthic organisms." *Annual Review of Ecology and Systematics*, 30, 363-395.

Hoagland, K. D., Roemer, S. C., and Rosowski, J. R. (1982). "Colonization and community structure of two periphyton assemblages, with emphasis on the diatoms (Bacillariophyceae)." *American Journal of Botany*, 69(2), 188-213.

Horner, R. R., and Welch, E. B. (1981). "Stream periphyton development in relation to current velocity and nutrients." *Canadian Journal of Fisheries and Aquatic Sciences*, 38, 449-457.

McCormick, P. V., and Stevenson, R. J. (1991). "Mechanisms of benthic algal succession in lotic environments." *Ecology*, 72(5), 1835-1848.

McIntire, C. D. (1966). "Some Effects of Current Velocity on Periphyton Communities in Laboratory Streams." *Hydrobiologia*, 27, 559-570.

Nikora, V. I., Goring, D. G., and Biggs, B. J. F. (1997). "On stream periphyton-turbulence interactions." *New Zealand Journal of Marine and Freshwater Research*, 31, 435-448.

Nikora, V. I., Suren, A. M., Brown, S. L. R., and Biggs, B. J. F. (1998). "The effects of the moss Fissidens rigidulus (Fissidentaceae : Musci) on near-bed flow structure in an experimental cobble bed flume." *Limnology and Oceanography*, 43(6), 1321-1331.

Nikora, V. I., Goring, D. G., and Biggs, B. J. F. (1998). "A simple model of stream periphyton-flow interactions." *Oikos*, 81(3), 607-611.

Nikora, V. I., Larned, S. T., and Biggs, B. J. F. (2002). "Hydrodynamic effects in aquatic ecosystems with a focus on periphyton." National Institute of Water and Atmospheric Research.

Peterson, C. G., and Stevenson, R. J. (1992). "Resistance and Resilience of Lotic Algal Communities - Importance of Disturbance Timing and Current." *Ecology*, 73(4), 1445-1461.

Poff, N. L., Voelz, N. J., Ward, J. V., and Lee, R. E. (1990). "Algal Colonization Under Four Experimentally-Controlled Current Regimes in A High Mountain Stream." *Journal of the North American Benthological Society*, 9(4), 303-318.

Poff, N. L., and Ward, J. V. (1990). "Physical Habitat Template of Lotic Systems - Recovery in the Context of Historical Pattern of Spatiotemporal Heterogeneity." *Environmental Management*, 14(5), 629-645.

Steinman, A. D., and McIntire, C. D. (1986). "Effects of current velocity and light energy on the structure of periphyton assemblages in laboratory streams." *Journal of Phycology*, 22, 352-361.

Steinman, A. D., Mulholland, P. J., Palumbo, A. V., Flum, T. F., Elwood, J. W., and DeAngelis, D. L. (1990). "Resistance of lotic ecosystems to a light elimination disturbance: a laboratory stream study." *Oikos*, 58, 80-90.

Stevenson, R. J. (1983). "Effects of current and conditions simulating autogenically changing microhabitats on benthic diatom immigration." *Ecology*, 64(6), 1514-1524.

Stevenson, R. J. (1990). "Benthic algal community dynamics in a stream during and after a spate." *Journal of the North American Benthological Society*, 9(3), 277-288.

Uehlinger, U., Buhrer, H., and Reichert, P. (1996). "Periphyton dynamics in a floodprone prealpine river: evaluation of significant processes by modeling." *Freshwater Biology*, 36, 249-263.

USGS (1997). "Hydrologic disturbance and response of aquatic biota in Big Darby Creek basin, Ohio." *Rep. No. Water resources investigations report, 96-4315*, United States Geological Survey.

Whitford, L. A. (1960). "The Current Effect and Growth of Fresh-Water Algae." *Transactions of the microbiological society*, 79, 302-309.

Appendix C: Supplementary information for Chapter 2

ADV data for the St. Maries and Potlatch reaches are summarized in Tables C.1 and C.2, respectively. The data has been categorized by cross-section (CS), stream unit, location, and depth. The table includes data for streamwise (U_s), transverse (U_t), and vertical (U_v) velocities, streamwise (TI_s), transverse (TI_t), vertical (TI_v), and turbulence intensity magnitude (TI_{mag}), turbulent kinetic energy (TKE), integral time (T) and Length (L) scales, normal (C_{ii}) and cross (C_{ij}) correlations, Reynolds shear stress (τ_R), streamwise (S_s), transverse (S_t), and vertical (S_v) skew, and streamwise (K_s), transverse (K_t), and vertical (K_v) kurtosis.

Figure C.1 contains time series coordinate velocity data for the St. Maries reach, cross-section 1, station 3, and relative depth of 0.6h. By definition, the mean transverse and vertical velocity components were equal to 0. Variation appears slightly higher in the streamwise velocity. Some evidence of cyclic patterns was also observed. Figure C.2 contains streamwise velocity time-series for run, riffle, and pool stream units. As expected, the riffle velocity was generally highest and the pool velocity was lowest. Additionally, velocity deviation from the mean was highest in the riffle and similar between the riffle and pool. Cyclic patterns were observed at high frequencies in the riffle and at lower frequencies in the pool. Streamwise velocity time series for different transverse locations are shown in Figure C.3. Although time dependent patterns appear similar between locations, the center measurement was generally the highest and the edge measurement was generally lowest. Finally, time series data for three depths (1cm, 5cm, and 0.8h) are shown in figure C.4. As expected, the velocity magnitude increased with relative depth. However, variations in velocity decreased with depth.

Skew and kurtosis profiles for all measurements are shown in Figures C.5 and C.6, respectively. As expected, the skew and kurtosis values were between -1 and 1 for all measurements. No trends were observed with depth. Deviations from zero were largest for the transverse and vertical velocity components. This was caused by secondary currents influences the Gaussian velocity distributions.

Normal and cross correlation profiles are shown in figures C.7 and C.8 respectively. Normal correlations displayed expected behavior with streamwise correlations the highest and vertical correlations the lowest. All correlations decreased as the water surface was approached. However, the cross correlation data contradicted previous open channel measurements. The streamwise-vertical cross correlation (Csv) is assumed to dominate the other correlation terms. In this study, it was found that the streamwise-transverse cross correlation (Cst) was also significant. The mean Cst value for all data points was higher than the mean Csv at 15.4 and 6.7 cm^2/s^2, respectively. This data further supports the study conclusion that bursting and bed shear are not the dominant processes for turbulence production in the study reaches.

Correlation coefficients are shown for different stream units and depths in Figures C.9 and C.10, respectively. As expected, the pool correlation coefficient went to zero much slower than the riffle and pool. Also, the riffle and run coefficients behaved similarly. This is consistent with integral time scale values, which are calculated as the integral of the correlation coefficient with respect to time. The correlation functions were similar with depth. This supports the concept that horizontal vortices, which are not as heavily influenced by the bed, were more dominant than vertical vortices created by bursting events.

Spectral density functions are shown for different stream units and depths in Figures C.11 and C.12, respectively. All data followed the theoretical -5/3 Kolmogoroff power law. Spectral distributions were very similar between stream units and depths. There seems to be slightly less scatter in the pool density distribution, compared to the run and riffle. The high density of data points near 25 Hz demonstrates that the instrument was not able to measure the highest frequency vortices. Therefore, micro and Kolmogoroff time and length scales were not calculated.

Results of quadrant analyses by stream unit and depth are shown in Figures C.13 and C.14, respectively. For all analyses, the hole size was set to 1. For all cases, the sweep and injections appeared stronger than the outward and inward interactions. The burst events appeared to have a lower intensity in the pool with similar intensities in the riffles and runs. The riffle seemed to have stronger sweeping events than the other units. As expected, the bursts were weakest near the surface (0.8h). Although the events had similar magnitudes at 1 and 3cm, several high intensity ejections and sweeps were observed at 3cm.

Figures C.15 through C.25 contain spatial distributions of velocity and turbulence variables. These figures were discussed in Chapter 3.

Table C.1. Summary of flow field data for the St. Maries Reach

CS	Unit	Loc.	z	Z/h	Us	Ut	Uv	U mag	TI s	TI t	TI v	TI mag	TKE	T	L
1	run	transition	1.00	0.02	13.23	1.40	-0.10	13.31	7.81	6.66	2.95	5.80	56.97	0.17	2.24
1	run	transition	2.00	0.04	20.14	-0.90	-0.28	20.16	8.48	6.69	3.64	6.27	65.00	0.18	3.62
1	run	transition	5.00	0.09	31.55	0.69	-0.55	31.56	9.37	7.26	3.94	6.86	78.02	0.33	10.53
1	run	transition	12.59	0.21	38.08	1.82	-0.01	38.12	8.77	6.87	4.50	6.71	72.12	0.80	30.45
1	run	transition	25.17	0.41	45.07	1.52	0.30	45.10	8.27	6.23	4.54	6.35	63.87	0.52	23.40
1	run	transition	37.76	0.61	48.42	-1.13	0.05	48.43	6.40	5.57	4.00	5.32	43.96	0.16	7.54
1	run	transition	50.34	0.81	50.12	-3.40	0.58	50.24	6.21	5.40	3.51	5.04	40.03	0.32	16.27
1	run	center	1.00	0.02	18.27	0.23	-1.20	18.31	7.85	6.27	5.03	6.38	63.11	0.12	2.16
1	run	center	2.00	0.04	22.88	-2.13	-2.37	23.10	8.00	7.17	4.31	6.49	66.95	0.29	6.72
1	run	center	5.00	0.09	25.01	-0.79	-2.07	25.10	10.60	9.71	4.77	8.36	114.67	0.10	2.44
1	run	center	12.09	0.21	30.87	0.69	-0.46	30.88	9.04	8.48	5.84	7.78	93.82	0.15	4.61
1	run	center	24.19	0.41	41.76	0.92	0.97	41.78	11.54	8.13	6.74	8.80	122.26	0.16	6.62
1	run	center	36.28	0.60	53.57	1.30	1.79	53.62	8.04	6.36	4.31	6.24	61.87	0.45	24.27
1	run	center	48.37	0.80	58.61	-0.23	3.34	58.71	6.65	5.75	3.43	5.28	44.54	0.29	16.92
1	run	transition	1.00	0.01	6.26	-2.10	-0.33	6.61	4.97	4.73	2.30	4.00	26.17	0.77	4.83
1	run	transition	2.00	0.03	7.94	-1.19	-0.59	8.05	5.42	5.72	3.30	4.81	36.48	0.21	1.70
1	run	transition	5.00	0.08	9.53	-1.00	-0.25	9.59	7.07	7.06	3.87	6.00	57.33	0.18	1.73
1	run	transition	10.00	0.18	10.24	-0.48	0.41	10.26	6.63	5.97	4.37	5.66	49.38	0.37	3.83
1	run	transition	21.36	0.39	23.61	1.34	-0.23	23.65	8.14	6.64	4.92	6.57	67.31	0.24	5.55
1	run	transition	32.04	0.59	31.16	1.48	0.61	31.20	7.51	6.29	4.37	6.06	57.50	0.22	6.74
1	run	transition	40.30	0.74	36.84	1.96	0.38	36.89	7.35	6.05	3.97	5.79	53.18	0.43	15.91
1	run	edge	1.00	0.04	23.01	-1.69	0.05	23.08	5.81	4.54	1.83	4.06	28.90	0.33	7.58
1	run	edge	2.00	0.07	24.47	-1.46	0.05	24.51	5.89	4.63	2.19	4.24	30.45	0.23	5.62
1	run	edge	5.00	0.15	29.02	-0.23	0.25	29.02	9.27	7.21	2.88	6.45	73.12	0.18	5.33
1	run	edge	6.73	0.51	38.85	1.15	-0.40	38.87	5.64	4.77	2.72	4.38	30.98	0.30	11.60
1	run	edge	13.47	0.71	40.68	2.23	0.05	40.74	5.45	4.52	2.70	4.23	28.73	0.24	9.77
1	run	edge	1.00	0.29	11.96	1.42	-0.23	12.04	5.20	4.28	2.99	4.16	27.15	0.12	1.46
1	run	edge	2.00	0.32	15.60	2.38	-0.56	15.79	5.46	4.46	3.00	4.31	29.35	0.16	2.56
1	run	edge	5.00	0.40	15.64	1.90	-0.38	15.76	8.01	7.10	3.98	6.36	65.18	0.09	1.33
1	run	edge	7.20	0.47	16.27	0.89	-0.36	16.30	5.37	5.85	3.84	5.02	38.93	0.34	5.53
1	run	edge	14.40	0.67	15.41	-2.02	0.69	15.56	5.53	5.53	4.49	5.18	40.61	0.20	3.02
1	run	edge	21.61	0.87	18.80	-4.57	0.84	19.37	6.44	6.32	5.33	6.03	54.95	0.18	3.35
2	run	transition	1.00	0.04	18.68	2.39	-0.71	18.85	8.32	8.44	4.35	7.04	79.67	0.12	2.18
2	run	transition	2.00	0.07	19.79	1.71	0.78	19.88	7.89	7.66	5.44	7.00	75.24	0.18	3.61
2	run	transition	5.00	0.17	23.21	-0.93	0.58	23.23	11.77	8.56	6.39	8.91	126.31	0.29	6.65
2	run	transition	6.16	0.21	25.10	-2.03	0.47	25.19	10.12	7.68	6.49	8.10	101.79	0.18	4.54
2	run	transition	12.33	0.41	41.30	-1.37	-0.43	41.32	9.37	6.76	5.09	7.07	79.64	0.33	13.55
2	run	transition	18.49	0.61	50.55	0.23	-0.69	50.56	6.61	5.33	3.67	5.20	42.79	0.26	13.34
2	run	center	1.00	0.04	32.55	1.85	0.37	32.61	14.43	10.85	5.47	10.25	177.90	0.13	4.12
2	run	center	2.00	0.06	38.15	2.59	0.77	38.24	10.68	10.84	6.18	9.24	134.92	0.13	5.08
2	run	center	5.00	0.12	44.74	3.28	-1.15	44.87	15.83	13.03	9.22	12.70	252.82	0.15	6.91
2	run	center	10.09	0.22	58.81	1.92	-1.07	58.85	15.17	13.04	9.39	12.53	244.15	0.21	12.16
2	run	center	20.19	0.42	73.05	-0.17	-1.01	73.06	13.80	10.98	7.81	10.86	186.02	0.27	19.89
2	run	center	30.28	0.62	84.01	-2.78	0.23	84.05	11.20	9.76	6.64	9.20	132.34	0.11	9.08
2	run	center	40.38	0.82	88.62	-6.69	1.86	88.89	9.23	8.68	5.45	7.79	95.12	0.11	9.35
2	run	transition	1.00	0.00	0.28	-1.58	1.64	2.29	6.38	5.53	2.86	4.92	39.69	0.11	0.03
2	run	transition	2.00	0.02	6.02	-0.73	1.51	6.24	4.63	5.24	3.30	4.39	29.83	0.18	1.07
2	run	transition	5.00	0.08	19.44	1.96	0.28	19.54	6.81	5.51	4.96	5.76	50.61	0.25	4.83
2	run	transition	10.09	0.18	26.90	4.94	-0.56	27.35	7.55	6.58	4.54	6.23	60.50	0.25	6.75
2	run	transition	20.19	0.38	35.86	0.51	-0.64	35.87	7.43	6.01	4.12	5.85	54.10	0.36	12.76
2	run	transition	30.28	0.58	41.97	-1.97	-1.13	42.03	5.73	5.00	3.23	4.65	34.13	0.22	9.21
2	run	transition	40.38	0.78	43.78	-3.13	-1.09	43.90	5.23	4.92	2.79	4.32	29.71	0.12	5.21
2	run	edge	1.00	0.01	1.61	9.30	-1.18	9.51	9.25	8.66	5.92	7.94	97.76	0.09	0.14
2	run	edge	2.00	0.04	2.86	5.04	-0.19	5.80	8.71	8.61	5.55	7.62	90.40	0.10	0.27
2	run	edge	5.00	0.14	10.37	-1.43	-2.15	10.69	11.08	9.86	6.59	9.18	131.69	0.10	1.05
2	run	edge	11.73	0.37	34.56	-7.64	0.04	35.40	10.70	8.39	5.43	8.17	107.19	0.12	4.22
2	run	edge	17.59	0.57	45.97	-5.27	3.49	46.40	7.65	6.44	4.06	6.05	58.30	0.11	5.06
2	run	edge	1.00	0.01	5.05	7.08	-1.88	8.90	6.20	5.75	2.41	4.79	38.65	0.17	0.87
2	run	edge	2.00	0.03	8.64	5.01	-0.45	9.99	5.66	4.86	3.22	4.58	32.98	0.46	3.93
2	run	edge	5.00	0.10	12.56	3.38	-0.01	13.01	7.77	6.92	4.01	6.23	62.15	0.10	1.20
2	run	edge	9.19	0.19	14.31	0.64	0.81	14.35	6.10	5.97	4.08	5.38	44.77	0.18	2.53
2	run	edge	18.38	0.39	22.78	-3.55	0.74	23.07	7.60	6.43	4.39	6.14	59.20	0.29	6.60
2	run	edge	27.56	0.59	31.81	-6.02	0.62	32.38	5.90	4.77	3.70	4.79	35.65	0.44	13.89
2	run	edge	34.00	0.73	33.73	-6.54	0.17	34.36	5.70	4.30	2.98	4.32	29.91	0.27	9.26

Table C.1 (continued). Summary of flow field data for the St. Maries Reach

CS	Unit	Loc.	z	Z/h	Us	Ut	Uv	U mag	TI s	TI t	TI v	TI mag	TKE	T	L
3	riffle	transition	1.00	0.03	18.95	-4.99	-1.87	19.68	12.95	11.23	5.93	10.04	164.51	0.19	3.58
3	riffle	transition	2.00	0.07	24.70	-2.72	-1.75	24.91	13.05	12.10	7.42	10.86	185.85	0.10	2.44
3	riffle	transition	5.70	0.20	34.13	-2.17	-0.19	34.20	16.07	14.11	9.43	13.21	273.23	0.11	3.79
3	riffle	transition	11.41	0.40	54.24	4.20	0.36	54.40	15.99	12.65	8.92	12.52	247.64	0.08	4.35
3	riffle	transition	17.11	0.60	70.19	5.68	3.45	70.50	14.42	10.33	7.67	10.81	186.78	0.10	6.97
3	riffle	center	1.00	0.02	12.90	-18.86	-3.20	23.07	12.88	13.39	8.88	11.72	212.02	0.07	0.88
3	riffle	center	2.00	0.04	17.34	-18.96	-4.61	26.10	12.79	14.30	9.21	12.10	226.35	0.07	1.14
3	riffle	center	5.00	0.11	21.20	-12.21	-3.78	24.75	14.32	17.16	11.67	14.38	317.91	0.15	3.19
3	riffle	center	8.16	0.19	27.48	-0.58	-1.29	27.51	16.96	17.04	12.03	15.34	361.41	0.09	2.60
3	riffle	center	16.32	0.39	55.65	10.80	1.09	56.70	21.88	18.15	13.01	17.68	488.57	0.08	4.71
3	riffle	center	24.47	0.59	80.32	18.90	5.87	82.72	17.98	16.97	13.04	16.00	390.69	0.09	7.25
3	riffle	center	28.00	0.68	87.10	20.90	5.91	89.77	17.34	16.46	13.85	15.88	381.71	0.08	7.29
3	riffle	transition	1.00	0.01	4.00	-19.66	-7.99	21.59	20.72	23.49	17.30	20.51	640.35	0.11	0.45
3	riffle	transition	2.00	0.03	25.39	-13.60	-9.49	30.33	21.69	16.18	15.41	17.76	484.98	0.07	1.84
3	riffle	transition	5.00	0.10	46.56	-1.53	-6.71	47.07	26.19	16.30	14.73	19.07	584.25	0.09	4.03
3	riffle	transition	8.57	0.18	71.97	3.75	-2.03	72.09	22.61	15.58	12.83	17.01	459.29	0.10	7.04
3	riffle	transition	17.13	0.38	81.40	10.90	7.11	82.43	12.18	13.15	11.15	12.16	222.96	0.06	4.73
3	riffle	transition	25.70	0.58	98.24	10.21	9.27	99.20	12.12	13.28	10.98	12.13	221.90	0.07	6.40
3	riffle	transition	30.95	0.71	106.62	9.93	9.83	107.53	13.69	14.95	15.94	14.86	332.57	0.04	3.81
3	riffle	edge	1.00	0.02	9.06	3.41	0.70	9.70	14.48	8.57	1.84	8.30	143.22	0.02	0.15
3	riffle	edge	2.00	0.04	41.69	-1.59	1.36	41.74	7.83	5.79	4.42	6.02	57.22	0.09	3.62
3	riffle	edge	5.00	0.11	47.00	-0.65	-0.13	47.00	9.73	7.80	4.62	7.38	88.42	0.06	2.73
3	riffle	edge	7.20	0.17	51.14	-1.17	-1.93	51.19	6.88	5.18	4.26	5.44	46.19	0.12	6.12
3	pool	edge	1.00	0.02	15.74	1.69	2.51	16.03	9.89	10.97	9.23	10.03	151.62	0.05	0.83
3	pool	edge	2.00	0.04	18.47	7.47	1.06	19.95	8.27	9.18	6.61	8.02	98.14	0.03	0.61
3	pool	edge	5.00	0.11	40.39	0.72	-1.36	40.42	14.13	10.58	8.67	11.12	193.31	0.06	2.48
3	pool	edge	6.61	0.15	43.07	-2.47	1.24	43.16	12.92	10.54	8.62	10.69	176.09	0.07	3.17
3	pool	edge	13.22	0.31	43.15	-5.95	0.10	43.56	11.98	10.18	10.02	10.73	173.81	0.08	3.48
3	pool	edge	19.83	0.46	35.84	-1.45	-3.55	36.05	11.08	10.84	9.58	10.50	165.96	0.08	2.75
4	pool	transition	1.00	0.02	3.79	1.45	-0.88	4.15	3.25	3.93	1.26	2.81	13.78	0.81	3.08
4	pool	transition	2.00	0.04	9.35	-2.77	-0.70	9.78	5.18	3.95	2.08	3.74	23.39	0.44	4.07
4	pool	transition	5.00	0.08	9.90	-4.44	-0.45	10.86	8.74	7.48	2.42	6.21	69.05	0.16	1.55
4	pool	transition	12.24	0.20	14.43	-2.73	0.26	14.69	5.85	5.55	3.45	4.95	38.50	0.65	9.40
4	pool	transition	24.49	0.40	17.23	0.91	0.60	17.26	6.23	5.80	3.61	5.21	42.70	0.53	9.07
4	pool	transition	36.73	0.60	21.84	2.68	0.73	22.02	6.63	6.21	3.73	5.52	48.21	0.55	12.04
4	pool	transition	48.98	0.80	24.70	4.89	0.45	25.18	6.24	5.79	3.30	5.11	41.62	1.28	31.50
4	pool	center	1.00	0.00	7.93	2.48	0.08	8.30	5.67	5.80	2.69	4.72	36.52	0.19	1.48
4	pool	center	2.00	0.02	10.18	0.90	0.16	10.22	6.99	6.32	3.34	5.55	49.94	0.20	2.03
4	pool	center	5.00	0.05	13.39	-1.87	-0.35	13.53	8.84	8.33	4.19	7.12	82.59	0.23	3.14
4	pool	center	16.15	0.19	27.90	-3.88	-2.53	28.28	10.83	7.33	5.03	7.73	98.19	0.50	14.07
4	pool	center	32.30	0.39	35.44	-2.74	-0.73	35.56	10.03	8.10	5.56	7.90	98.57	0.49	17.20
4	pool	center	48.46	0.59	48.29	-0.38	0.48	48.29	9.48	7.14	5.16	7.26	83.76	0.41	19.64
4	pool	center	64.61	0.79	49.12	1.61	1.49	49.17	8.19	6.72	4.35	6.42	65.61	0.79	38.83
4	pool	center	70.00	0.86	51.09	3.88	1.41	51.26	7.55	6.93	4.36	6.28	61.98	0.39	20.02
4	pool	transition	1.00	0.00	6.46	1.87	0.67	6.76	6.43	6.10	2.63	5.05	42.71	0.24	1.56
4	pool	transition	2.00	0.02	9.33	1.61	-0.24	9.47	7.42	7.48	3.83	6.24	62.85	0.58	5.41
4	pool	transition	5.00	0.05	10.45	-1.06	-0.60	10.52	10.32	9.85	5.03	8.40	114.40	0.12	1.30
4	pool	transition	16.10	0.19	20.51	-0.73	-1.33	20.57	9.73	7.18	5.34	7.42	87.39	0.43	8.81
4	pool	transition	32.19	0.39	28.47	0.06	-0.58	28.48	10.30	6.93	5.12	7.45	90.21	0.65	18.39
4	pool	transition	48.29	0.59	35.23	0.06	-0.27	35.23	9.39	7.79	5.29	7.49	88.37	0.49	17.28
4	pool	transition	64.38	0.79	40.67	-0.39	1.37	40.70	9.23	7.35	5.00	7.19	82.13	0.55	22.47
4	pool	transition	70.00	0.86	43.08	-1.41	0.96	43.11	9.10	7.26	4.67	7.01	78.71	1.27	54.86
4	pool	edge	1.00	0.02	-0.45	-0.26	-0.12	0.53	3.92	3.31	1.20	2.81	13.88	0.21	-0.09
4	pool	edge	2.00	0.03	0.13	-0.42	-0.18	0.47	2.46	1.68	0.77	1.64	4.74	1.16	0.16
4	pool	edge	5.00	0.08	-1.26	0.54	0.10	1.38	5.90	5.24	1.94	4.36	33.02	0.04	-0.05
4	pool	edge	7.20	0.12	-0.84	-0.26	0.01	0.88	3.78	3.56	1.35	2.90	14.38	0.02	-0.02
4	pool	edge	24.65	0.40	-1.08	-0.66	0.09	1.27	4.89	4.61	1.55	3.68	23.77	0.02	-0.02
4	pool	edge	36.97	0.60	-0.65	1.23	0.27	1.42	3.05	2.45	1.33	2.28	8.54	2.81	-1.84
4	pool	edge	49.30	0.80	-0.24	-0.16	-0.18	0.34	2.42	2.19	1.12	1.91	5.96	2.58	-0.61
4	pool	edge	1.00	0.01	1.75	0.84	-0.25	1.96	4.46	4.85	1.15	3.49	22.35	0.37	0.65
4	pool	edge	2.00	0.03	0.06	3.00	-0.53	3.04	2.85	2.94	1.08	2.29	8.98	0.56	0.03
4	pool	edge	5.00	0.07	2.18	1.86	-0.50	2.91	6.15	7.45	1.94	5.18	48.53	1.27	2.77
4	pool	edge	13.51	0.20	1.70	4.30	0.05	4.62	2.82	2.97	2.09	2.63	10.57	0.23	0.39
4	pool	edge	27.03	0.40	1.72	-0.19	0.49	1.80	3.58	4.86	2.65	3.70	21.75	0.43	0.73
4	pool	edge	40.54	0.60	1.99	-3.19	0.41	3.78	4.90	3.98	3.66	4.18	26.58	1.44	2.86
4	pool	edge	54.05	0.80	1.94	-6.61	0.33	6.90	4.95	5.32	2.46	4.24	29.45	2.23	4.34

Table C.1 (continued). Summary of flow field data for the St. Maries Reach

CS	Unit	Loc.	Cuu	Cvv	Cww	Cuv	Cuw	Cvw	τ_R	Ss	St	Sv	Ks	Kt	Kv
3	riffle	transition	167.67	126.16	35.18	-40.83	-25.84	2.59	2.46	0.24	-0.09	-0.39	-0.17	-0.22	0.14
3	riffle	transition	170.34	146.30	55.05	-29.43	-34.16	3.42	-2.36	0.16	-0.01	-0.24	-0.29	-0.13	0.10
3	riffle	transition	258.36	199.14	88.97	-26.23	-32.96	3.30	-33.72	0.10	0.00	-0.17	-0.15	-0.24	-0.08
3	riffle	transition	255.81	159.90	79.58	-7.80	-47.71	4.78	-29.13	-0.23	0.02	0.30	-0.34	-0.17	-0.10
3	riffle	transition	207.97	106.75	58.84	-3.07	-25.48	2.55	-10.46	-0.32	0.00	0.26	0.25	0.03	0.04
3	riffle	center	166.01	179.18	78.85	-45.12	-40.92	4.10	43.51	0.17	0.21	0.19	-0.19	0.06	0.50
3	riffle	center	163.51	204.36	84.83	-44.31	-33.67	3.37	40.30	0.07	0.39	0.25	-0.27	0.57	0.08
3	riffle	center	205.08	294.52	136.22	-14.80	-37.78	3.78	13.93	0.11	0.16	0.20	0.09	-0.03	0.30
3	riffle	center	287.59	290.44	144.79	55.99	-65.10	6.52	23.19	0.32	-0.01	0.06	0.11	-0.22	0.10
3	riffle	center	478.53	329.28	169.33	181.86	-74.99	7.51	1.44	0.05	-0.05	0.16	-0.23	-0.40	0.13
3	riffle	center	323.10	288.14	170.14	108.64	-22.90	2.29	-15.23	-0.28	-0.44	2.67	0.17	0.03	20.11
3	riffle	center	300.75	270.82	191.85	70.09	-1.00	0.10	-11.26	0.01	-0.49	3.12	0.11	0.57	21.33
3	riffle	transition	429.44	551.85	299.41	217.41	-19.90	1.99	-50.95	0.44	-1.51	0.64	-0.09	4.79	0.52
3	riffle	transition	470.61	261.87	237.47	184.04	4.40	-0.44	93.00	0.53	0.18	0.33	0.00	-0.29	0.15
3	riffle	transition	685.82	265.60	217.08	238.59	-21.90	2.19	58.77	-0.15	-0.15	-0.03	-0.59	-0.29	-0.02
3	riffle	transition	511.08	242.85	164.67	135.51	-14.63	1.46	12.97	-0.50	-1.22	0.65	-0.14	6.20	2.36
3	riffle	transition	148.46	173.05	124.42	22.46	8.69	-0.87	-8.93	-0.07	-3.88	0.69	-0.05	28.89	3.55
3	riffle	transition	147.00	176.28	120.51	9.65	-5.07	0.51	-22.64	-0.23	-4.24	1.09	-0.24	30.97	4.89
3	riffle	transition	187.50	223.45	254.20	3.69	-18.54	1.86	100.61	-0.60	-2.68	0.19	1.86	18.70	2.89
3	riffle	edge	209.55	73.49	3.40	22.26	-3.08	0.31	-4.24	-0.08	0.01	-0.46	-0.32	0.02	1.46
3	riffle	edge	61.33	33.56	19.55	10.59	-14.48	1.45	-1.99	-0.41	-0.04	-0.18	0.13	0.22	-0.07
3	riffle	edge	94.58	60.90	21.35	4.27	-12.90	1.29	-1.70	-0.29	0.01	0.23	0.10	0.14	0.17
3	riffle	edge	47.38	26.83	18.17	2.41	-10.81	1.08	-1.48	-0.52	0.01	0.44	1.02	0.04	0.31
3	pool	edge	97.80	120.24	85.20	-6.99	8.75	-0.88	-45.94	0.02	0.01	-0.04	0.18	-0.20	0.05
3	pool	edge	68.45	84.19	43.64	4.56	-18.41	1.84	-11.24	-0.02	-0.25	-0.12	0.46	0.14	-0.22
3	pool	edge	199.57	111.87	75.18	-19.15	-46.44	4.65	6.74	-0.17	-0.15	0.14	-0.21	0.08	-0.04
3	pool	edge	166.84	111.03	74.30	-19.79	-32.88	3.29	6.84	-0.15	0.03	0.14	0.04	-0.05	0.14
3	pool	edge	143.49	103.73	100.40	-6.04	37.37	-3.74	3.29	0.27	-0.16	-0.10	0.10	0.07	-0.26
3	pool	edge	122.71	117.42	91.79	-12.90	25.16	-2.52	-4.26	0.34	-0.20	0.42	0.07	0.11	-0.10
4	pool	transition	10.55	15.41	1.60	2.16	-0.52	0.05	-3.06	0.12	0.35	-0.04	0.20	0.13	0.14
4	pool	transition	26.82	15.62	4.34	2.72	-2.88	0.29	1.50	0.46	0.35	0.02	-0.16	0.29	0.27
4	pool	transition	76.37	55.90	5.84	7.51	5.81	-0.58	-1.45	0.03	0.32	-0.17	0.32	0.31	0.34
4	pool	transition	34.27	30.81	11.91	11.15	-5.75	0.58	-4.94	-0.03	0.34	0.11	-0.05	-0.03	0.39
4	pool	transition	38.75	33.59	13.05	4.99	-6.95	0.70	-5.36	0.22	0.21	-0.04	0.12	0.02	0.03
4	pool	transition	43.94	38.56	13.92	14.00	-6.08	0.61	-3.99	0.19	-0.02	0.00	-0.06	-0.18	-0.15
4	pool	transition	38.90	33.48	10.86	6.01	-4.74	0.47	-2.34	-0.06	0.28	0.16	-0.30	0.09	-0.25
4	pool	center	32.19	33.62	7.23	11.88	-6.38	0.64	-1.91	0.13	-0.15	-0.06	0.13	-0.05	0.19
4	pool	center	48.82	39.88	11.19	12.37	-4.32	0.43	0.02	0.34	-0.05	-0.10	0.09	0.17	0.29
4	pool	center	78.17	69.42	17.59	5.79	-8.95	0.90	-1.77	0.24	-0.12	-0.06	0.02	0.05	-0.09
4	pool	center	117.35	53.76	25.26	21.22	-19.93	1.99	-3.20	0.14	-0.07	0.15	-0.24	-0.07	0.03
4	pool	center	100.69	65.56	30.90	27.46	-13.31	1.33	-5.22	0.08	-0.02	0.09	-0.22	-0.14	0.17
4	pool	center	89.85	51.04	26.63	13.40	-10.62	1.06	-3.39	-0.29	-0.11	0.22	-0.13	-0.08	0.25
4	pool	center	67.15	45.16	18.90	5.12	-1.18	0.12	-5.47	0.09	-0.28	0.17	0.16	0.22	0.12
4	pool	center	57.02	47.96	18.99	-6.14	2.45	-0.25	-7.40	-0.11	-0.21	0.02	-0.04	0.20	0.25
4	pool	transition	41.28	37.23	6.90	11.90	-5.02	0.50	0.86	-0.03	-0.18	-0.22	0.08	0.17	0.73
4	pool	transition	55.01	55.98	14.71	20.68	-2.70	0.27	5.14	0.25	-0.17	-0.04	-0.03	-0.22	0.24
4	pool	transition	106.53	96.96	25.30	-0.76	-2.53	0.25	5.73	0.05	0.10	-0.12	0.18	0.08	0.01
4	pool	transition	94.65	51.56	28.56	-1.89	-18.69	1.87	-0.06	0.30	-0.13	0.20	-0.38	-0.13	0.02
4	pool	transition	106.13	48.04	26.24	-3.29	-14.84	1.49	-3.78	0.11	0.09	-0.16	-0.40	-0.19	-0.21
4	pool	transition	88.11	60.61	28.03	2.59	-9.69	0.97	-2.05	-0.30	-0.11	0.13	0.09	-0.12	0.07
4	pool	transition	85.17	54.04	25.03	-8.33	-7.83	0.78	-2.97	0.19	-0.09	0.13	-0.27	0.02	-0.20
4	pool	transition	82.89	52.67	21.85	-9.07	-8.53	0.85	-0.78	0.00	0.08	0.29	-0.24	0.03	0.07
4	pool	edge	15.35	10.97	1.44	-1.43	-3.46	0.35	-0.56	-0.03	0.00	0.06	0.28	0.21	0.34
4	pool	edge	6.06	2.83	0.59	0.07	-1.07	0.11	-0.34	0.09	0.12	-0.19	-0.03	0.13	0.07
4	pool	edge	34.83	27.46	3.76	-2.76	-8.74	0.88	-1.62	-0.08	-0.02	0.08	0.40	0.32	0.56
4	pool	edge	14.28	12.67	1.81	-1.33	-3.92	0.39	-0.89	0.11	-0.01	-0.07	0.47	0.38	0.45
4	pool	edge	23.89	21.24	2.41	-4.06	-5.94	0.59	-0.37	-0.05	0.01	0.05	0.24	0.31	0.42
4	pool	edge	9.29	6.00	1.78	0.45	-2.88	0.29	-0.65	0.37	0.27	-0.36	0.34	0.76	0.41
4	pool	edge	5.86	4.81	1.24	0.25	-1.32	0.13	-0.52	0.08	0.26	-0.29	-0.14	0.52	0.07
4	pool	edge	19.85	23.53	1.32	-0.99	1.46	-0.15	-1.62	-0.24	-0.05	-0.09	0.57	0.15	0.42
4	pool	edge	8.13	8.67	1.16	1.04	0.31	-0.03	-1.05	0.07	-0.43	-0.16	0.09	0.47	0.55
4	pool	edge	37.84	55.46	3.77	-6.45	5.37	-0.54	-5.02	0.01	0.00	-0.10	0.37	0.30	0.29
4	pool	edge	7.94	8.83	4.37	-1.63	1.17	-0.12	-0.52	-0.12	-0.09	0.09	0.63	0.24	0.19
4	pool	edge	12.85	23.63	7.01	0.69	-0.89	0.09	1.11	-0.15	-0.67	0.15	0.07	0.61	0.37
4	pool	edge	23.98	15.81	13.37	0.86	-5.18	0.52	0.66	-0.05	0.13	0.03	-0.64	-0.04	-0.54
4	pool	edge	24.54	28.31	6.04	2.12	1.01	-0.10	3.50	-0.30	-0.19	-0.45	-0.37	-0.15	0.21

Table C.2. Summary of flow field data for the Potlatch Reach

CS	Unit	Loc.	z	Z/h	Us	Ut	Uv	U mag	TI s	TI t	TI v	TI mag	TKE	T	L
1	riffle	edge	1.00	0.03	16.06	7.03	0.33	17.54	5.98	5.89	4.35	5.41	44.74	0.10	1.66
1	riffle	edge	2.00	0.05	18.56	3.85	-1.15	18.99	6.28	6.16	4.13	5.52	47.22	0.11	2.13
1	riffle	edge	5.00	0.12	25.54	-1.26	-0.02	25.57	8.39	8.00	4.61	7.00	77.84	0.13	3.30
1	riffle	edge	8.70	0.21	31.51	-2.03	0.16	31.58	8.67	7.78	4.95	7.13	80.05	0.20	6.37
1	riffle	edge	17.50	0.41	41.80	-2.29	1.03	41.87	8.59	6.96	5.50	7.02	76.29	0.19	7.95
1	riffle	edge	26.20	0.61	46.98	-2.43	0.31	47.04	8.34	7.09	5.76	7.06	76.51	0.13	6.16
1	riffle	edge	31.93	0.74	51.22	-2.87	-0.65	51.30	7.43	6.57	5.50	6.50	64.33	0.13	6.81
1	riffle	center	1.00	0.03	6.78	-1.75	-1.92	7.26	8.44	7.76	5.34	7.18	79.98	0.12	0.82
1	riffle	center	2.00	0.05	15.13	1.07	-1.86	15.28	10.81	9.35	6.26	8.81	121.73	0.23	3.53
1	riffle	center	5.00	0.12	18.77	2.05	-2.48	19.04	12.34	10.86	6.83	10.01	158.37	0.15	2.83
1	riffle	center	8.82	0.20	24.57	4.98	0.10	25.07	12.88	11.36	8.27	10.84	181.68	0.33	8.13
1	riffle	center	17.64	0.40	28.54	1.49	3.31	28.77	12.53	11.90	10.49	11.64	204.26	0.36	10.16
1	riffle	center	26.46	0.60	23.79	-3.70	2.47	24.20	12.36	12.95	10.25	11.85	212.70	0.19	4.49
1	riffle	center	35.29	0.80	20.12	-4.14	0.38	20.54	11.81	12.04	10.03	11.29	192.55	0.22	4.46
1	riffle	edge	1.00	0.01	1.37	-3.24	-0.97	3.65	6.22	7.51	6.29	6.67	67.36	0.10	0.13
1	riffle	edge	2.00	0.04	10.71	-1.25	-4.34	11.62	10.23	10.56	7.22	9.34	134.15	0.16	1.69
1	riffle	edge	5.00	0.13	12.80	-1.14	-0.16	12.85	12.72	10.59	8.64	10.65	174.29	0.18	2.34
1	riffle	edge	7.11	0.20	18.51	-1.42	-0.73	18.58	13.42	11.74	8.85	11.34	198.20	0.15	2.70
1	riffle	edge	13.78	0.40	29.37	0.80	0.90	29.40	15.25	14.38	10.59	13.41	275.72	0.12	3.38
1	riffle	edge	20.68	0.61	35.39	2.80	1.81	35.55	16.91	13.89	11.23	14.01	302.43	0.12	4.21
1	riffle	edge	21.53	0.63	36.05	3.45	3.49	36.38	17.35	13.36	10.54	13.75	295.22	0.14	4.91
2	run	edge	1.00	0.12	24.95	-0.71	-2.57	25.10	8.07	7.34	5.71	7.04	75.75	0.60	15.04
2	run	edge	2.00	0.14	26.61	-2.58	-1.60	26.78	9.36	7.20	3.58	6.72	76.17	0.24	6.26
2	run	edge	5.00	0.22	37.03	-6.32	-0.91	37.58	8.30	6.32	3.67	6.10	61.22	0.20	7.44
2	run	edge	7.57	0.29	39.39	-2.08	1.09	39.46	10.23	8.97	4.66	7.96	103.44	0.14	5.38
2	run	edge	15.14	0.49	41.63	0.08	0.68	41.63	8.03	7.49	4.95	6.82	72.53	0.16	6.85
2	run	edge	22.70	0.69	44.67	5.66	1.49	45.05	7.25	7.10	4.45	6.27	61.39	0.15	6.87
2	run	edge	27.00	0.80	44.44	5.95	1.82	44.87	6.91	7.56	4.37	6.28	62.04	0.15	6.48
2	run	center	1.00	0.06	15.18	3.30	-0.31	15.54	8.14	8.15	4.84	7.04	78.03	0.11	1.67
2	run	center	2.00	0.09	18.71	1.17	0.29	18.75	8.55	7.08	5.08	6.90	74.52	0.10	1.93
2	run	center	5.00	0.18	29.83	0.21	0.18	29.83	8.61	7.34	4.27	6.74	73.12	0.18	5.31
2	run	center	6.59	0.23	31.57	0.18	0.61	31.58	7.05	5.92	4.27	5.75	51.52	0.81	25.71
2	run	center	13.18	0.43	34.30	-2.18	-0.14	34.37	6.09	5.43	4.10	5.21	41.71	0.15	5.09
2	run	center	20.00	0.63	34.80	-2.68	-0.62	34.91	5.87	4.93	3.88	4.90	36.94	0.12	4.15
2	run	edge	1.00	0.05	6.17	1.10	-0.58	6.29	7.38	8.14	2.59	6.04	63.73	0.19	1.14
2	run	edge	2.00	0.08	10.45	0.29	-0.78	10.48	5.82	5.57	3.05	4.81	37.11	0.15	1.54
2	run	edge	5.00	0.17	15.60	0.42	-1.68	15.69	9.02	9.07	4.11	7.40	90.30	0.07	1.08
2	run	edge	6.60	0.22	16.06	1.27	-1.29	16.16	6.81	8.08	4.07	6.32	64.14	0.10	1.61
2	run	edge	13.20	0.42	16.70	-0.94	1.11	16.76	6.26	7.24	4.29	5.93	55.01	0.09	1.44
2	run	edge	19.50	0.61	16.95	-2.13	3.22	17.39	6.14	7.46	5.24	6.28	60.39	0.07	1.15
3	pool	edge	5.00	0.07	6.94	0.63	0.31	6.98	4.80	4.32	1.36	3.50	21.81	0.33	2.31
3	pool	edge	16.00	0.21	9.13	0.62	0.01	9.15	3.36	2.79	1.54	2.56	10.71	2.67	24.37
3	pool	edge	32.00	0.41	11.47	0.07	-0.08	11.47	3.24	2.98	1.53	2.58	10.85	0.81	9.32
3	pool	edge	47.70	0.61	10.82	-0.15	0.00	10.82	3.24	3.05	1.56	2.62	11.11	0.45	4.87
3	pool	edge	63.00	0.80	8.73	-0.47	-0.27	8.74	3.50	2.86	1.40	2.59	11.22	0.53	4.67
3	pool	edge	69.00	0.88	8.48	-0.70	0.03	8.51	3.08	2.87	1.34	2.43	9.76	0.17	1.43
3	pool	center	1.20	0.05	10.34	0.86	0.28	10.38	4.00	3.12	1.43	2.85	13.90	0.67	6.88
3	pool	center	2.07	0.06	11.15	0.42	0.30	11.16	4.34	3.23	1.64	3.07	15.99	0.57	6.38
3	pool	center	4.88	0.10	13.89	0.16	-0.07	13.89	7.75	7.04	2.27	5.69	57.39	0.16	2.16
3	pool	center	14.00	0.21	15.84	0.02	-0.25	15.85	4.41	4.22	2.27	3.64	21.25	0.29	4.66
3	pool	center	27.95	0.39	19.76	-0.06	-0.40	19.76	4.57	3.92	2.35	3.61	20.86	0.35	6.90
3	pool	center	41.93	0.56	21.27	-0.78	-0.02	21.28	3.99	3.91	2.12	3.34	17.83	0.59	12.45
3	pool	center	55.90	0.74	23.62	-0.61	0.16	23.63	3.92	3.64	1.73	3.10	15.81	0.23	5.49
3	pool	edge	1.10	0.00	1.01	-0.42	0.11	1.10	5.12	7.05	1.12	4.43	38.64	0.02	0.02
3	pool	edge	2.10	0.02	1.11	0.25	0.08	1.14	1.67	1.58	0.78	1.34	2.96	0.31	0.34
3	pool	edge	5.55	0.08	4.76	0.66	-0.56	4.84	3.44	2.91	1.39	2.58	11.13	0.21	1.01
3	pool	edge	14.47	0.23	6.30	0.68	0.03	6.34	3.72	3.40	1.83	2.98	14.38	0.51	3.22
3	pool	edge	28.80	0.47	7.53	0.11	0.14	7.53	3.36	3.15	1.79	2.77	12.21	0.37	2.80
3	pool	edge	37.30	0.61	10.84	-0.11	-0.10	10.84	4.28	3.53	1.89	3.23	17.17	0.85	9.16
3	pool	edge	49.70	0.81	13.29	-1.18	0.30	13.35	4.14	3.10	1.69	2.98	14.80	0.50	6.66

Table C.2 (continued). Summary of flow field data for the Potlatch Reach

CS	Unit	Loc.	Cuu	Cvv	Cww	Cuv	Cuw	Cvw	τ_R	Ss	St	Sv	Ks	Kt	Kv
1	riffle	edge	35.82	34.75	18.91	9.86	-5.51	4.46	0.55	0.09	-0.05	5.45	-0.02	0.04	143.46
1	riffle	edge	39.45	37.95	17.04	6.27	-10.75	6.48	1.08	0.12	-0.02	-0.10	-0.09	-0.11	-0.05
1	riffle	edge	70.43	63.97	21.28	10.65	-16.61	-0.50	1.66	0.18	0.00	-0.05	-0.13	-0.08	0.14
1	riffle	edge	75.10	60.50	24.50	0.91	-20.33	1.83	2.04	-0.06	0.06	0.15	-0.13	0.01	-0.09
1	riffle	edge	73.84	48.50	30.24	-4.96	-18.35	1.06	1.84	0.11	0.01	-0.05	-0.10	0.11	-0.10
1	riffle	edge	69.60	50.29	33.12	-4.98	-16.83	-3.03	1.69	-0.10	-0.02	0.06	-0.14	0.06	-0.08
1	riffle	edge	55.24	43.15	30.28	-3.00	-10.92	-1.65	1.09	-0.14	0.02	0.36	-0.04	0.04	0.12
1	riffle	center	71.23	60.21	28.51	12.01	-4.02	9.86	0.40	0.05	0.19	2.52	0.32	0.63	45.20
1	riffle	center	116.87	87.39	39.19	26.73	-4.65	11.05	0.46	0.07	0.18	-0.17	0.02	0.11	0.15
1	riffle	center	152.27	117.89	46.59	34.80	-11.98	7.68	1.20	0.18	0.21	-0.09	0.04	-0.04	0.23
1	riffle	center	165.85	129.04	68.47	66.60	0.37	10.38	-0.04	0.22	0.17	-0.07	-0.16	-0.15	0.14
1	riffle	center	156.99	141.54	109.99	52.88	28.26	8.23	-2.83	0.03	0.25	0.11	-0.20	-0.05	-0.29
1	riffle	center	152.70	167.61	105.09	47.32	25.75	17.67	-2.58	0.19	0.45	0.20	-0.22	0.16	-0.03
1	riffle	center	139.51	144.98	100.61	32.19	17.75	10.98	-1.78	0.17	0.35	0.26	-0.01	-0.08	0.16
1	riffle	edge	38.69	56.46	39.58	0.03	-13.06	17.36	1.31	-0.05	-0.42	3.73	0.41	2.52	60.77
1	riffle	edge	104.62	111.53	52.15	29.21	-28.32	26.01	2.83	0.30	0.05	0.14	0.05	-0.22	0.40
1	riffle	edge	161.68	112.19	74.71	35.49	-20.72	13.62	2.07	0.38	0.24	-0.31	-0.09	-0.18	0.20
1	riffle	edge	180.21	137.92	78.28	30.31	-26.95	11.46	2.70	0.33	0.20	-0.18	-0.16	-0.10	-0.22
1	riffle	edge	232.43	206.78	112.23	24.41	-17.07	-9.32	1.71	0.07	0.10	-0.10	-0.32	-0.49	-0.21
1	riffle	edge	285.95	192.87	126.05	-16.06	-30.86	-5.00	3.09	0.17	-0.18	0.06	-0.18	-0.36	-0.30
1	riffle	edge	300.99	178.45	111.01	-35.29	-31.42	-2.50	3.15	0.12	-0.26	0.11	-0.35	-0.32	-0.23
2	run	edge	65.08	53.81	32.60	10.73	-9.16	-11.51	0.92	-0.04	0.24	12.14	0.00	0.08	251.68
2	run	edge	87.66	51.83	12.85	10.63	-12.25	-11.17	1.23	-0.07	0.26	-0.01	-0.30	0.24	-0.17
2	run	edge	68.96	40.00	13.48	15.32	-7.80	-4.94	0.78	-0.21	0.10	0.09	0.01	0.05	-0.02
2	run	edge	104.60	80.52	21.76	14.05	1.94	-10.07	-0.19	-0.10	-0.01	0.02	0.03	-0.05	-0.09
2	run	edge	64.41	56.16	24.49	11.82	-10.22	-7.08	1.02	-0.13	-0.10	0.12	-0.15	-0.01	0.13
2	run	edge	52.62	50.36	19.79	10.27	-3.88	-6.04	0.39	-0.09	-0.32	0.29	-0.12	0.19	0.27
2	run	edge	47.74	57.22	19.12	10.78	-4.31	-5.79	0.43	0.07	-0.17	0.23	-0.01	0.11	0.21
2	run	center	66.26	66.40	23.41	-2.03	-19.42	-7.22	1.94	0.26	0.07	-0.07	-0.01	-0.21	-0.19
2	run	center	73.07	50.16	25.82	-6.77	-23.37	-4.90	2.34	0.00	0.12	0.17	-0.26	-0.15	-0.45
2	run	center	74.18	53.86	18.20	-3.15	-12.23	-7.29	1.22	-0.09	-0.06	0.24	0.10	-0.01	0.15
2	run	center	49.67	35.10	18.27	-0.47	-10.75	-2.66	1.08	-0.13	-0.08	0.16	0.03	-0.02	0.04
2	run	center	37.04	29.53	16.85	-0.64	-7.08	-0.57	0.71	-0.03	0.06	-0.03	-0.07	-0.13	0.11
2	run	center	34.51	24.32	15.05	-0.49	-4.33	0.52	0.43	-0.05	0.00	-0.08	-0.13	0.06	0.06
2	run	edge	54.50	66.24	6.70	-13.40	-9.20	-3.52	0.92	-0.09	0.03	-0.08	-0.10	0.23	-0.16
2	run	edge	33.85	31.07	9.29	0.06	-6.04	-2.99	0.61	0.08	-0.10	-0.25	0.20	0.08	0.02
2	run	edge	81.44	82.26	16.91	-9.15	-8.14	4.80	0.82	0.06	-0.01	-0.21	0.13	0.12	0.14
2	run	edge	46.42	65.30	16.55	-4.62	-7.60	5.70	0.76	0.04	-0.14	-0.22	0.12	-0.04	-0.04
2	run	edge	39.21	52.40	18.41	-2.10	-2.12	0.68	0.21	0.12	-0.21	-0.12	-0.10	-0.04	0.12
2	run	edge	37.69	55.61	27.47	-4.49	1.23	0.55	-0.12	0.08	-0.25	-0.25	0.06	-0.10	0.04
3	pool	edge	23.06	18.70	1.86	-0.88	0.37	0.53	-0.04	-0.09	0.11	0.03	0.16	0.33	0.14
3	pool	edge	11.31	7.76	2.36	-0.35	-1.02	0.09	0.10	-0.27	0.03	-0.18	0.00	0.08	-0.18
3	pool	edge	10.50	8.87	2.33	1.52	0.14	-0.09	-0.01	-0.07	0.05	0.28	0.35	0.06	-0.12
3	pool	edge	10.49	9.28	2.44	1.51	0.44	-0.50	-0.04	0.05	0.09	-0.31	0.22	0.01	0.25
3	pool	edge	12.28	8.18	1.97	1.89	0.81	-0.24	-0.08	0.09	0.08	0.11	-0.05	0.07	-0.24
3	pool	edge	9.47	8.26	1.80	0.05	0.60	-0.14	-0.06	-0.01	0.08	0.27	0.12	0.28	0.13
3	pool	center	16.01	9.74	2.05	-0.65	-0.52	-0.59	0.05	0.11	0.00	-0.04	-0.17	0.06	0.16
3	pool	center	18.81	10.46	2.70	0.04	-1.46	-0.51	0.15	0.28	0.18	-0.04	-0.22	0.35	-0.08
3	pool	center	60.03	49.61	5.13	-6.03	0.85	-0.88	-0.09	0.03	0.05	-0.09	0.14	0.29	0.05
3	pool	center	19.49	17.83	5.17	-0.61	-1.65	-1.35	0.16	0.10	0.17	0.15	0.00	0.06	-0.30
3	pool	center	20.86	15.33	5.52	-0.43	-3.62	0.32	0.36	-0.24	0.05	0.32	0.04	0.05	-0.04
3	pool	center	15.91	15.25	4.49	-0.52	-1.89	0.14	0.19	-0.14	0.03	0.23	0.09	-0.09	-0.08
3	pool	center	15.36	13.25	3.01	-0.07	-0.41	-0.30	0.04	-0.06	-0.06	0.17	0.13	-0.03	0.01
3	pool	edge	26.26	49.76	1.26	1.76	-1.40	-1.82	0.14	0.29	-0.36	0.12	0.30	0.09	0.19
3	pool	edge	2.80	2.50	0.61	0.48	0.06	-0.26	-0.01	0.06	0.09	-0.45	0.21	0.98	0.28
3	pool	edge	11.84	8.49	1.92	-1.22	-1.03	0.80	0.10	0.00	-0.11	-0.22	-0.01	0.31	0.10
3	pool	edge	13.84	11.58	3.34	-2.32	-1.17	0.80	0.12	0.21	0.04	-0.01	0.03	0.00	0.21
3	pool	edge	11.32	9.92	3.19	-1.90	-0.60	-0.08	0.06	0.13	0.03	0.20	0.19	0.13	0.23
3	pool	edge	18.31	12.46	3.58	-3.36	-1.06	0.09	0.11	-0.08	0.07	-0.02	-0.16	-0.01	0.12
3	pool	edge	17.17	9.59	2.85	-2.43	-1.47	0.14	0.15	0.04	0.02	0.47	0.69	0.37	0.57

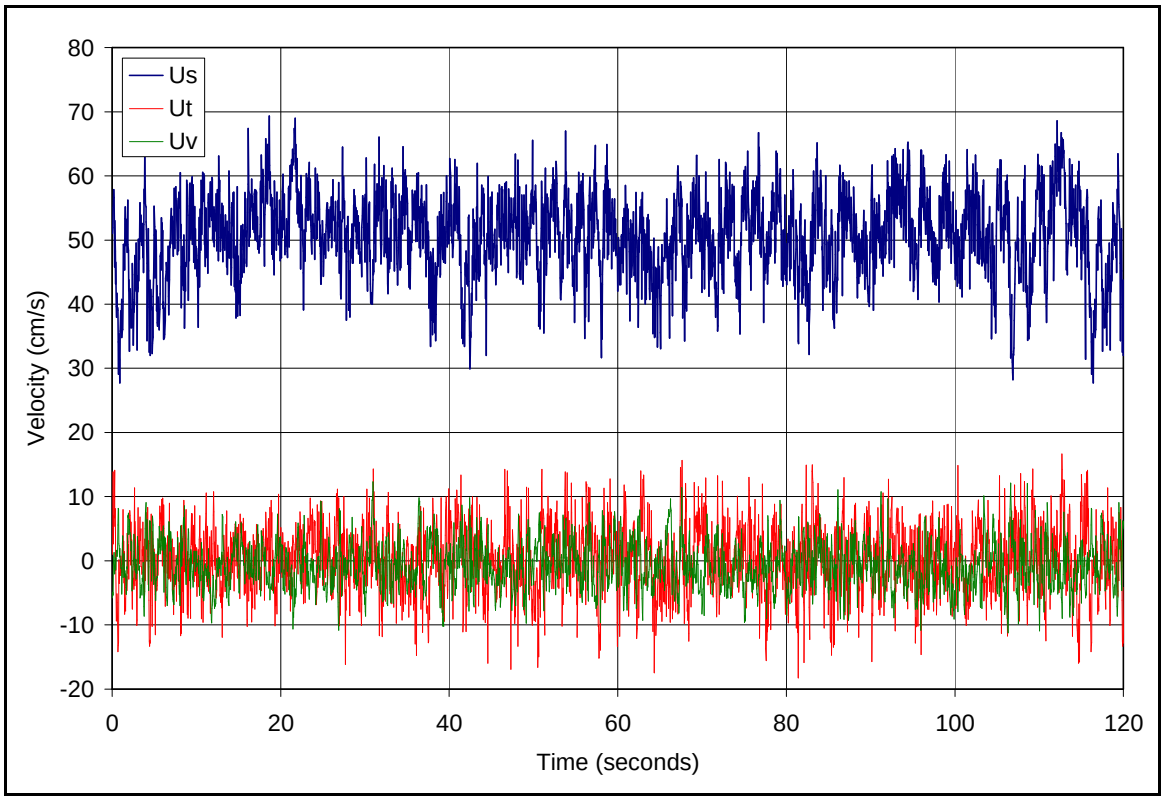

Figure C.1. Time series velocity for St. Maries C.S. 1, Station 3, 0.6h

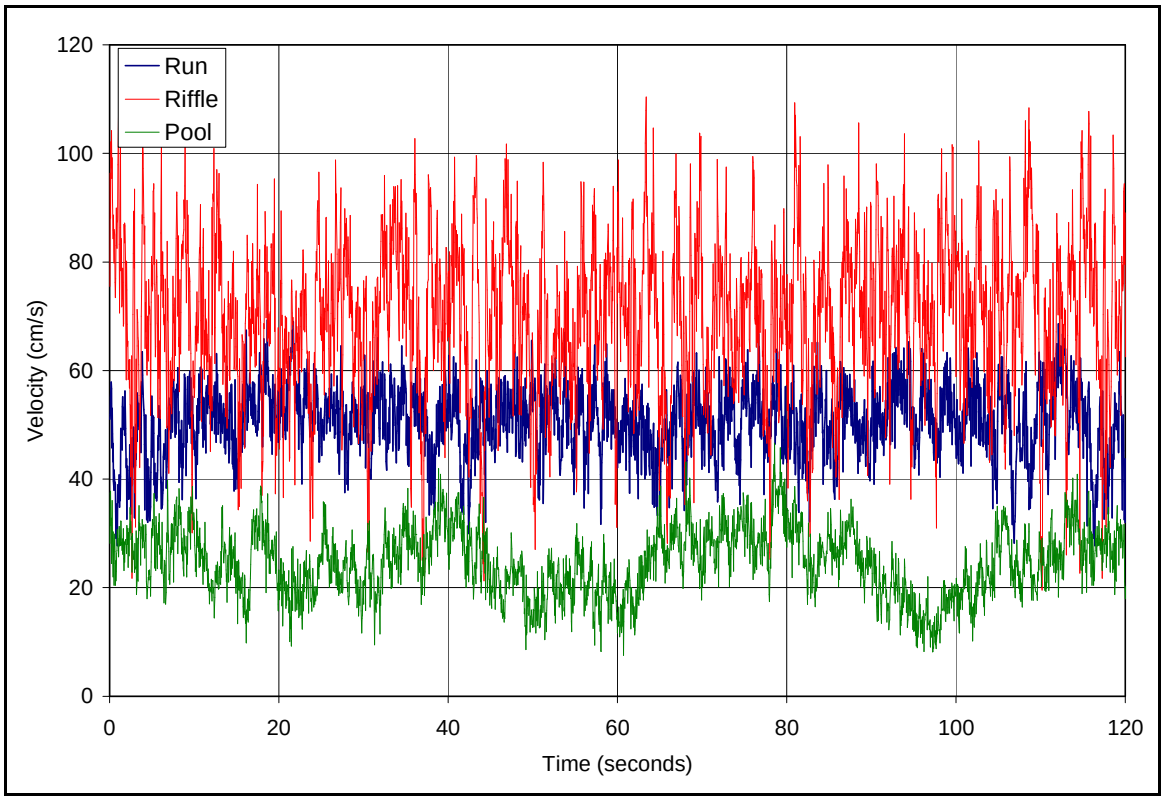

Figure C.2. Time series by unit for the St. Maries reach at 0.6h

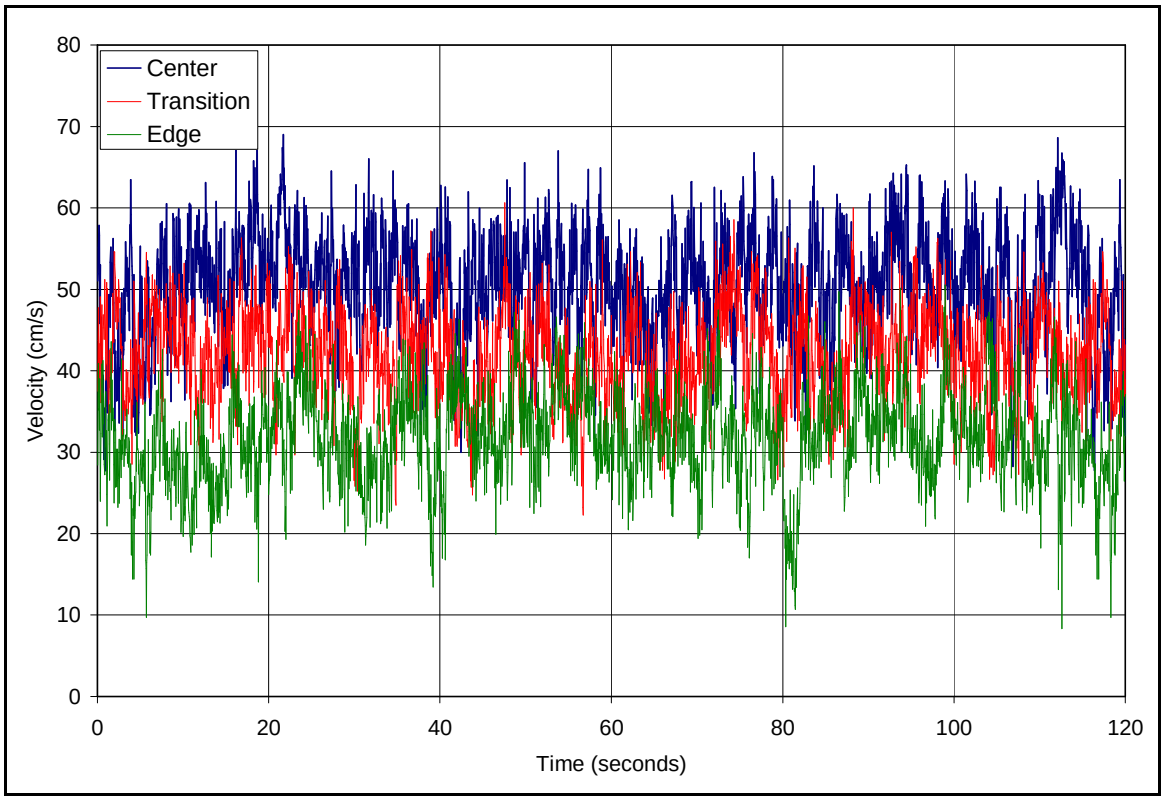

Figure C.3. Time series data by transverse location for the St. Maries, C.S. 2

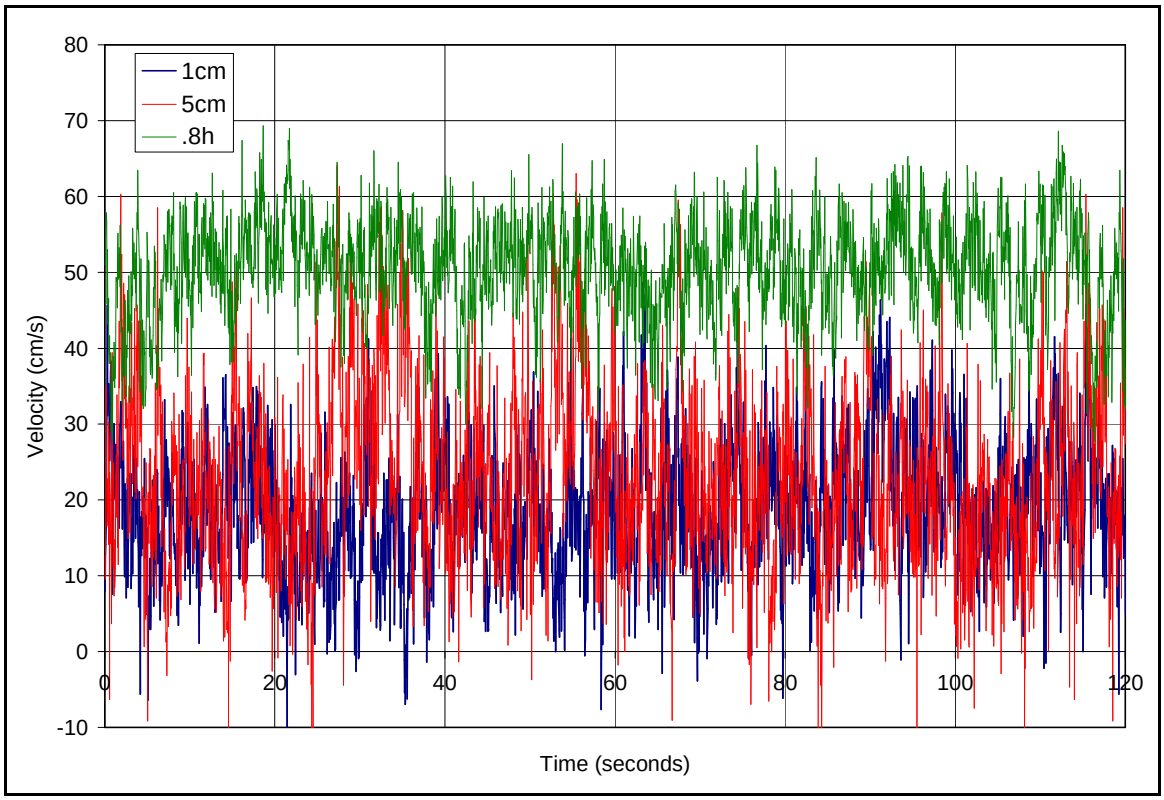

Figure C.4. Time series data by vertical location for the St. Maries, C.S. 2

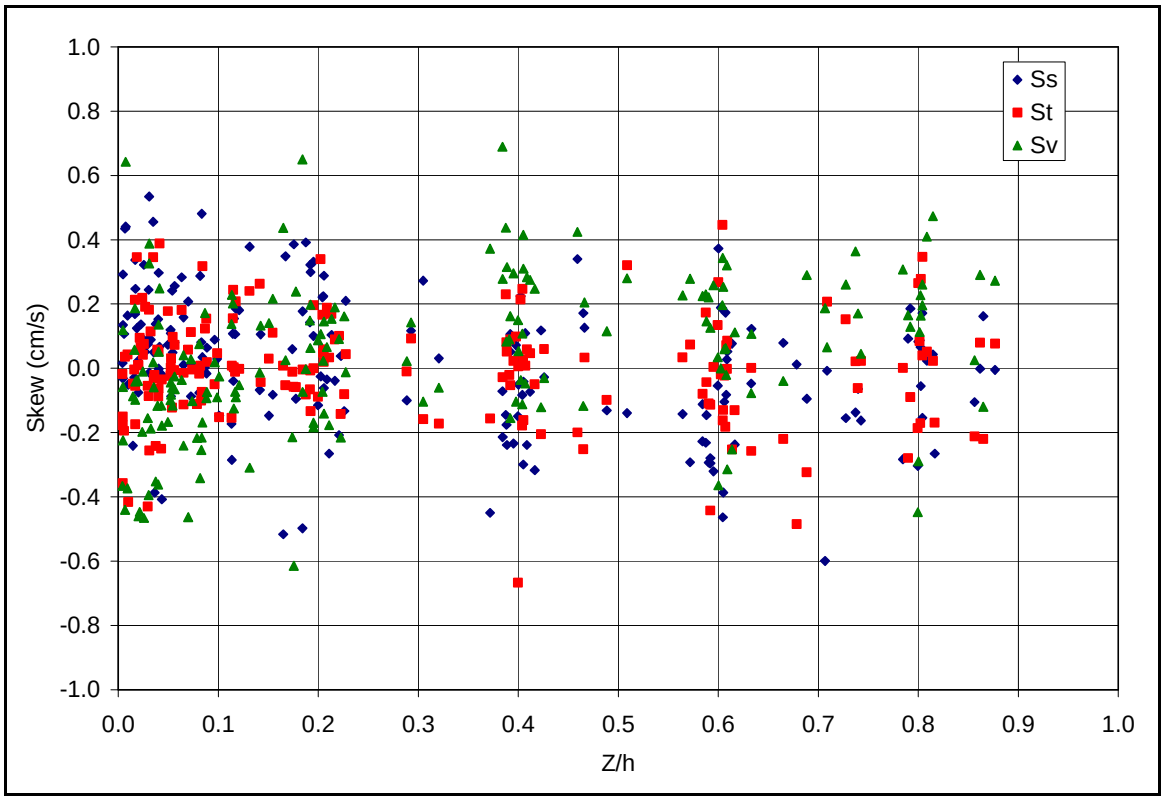

Figure C.5. Velocity skew vertical profiles

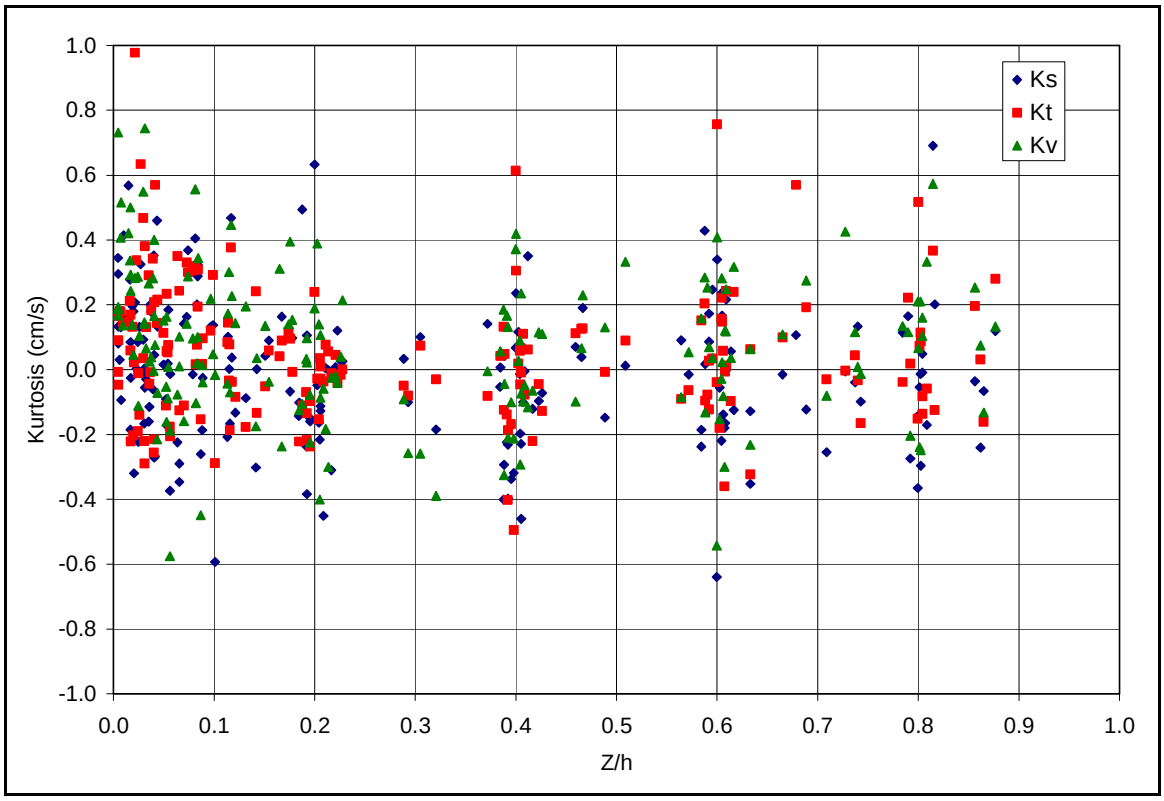

Figure C.6. Velocity kurtosis vertical profiles

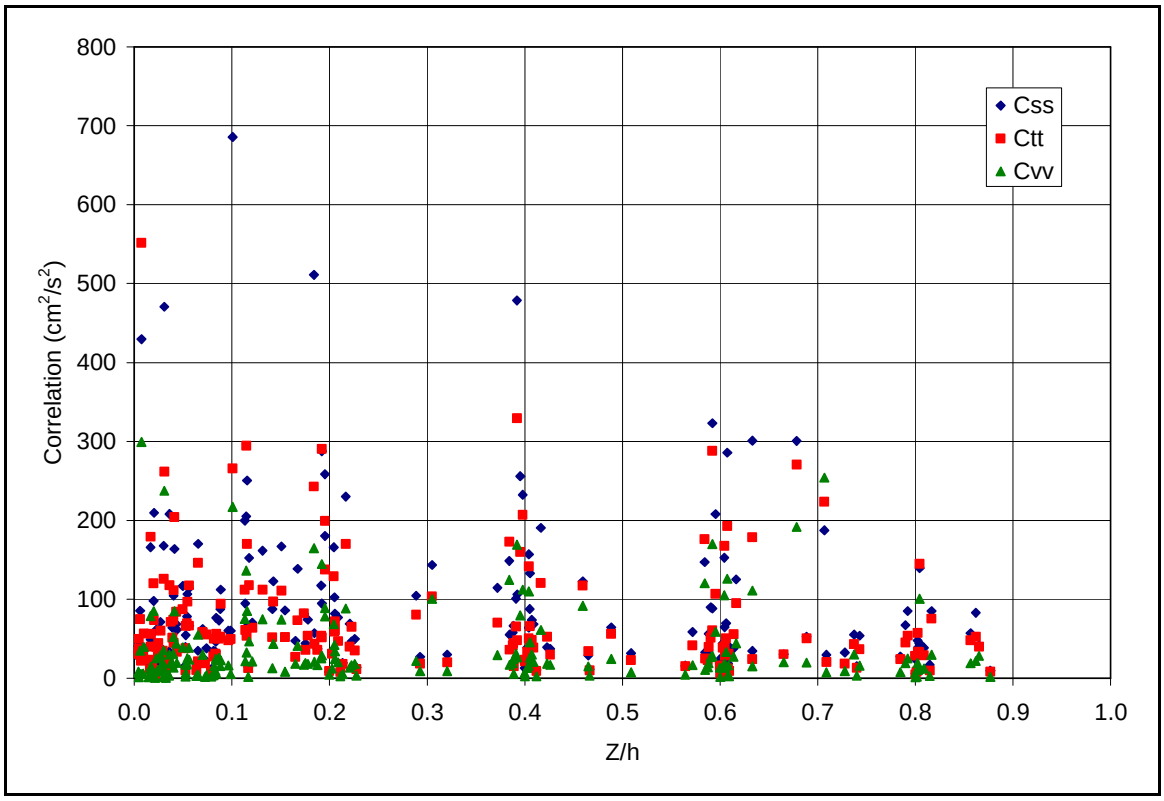

Figure C.7. Normal correlation profiles

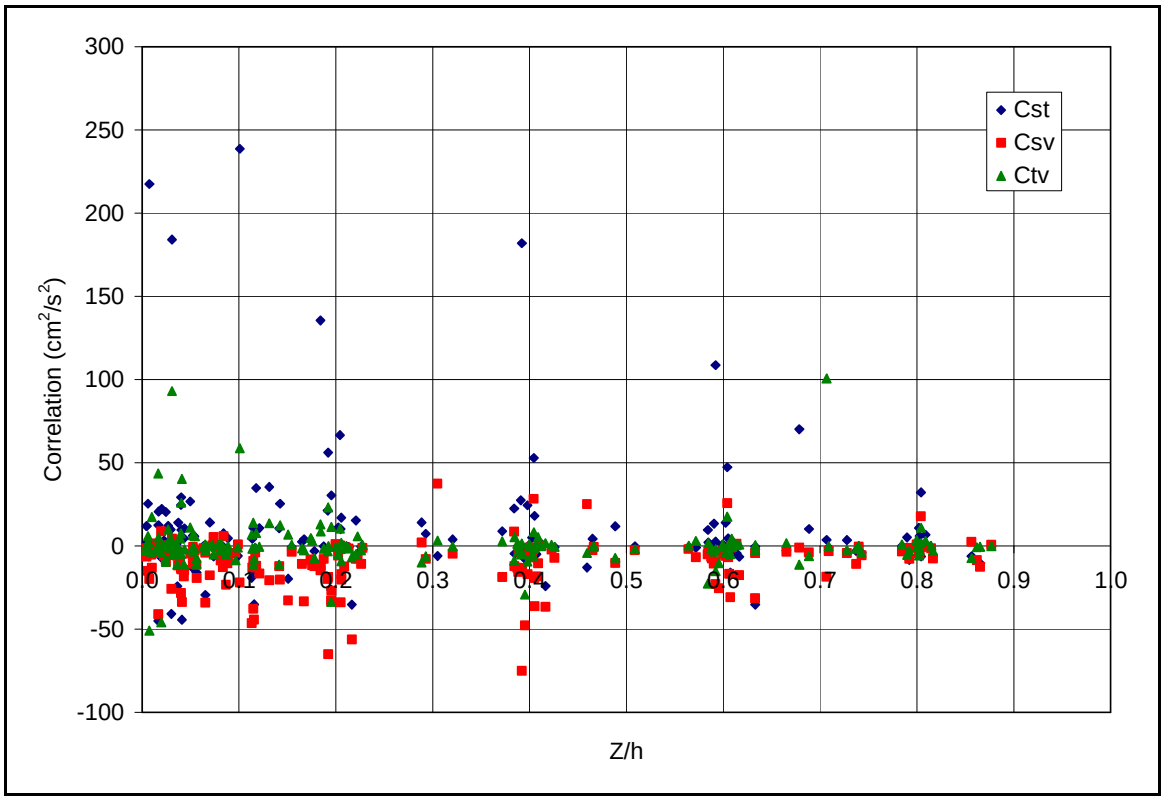

Figure C.8. Cross correlation profiles

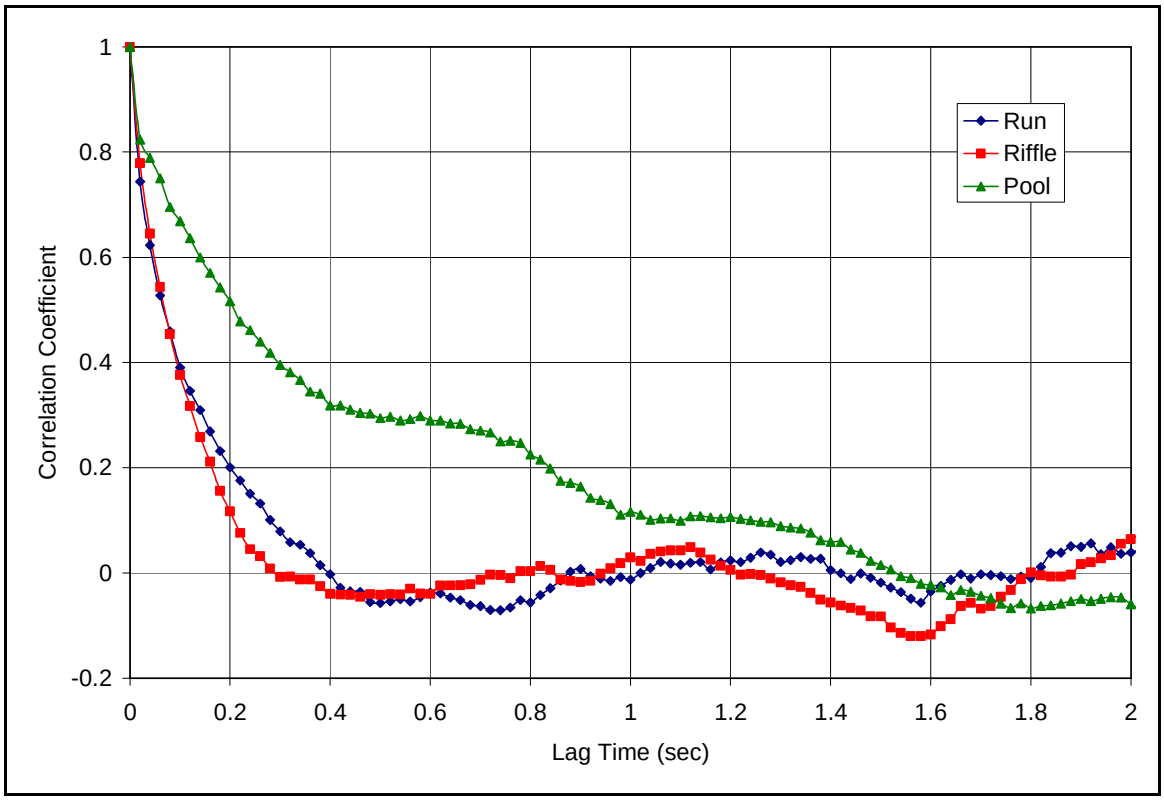

Figure C.9. Correlation coefficients by stream unit

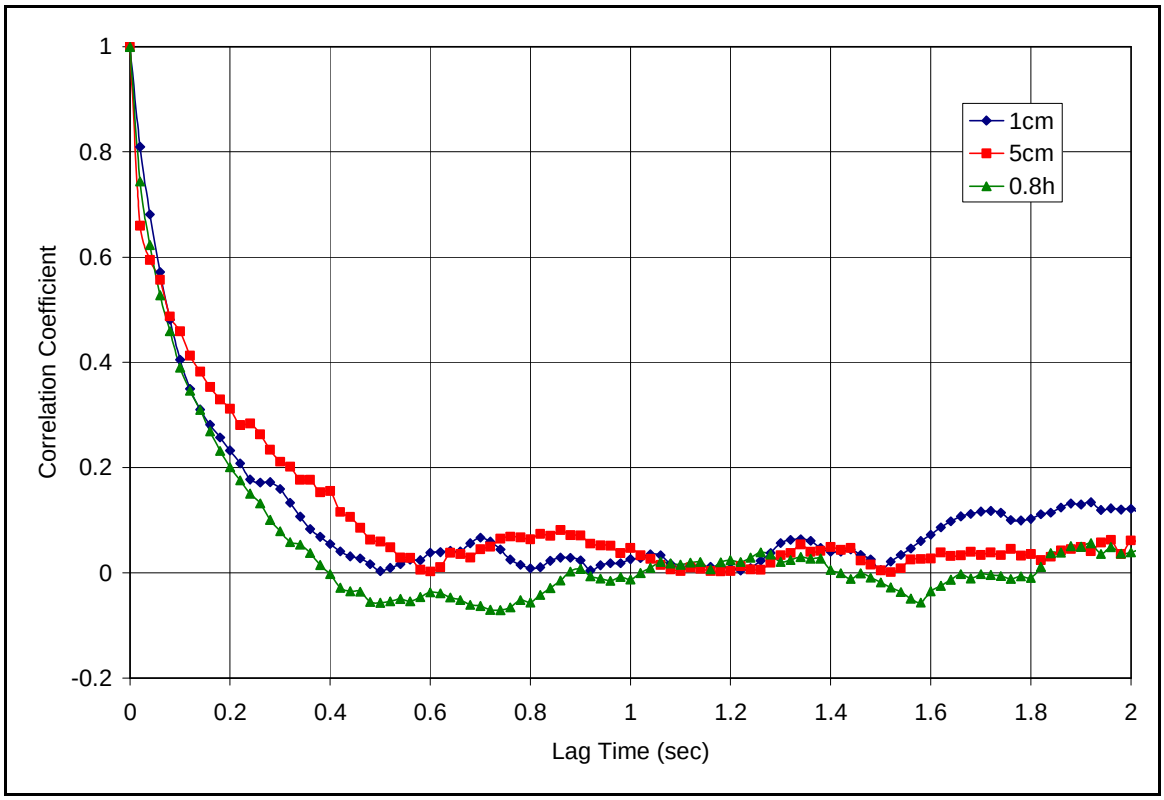

Figure C.10. Correlation coefficients by vertical location

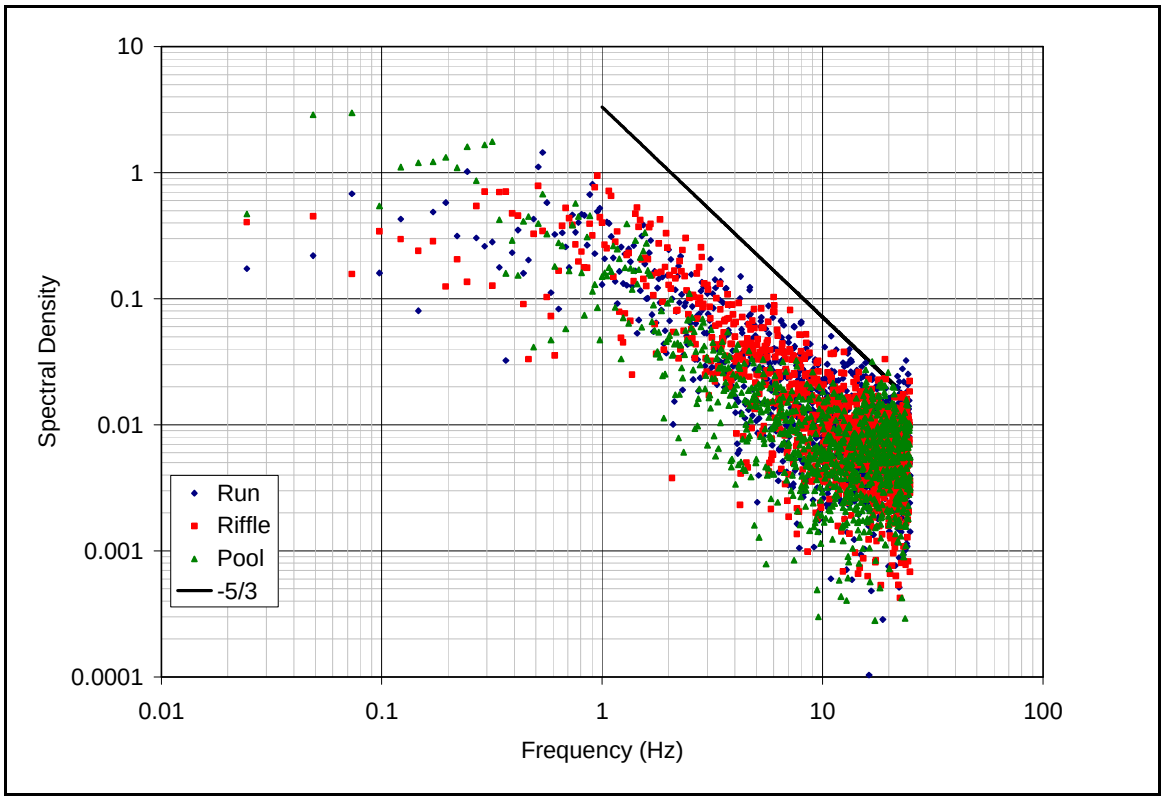

Figure C.11. Spectral density versus frequency by stream unit, St. Maries Reach

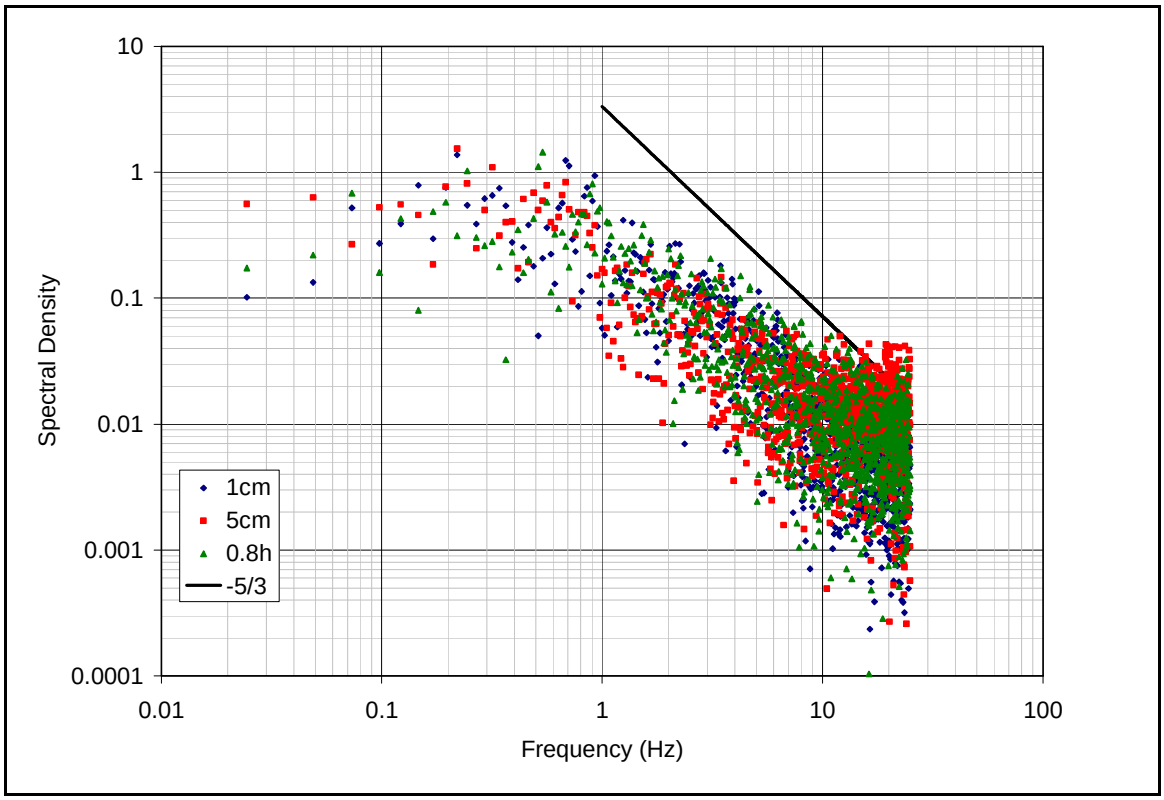

Figure C.12. Spectral density versus frequency by vertical location St. Maries Reach

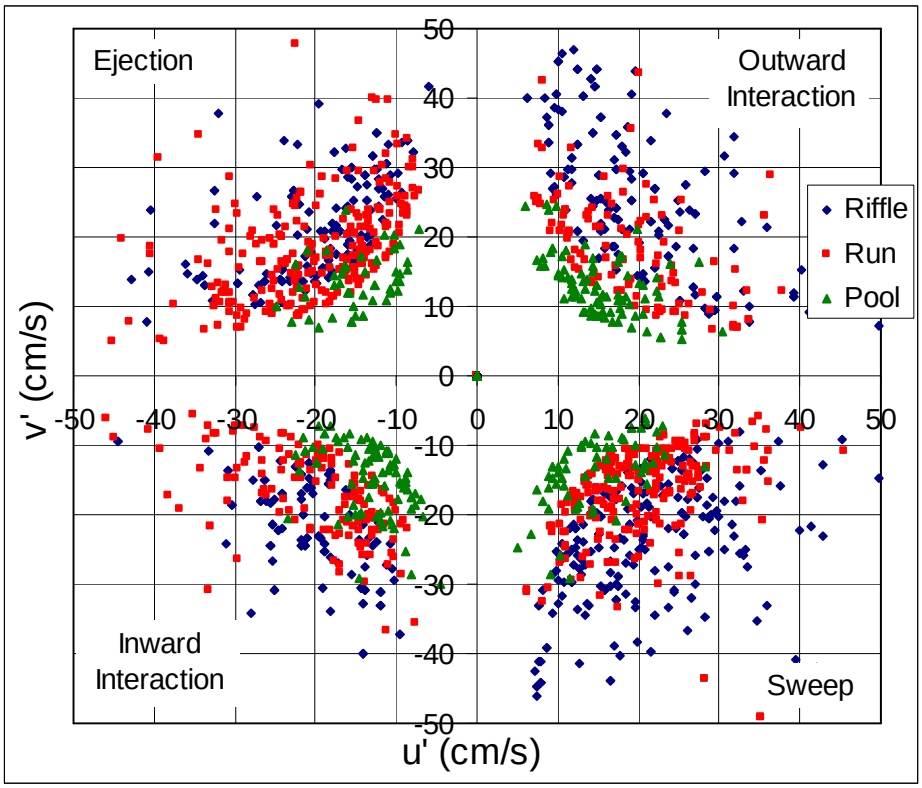

Figure C.13. Quadrant data by stream unit, St. Maries Reach, 3cm

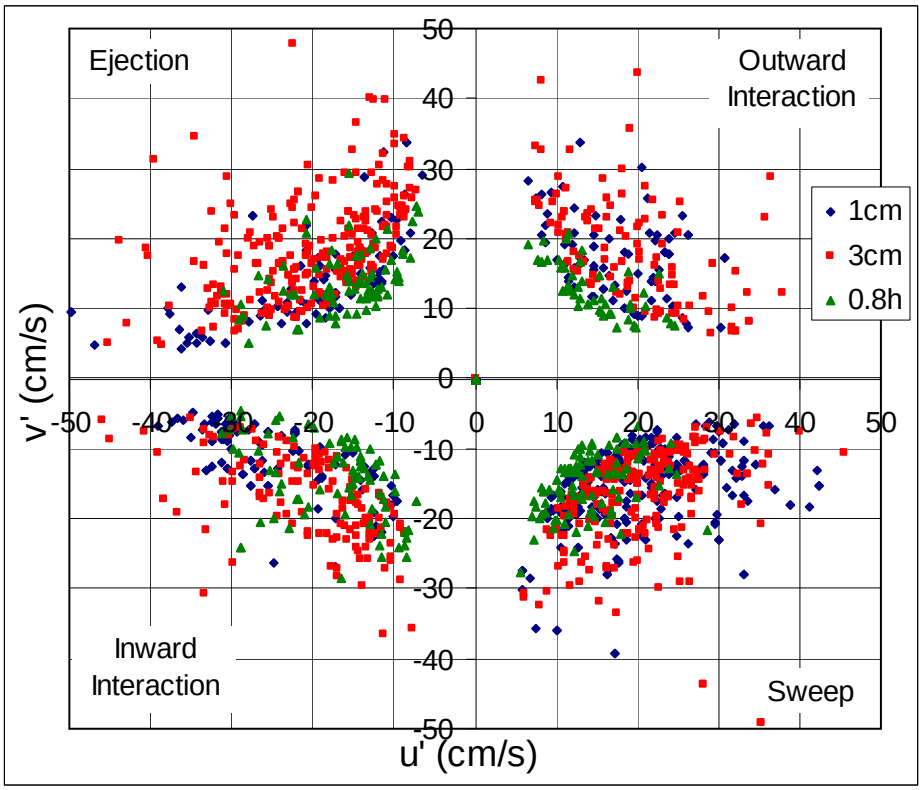

Figure C.14. Quadrant analysis by vertical location, St. Maries, C.S. 2, St. 2

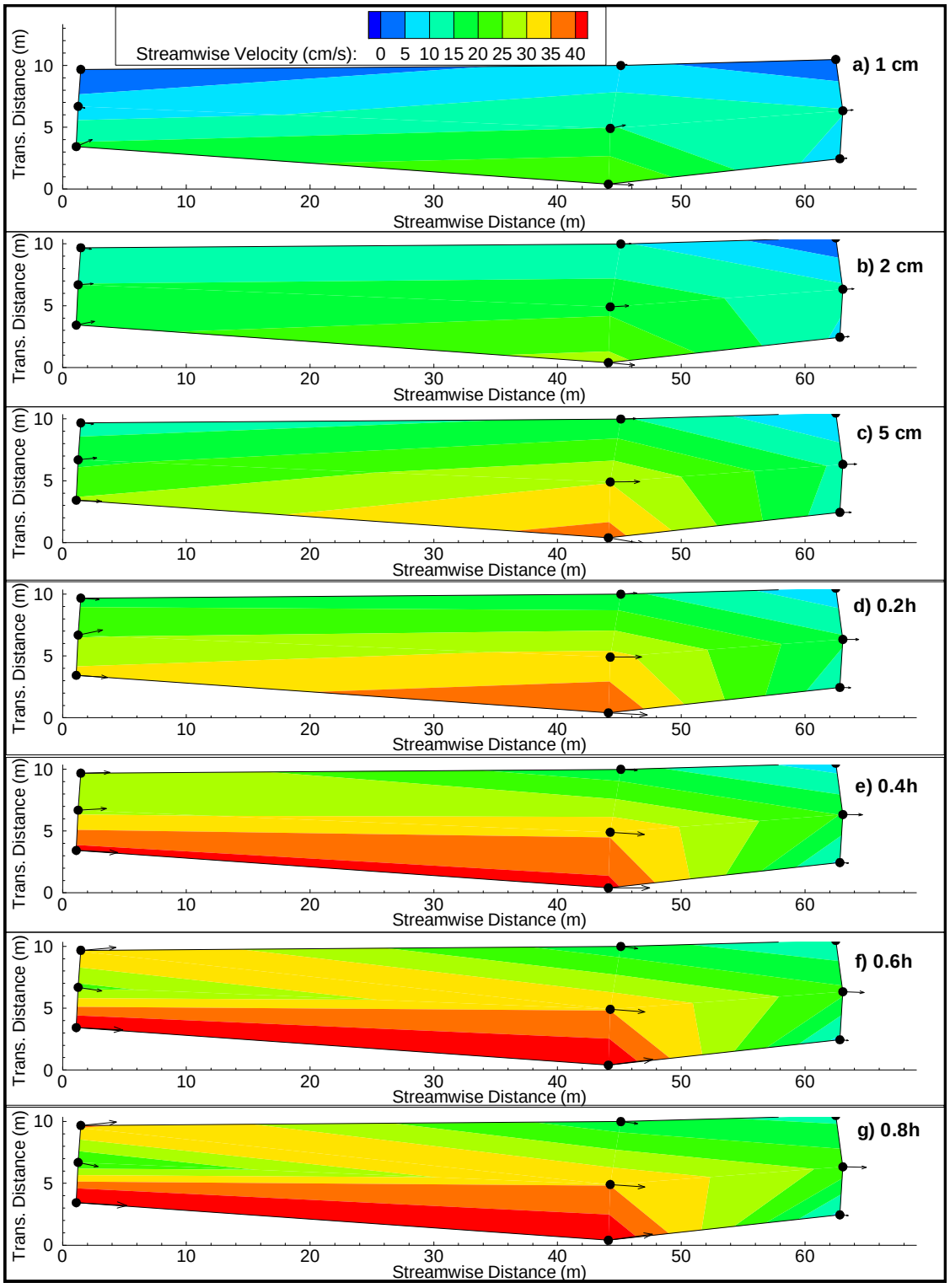

Figure C.15. Potlatch reach streamwise velocity distributions and velocity vectors

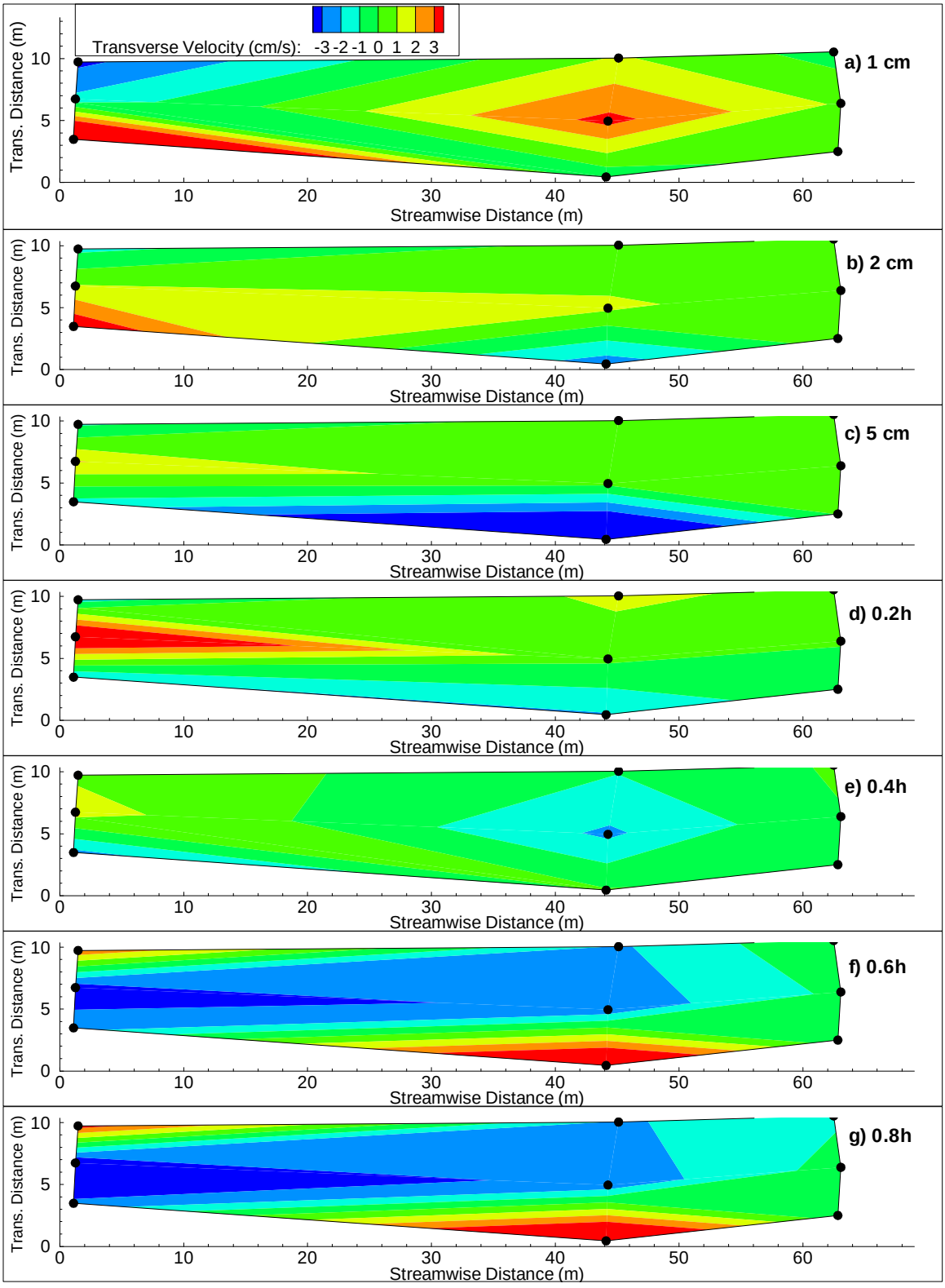

Figure C.16. Potlatch reach transverse velocity distributions

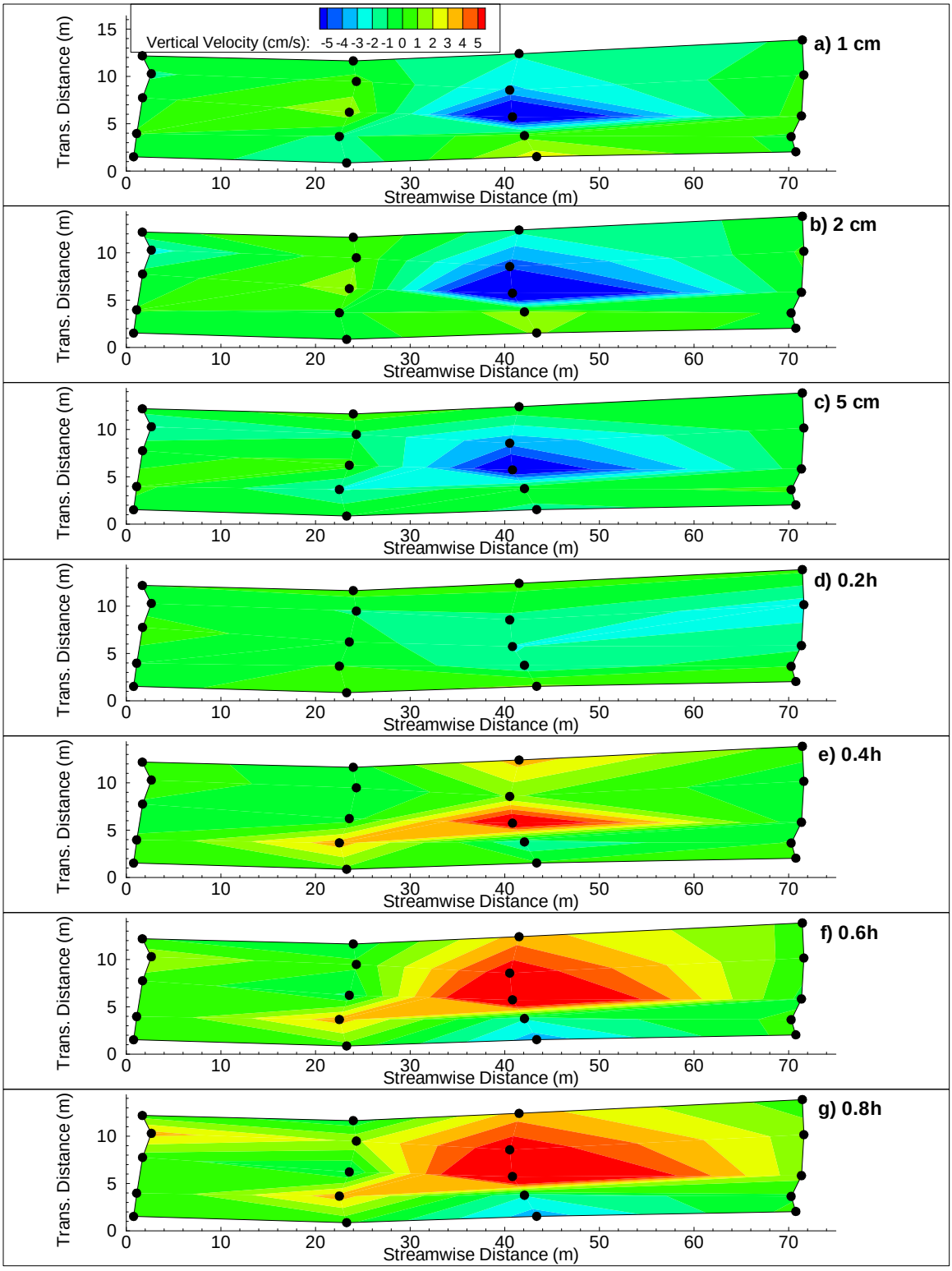

Figure C.17. St. Maries reach vertical velocity distributions

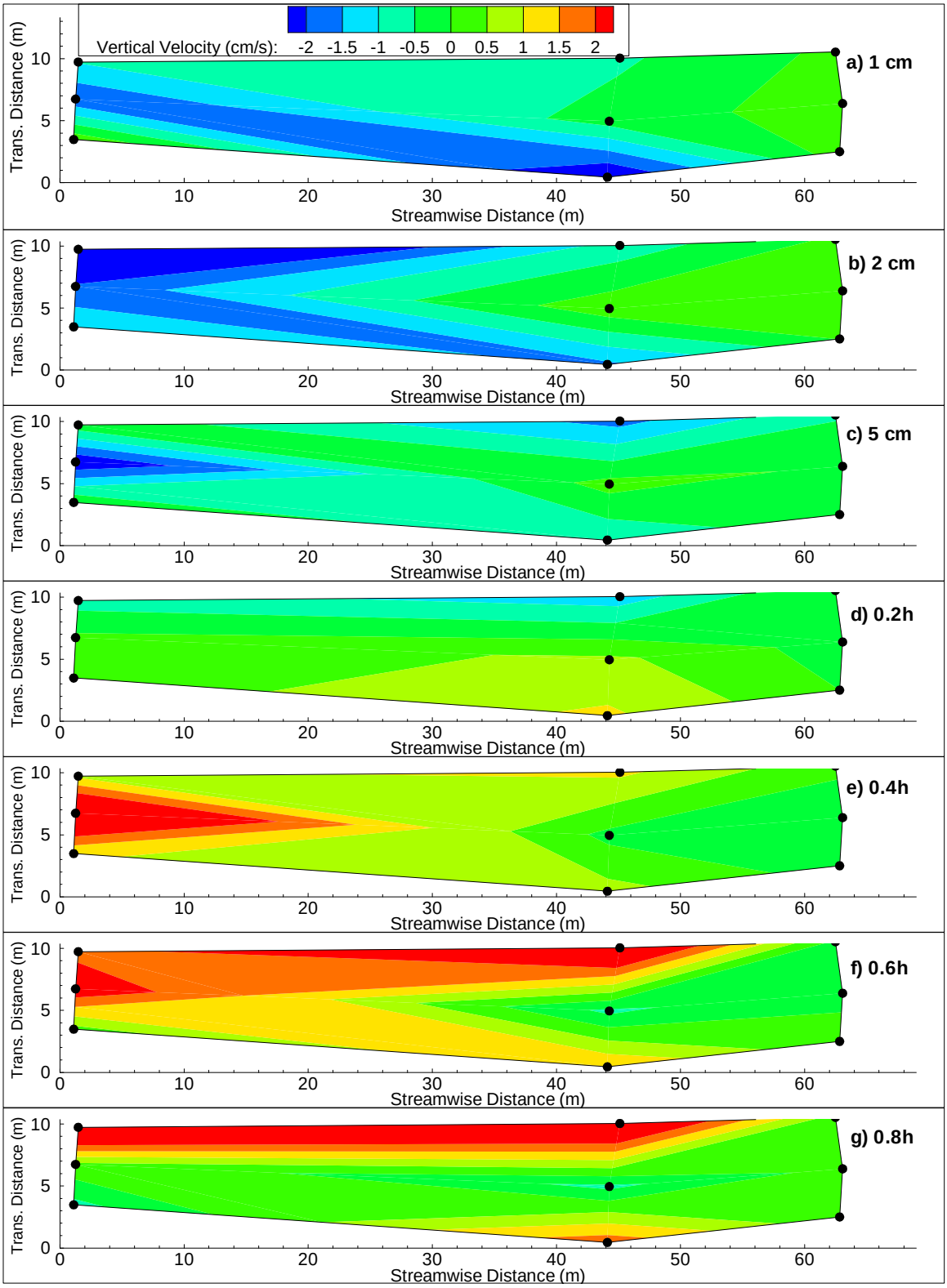

Figure C.18. Potlatch reach vertical velocity distributions

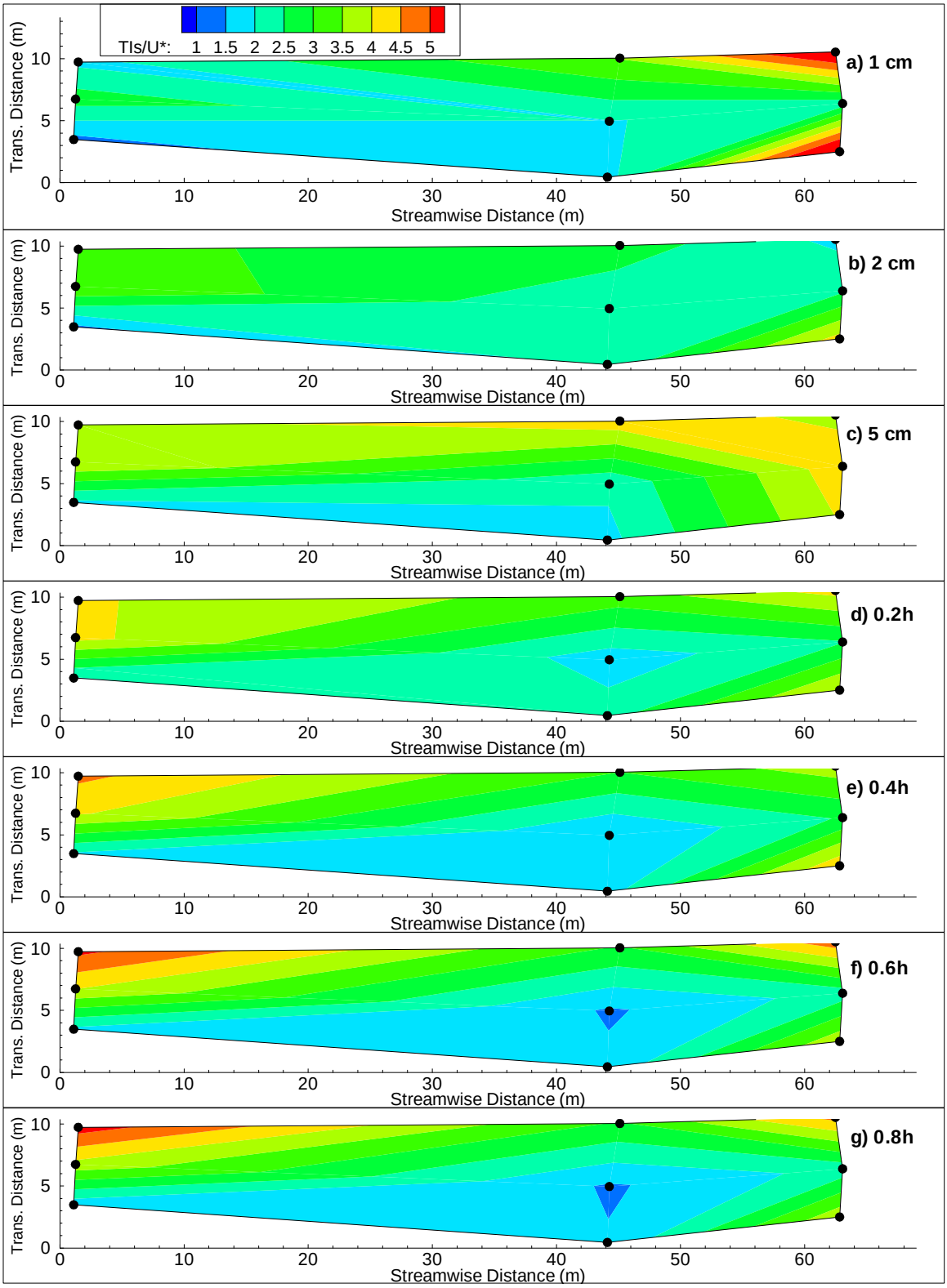

Figure C.19. Potlatch reach streamwise turbulence intensity distributions

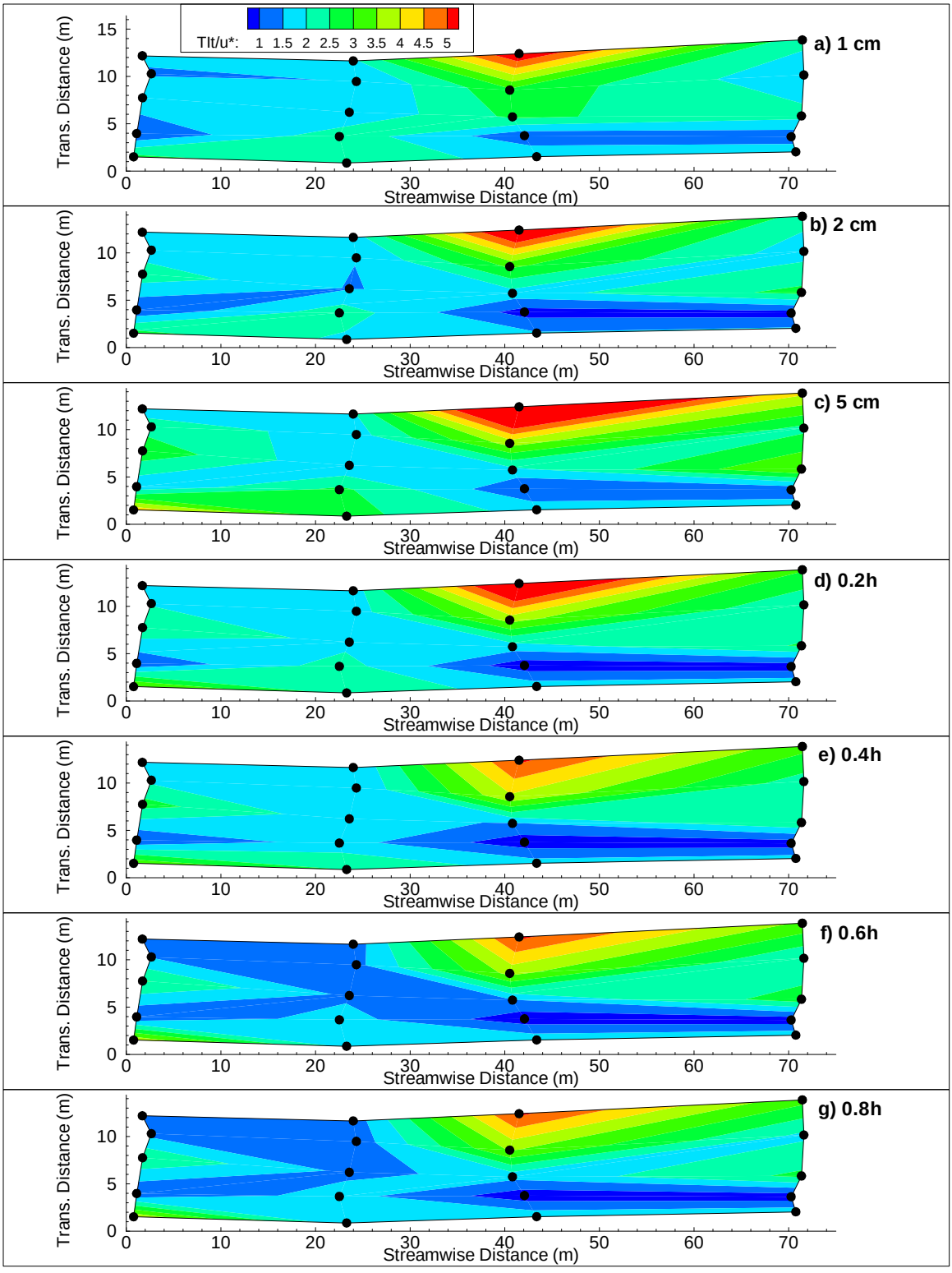

Figure C.20. St. Maries reach transverse TI distributions

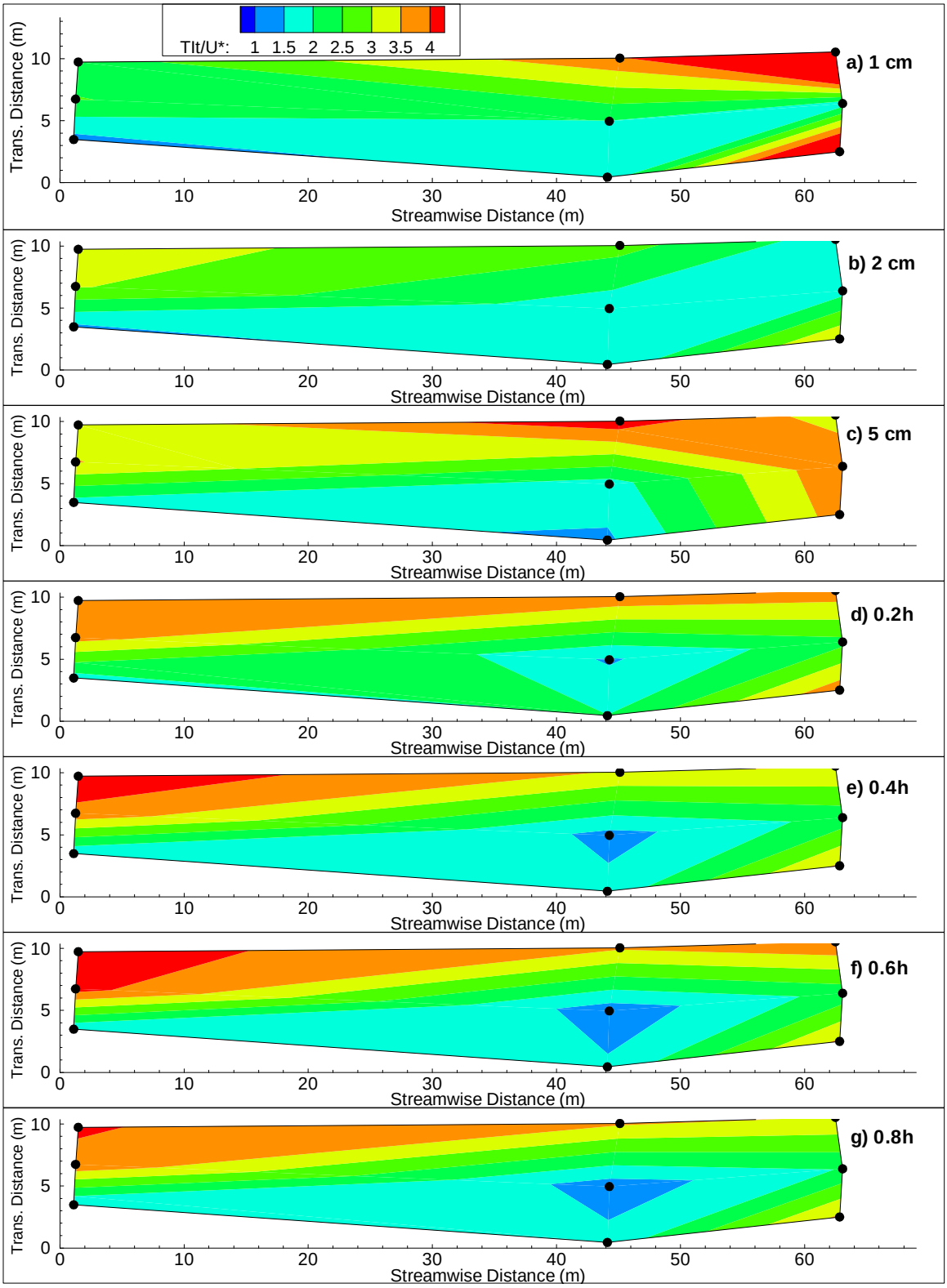

Figure C.21. Potlatch reach transverse TI distributions

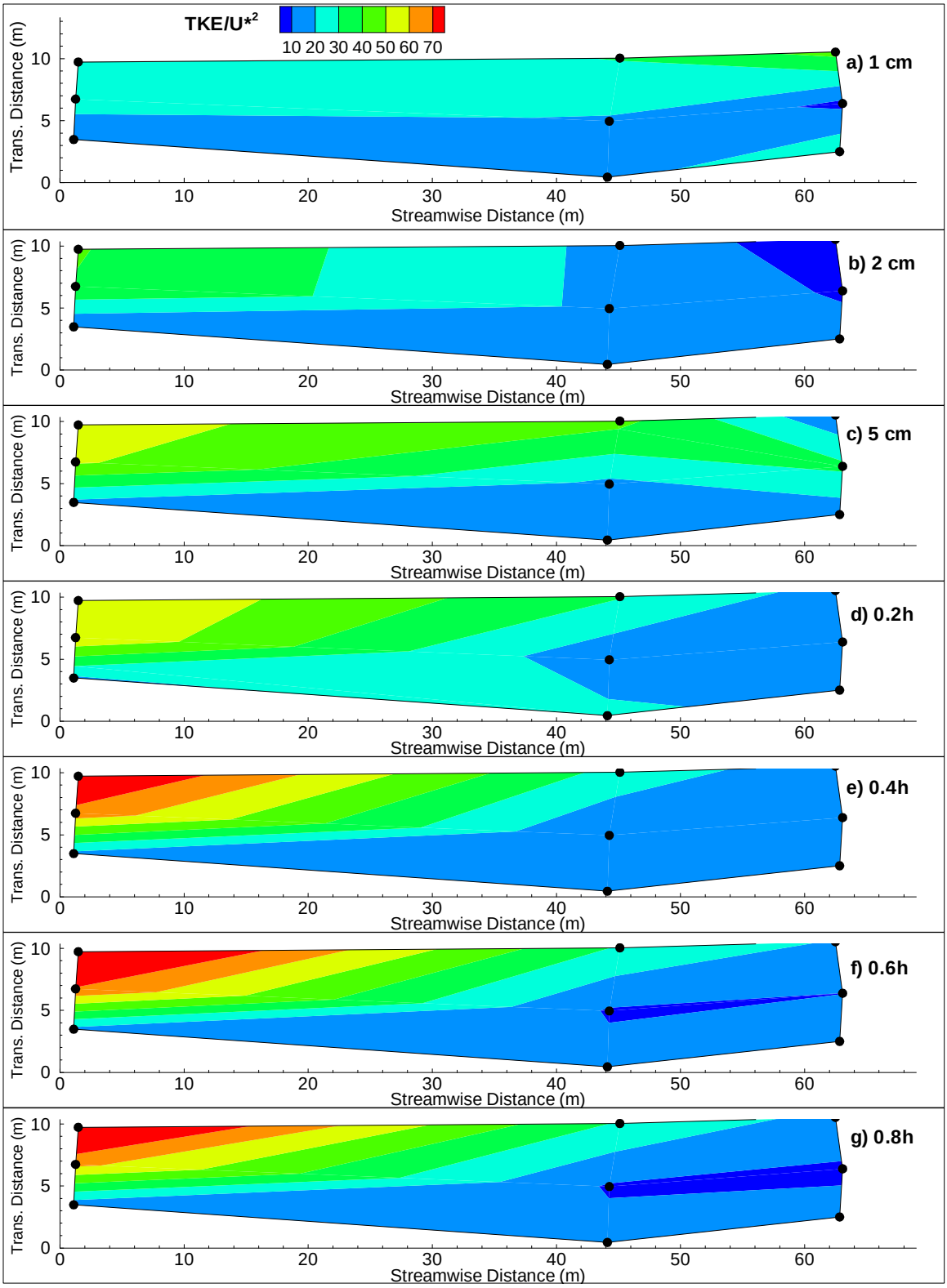

Figure C.22. Potlatch reach TKE distributions

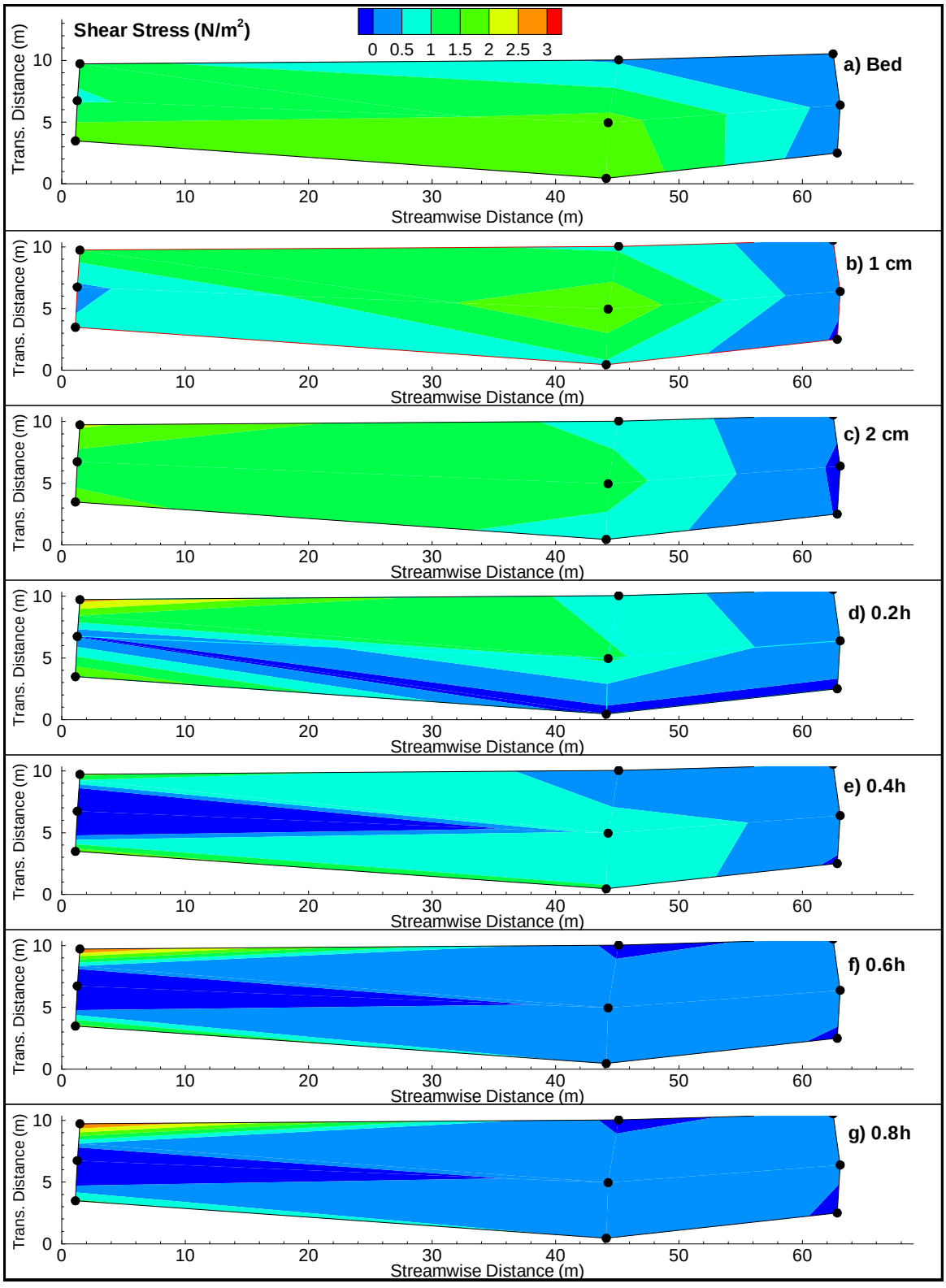

Figure C.23. Potlatch reach shear stress distributions

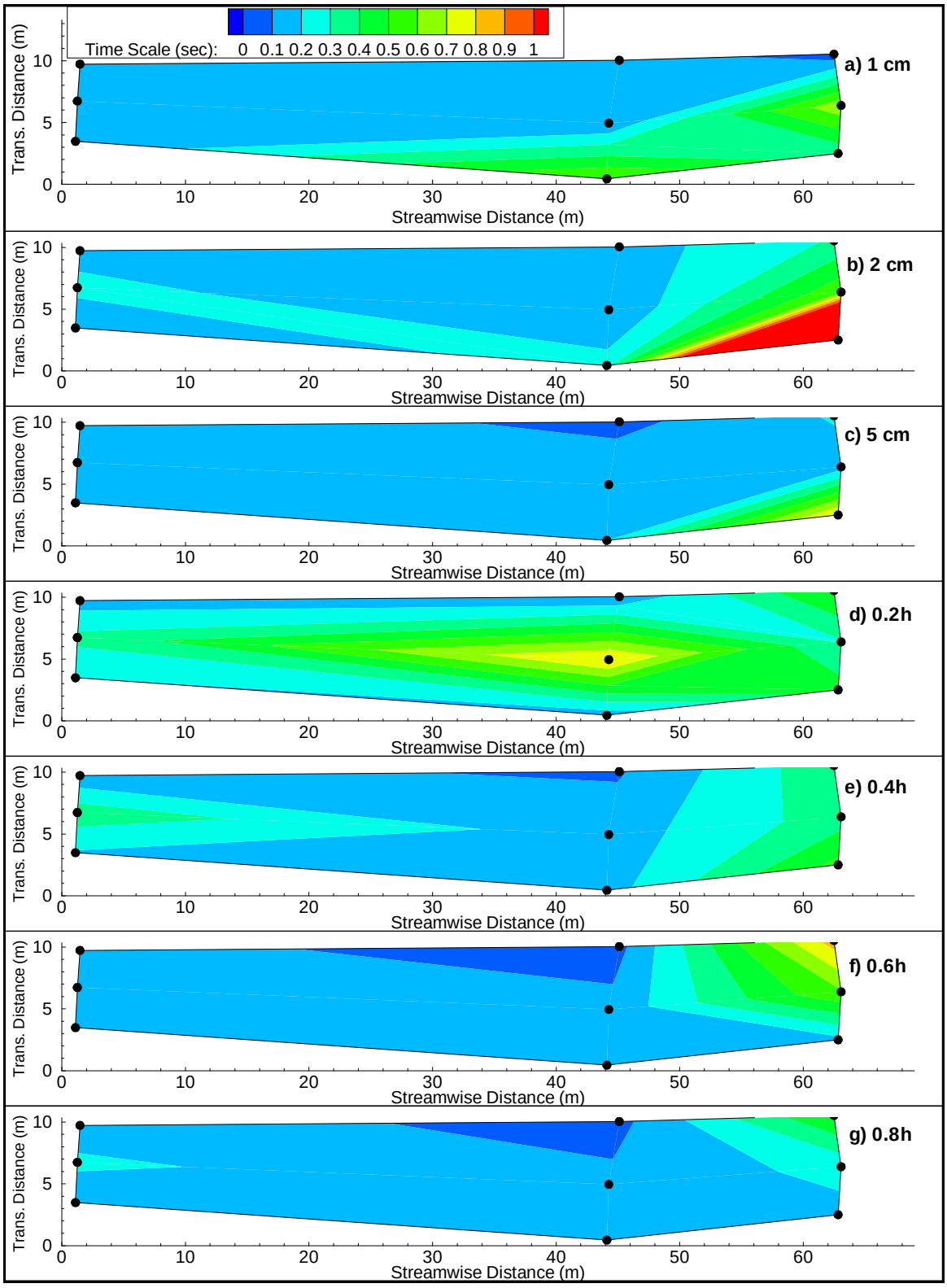

Figure C.24. Potlatch reach integral time scale distributions

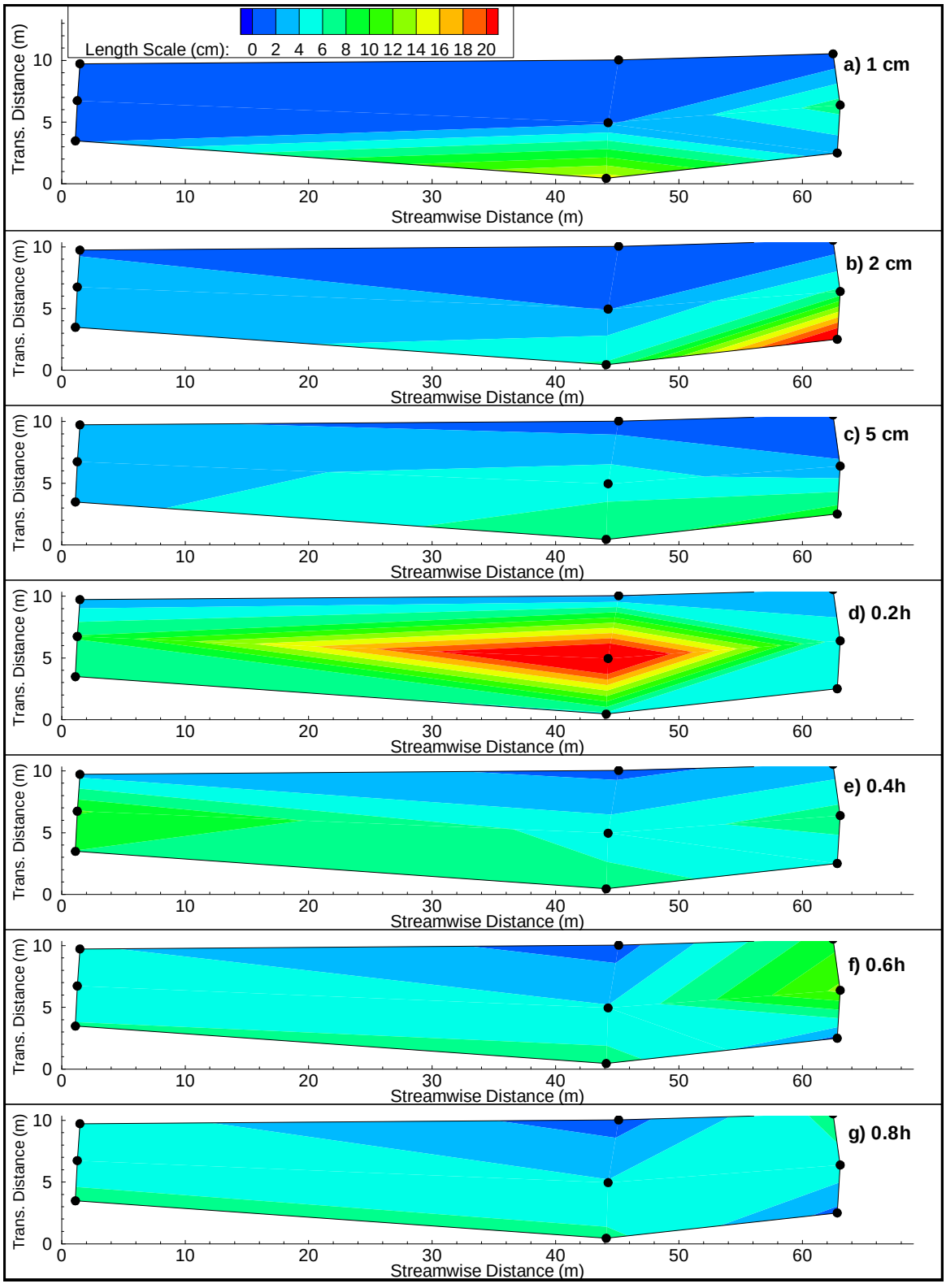

Figure C.25. Potlatch reach integral length scale distributions

Appendix D: Supplementary information for Chapter 3

Table D.1. Summary of ADV data from the Potlatch reach

River	Station	z/h	Umag	Us	Ut	Uv	TI s	TI t	TI v	Csv
Potlatch	1	0.01	39.48	38.86	5.81	-3.93	12.65	14.86	13.68	-22.50
Potlatch	1	0.02	44.65	43.41	8.93	-5.47	11.67	10.22	9.27	-38.93
Potlatch	1	0.05	54.91	54.65	4.04	-3.44	13.54	10.14	9.69	-36.64
Potlatch	1	0.07	58.65	58.61	1.52	-1.49	12.73	10.37	11.33	-27.65
Potlatch	1	0.10	62.52	62.51	0.64	-0.97	13.88	10.34	12.06	-29.13
Potlatch	1	0.15	69.45	69.45	-0.65	0.02	13.80	10.54	15.68	-38.80
Potlatch	1	0.23	73.34	73.33	-0.58	0.42	13.94	10.23	14.34	-49.37
Potlatch	1	0.31	80.38	80.37	-0.07	1.25	13.10	9.73	13.70	-21.58
Potlatch	1	0.46	91.59	91.58	-0.40	0.92	11.56	8.94	14.93	-22.95
Potlatch	1	0.62	92.85	92.85	-0.37	-0.15	9.53	7.64	14.04	-7.75
Potlatch	2	0.02	42.40	42.27	-0.72	-3.20	15.98	11.87	11.97	-65.06
Potlatch	2	0.06	49.17	48.58	7.06	-2.79	14.45	11.56	9.62	-41.77
Potlatch	2	0.12	65.32	65.22	3.29	-1.65	14.74	9.52	10.59	-43.99
Potlatch	2	0.24	76.80	76.79	0.24	-1.10	13.43	9.08	8.54	-36.38
Potlatch	2	0.36	85.75	85.75	0.44	-0.42	11.51	8.60	13.73	-16.14
Potlatch	2	0.48	90.23	90.23	0.07	-0.85	10.10	7.70	13.32	-16.61
Potlatch	2	0.60	93.56	93.56	-0.02	-0.86	11.82	6.98	15.65	-23.24
Potlatch	2	0.71	94.59	94.59	-0.68	1.06	9.23	6.91	16.54	-7.84
Potlatch	2	0.76	97.20	97.18	0.04	2.18	9.26	6.50	11.60	-8.11
Potlatch	3	0.01	14.41	12.27	7.26	-2.10	8.59	7.65	5.07	-4.04
Potlatch	3	0.02	22.08	20.26	7.87	-3.88	11.18	12.25	8.13	-19.43
Potlatch	3	0.03	30.09	27.44	11.05	-5.53	11.36	12.64	8.39	-27.59
Potlatch	3	0.11	47.84	47.82	0.66	1.17	13.38	11.42	12.96	-78.01
Potlatch	3	0.21	65.76	65.71	-2.45	0.87	16.56	9.69	13.86	-43.58
Potlatch	3	0.32	74.79	74.76	-1.91	0.93	13.55	9.73	16.26	-1.11
Potlatch	3	0.43	81.44	81.41	-1.90	-0.09	14.01	9.21	14.45	-29.56
Potlatch	3	0.53	89.82	89.73	-3.12	2.49	12.77	9.82	20.89	-12.70
Potlatch	3	0.64	93.19	93.14	-3.03	-0.57	11.71	8.54	14.82	-29.23
Potlatch	3	0.85	94.69	94.66	-2.24	0.86	9.15	8.78	20.51	-12.47
Potlatch	3	0.94	92.95	92.52	-7.03	5.58	11.46	10.78	19.43	-3.09
Potlatch	4	0.01	12.52	10.97	5.77	1.74	7.39	6.25	3.95	2.36
Potlatch	4	0.02	35.03	34.44	6.32	0.69	11.64	12.38	9.70	-23.41
Potlatch	4	0.04	38.99	38.56	5.76	-0.26	13.42	12.30	10.14	-28.53
Potlatch	4	0.06	41.99	41.78	4.20	-0.64	13.47	10.39	8.30	-44.66
Potlatch	4	0.12	59.52	59.44	3.01	-0.59	13.11	9.89	12.26	-28.99
Potlatch	4	0.24	72.55	72.55	0.05	-0.35	12.26	9.30	13.14	-28.43
Potlatch	4	0.36	82.19	82.19	-0.61	-0.18	12.86	8.04	14.99	-15.95
Potlatch	4	0.48	86.98	86.97	-1.18	-0.27	9.49	7.34	17.23	7.16
Potlatch	4	0.60	90.95	90.93	-2.08	-0.19	7.87	7.45	17.21	-1.51
Potlatch	4	0.84	90.98	90.89	-3.31	2.20	6.42	6.80	15.63	3.48
Potlatch	5	0.01	22.18	20.44	8.61	0.32	7.14	6.70	2.89	1.39
Potlatch	5	0.02	32.70	32.49	3.53	-1.03	9.94	9.57	10.13	-29.29
Potlatch	5	0.04	36.26	36.23	0.98	-0.85	12.46	10.50	13.64	-33.81
Potlatch	5	0.06	41.99	41.99	-0.05	-0.35	10.55	8.98	10.80	-23.31
Potlatch	5	0.12	54.52	54.51	-0.90	0.56	10.67	8.32	13.98	-33.38
Potlatch	5	0.25	63.87	63.87	0.61	-0.17	10.77	7.64	13.93	-31.20
Potlatch	5	0.37	71.27	71.27	0.28	-0.01	6.18	6.41	1.72	2.50
Potlatch	5	0.49	76.73	76.73	0.10	-0.04	6.32	6.37	1.66	2.53

Table D.2. Summary of ADV data for the St. Maries reach

River	Station	z/h	Umag	Us	Ut	Uv	Tl s	Tl t	Tl v	Csv
St. Maries	1	0.01	33.27	33.26	0.75	-0.49	9.04	11.58	3.17	-1.92
St. Maries	1	0.02	40.88	40.76	-1.33	2.79	15.73	13.03	12.76	-18.35
St. Maries	1	0.03	43.98	43.93	1.20	1.52	10.17	11.56	9.49	-23.42
St. Maries	1	0.05	48.61	48.53	-1.07	2.58	12.28	9.53	11.51	-40.35
St. Maries	1	0.09	57.13	57.11	-0.01	1.73	12.01	8.78	11.24	-32.13
St. Maries	1	0.19	66.60	66.60	-0.46	0.21	10.95	7.05	10.29	-15.56
St. Maries	1	0.38	75.61	75.61	0.14	0.05	8.26	5.96	12.32	-7.03
St. Maries	1	0.47	79.01	79.01	0.35	-0.26	7.71	5.62	12.34	-18.43
St. Maries	1	0.66	82.58	82.56	0.53	-1.51	6.43	4.97	14.66	-21.12
St. Maries	1	0.90	81.05	80.95	-3.94	-0.37	5.54	4.52	9.35	-5.87
St. Maries	2	0.01	28.28	25.64	-10.83	5.01	10.62	13.22	8.24	-15.06
St. Maries	2	0.03	35.41	34.23	-8.12	4.03	11.87	13.77	9.87	-32.43
St. Maries	2	0.04	44.70	44.51	-2.16	3.48	12.55	10.83	10.69	-53.67
St. Maries	2	0.09	51.81	51.78	0.60	1.41	13.12	9.26	9.99	-34.21
St. Maries	2	0.18	66.08	66.07	0.87	0.59	10.42	8.48	11.14	-22.37
St. Maries	2	0.35	76.00	75.98	1.70	-0.18	11.35	6.94	14.62	-23.49
St. Maries	2	0.53	88.04	88.00	0.83	-2.39	8.97	6.59	17.07	-21.87
St. Maries	2	0.71	88.03	88.01	0.96	-1.61	6.81	5.45	21.37	-0.44
St. Maries	2	0.88	85.57	85.52	-2.72	-1.30	5.29	5.35	17.86	-2.84
St. Maries	3	0.01	26.63	26.41	3.40	0.57	7.23	6.21	3.37	-3.44
St. Maries	3	0.02	34.52	33.94	5.38	3.23	8.79	6.72	2.60	7.40
St. Maries	3	0.03	51.25	50.89	6.04	0.70	12.43	11.02	9.97	-18.20
St. Maries	3	0.11	61.07	61.03	1.96	-0.97	9.77	7.68	10.90	-21.47
St. Maries	3	0.23	71.98	71.97	-1.11	0.40	8.30	5.66	12.04	-13.54
St. Maries	3	0.46	77.12	77.01	-4.18	0.02	4.92	3.69	15.92	-23.08
St. Maries	3	0.69	78.53	78.53	0.20	0.48	8.65	6.69	14.75	-16.66
St. Maries	3	0.92	79.18	78.95	-6.06	0.89	4.47	4.20	9.26	-6.88
St. Maries	4	0.01	20.66	18.86	8.45	0.34	7.49	7.76	3.99	-4.32
St. Maries	4	0.02	30.94	29.76	8.33	-1.30	9.30	9.56	6.71	-27.45
St. Maries	4	0.03	34.39	33.41	7.88	-2.18	10.66	9.76	7.74	-24.75
St. Maries	4	0.05	41.47	41.13	5.11	-1.19	10.74	8.14	6.60	-27.24
St. Maries	4	0.10	52.60	52.43	4.16	-0.74	10.71	8.03	5.85	-14.02
St. Maries	4	0.20	67.98	67.97	1.10	-1.01	10.42	8.32	7.42	-7.82
St. Maries	4	0.29	74.05	74.04	-1.17	0.86	10.04	7.32	5.93	-11.31
St. Maries	4	0.39	87.15	87.08	-3.54	0.94	7.25	5.54	6.42	-1.66
St. Maries	4	0.59	86.96	86.77	-5.58	1.15	6.69	4.77	5.11	-2.43
St. Maries	4	0.83	85.53	85.25	-5.74	3.91	5.42	4.45	4.27	0.82

Table D.3. Summary of ADCP data for the Potlatch reach

River	Station	z/h	mag	Us	Ut	Uv	TI s	TI t	TI v	Csv
Potlatch	1	0.06	70.44	54.77	3.26	-3.93	40.23	39.08	10.02	55.66
Potlatch	1	0.14	77.79	62.98	8.30	-2.09	33.01	32.78	8.71	126.36
Potlatch	1	0.22	76.71	69.23	3.02	-0.76	27.27	25.89	6.81	80.68
Potlatch	1	0.29	77.76	72.12	1.52	-0.71	29.05	27.79	7.27	50.67
Potlatch	1	0.37	82.52	77.27	0.28	-1.42	27.76	27.66	7.00	41.60
Potlatch	1	0.45	86.38	81.82	0.76	-1.94	27.59	26.93	7.19	45.75
Potlatch	2	0.15	69.86	60.92	-0.70	-0.10	31.00	27.19	7.21	42.73
Potlatch	2	0.21	70.01	67.59	-1.06	-0.02	27.84	27.79	7.05	34.54
Potlatch	2	0.27	77.56	71.67	-0.76	-0.39	27.23	28.13	7.12	42.64
Potlatch	2	0.33	81.11	75.82	-1.21	-0.34	28.30	27.16	7.24	49.15
Potlatch	2	0.39	84.79	79.91	-1.02	-0.76	27.60	27.21	7.15	46.83
Potlatch	2	0.45	88.97	84.12	-0.47	-0.80	28.27	27.77	7.22	43.78
Potlatch	2	0.51	90.08	85.80	0.12	-1.09	27.64	26.44	6.99	36.07
Potlatch	2	0.57	92.52	88.63	-0.67	-1.46	26.88	25.61	7.07	39.28
Potlatch	3	0.14	67.68	60.46	1.62	0.30	33.24	26.86	8.30	115.24
Potlatch	3	0.19	74.44	66.55	1.08	0.22	31.56	26.58	7.79	86.10
Potlatch	3	0.24	76.59	70.67	0.77	0.85	29.26	27.88	7.43	42.91
Potlatch	3	0.30	79.27	73.24	0.01	1.21	28.58	28.56	7.13	43.01
Potlatch	3	0.35	81.04	75.68	0.40	0.90	28.74	27.38	7.04	43.26
Potlatch	3	0.40	85.11	80.00	-0.50	0.96	28.48	27.68	7.28	43.03
Potlatch	3	0.46	86.96	82.18	-0.31	0.70	28.17	27.46	7.39	39.68
Potlatch	3	0.51	90.32	85.62	-2.09	0.59	28.58	27.68	7.38	30.15
Potlatch	3	0.56	92.00	87.73	-1.01	0.15	27.03	26.98	7.19	42.82
Potlatch	3	0.62	94.98	90.79	-0.77	-0.19	27.29	26.89	7.25	45.93
Potlatch	4	0.14	68.77	62.01	2.56	0.16	28.34	27.48	7.74	48.06
Potlatch	4	0.20	68.85	66.35	4.07	1.08	27.64	27.35	7.13	38.58
Potlatch	4	0.27	75.30	69.50	3.29	0.40	28.93	27.34	7.09	40.64
Potlatch	4	0.33	80.23	74.95	1.75	0.25	27.14	27.28	7.01	28.02
Potlatch	4	0.39	85.47	80.36	2.96	-0.28	27.12	28.29	7.42	36.18
Potlatch	4	0.45	87.37	82.87	1.20	-0.08	26.33	27.07	6.98	29.75
Potlatch	4	0.51	88.86	84.74	0.05	-0.07	27.33	25.64	6.75	32.32
Potlatch	4	0.57	92.12	87.86	-0.54	-0.79	27.17	26.83	6.88	26.87
Potlatch	5	0.12	59.30	43.86	-1.61	-1.17	32.10	35.48	8.71	81.91
Potlatch	5	0.19	58.18	46.87	2.62	0.05	28.55	31.88	7.80	48.61
Potlatch	5	0.25	61.66	54.94	3.75	0.06	27.37	25.51	6.87	35.24
Potlatch	5	0.31	67.26	61.28	4.76	-0.09	27.13	25.81	6.94	26.81
Potlatch	5	0.37	71.03	65.23	3.17	-0.14	27.08	26.52	7.03	30.76
Potlatch	5	0.43	73.93	68.52	2.91	-0.35	27.01	26.25	6.67	18.48
Potlatch	5	0.49	76.15	71.14	1.46	-0.30	26.52	25.86	6.78	27.18
Potlatch	5	0.56	76.74	72.16	1.36	-0.42	25.56	25.29	6.77	28.20

Table D.4. Summary of ADCP data for the St. Maries reach

River	Station	z/h	mag	Us	Ut	Uv	TI s	TI t	TI v	Csv
St. Maries	1	0.14	63.04	56.36	0.86	-0.41	26.58	26.40	6.91	16.38
St. Maries	1	0.19	66.25	60.30	-0.49	-0.47	25.98	25.94	6.90	28.15
St. Maries	1	0.24	69.79	63.66	-0.79	-0.46	27.34	26.51	6.82	26.36
St. Maries	1	0.28	71.57	65.65	-0.43	-0.46	27.01	27.23	6.80	22.73
St. Maries	1	0.33	72.71	67.15	0.03	-0.26	26.96	26.52	6.71	22.19
St. Maries	1	0.38	74.35	69.24	-0.74	-0.49	26.83	25.67	6.75	15.54
St. Maries	1	0.42	75.66	70.52	-1.86	-0.55	25.63	26.25	6.79	21.68
St. Maries	1	0.47	76.72	71.81	-1.21	-0.43	26.43	26.00	6.59	24.20
St. Maries	1	0.52	78.69	74.11	-0.58	-0.65	26.21	25.47	6.80	17.60
St. Maries	1	0.57	79.92	75.35	-1.39	-0.82	25.75	25.59	6.73	19.73
St. Maries	1	0.61	80.80	76.55	-1.32	-1.07	25.54	24.83	6.73	16.20
St. Maries	1	0.66	80.90	76.67	-0.60	-1.22	25.31	25.07	6.65	22.94
St. Maries	2	0.68	76.69	72.87	-2.23	-0.38	31.76	23.17	7.22	-9.16
St. Maries	2	0.64	76.47	72.58	-1.81	-0.04	31.59	23.32	7.08	-8.40
St. Maries	2	0.59	75.07	70.97	-2.57	0.34	31.44	23.39	7.05	-12.14
St. Maries	2	0.55	75.78	71.52	-2.38	0.49	31.79	24.58	7.55	-14.78
St. Maries	2	0.50	73.37	68.93	-1.02	0.21	31.78	24.56	7.17	-4.08
St. Maries	2	0.46	72.44	67.39	-0.13	-0.19	31.71	25.61	7.31	-15.53
St. Maries	2	0.42	70.96	65.83	0.44	0.02	31.80	25.56	7.36	-22.46
St. Maries	2	0.37	69.25	63.90	0.45	0.09	31.48	26.09	7.60	-22.99
St. Maries	2	0.33	68.01	62.54	0.29	0.13	30.81	25.71	7.47	-14.33
St. Maries	2	0.28	65.30	59.71	-0.08	0.20	31.48	24.89	7.47	-22.22
St. Maries	2	0.24	61.96	56.12	2.43	-0.14	30.36	25.15	7.65	-20.94
St. Maries	2	0.19	60.00	53.47	2.12	-0.34	29.36	25.95	7.68	-15.67
St. Maries	2	0.15	56.96	50.62	3.10	-0.10	28.54	24.61	7.66	-14.48
St. Maries	2	0.11	22.37	17.00	1.66	-0.36	28.30	22.83	7.48	-23.58
St. Maries	3	0.13	65.36	57.67	2.90	0.63	35.78	27.17	8.14	100.94
St. Maries	3	0.18	63.35	56.02	4.62	-0.54	27.74	26.59	6.78	27.78
St. Maries	3	0.24	65.87	60.04	4.81	-0.21	26.03	25.30	6.71	18.49
St. Maries	3	0.30	68.52	62.81	1.81	-0.27	26.29	25.95	6.40	18.21
St. Maries	3	0.36	69.27	63.99	-0.27	0.02	27.15	25.19	6.58	33.41
St. Maries	3	0.41	72.56	67.42	0.27	-0.07	26.65	25.40	6.54	16.35
St. Maries	3	0.47	74.58	69.93	0.03	-0.07	25.64	24.96	6.61	24.93
St. Maries	3	0.53	75.12	70.41	-0.10	-0.25	26.58	25.30	6.61	19.87
St. Maries	3	0.59	75.84	71.18	-0.35	-0.69	25.31	25.10	6.58	8.48
St. Maries	4	0.16	59.34	49.97	2.45	0.97	26.28	30.65	7.46	23.73
St. Maries	4	0.21	60.47	53.47	1.95	0.54	27.41	25.86	6.73	27.20
St. Maries	4	0.25	63.79	57.13	0.78	0.98	27.11	26.78	-21.34	29.25
St. Maries	4	0.30	64.33	57.91	1.19	0.93	25.95	26.52	-22.52	26.66
St. Maries	4	0.35	66.90	61.11	0.13	0.57	26.35	25.90	-23.58	28.38
St. Maries	4	0.40	69.86	64.67	-0.60	0.54	26.38	25.09	-24.43	24.74
St. Maries	4	0.45	71.67	66.16	-1.15	0.65	26.28	26.39	-24.74	17.94
St. Maries	4	0.50	73.47	67.88	-0.57	0.63	27.18	26.66	-25.06	27.92
St. Maries	4	0.55	74.22	69.51	-1.56	0.39	25.96	24.92	-26.66	20.00
St. Maries	4	0.60	74.34	69.55	0.24	0.14	25.44	25.09	-27.02	21.95
St. Maries	4	0.6471	75.199	70.475	-1.633	-0.123	25.019	25.187	-27.334	28.992

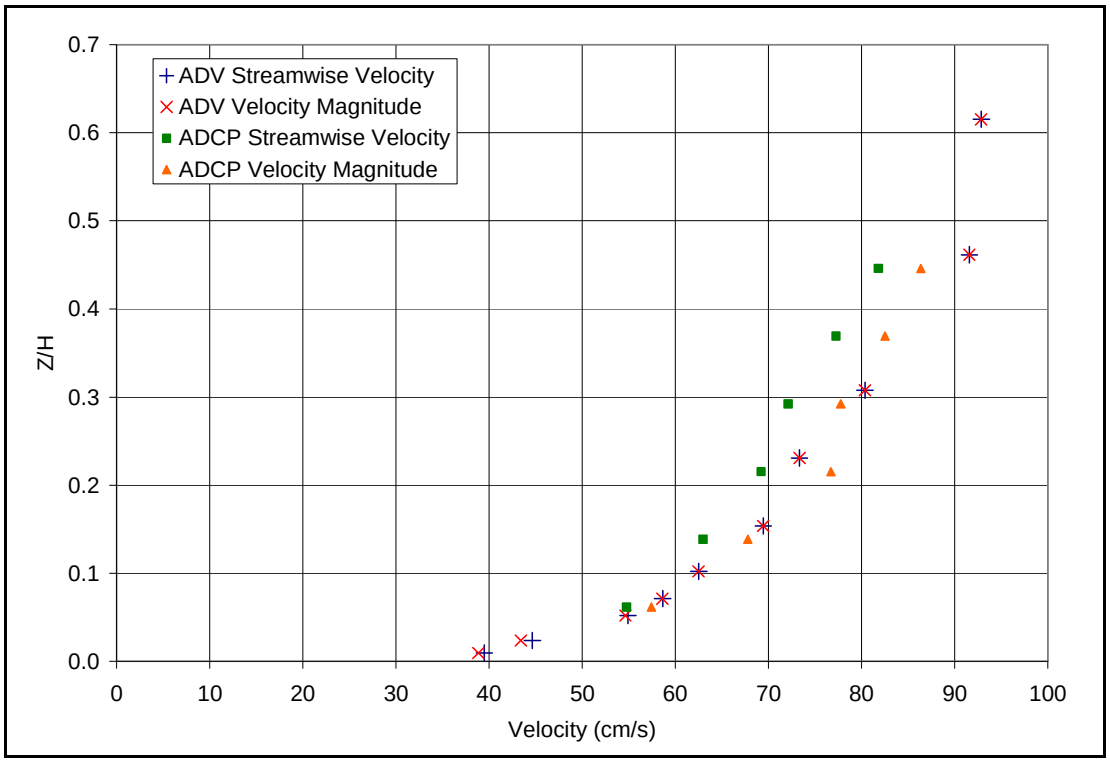

Figure D.1. ADV and ADCP streamwise velocity and velocity magnitude profiles for the Potlatch reach, Station 2, Z=0.5H

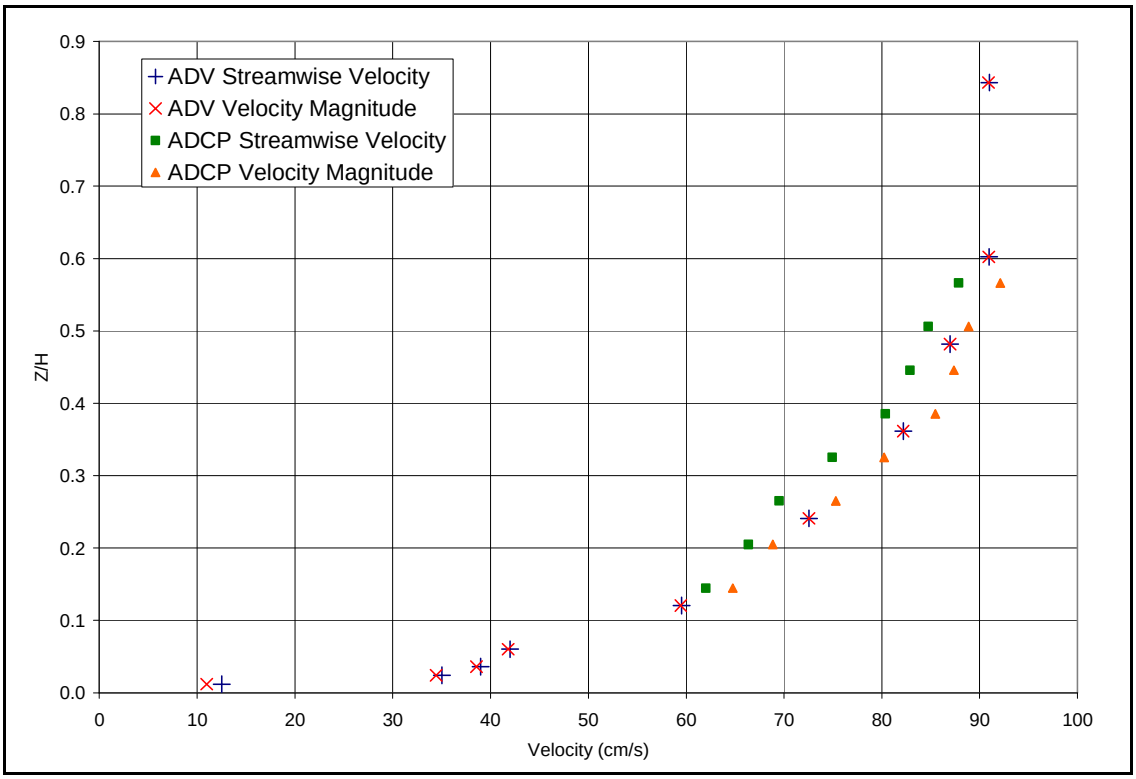

Figure D.2. ADV and ADCP streamwise velocity and velocity magnitude profiles for the Potlatch reach, Station 5, Z=0.5H

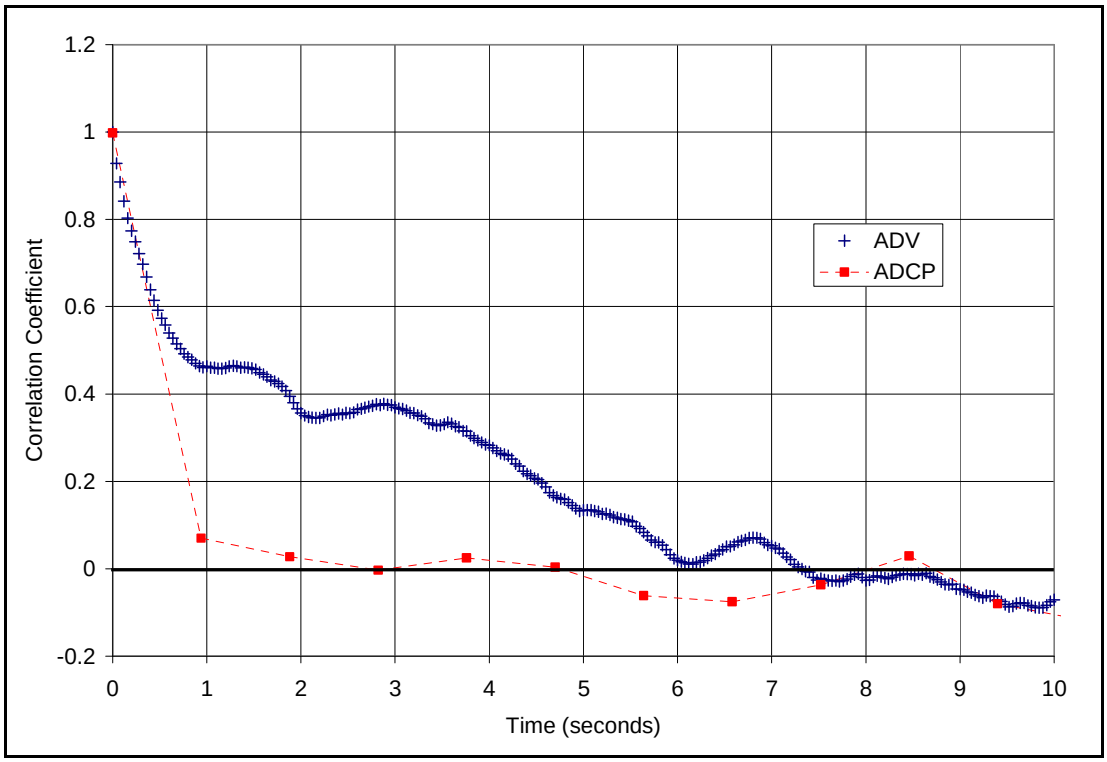

Figure D.3. ADV and ADCP autocorrelation coefficients for the Potlatch reach, Station 2, Z=0.5H

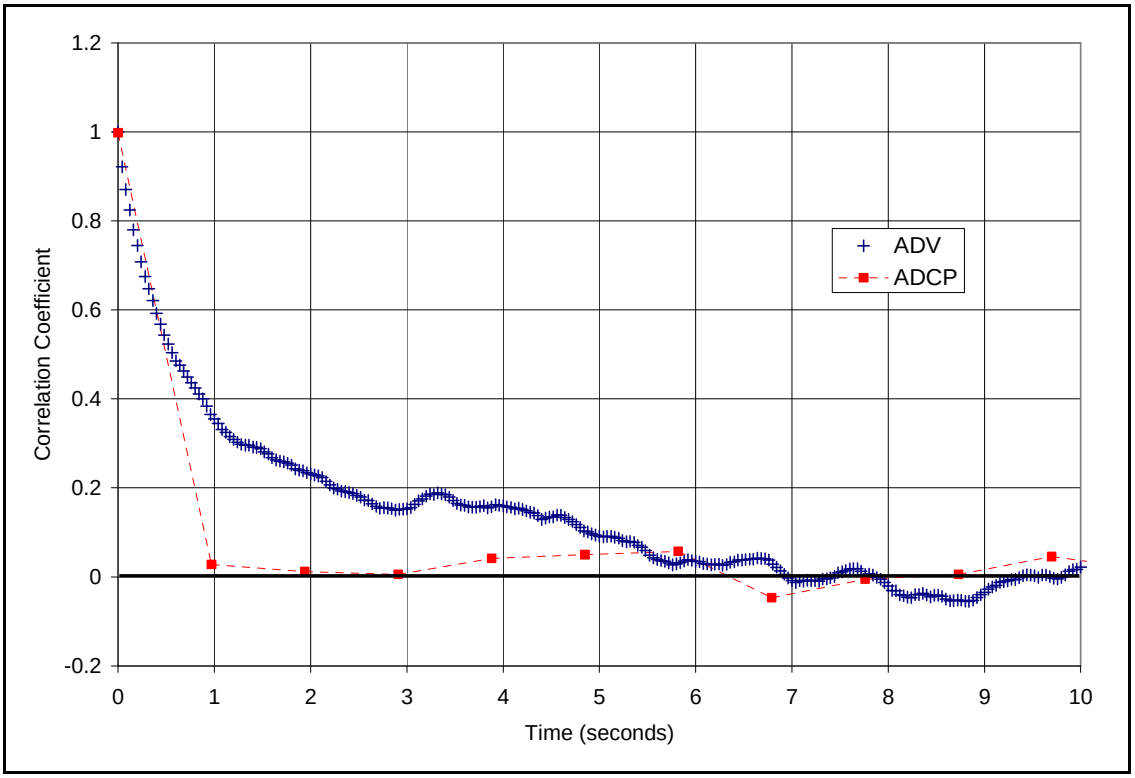

Figure D.4. ADV and ADCP autocorrelation coefficients for the Potlatch reach, Station 2, Z=0.5H

Appendix E: Supplementary information for Chapter 4

Table E.1. Ash free dry mass data for periphyton samples

Sample	Set	Age	Shear	AFDM	Scour	% Scour
1	1	1	0	0.0011	0.0000	0.00
2	1	1	0	0.0011	0.0000	0.00
3	1	1	1	0.0016	0.0007	30.43
4	1	1	1	0.0016	0.0007	30.43
5	1	1	2	0.0020	0.0003	13.04
6	1	1	2	0.0016	0.0007	30.43
7	1	1	3	0.0012	0.0011	47.83
8	1	1	3	0.0002	0.0021	91.74
9	1	1	4	0.0002	0.0021	91.30
10	1	1	4	0.0003	0.0020	86.96
11	1	2	0	0.0046	0.0000	0.00
12	1	2	0	0.0034	0.0000	0.00
13	1	2	1	0.0038	0.0002	5.00
14	1	2	1	0.0030	0.0010	25.00
15	1	2	2	0.0036	0.0004	10.00
16	1	2	2	0.0036	0.0004	10.00
17	1	2	3	0.0024	0.0016	40.00
18	1	2	3	0.0016	0.0024	60.00
19	1	2	4	0.0025	0.0015	37.50
20	1	2	4	0.0023	0.0017	42.50
21	2	1	0	0.0016	0.0000	0.00
22	2	1	0	0.0025	0.0000	0.00
23	2	1	1	0.0029	0.0016	35.56
24	2	1	1	0.0043	0.0002	4.44
25	2	1	2	0.0028	0.0017	37.78
26	2	1	2	0.0012	0.0033	73.33
27	2	1	2	0.0026	0.0019	42.22
28	2	1	3	0.0000	0.0045	100.00
29	2	1	3	0.0003	0.0042	93.33
30	2	1	4	0.0000	0.0045	100.00
31	2	1	4	0.0000	0.0045	100.00
32	2	3	0	0.0075	0.0000	0.00
33	2	3	0	0.0060	0.0000	0.00
34	2	3	0	0.0050	0.0000	0.00
35	2	3	1	0.0056	0.0033	37.08
36	2	3	1	0.0046	0.0043	48.31
37	2	3	2	0.0077	0.0012	13.48
38	2	3	2	0.0048	0.0041	46.07
39	2	3	3	0.0055	0.0034	38.20
40	2	3	3	0.0072	0.0017	19.10
41	2	3	4	0.0049	0.0040	44.94
42	2	3	4	0.0011	0.0078	87.64
43	2	3	4	0.0027	0.0062	69.66
44	3	1	0	0.0034	0.0000	0.00
45	3	1	0	0.0086	0.0000	0.00
46	3	1	0	0.0022	0.0000	0.00
47	3	1	0	0.0039	0.0000	0.00
48	3	1	1	0.0040	0.0002	4.76
49	3	1	1	0.0033	0.0009	21.43
50	3	1	2	0.0021	0.0021	50.00
51	3	1	2	0.0014	0.0028	66.67
52	3	1	3	0.0026	0.0016	38.10
53	3	1	3	0.0002	0.0040	95.24
54	3	1	4	0.0000	0.0042	100.00
55	3	1	4	0.0005	0.0037	88.10

Table E.1 (continued). Ash free dry mass data for periphyton samples

Sample	Set	Age	Shear	AFDM	Scour	% Scour
56	3	4	0	0.0045	0.0000	0.00
57	3	4	0	0.0044	0.0000	0.00
58	3	4	0	0.0085	0.0000	0.00
59	3	4	1	0.0028	0.0002	2.11
60	3	4	1	0.0051	0.0014	14.74
61	3	4	1	0.0038	0.0022	23.16
62	3	4	2	0.0081	0.0026	27.37
63	3	4	2	0.0067	0.0027	28.42
64	3	4	3	0.0069	0.0028	29.47
65	3	4	3	0.0068	0.0044	46.32
66	3	4	4	0.0073	0.0057	60.00
67	3	4	4	0.0093	0.0067	70.53
68	4	1	0	0.0082	0.0000	0.00
69	4	1	0	0.0069	0.0000	0.00
70	4	1	0	0.0080	0.0000	0.00
71	4	1	1	0.0082	0.0000	0.00
72	4	1	1	0.0064	0.0036	36.00
73	4	1	2	0.0070	0.0030	30.00
74	4	1	2	0.0081	0.0019	19.00
75	4	1	3	0.0097	0.0003	3.00
76	4	1	3	0.0099	0.0001	1.00
77	4	1	3	0.0051	0.0049	49.00
78	4	1	4	0.0032	0.0068	68.00
79	4	1	4	0.0023	0.0077	77.00
80	4	5	0	0.0021	0.0079	79.00
81	4	5	0	0.0020	0.0080	80.00
82	4	5	1	0.0042	0.0058	58.00
83	4	5	1	0.0056	0.0044	44.00
84	4	5	2	0.0019	0.0081	81.00
85	4	5	2	0.0045	0.0055	55.00
86	4	5	2	0.0032	0.0068	68.00
87	4	5	3	0.0061	0.0039	39.00
88	4	5	3	0.0014	0.0086	86.00
89	4	5	4	0.0011	0.0089	89.00
90	4	5	4	0.0014	0.0086	86.00
91	4	5	4	0.0013	0.0087	87.00
92	5	1	0	0.0141	0.0000	0.00
93	5	1	0	0.0125	0.0000	0.00
94	5	1	0	0.0140	0.0000	0.00
95	5	1	1	0.0138	0.0000	0.00
96	5	1	1	0.0205	0.0005	2.38
97	5	1	2	0.0175	0.0035	16.67
98	5	1	2	0.0205	0.0005	2.38
99	5	1	3	0.0200	0.0010	4.76
100	5	1	3	0.0118	0.0092	43.81
101	5	1	3	0.0171	0.0039	18.57
102	5	1	4	0.0113	0.0097	46.19
103	5	1	4	0.0157	0.0053	25.24
104	5	6	0	0.0186	0.0024	11.43
105	5	6	0	0.0184	0.0026	12.38
106	5	6	1	0.0093	0.0117	55.71
107	5	6	1	0.0177	0.0033	15.71
108	5	6	2	0.0145	0.0065	30.95
109	5	6	2	0.0136	0.0074	35.24
110	5	6	2	0.0083	0.0127	60.48
111	5	6	3	0.0089	0.0121	57.62
112	5	6	3	0.0121	0.0089	42.38
113	5	6	4	0.0147	0.0063	30.00
114	5	6	4	0.0122	0.0088	41.90
115	5	6	4	0.0137	0.0073	34.76

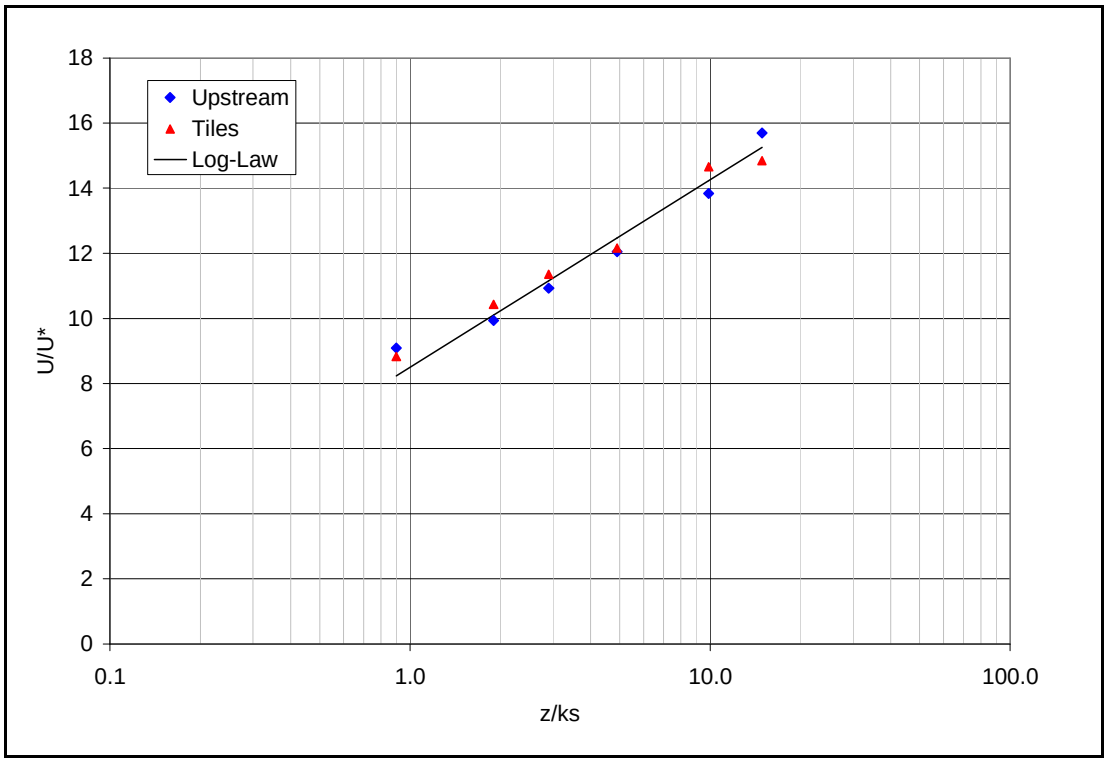

Figure E.1. Log-law 1 meter upstream and directly over the tiles for shear stress of 10 N/m^2

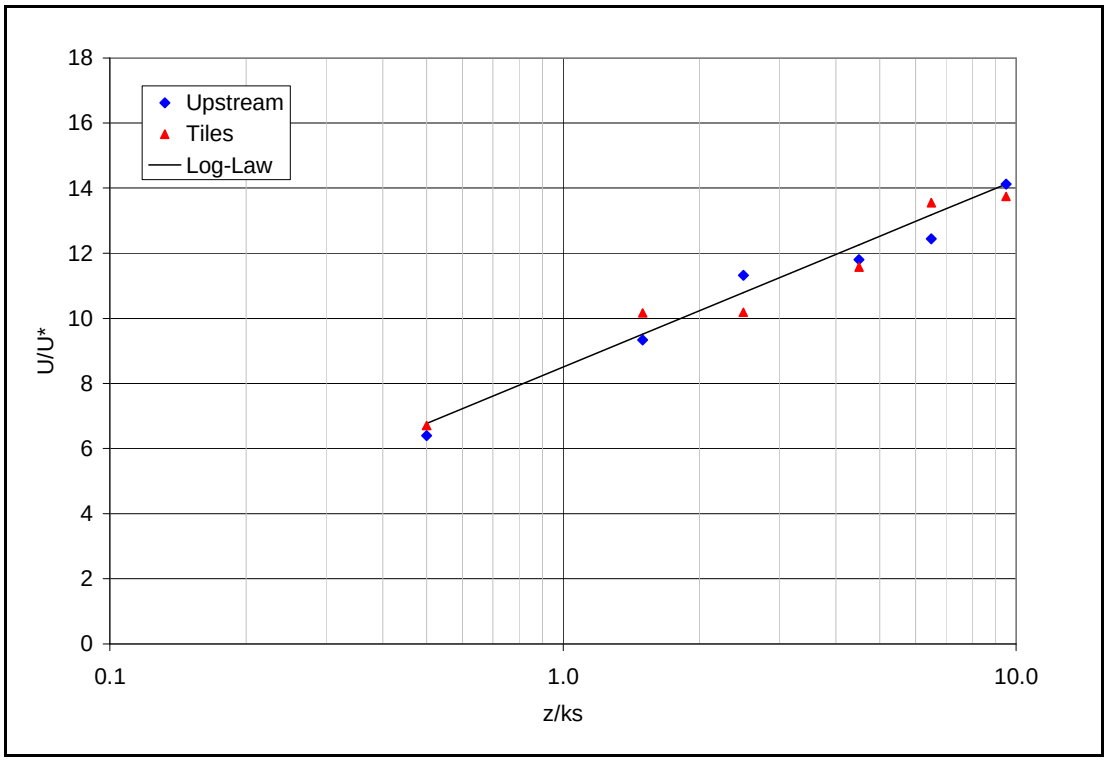

Figure E.2. Log-law 1 meter upstream and directly over the tiles for shear stress of 20 N/m^2

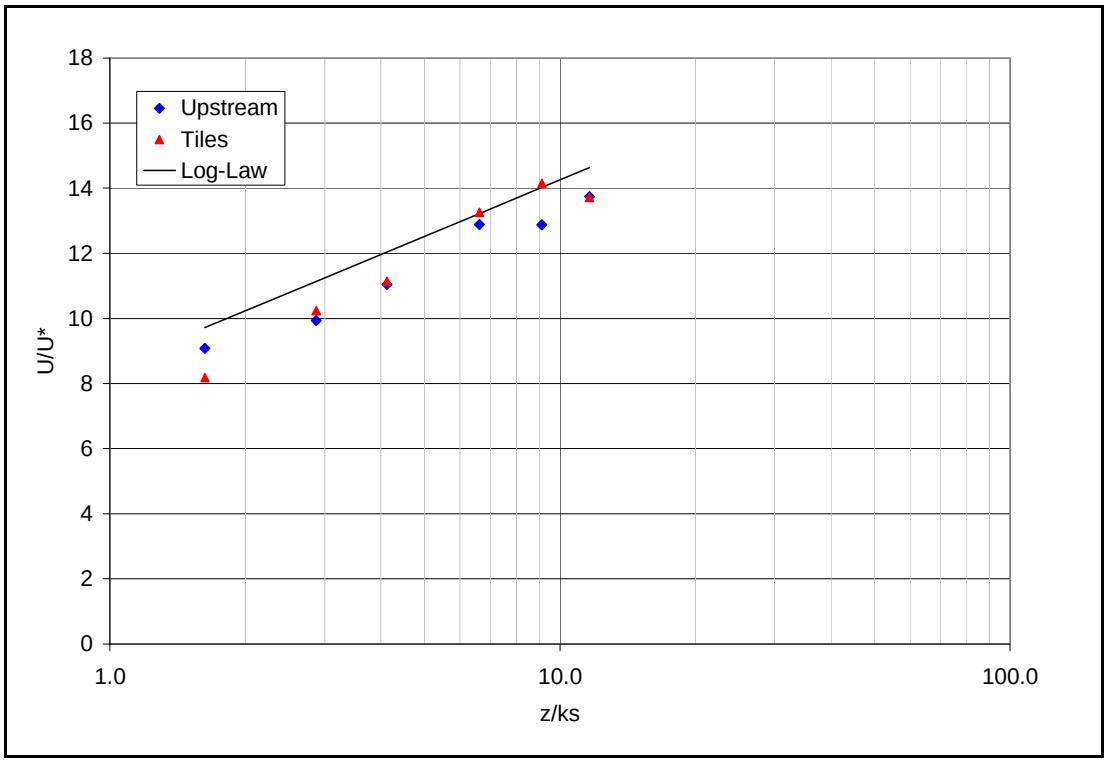

Figure E.3. Log-law 1 meter upstream and directly over the tiles for shear stress of 30 N/m^2

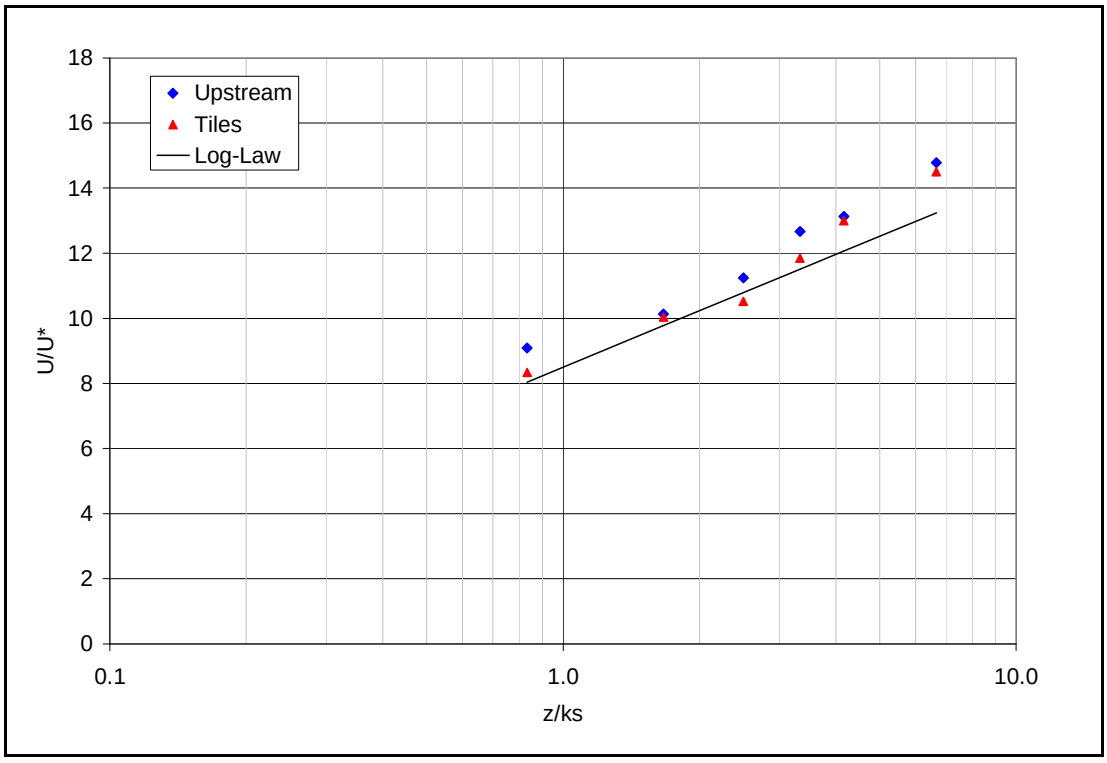

Figure E.4. Log-law 1 meter upstream and directly over the tiles for shear stress of 40 N/m^2

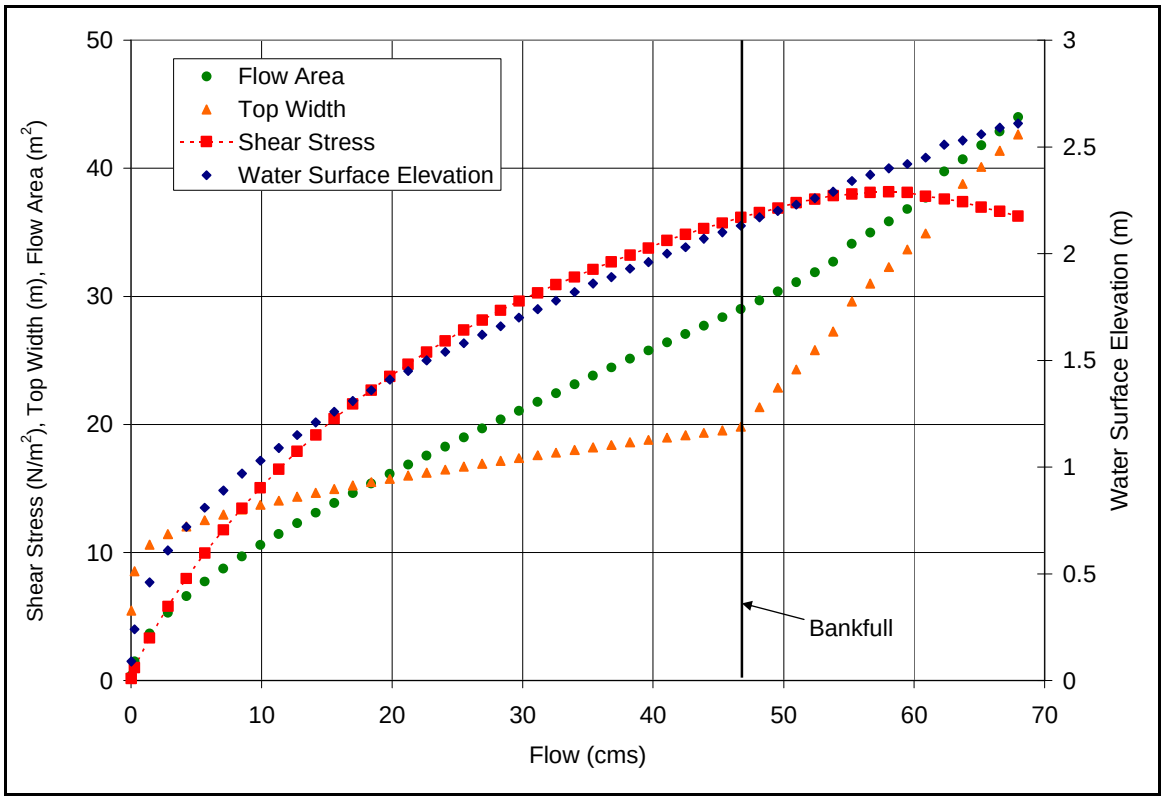

Figure E.5. Flow area, top width, shear stress, and water surface elevations versus discharge for the colonization reach

Appendix F: FORTRAN Code

Following is the FORTRAN code used for analyzing ADV and ADCP velocity time-series data including rotation and calculation of mean and turbulence parameters.

File: turbo.dsw

```
!!    Analyzes time series velocities to calculate turbulence parameters implicit none
INTEGER aa,b,c,n,nbatch
double precision
time1(6000),u(6000),v(6000),w(6000),um,uadev,usdev,uvar,uskew,ukurt,vm,vadev,vsde
v,vvar,vskew,vkurt,wm,wadev,wsdev,wvar,wskew,wkurt,uucov,vvcov,wwcov,uvcov,uw
cov,vwcov,tke,ti, real cor,area
CHARACTER*16       batch,summary,input,spout,corout

                print*,'Now running TurboSweet V2.0'
                        summary='summary.txt'
                        b=1024
                        nbatch=2
                call filemaker()
                call replace()
                call rotate()

   10    open(10,file='turbo.prn')
                open(98,file=summary)
                write(98,1000)

   15           do 100 aa=1,1000

                        read (10,*,end=101)input,spout,corout
                        open (11,file=input)

   20           do n=1,6000
                        read (11,*,end=25)time1(n),u(n),v(n),w(n)
                end do
   25          continue
   26                   close (11)
                        n=n-1
                        call moment(u,n,um,uadev,usdev,uvar,uskew,ukurt)
                        call moment(v,n,vm,vadev,vsdev,vvar,vskew,vkurt)
                        call moment(w,n,wm,wadev,wsdev,wvar,wskew,wkurt)
                                        ti=((usdev+vsdev+wsdev)/3)
                        call spectra(u,n,b,nbatch,input,spout,corout,area)

                  call covariance(u,u,n,uucov)
```

```
                    call covariance(v,v,n,vvcov)
                    call covariance(w,w,n,wwcov)
                          call covariance(u,v,n,uvcov)
                          call covariance(u,w,n,uwcov)
                          call covariance(v,w,n,vwcov)
                  tke=(0.5*(uucov+vvcov+wwcov))

                          write
(98,1100)input,spout,corout,um,vm,wm,usdev,vsdev,wsdev,ti,tke,area,uucov,vvcov,wwc
ov,uvcov,uwcov,vwcov,uskew,vskew,wskew,ukurt,vkurt,wkurt
          !
          print*,input,spout,corout,um,vm,wm,usdev,vsdev,wsdev,ti,tke,area,uucov,vvcov,
wwcov,uvcov,uwcov,vwcov,uskew,vskew,wskew,ukurt,vkurt,wkurt

           100  continue
           101  continue
                     close (10)
                          close (98)

                                print*,'End of program!'
                                read(*,*)

1000  format ('input',11x,',Spectra',9x,',Correlation',5x,',U Mean',4x,',V Mean',4x,',W
Mean',4x,',X TI',6x,',Y TI',6x,',Z TI',6x,',Ave TI',4x,',TKE',7x,',Time S',4x,',UU
Cor',4x,',VV Cor',4x,',WW Cor',4x,',UV Cor',4x,',UW Cor',4x,',VW Cor',4x,',U
Skew',4x,',V Skew',4x,',W Skew',4x,',U Kurt',4x,',V Kurt',4x,',W Kurt')
1100  format (a16,',',a16,',',a16,',',f10.4,',',f10.4,',',f10.4,',',f10.4,',',f10.4,',',f10.4,',
',f10.4,',',f10.4,',',f10.8,',',f10.4,',',f10.4,',',f10.4,',',f10.4,',',f10.4,',',f10.4,',',f10.4,',',f
10.4,',',f10.4,',',f10.4,',',f10.4)
          end
```

SUBROUTINE filemaker()

```
!! This subroutine creates the output files for processed data
!!-------------------------------------------------------------
     character*16  batch
           character*10   file(200)
     integer*2   i,l,number
!      print*,'What is the batch file name?'
                  batch='input.txt'
 20   open(10,file=batch,status='old')
           open(11,file='replace.prn')
           open(12,file='batch.prn')
           open(13,file='rotate.prn')
           open(14,file='orientation.prn')
           open(15,file='turbo.prn')
```

```
21      do 31 i=1,200
              read (10,*,end=32)file(i)
31      continue
32  continue
              close(10)
              number=i-1

40      do 45 l=1,number
              write(11,*)file(l),'.Vf',',',file(l),'.rp'
              write(12,*)file(l),'.rp',',',file(l),'.rep'
              write(13,*)file(l),'.rep',',',file(l),'.rot'
              write(14,*)file(l),'.rep'
              write(15,*)file(l),'.rot',',',file(l),'.spe',',',file(l),'.cor'
45      continue

        close(11)
        close(12)
        close(13)
        close(14)
        close(15)
              end
```

SUBROUTINE replace()

```
!! This subroutine replaces the semi-colon delineated files with commas
!!--------------------------------------------------------------------
        character*40 in,out
        character*15 batch,input,output,com
        integer a,b,c,d,e,f,l,m,n,i,j,k,s1,s2,s3,s4,s5,s6,time,points,frq

10      open (10,file='replace.prn')
12      do 41 i=1,1000

              read(10,*,end=42) input,output
              open (11,file=input)
              open (12,file=output)

24      do 25 j=1,8
              read (11,*) com
25      continue

26      do 39 l=1,10000
31  read (11,*,end=41)in

              s1=index(in,';')
              s2=index(in(s1+1:),';')+s1
              s3=index(in(s2+1:),';')+s2
```

```
              s4=index(in(s3+1:),';')+s3
              s5=index(in(s4+1:),';')+s4
              s6=index(in(s5+1:),';')+s5
          out=in(1:s1-1)//','//in(s3+1:s4-1)//','//in(s4+1:s5-1)//','//in(s5+1:s6-1)

              a=ichar(in(1:1))
              b=ichar(in(2:2))
              c=ichar(in(3:3))
              d=ichar(in(s3+1:s3+1))
              e=ichar(in(s3+2:s3+2))
              f=ichar(in(s3+3:s3+3))

               if(d.eq.45) then
                     if(e.eq.57) then
                           if(f.eq.57) then
                goto 39
                else
                goto 32
                end if
                end if
                end if
32            write (12,*)out

33             if(a.eq.49) then
                     if(b.eq.50) then
                           if(c.eq.48) then
                goto 40
                else
                goto 39
                end if
                end if
                end if

39      continue
40            close (11)
              close (12)
41      continue
42      continue
              close(10)
       end
```

SUBROUTINE rotate()

```
!! This subroutine rotates the data to a streamwise coordiante system
!!-----------------------------------------------------------------
    character*16  obatch,batch,oreo(100),in,out,sum
    integer*2   opoints,i,k,l,o,p
```

```
      integer*2       q,r,s,t,h(100),a,b,c,d,e,m,n
      integer*4       number
      real            time(6000),u(20,6000),v(20,6000),w(20,6000)
      real      u1(20,6000),v1(20,6000),w1(20,6000)
      real      u2(20,6000),v2(20,6000),w2(20,6000)
      real      u3(6000),v3(6000),w3(6000)
      real            up(6000),vp(6000),wp(6000),ur(6000),vr(6000),wr(6000)
      real            uc(6000),vc(6000),wc(6000),uvc(6000),uwc(6000),vwc(6000)
      double precision      vw,vv,ww,vwm,vvm,wwm
      double precision      usum,vsum,wsum,um,vm,wm,theta,phi,u1m,v1m,w1m,psi

            obatch='orientation.prn'
            batch='rotate.prn'
            sum='rotsum.prn'
!!    print*,'What is the rotation sum file?'
!!          read*,sum
            number=0
 20   open (10,file=obatch,status='old')
      open(99,file=sum)
      write(99,*) 'Rotation files:'

 21   do 31 i=1,100
            read (10,*,end=32)oreo(i)
            open (11,file=oreo(i))
            write(99,*)oreo(i)
 22   do 25 l=1,6000
       read (11,*,end=26)time(l),u(i,l),v(i,l),w(i,l)
                  usum=usum+u(i,l)
                  vsum=vsum+v(i,l)
                  wsum=wsum+w(i,l)
                  number=number+1
 25    continue
 26    continue
 30          close (11)
            h(i)=l-1
 31   continue
 32   continue

 33          close (10)
            opoints=i-1
!*************************************************************************
                  um=usum/number
                  vm=vsum/number
                  wm=wsum/number
                  theta=atan(vm/um)
                  usum=0.0
```

```
                    vsum=0.0
                    wsum=0.0

41          do 50 o=1,opoints
42          do 49 p=1,h(o)

            u1(o,p)=u(o,p)*cos(theta)+v(o,p)*sin(theta)
            v1(o,p)=-u(o,p)*sin(theta)+v(o,p)*cos(theta)
            w1(o,p)=w(o,p)
                    usum=usum+u1(o,p)
                    vsum=vsum+v1(o,p)
                    wsum=wsum+w1(o,p)
49          continue
50          continue

                    u1m=usum/number
                    v1m=vsum/number
                    w1m=wsum/number
                    phi=atan(w1m/u1m)
                    q = 0
                    r = 0
                    vw=0.0
                    vv=0.0
                    ww=0.0

61          do 70 q=1,opoints
62          do 69 r=1,h(q)
            u2(q,r)=u1(q,r)*cos(phi)+w1(q,r)*sin(phi)
            v2(q,r)=v1(q,r)
            w2(q,r)=-u1(q,r)*sin(phi)+w1(q,r)*cos(phi)
                    vw=vw+v2(q,r)*w2(q,r)
                    vv=vv+v2(q,r)*v2(q,r)
                    ww=ww+w2(q,r)*w2(q,r)

69          continue
70          continue
                    vwm=vw/number
                    vvm=vv/number
                    wwm=ww/number
                    psi=atan((2*vwm)/(vvm-wwm))
        write(99,*)'This data has been rotated:'
        write(99,1200)theta,phi,psi

100   open (30,file=batch,status='old')
110    do 200 a=1,500
            read (30,*,end=201)in,out
```

```
                open(50,file=in)
                open(51,file=out)

 150    do 190 d=1,6000
                read (50,*,end=195)time(d),u(1,d),v(1,d),w(1,d)

                u1(1,d)=u(1,d)*cos(theta)+v(1,d)*sin(theta)
                v1(1,d)=-u(1,d)*sin(theta)+v(1,d)*cos(theta)
                w1(1,d)=w(1,d)

                u2(1,d)=u1(1,d)*cos(phi)+w1(1,d)*sin(phi)
                v2(1,d)=v1(1,d)
                w2(1,d)=-u1(1,d)*sin(phi)+w1(1,d)*cos(phi)

                u3(d)=u2(1,d)
                v3(d)=v2(1,d)*cos(psi)+w2(1,d)*sin(psi)
                w3(d)=-v2(1,d)*sin(psi)+w2(1,d)*cos(psi)
                write(51,1300)time(d),u3(d),v3(d),w3(d)

 190  continue
 195  continue
                close (50)
                close (51)
 200  continue
 201  continue
                close (30)
 1200  format ('theta,',f8.6,',','phi,',f8.6,',','psi,',f8.6)
 1300  format (f7.3,',',f10.5,',',f10.5,',',f10.5)
                end
```

SUBROUTINE moment (data1,n,ave,adev,sdev,var,skew,kurt)

```
!! This subroutine calculates basic velocity statistical properties
!!---------------------------------------------------------------------
    INTEGER n
        double precision adev,ave,kurt,sdev,skew,var,data1(n)
    INTEGER j
        double precision p,s,ep
    if(n.le.1)pause 'n must be at least 2 in moment'
    s=0.
    do 11 j=1,n
      s=s+data1(j)
11    continue
    ave=s/n
    adev=0.0
    var=0.0
    skew=0.0
```

```
      kurt=0.0
      ep=0.
      do 12 j=1,n
        s=data1(j)-ave
        ep=ep+s
        adev=adev+abs(s)
        p=s*s
        var=var+p
        p=p*s
        skew=skew+p
        p=p*s
        kurt=kurt+p
12    continue
      adev=adev/n
      var=(var-ep**2/n)/(n-1)
      sdev=sqrt(var)
      if(var.ne.0.)then
        skew=skew/(n*sdev**3)
        kurt=kurt/(n*var**2)-3.
      else
        pause 'no skew or kurtosis when zero variance in moment'
      endif
      return
      END
```

Subroutine spectra (u,r,n,nbatch,input,spout,corout,area)

```
!! This subroutine prepares the data for the spectral analysis
!!--------------------------------------------------------------------
      INTEGER r
          double precision u(r)
      real vdata(r)
          character*16 input,spout,corout

      do i=1,r
          vdata(i)=u(i)
      end do
      CALL SPECTR(vdata,n,nbatch,input,spout,corout,area)
      RETURN
      END
```

SUBROUTINE SPECTR (vdata,n,nbatch,input,spout,corout,area)

```
      COMMON /SPECT/ AMPLIT( 2048),POWER( 2048),TIME(1024),SPLOT( 2048)
      COMMON /DAT100/ WORK(2, 2048),VEL(2, 2048)
      REAL*4 VDATA(N,NBATCH)
      INTEGER*4 NROWS
      REAL*4 XMIN,XMAX
```

```
      REAL*8 VMEAN,STDEV,SKEW,RKURT
      LOGICAL HPTERM,YSNO$A,YES,ONEFIL
      integer trntyp
      common /xy$tg/trntyp
      CHARACTER C_OUT*160
           character*16 input,spout,corout

      DATA ISYM1,ISYM2,SIZE1,SIZE2,LINE1,LINE2,IPEN1,IPEN2/
     &          0,    0,0.125,0.125,    1,    0,   15,  0/

           HZ=12.5
      RNPT=N
      PI=3.141592654
      NT2=2*N

C Computing the mean velocity using all data files
           nrows=nbatch*n

      CALL mom(VDATA,NROWS,XMIN,XMAX,VMEAN,STDEV,SKEW,RKURT)
      NFP=N
      DO 7000 I=1,NFP
      TIME(I)=(I-1)/HZ
 7000 CONTINUE
           DSTDEV=1.0/STDEV

      DO 285 I=1,NT2
        AMPLIT(I)=0.0
285     POWER(I)=0.0

      DO 295 IBATCH=1,NBATCH

           DO 230 I=1,N
            VDATA(I,IBATCH)=(VDATA(I,IBATCH)-VMEAN)*DSTDEV
 230   CONTINUE

 295 continue

      CALL mom(VDATA,NROWS,XMIN,XMAX,VMEAN,STDEV,SKEW,RKURT)

C     Computing the Spectral Energy Curve

      FREQ=HZ/N
      DO 7800 I=1,N
      TIME(I)=FREQ*(I-1)
 7800 CONTINUE
```

```
      DO 7290 IBATCH=1,NBATCH

C Setting imaginary part of array to zero
C
       DO 430  J=1,NT2
         VEL(2,J)=0.0
430     CONTINUE
C
C Adding zeros to last half of velocity array
C
       I=N+1
       DO 437 J=I,NT2
437       VEL(1,J)=0.0
C
C move the normalized data into VEL to pass it all to the FFT subroutine.
C
       DO 5000 J=1,N
         VEL(1,J)=VDATA(J,IBATCH)
 5000    CONTINUE

C Calling FFT subroutine
       ISIGN =-1
       CALL FOURG(NT2,ISIGN)

C Ensemble averaging the frequency transforms for each batch
       DO 450 I=1,NT2
         A=(VEL(1,I)**2+VEL(2,I)**2)
         POWER(I)=POWER(I)+A*2.0/(RNPT*HZ)
            AMPLIT(I)=AMPLIT(I)+SQRT(A)*2.0/RNPT
450     CONTINUE

 7290 CONTINUE

      DBATCH=1.0/FLOAT(NBATCH)
      DO 478 III=1,NT2
        AMPLIT(III)=AMPLIT(III)*DBATCH
478     POWER(III)=POWER(III)*DBATCH

C     Storing the ensemble averaged spectral energy curve for
C     computing the autocorrelation

      DO 500 I=1,NT2
500     VEL(1,I)=POWER(I)
C
C Integration of the spectral energy curve (trapezoidal rule is used)
C
```

```
      AREA=0.5*(POWER(1)+POWER(N))
      K=N-1
      DO 1024 I=2,K
1024    AREA=AREA+POWER(I)
      BNDWTH=HZ/(2.0*RNPT)
      AREA=AREA*HZ/(2.0*RNPT)
!      WRITE(*,1029) AREA
!1029  FORMAT(/' The area under the power spectral curve is 'F12.5)

      NPTS=N
      NPTA=1
          DO 504 I=1,NPTS
            SPLOT(I)=POWER(I)
 504    CONTINUE

          NROWS=NPTS
          lur=12
          open(file=spout,unit=lur,status='unknown')
          write(lur,*)area
          write(lur,'(2g16.7)')(time(i),splot(i),i=1,nrows)
          close(lur)

      DO 1032 I=1,NT2
        VEL(1,I)=0.5*VEL(1,I)
        VEL(2,I)=0.0
1032  CONTINUE

C Calling FFT subroutine
      ISIGN=+1
      CALL FOURG(NT2,ISIGN)

C Finding magnitude of autocorr coeffs.
      HZDEV2=HZ*0.5
      DO 1034 I=1,N

1034    VEL(1,I)=VEL(1,I)*HZDEV2/FLOAT(N-I+1)

C Integration of the auto correlation curve to find the integral
C time scale (trapezoidal rule is used).  Integration stops at
C at first negative autocorrelation point.
      AREA=0.0
      DELT=1.0/HZ
      M=N-1
      DO 920 I=2,M
        AREA=AREA+VEL(1,I)
920     IF(VEL(1,I+1) .LT. 0.0)GOTO 930
```

```
930   CONTINUE
      AREA=AREA+0.5*(VEL(1,1)+VEL(1,I+1))
      AREA=AREA*DELT
!       WRITE(*,940)AREA
! 940   FORMAT(/' The integral time scale is ',F12.5,' seconds.')

      DO 7950 I=1,N
      SPLOT(I)=VEL(1,I)
      TIME(I)=(I-1)/HZ
 7950 CONTINUE

      NROWS=N
      lur=12
      open(file=corout,unit=lur,status='unknown')
           write(lur,*)area
      write(lur,'(2g16.7)')(time(i),splot(i),i=1,nrows)
      close(lur)
      RETURN
      END

SUBROUTINE FOURG (N,ISIGN)
!! This subroutine is used in the Fast Fourier Transform
!!-----------------------------------------------------------------------
!! Written by Norman Brenner, MIT Lincoln Laboratory
      DIMENSION IFACT(32)
      COMMON /DAT100/ WORK(2* 2048),data(2* 2048)

      TWOPI=6.283185307*FLOAT(ISIGN)

      IF=0
      NPART=N
      DO 50 ID=1,N,2
      IDIV=ID
      IF(ID-1) 10,10,20
   10 IDIV=2
   20 IQUOT=NPART/IDIV
      IF(NPART-IDIV*IQUOT) 40,30,40
   30 IF=IF+1
      IFACT(IF)=IDIV
      NPART=IQUOT
      GOTO 20
   40 IF(IQUOT-IDIV) 60,60,50
   50 CONTINUE
   60 IF(NPART-1) 80,80,70
   70 IF=IF+1
      IFACT(IF)=NPART
```

```
 80 NFACT=IF

    IP0=2
    IP3=IP0*N
    IWORK=1
    I3REV=1
    DO 110 I3=1,IP3,IP0
    WORK(IWORK)=DATA(I3REV)
    NN=IWORK + 1
    LLL = I3REV +1
    WORK(NN)=DATA(LLL)
    IP2=IP3
    DO 100 IF=1,NFACT
    IP1=IP2/IFACT(IF)
    I3REV=I3REV+IP1
    IF(I3REV-IP2)110,110,90
 90 I3REV=I3REV-IP2
100 IP2=IP1
110 IWORK=IWORK+IP0
    IWORK=1
    DO 120 I3=1,IP3,IP0
    DATA(I3)=WORK(IWORK)
    NN=I3 +1
    LLL=IWORK + 1
    DATA(NN)=WORK(LLL)
120 IWORK=IWORK+IP0
C     PHASE-SHIFTED FOURIER TRANSFORM OF LENGTH IFACT(IF)
    IF=0
    IP1=IP0
130 IF(IP1-IP3) 140,240,240
140 IF=IF+1
    IFCUR=IFACT(IF)
    IP2=IP1*IFCUR
    THETA=TWOPI/FLOAT(IFCUR)
    SINTH=SIN(0.5*THETA)
    ROOTR=-2.*SINTH*SINTH
C     COS(THETA)-1, FOR ACCURACY
    ROOTI=SIN(THETA)
    THETA=TWOPI/FLOAT(IP2/IP0)
    SINTH=SIN(0.5*THETA)
    WSTPR=-2.*SINTH*SINTH
    WSTPI=SIN(THETA)
    WMINR=1.
    WMINI=0.
    DO 230 I1=1,IP1,IP0
    IF(IFCUR-2) 150,150,170
```

```
150 DO 160 I3=I1,IP3,IP2
   J0=I3
   J1=I3+IP1
   LLL=J0 +1
   NN =J1 +1
   TEMPR=WMINR*DATA(J1)-WMINI*DATA(NN)
   TEMPI=WMINR*DATA(NN)+WMINI*DATA(J1)
   DATA(J1)=DATA(J0)-TEMPR
   DATA(NN)=DATA(LLL)-TEMPI
   DATA(J0)=DATA(J0)+TEMPR
160 DATA(LLL)=DATA(LLL)+TEMPI
   GOTO 220
170 IWMAX=IP0*IFCUR
   DO 210 I3=I1,IP3,IP2
   I2MAX=I3+IP2-IP1
   WR=WMINR
   WI=WMINI
   DO 200 IWORK=1,IWMAX,IP0
   I2=I2MAX
   NN =I2 + 1
   SUMR=DATA(I2)
   SUMI=DATA(NN)
180 I2=I2-IP1
   NN= I2 +1
   TEMPR=SUMR
   SUMR=WR*SUMR-WI*SUMI+DATA(I2)
   SUMI=WR*SUMI+WI*TEMPR+DATA(NN)
   IF(I2-I3) 190,190,180
190 WORK(IWORK)=SUMR
   LLL = IWORK + 1
   WORK(LLL)=SUMI
   TEMPR=WR
   WR=WR*ROOTR-WI*ROOTI+WR
200 WI=TEMPR*ROOTI+WI*ROOTR+WI
   IWORK=1
   DO 210 I2=I3,I2MAX,IP1
   DATA(I2)=WORK(IWORK)
   NN = IWORK + 1
   LLL = I2 + 1
   DATA(LLL)=WORK(NN)
210 IWORK=IWORK+IP0
220 TEMPR=WMINR
   WMINR=WMINR*WSTPR-WMINI*WSTPI+WMINR
230 WMINI=TEMPR*WSTPI+WMINI*WSTPR+WMINI
   IP1=IP2
   GOTO 130
```

```
  240 RETURN
      END

SUBROUTINE four1 (data,nn,isign)
!! This subroutine performs the Fast Fourier Transform
!!---------------------------------------------------------------------
      INTEGER isign,nn
      REAL data(2*nn)
      INTEGER i,istep,j,m,mmax,n
      REAL veli,velr
      DOUBLE PRECISION theta,wi,wpi,wpr,wr,wvel
      n=2*nn
      j=1

      do 11 i=1,n,2
        if(j.gt.i)then
          velr=data(j)
          veli=data(j+1)
          data(j)=data(i)
          data(j+1)=data(i+1)
          data(i)=velr
          data(i+1)=veli
        endif
        m=n/2
1       if ((m.ge.2).and.(j.gt.m)) then
          j=j-m
          m=m/2
        goto 1
        endif
        j=j+m
11    continue
      mmax=2
2     if (n.gt.mmax) then
        istep=2*mmax
        theta=6.28318530717959d0/(isign*mmax)
        wpr=-2.d0*sin(0.5d0*theta)**2
        wpi=sin(theta)
        wr=1.d0
        wi=0.d0
        do 13 m=1,mmax,2
          do 12 i=m,n,istep
            j=i+mmax
            velr=sngl(wr)*data(j)-sngl(wi)*data(j+1)
            veli=sngl(wr)*data(j+1)+sngl(wi)*data(j)
            data(j)=data(i)-velr
            data(j+1)=data(i+1)-veli
```

```
          data(i)=data(i)+velr
          data(i+1)=data(i+1)+veli
12        continue
         wvel=wr
         wr=wr*wpr-wi*wpi+wr
         wi=wi*wpr+wvel*wpi+wi
13       continue
        mmax=istep
      goto 2
      endif

      return
      END
```

SUBROUTINE realft (ans,N1,isign)

```
!! This subroutine is used in the Fast Fourier Transform
!!---------------------------------------------------------------------
      INTEGER isign,N1
      REAL ans(N1)
CU    USES four1
      INTEGER i,i1,i2,i3,i4,n2p3
      REAL c1,c2,h1i,h1r,h2i,h2r,wis,wrs
      DOUBLE PRECISION theta,wi,wpi,wpr,wr,wtemp
      theta=3.141592653589793d0/dble(N1/2)
      c1=0.5
      if (isign.eq.1) then
        c2=-0.5
        call four1(ans,N1/2,+1)
      else
        c2=0.5
        theta=-theta
      endif
      wpr=-2.0d0*sin(0.5d0*theta)**2
      wpi=sin(theta)
      wr=1.0d0+wpr
      wi=wpi
      n2p3=N1+3
      do 11 i=2,N1/4
        i1=2*i-1
        i2=i1+1
        i3=n2p3-i2
        i4=i3+1
        wrs=sngl(wr)
        wis=sngl(wi)
        h1r=c1*(ans(i1)+ans(i3))
        h1i=c1*(ans(i2)-ans(i4))
```

```
      h2r=-c2*(ans(i2)+ans(i4))
      h2i=c2*(ans(i1)-ans(i3))
      ans(i1)=h1r+wrs*h2r-wis*h2i
      ans(i2)=h1i+wrs*h2i+wis*h2r
      ans(i3)=h1r-wrs*h2r+wis*h2i
      ans(i4)=-h1i+wrs*h2i+wis*h2r
      wtemp=wr
      wr=wr*wpr-wi*wpi+wr
      wi=wi*wpr+wtemp*wpi+wi
11    continue
     if (isign.eq.1) then
      h1r=ans(1)
      ans(1)=h1r+ans(2)
      ans(2)=h1r-ans(2)
     else
      h1r=ans(1)
      ans(1)=c1*(h1r+ans(2))
      ans(2)=c1*(h1r-ans(2))
      call four1(ans,N1/2,-1)
     endif
     return
     END
```

SUBROUTINE twofft (data1,data2,fft1,fft2,N1)

```
!! This subroutine is used in the Fast Fourier Transform
!!-----------------------------------------------------------------------
     INTEGER N1
     REAL data1(N1),data2(N1),fft(N1)
     COMPLEX fft1(N1),fft2(N1)
CU    USES four1
     INTEGER j,N2
     COMPLEX h1,h2,c1,c2
     c1=cmplx(0.5,0.0)
     c2=cmplx(0.0,-0.5)
     do 11 j=1,N1
      fft1(j)=cmplx(data1(j),data2(j))
11    continue
     call four1(fft1,N1,1)
     fft2(1)=cmplx(aimag(fft1(1)),0.0)
     fft1(1)=cmplx(real(fft1(1)),0.0)

         do 12 j=1,N1
         fft(j)=cmplx(real(fft1(j)))
12       continue

     N2=N1+2
```

```
      do 15 j=2,N1/2+1
        h1=c1*(fft1(j)+conjg(fft1(N2-j)))
        h2=c2*(fft1(j)-conjg(fft1(N2-j)))
        fft1(j)=h1
        fft1(N2-j)=conjg(h1)
        fft2(j)=h2
        fft2(N2-j)=conjg(h2)
15    continue
      return
      END
```